



**HAL**  
open science

# State observer for diagnosis of dynamic behavior of vehicle in its environment

Bin Wang

► **To cite this version:**

Bin Wang. State observer for diagnosis of dynamic behavior of vehicle in its environment. Other [cs.OH]. Université de Technologie de Compiègne, 2013. English. NNT : 2013COMP2126 . tel-01016796

**HAL Id: tel-01016796**

**<https://theses.hal.science/tel-01016796>**

Submitted on 1 Jul 2014

**HAL** is a multi-disciplinary open access archive for the deposit and dissemination of scientific research documents, whether they are published or not. The documents may come from teaching and research institutions in France or abroad, or from public or private research centers.

L'archive ouverte pluridisciplinaire **HAL**, est destinée au dépôt et à la diffusion de documents scientifiques de niveau recherche, publiés ou non, émanant des établissements d'enseignement et de recherche français ou étrangers, des laboratoires publics ou privés.

Par **Bin WANG**

*Observateurs d'état pour le diagnostic de comportement dynamique de véhicules automobiles en environnement réel de conduite*

Thèse présentée  
pour l'obtention du grade  
de Docteur de l'UTC



Soutenue le 11 décembre 2013

**Spécialité** : Technologies de l'Information et des Systèmes

D2126

# Université de Technologie de Compiègne

Technologies de l'Information et des Systèmes

Par Bin WANG

## Observateurs d'état pour le diagnostic de comportement dynamique de véhicules automobiles en environnement réel de conduite

## State Observer for Diagnosis of Dynamic Behavior of Vehicle in Its Environment

Thèse soutenue le 11 Décembre 2013 devant le jury composé de :

Michel BASSET	Professeur	UHA-ENSISA, Mulhouse	<i>Rapporteur</i>
Xavier MOREAU	Professeur	Univ. Bordeaux, IPB, Bordeaux	<i>Rapporteur</i>
Dominique MEIZEL	Professeur	ENSIL, Limoges	<i>Examineur</i>
Philippe BONNIFAIT	Professeur	UTC, Compiègne	<i>Examineur</i>
Ali CHARARA	Professeur	UTC, Compiègne	<i>Directeur de thèse</i>
Alessandro VICTORINO	MCF-HDR	UTC, Compiègne	<i>Directeur de thèse</i>



*“Determine that the thing can and shall be done, and then we shall find the way.”*

Abraham Lincoln, 1848



# Acknowledgements

First of all, we would like to express my sincerely gratitude to all these who help me during my three years Ph.D study. If I forget to mention some people who may be deserved, I will apologize in advance to thank you for whatever you did for me.

The high tribute should be paid firstly to my supervisor, professor Ali Charara and associate professor Alessandro Correa Victorino at Université de Technologie de Compiègne, for their instructive advice, insightful criticism and continuous encouragement. Without their knowledge, patience and fully support, the completion of this thesis would not be possible. What I learned from them, it is not only the research method but also the attitude towards conducting oneself in society.

I am indebted to the reporters, professor Xavier Moreau and professor Michel Basset, thank you for being my rappers to check and approve this dissertation. Thank you for all the members of the thesis committee, professor Dominique Meizel, professor Philippe Bonnifait, for your time, encouragement, and insightful feedback.

I would like to send specific acknowledgments to my family, for their loving considerations and forgiveness during these three years in China. Even though I am far in overseas, I still can feel their everlasting love and great confidence.

Thank you to the engineers in our team, Gérald Dherbomez, Thierry Monglon, Paul Crubille and Pierre Hudelaine. They have made a great effort on the implementation of the embedded system and equipped sensors. Thank you for the arrangement of the experimental validation at CERAM and quotidian tests. Without them, the experimental part is impossible to be completed.

It's my pleasure to have an excellent exchange program at Technische Universität Ilmenau in Germany for two weeks, thank you for the warm reception from professor Valentin Ivanov and doctor Kristian Höpping in the framework of project VERVE. Thank you for their cooperation for the joint research, experimental test as well as the publication.

I would like to show heartfelt gratitude for my colleagues, Danilo Alves de lima, Kaci Bader, Bihao Wang, Hoda Dandach, Nicole El zoghby, Adam Houenou, Marek Kurdej, Jiqiong Qiu , Gilles Tagne fokam, Zui Tao, Clement Zinoune, Xiao Liu. Thank you for all of you, for taking the comfortable environment and conviviality within the research life. Especially for Julien Moras, who provides a tremendous assist for me to solve the difficulty encountered and wide knowledge of French language which helped me to familiar with French cultures.

Finally, thank you for Huiyuan Cao, Huyan Pengfei, Peng Cao, Qiang Li, Yingjuan Zhao, we came from in the same exchange program, it's my pleasure to spend four years life with you together in France. Thank you for your support and consolation in my life, and the trip we had experienced would not be forgotten in my memory. Besides, I would like to express my gratitude to all my friends both in China and France. Thank you for your support and encouragement.



# Abstract

Nowadays, a variety of advanced driving assistance systems are being developed by research centers and automobile manufactures. Stability control is an essential topic in the modern industrial automobile society. Driving safety is widely concerned in the passenger cars to prevent potential risks. More and more electronic active safety systems are fitted out as a standard option, such as Electronic Stability Control (ESC) and Traction Control System (TCS).

These safety systems are efficient in helping the driver maintain control of the car and also are considered highly cost-effective. However, for the future development trend of these systems, a more complex and integrated control unit requires more information about the vehicle dynamics. Some fundamental parameters such as tire road forces and sideslip angle are effective in describing vehicle dynamics. Nevertheless, it is lacking an effective and low-cost sensor to measure directly. Therefore, this study presents a method to estimate these parameters using observer technologies and low-cost sensors which are available on the passenger cars in real environment. In addition, these systems are designed for dealing with vehicle current state where danger situation has always occurred, the capacity of these systems is limited to minimize the effects. We were wondering whether shall we predict and effectively avoid a crash before it occurred. Therefore, this work is also addressed to develop a risk prediction method for proposing driver a safe speed to negotiate the upcoming curves.

First, this dissertation develops a new approach to estimate the vertical load distribution in real environment. The influence of bank angle is considered in the phase of reconstruction of vehicle model. The vertical tire force on banked road is estimated by using Kalman filter. In order to estimate the lateral tire force, two nonlinear observers are addressed to solve the nonlinearity of vehicle model. The Extended Kalman filter is widely discussed in the previous literature, while we firstly use a Particle filter to estimate the vehicle dynamics parameters. Two different observer technologies are proposed and compared using the experimental data.

Second, extending the consideration of road safety to the future instant. Prediction of vehicle dynamics parameters, evaluation of potential risk as well as establishment of advisory speed on curves are introduced to reduce the possibility of crash occurrence on curves.

Last but not least, the real-time sampling and process system is presented, the estimator with EKF and PF has been developed as a real-time application. Experimental results are performed to demonstrate the performance of these integrated systems in real-time.

**Keywords:** Vehicle dynamics; Tire/road force; State observer; Curve risk prediction; Experimental validation.



# Résumé

Le contrôle de stabilité est un sujet essentiel dans les systèmes avancés d'aide à la conduite développés par les constructeurs et équipementiers automobiles. Les systèmes de sécurité actifs sont devenus un standard dans les véhicules particuliers, tels que : le contrôle électronique de la stabilité (ESC) et le système de contrôle de traction (TCS).

La description du comportement dynamique du véhicule pendant le mouvement, est fondamental dans le fonctionnement des nouveaux systèmes de sécurité active. Certains systèmes actifs sont déjà implémentés dans des véhicules standards comme des options supplémentaires, pour améliorer la sécurité sur la route ou pour le confort du conducteur et des passagers. Cependant, ces systèmes ont besoin d'informations sur la dynamique de véhicule, qui représente les caractéristiques de mouvement du véhicule sur la route. L'accès à ces informations est souvent difficile, pour des raisons technologiques ou économiques. De ce fait, nous développons des algorithmes, basés sur la technique d'observation d'état, pour estimer une partie de ces variables notamment, les efforts dynamiques du contact pneumatique/chaussée et l'angle de dérive dans son environnement. En revanche, ces systèmes sont conçus pour faire face à l'état actuel du véhicule où la situation de danger a toujours eu lieu, la capacité de ces systèmes est limitée à minimiser les effets de danger. L'objectif ultime est de prévoir et d'éviter efficacement un accident avant qu'il se produise. Par conséquent, ce travail est dédié aussi à développer une méthode de prédiction des risques pour rappeler au conducteur la vitesse de sécurité pour négocier les virages à venir.

Dans un premier temps, nous développons dans ce mémoire une nouvelle approche pour estimer la répartition de la charge verticale sur chaque roue dans un environnement réel. L'influence de l'angle de pente est considérée dans la phase de reconstruction du modèle du véhicule. Les forces verticales sont estimées en utilisant un filtre de Kalman. Afin d'estimer la force latérale du pneu, un filtre de Kalman étendu et un filtre Particulaire sont appliqués pour tenir compte des non-linéarités du modèle de véhicule. Deux techniques différentes d'observateurs sont proposées et comparées avec des données expérimentales.

Dans un deuxième temps, nous étendons, à l'instant futur, la prise en compte de l'évaluation de risque d'accidents. La prédiction des paramètres de la dynamique du véhicule, l'évaluation du risque potentiel ainsi que la détermination d'une vitesse d'alerte à l'approche des virages, sont introduites pour réduire le risque potentiel d'accident dans les virages.

Enfin, la dernière partie du mémoire est consacrée à l'application en temps réel, sur un véhicule démonstrateur, du processus d'observation d'état développé précédemment. Les résultats expérimentaux sont réalisés pour démontrer la performance des estimateurs intégrés en temps réel.

**Mots-clés :** Dynamique du véhicule; Adhérence du contact pneumatique/chaussée; Observateur d'état; Anticipation de risque en virage; Validation expérimentale.



# Contents

<b>Acknowledgements</b>	<b>iii</b>
<b>Abstract</b>	<b>v</b>
<b>Résumé</b>	<b>vii</b>
<b>Contents</b>	<b>xii</b>
<b>List of Figures</b>	<b>xvi</b>
<b>List of Tables</b>	<b>xvii</b>
<b>Nomenclature</b>	<b>xix</b>
<b>Glossary</b>	<b>xxi</b>
<b>Publications</b>	<b>xxiii</b>
<b>1 Introduction</b>	<b>1</b>
1.1 Motivation . . . . .	1
1.2 Objective and contribution . . . . .	2
1.3 Work frame . . . . .	3
1.4 Thesis structure . . . . .	4
<b>2 State of the art</b>	<b>7</b>
2.1 Introduction . . . . .	7
2.2 Road safety and safe system approach . . . . .	8
2.2.1 Electronic Stability Control . . . . .	9
2.2.2 Active Rollover Prevention . . . . .	11
2.3 Tire model . . . . .	12
2.3.1 Basic tire characteristics . . . . .	12
2.3.2 Tire axis frame and terminology . . . . .	13
2.3.3 Tire forces and moments . . . . .	14
2.3.3.1 Longitudinal force and slip ratio . . . . .	14
2.3.3.2 Lateral force and slip angle . . . . .	16
2.3.3.3 Vertical force . . . . .	16
2.3.4 Steady-state tire model . . . . .	18
2.3.4.1 Linear model . . . . .	18
2.3.4.2 Dugoff tire model . . . . .	19
2.3.4.3 Magic tire model . . . . .	21
2.3.5 Wheel ground vertical contact forces . . . . .	25
2.3.5.1 Wheel vertical planar dynamics . . . . .	25
2.3.5.2 Wheel vertical dynamics on banked road . . . . .	27
2.4 Vehicle model . . . . .	28

2.4.1	Vehicle vertical dynamics model . . . . .	29
2.4.1.1	Suspension model . . . . .	29
2.4.2	Vehicle longitudinal and lateral dynamics model . . . . .	31
2.4.2.1	Bicycle vehicle model . . . . .	31
2.4.2.2	Four wheels vehicle model . . . . .	32
2.5	Road-traffic risk assessment . . . . .	35
2.5.1	Excessive driving speed . . . . .	36
2.5.2	Time to collision . . . . .	37
2.5.3	Lateral load transfer . . . . .	38
2.5.4	Lateral acceleration appraisal . . . . .	39
2.5.5	Vehicle yaw stability . . . . .	39
2.5.6	Lane departure indicator . . . . .	39
2.6	Conclusion . . . . .	40
<b>3</b>	<b>Observer theory</b>	<b>43</b>
3.1	Introduction . . . . .	43
3.2	Observer design . . . . .	44
3.2.1	Linear system . . . . .	45
3.2.2	Nonlinear system . . . . .	46
3.3	Kalman filter . . . . .	47
3.4	Extended Kalman filter . . . . .	48
3.5	Particle filter . . . . .	50
3.5.1	Sequential importance sampling (SIS) . . . . .	51
3.5.2	Sequential importance resampling (SIR) . . . . .	52
3.5.3	Particle filter algorithm . . . . .	52
3.6	Conclusion . . . . .	53
<b>4</b>	<b>Vehicle vertical dynamics estimation on banked road</b>	<b>55</b>
4.1	Introduction . . . . .	55
4.2	Analysis of existing method limitation . . . . .	57
4.2.1	Validation of existing vertical tire model . . . . .	57
4.2.2	Analysis of model limitation . . . . .	59
4.3	Vertical tire force model on banked road . . . . .	60
4.3.1	Acceleration measurement . . . . .	61
4.3.2	Roll dynamics of the vehicle body . . . . .	61
4.3.3	Pitch angle calculation . . . . .	64
4.3.4	Vertical force modeling . . . . .	65
4.3.4.1	Analysis of two models with open-loop method . . . . .	69
4.4	Observer design $O_{F_z}$ . . . . .	71
4.4.1	Discrete time state-space representation . . . . .	71
4.4.2	Observability analysis . . . . .	73
4.5	Simulation validation . . . . .	74
4.5.1	Simulation environment . . . . .	74
4.5.2	Observer regulation . . . . .	74
4.5.3	Validation test . . . . .	76
4.5.3.1	Steering wheel alternation slalom test on leveled road . . . . .	76
4.5.3.2	Steering wheel alternation test on 10% banked road . . . . .	77

4.5.3.3	ISO lane change on 18% banked road . . . . .	79
4.5.3.4	Summary . . . . .	82
4.6	Conclusion . . . . .	84
<b>5</b>	<b>Vehicle lateral dynamics estimation</b>	<b>87</b>
5.1	Introduction . . . . .	87
5.2	Retrospection of estimation of lateral dynamics parameters . . . . .	89
5.2.1	Estimation of lateral force . . . . .	89
5.2.2	Estimation of sideslip angle . . . . .	90
5.2.3	Analysis of relationship between lateral force and slip angle . . . . .	90
5.3	Vehicle and tire model . . . . .	91
5.3.1	Double track vehicle model . . . . .	91
5.3.2	Tire force modeling . . . . .	92
5.3.2.1	Vertical tire force model . . . . .	92
5.3.2.2	Lateral tire force model . . . . .	93
5.4	Estimation process in real-time . . . . .	94
5.5	Nonlinear observer modeling . . . . .	95
5.5.1	State-space representation . . . . .	95
5.5.2	Implementation of filter technique . . . . .	96
5.5.2.1	Observability analysis . . . . .	96
5.5.2.2	EKF algorithm: . . . . .	96
5.5.2.3	Bootstrap PF algorithm: . . . . .	97
5.5.3	Observer tuning . . . . .	98
5.6	Experimental validation . . . . .	100
5.6.1	Slalom test on dry pavement . . . . .	101
5.6.2	Slalom test on wet pavement . . . . .	102
5.6.3	Closed circle test on bumpy road . . . . .	107
5.6.4	Summary . . . . .	111
5.6.5	Robustness with respect to vehicle parameters . . . . .	112
5.7	Conclusion . . . . .	112
<b>6</b>	<b>Prediction system for curve negotiation</b>	<b>117</b>
6.1	Introduction . . . . .	117
6.2	Existing method of risk anticipation . . . . .	118
6.2.1	Road departure prediction . . . . .	119
6.2.2	Vehicle rollover prediction . . . . .	119
6.2.3	Curve speed prediction . . . . .	119
6.2.4	Vehicle dynamics state prediction . . . . .	120
6.3	Methodology of the prediction system for safe curve negotiation . . . . .	120
6.3.1	Coordinate system and transformation . . . . .	121
6.3.2	Reconstruction of the vehicle dynamics parameters . . . . .	122
6.3.2.1	Lateral acceleration . . . . .	123
6.3.2.2	Yaw rate . . . . .	123
6.3.2.3	Steering wheel angle . . . . .	123
6.3.2.4	Wheel velocity . . . . .	123
6.3.3	Methodology of the prediction system . . . . .	124
6.3.3.1	Global information collection system . . . . .	125

---

6.3.3.2	Risk prediction system . . . . .	127
6.4	Simulation validation . . . . .	129
6.5	Conclusion . . . . .	137
<b>7</b>	<b>Implementation of embedded system and experimental validation</b>	<b>139</b>
7.1	Introduction . . . . .	139
7.2	Experimental vehicle-infrastructure integration . . . . .	139
7.2.1	Embedded sensors . . . . .	140
7.2.2	Software modules . . . . .	143
7.2.2.1	Architecture of the acquisition system . . . . .	143
7.2.2.2	Software architecture . . . . .	145
7.3	Experimental validation . . . . .	146
7.3.1	Vehicle dynamics parameters estimation . . . . .	147
7.3.1.1	Road circuit test . . . . .	147
7.3.2	Risk predication and curve speed warning system . . . . .	155
7.4	Conclusion . . . . .	166
<b>8</b>	<b>Conclusions and perspectives</b>	<b>167</b>
8.1	Conclusions . . . . .	167
8.2	Future work . . . . .	168
	<b>Bibliography</b>	<b>171</b>

# List of Figures

2.1	The catalogue of Advanced Driver Assistance System [Gunia 2008]	9
2.2	ESC interventions for understeering and oversteering [NHTSA 2006]	10
2.3	Number of currently licensed passenger cars and vans analyzed (n) and number matched to crash data	11
2.4	Integration of the basic Electronic Stability Program ESP and the Hybrid Rollover Mitigation Controller(HRMC) in the structure of the entire vehicle stabilizing system from Bosch [Liebemann 2004]	12
2.5	The exploded view of sample radial tire interior components	13
2.6	SAE tire axis coordinate frame [Smith 2004]	14
2.7	Relation between longitudinal friction coefficient and slip ratio	15
2.8	Relation between lateral force and slip angle [Hsu 2007]	17
2.9	Classification of tire models	19
2.10	Dugoff longitudinal force model characteristics	20
2.11	Dugoff lateral force model characteristics	21
2.12	Magic formula factors	22
2.13	Magic longitudinal force model characteristics	24
2.14	Magic lateral force model characteristics	24
2.15	Magic aligning moment model characteristics	25
2.16	Vertical load distribution	27
2.17	Vertical load distribution on banked road	27
2.18	Vehicle body coordinate frame	29
2.19	A quarter vehicle suspension system	30
2.20	Bicycle model	31
2.21	Four wheel vehicle model	33
3.1	Observer employed in control system	45
4.1	Maneuver time history of the slalom test	58
4.2	Vertical forces at front wheels calculated with open-loop	58
4.3	DLC test with 10% bank angle: vertical force at front wheels	59
4.4	DLC test with 10% bank angle: vertical force at rear wheels	60
4.5	Lateral acceleration measurement on flat road	61
4.6	Lateral acceleration measurement and roll dynamics on banked road	62
4.7	Comparison of the calculated roll angle from suspension deflection and the simulation with 10% bank angle	63
4.8	Vehicle lateral view	64
4.9	Vehicle model on inclined road	65
4.10	Vehicle and suspension model on banked road	67
4.11	Vehicle and suspension model with banked angle	69
4.12	Comparison of multi-models of vertical front tire force with 18% bank angle	70
4.13	Comparison of multi-models of vertical rear tire force with 18% bank angle	71
4.14	A scenario of video replay: illustration of the vehicle test on banked road	75

4.15	The trajectory of vehicle body movement: steering wheel alternation test on leveled road . . . . .	77
4.16	Maneuver time history: steering wheel alternation test on leveled road . . . . .	78
4.17	Comparison of front vertical tire forces: steering wheel alternation test on leveled road . . . . .	78
4.18	Comparison of rear vertical tire forces: steering wheel alternation test on leveled road . . . . .	79
4.19	Maneuver time history: steering wheel alternation test on 10% banked road . . . . .	80
4.20	The trajectory of vehicle body movement: steering wheel alternation test on 10% banked road . . . . .	80
4.21	Roll angle model: steering wheel alternation test on 10% banked road . . . . .	80
4.22	Comparison of front vertical tire forces: steering wheel alternation test on 10% banked road . . . . .	81
4.23	Comparison of rear vertical tire forces: steering wheel alternation test on 10% banked road . . . . .	81
4.24	Maneuver time history: ISO lane change on 18% banked road . . . . .	82
4.25	The trajectory of vehicle body movement: ISO lane change on 18% banked road . . . . .	83
4.26	Roll angle model: ISO lane change on 18% banked road . . . . .	83
4.27	Comparison of front vertical tire forces: ISO lane change on 18% banked road . . . . .	83
4.28	Comparison of rear vertical tire forces: ISO lane change on 18% banked road . . . . .	83
5.1	Typical lateral force versus slip angle . . . . .	91
5.2	Lateral tire force estimation schema . . . . .	94
5.3	Comparison of two resample algorithms . . . . .	99
5.4	Maneuver time history: slalom test on dry pavement . . . . .	101
5.5	The trajectory of vehicle body movement: slalom test on dry pavement . . . . .	102
5.6	Comparison of front vertical tire forces: slalom test on dry pavement . . . . .	103
5.7	Comparison of front lateral tire forces: slalom test on dry pavement . . . . .	103
5.8	Comparison of sideslip angle: slalom test on dry pavement . . . . .	104
5.9	Maneuver time history: slalom test on wet pavement . . . . .	105
5.10	The trajectory of vehicle body movement: slalom test on wet pavement . . . . .	105
5.11	Comparison of front vertical tire forces: slalom test on wet pavement . . . . .	106
5.12	Comparison of front lateral tire forces: slalom test on wet pavement . . . . .	106
5.13	Comparison of sideslip angle: slalom test on wet pavement . . . . .	107
5.14	Maneuver time history: closed circle on bumpy road . . . . .	108
5.15	The trajectory of vehicle body movement: closed circle on bumpy road . . . . .	108
5.16	Comparison of front vertical tire forces: closed circle on bumpy road . . . . .	109
5.17	Comparison of rear vertical tire forces: closed circle on bumpy road . . . . .	109
5.18	Comparison of front lateral tire forces: closed circle on bumpy road . . . . .	110
5.19	Comparison of rear lateral tire forces: closed circle on bumpy road . . . . .	110
5.20	Comparison of sideslip angle: closed circle on bumpy road . . . . .	110
5.21	Closed circle test on bumpy road: $m : -30\% : 10 : 30\%$ , $m$ at $0\% = 1667kg$ . . . . .	113
5.22	Closed circle test on bumpy road: $\mu : -30\% : 10 : 30\%$ , $\mu$ at $0\% = 1.0$ . . . . .	114
6.1	Geodetic and ECEF coordinate systems [Cai 2011] . . . . .	121
6.2	Ackermann steering mechanism . . . . .	124
6.3	Reconstruction of the vehicle dynamics parameters . . . . .	125

---

6.4	Risk prediction and curve speed warning systems . . . . .	126
6.5	The schema of implemented prediction system . . . . .	128
6.6	The trajectory of modified double lane change maneuver: four curves identified on the Cartesian coordinate . . . . .	131
6.7	The predicted value of vehicle dynamics input parameters in the first curve . . .	131
6.8	The predicted value of vertical tire force in the first curve . . . . .	132
6.9	The predicted value of lateral tire force in the first curve . . . . .	132
6.10	The evaluation of potential risk and safe negotiation speed in the first curve . . .	133
6.11	The evaluation of potential risk and safe negotiation speed in the second curve .	134
6.12	The evaluation of potential risk and safe negotiation speed in the third curve . .	135
6.13	The evaluation of potential risk and safe negotiation speed in the fourth curve . .	136
6.14	The trajectory of modified double lane change maneuver: four curves identified on the Cartesian coordinate . . . . .	136
7.1	Heudiasyc laboratory experimental vehicle: DYNA . . . . .	140
7.2	The Correvit installed at place of the spare wheel . . . . .	141
7.3	Kistler wheel force transducers at front left wheel . . . . .	141
7.4	Laser sensor for chassis height measurement . . . . .	141
7.5	Suspension deflection sensor . . . . .	141
7.6	Laser sensor installed at front bumper . . . . .	142
7.7	Embedded electronics and computer in the trunk . . . . .	142
7.8	Laboratory experimental vehicle equipped with sensors . . . . .	142
7.9	Software architecture . . . . .	145
7.10	Application architecture of the vehicle dynamics parameter estimation and risk prediction . . . . .	146
7.11	Real-time vehicle dynamics parameters estimation process schema . . . . .	147
7.12	Onboard real-time estimation surveillance interface . . . . .	148
7.13	The trajectory of road circuit on plan . . . . .	148
7.14	Maneuver time history: S-curve test . . . . .	149
7.15	The trajectory of vehicle body movement: S-curve test . . . . .	150
7.16	Lateral load transfer: S-curve test . . . . .	150
7.17	Comparison of front vertical tire forces: S-curve test . . . . .	150
7.18	Comparison of rear vertical tire forces: S-curve test . . . . .	150
7.19	Comparison of front lateral tire forces: S-curve test . . . . .	151
7.20	Comparison of rear lateral tire forces: S-curve test . . . . .	151
7.21	Maneuver time history: Bend test . . . . .	152
7.22	The trajectory of vehicle body movement: Bend test . . . . .	153
7.23	Lateral load transfer: Bend test . . . . .	153
7.24	Comparison of front vertical tire forces: Bend test . . . . .	153
7.25	Comparison of rear vertical tire forces: Bend test . . . . .	153
7.26	Comparison of front lateral tire forces: Bend test . . . . .	154
7.27	Comparison of rear lateral tire forces: Bend test . . . . .	154
7.28	NRMSE analysis of S-curve test . . . . .	154
7.29	NRMSE analysis of bend test . . . . .	155
7.30	Architecture of real-time risk prediction and advisory curve speed warning system	156
7.31	Road-side unit located on Google map . . . . .	156

---

7.32	Road-side infrastructure . . . . .	156
7.33	Tracked trajectory on Google map . . . . .	157
7.34	Reconstructed Cartesian coordinate of trajectory . . . . .	157
7.35	Captured instantaneous scenario that entering the curve . . . . .	158
7.36	Captured instantaneous scenario that undergoing the curve . . . . .	158
7.37	Captured instantaneous scenario that leaving the curve . . . . .	159
7.38	Final illustration of the overall experimental test around the campus . . . . .	159
7.39	Predicted input parameters for the risk prediction system: first sequence . . . . .	160
7.40	Predicted vertical force: first sequence . . . . .	161
7.41	Predicted lateral force: first sequence . . . . .	161
7.42	Predicted lateral load transfer ratio: first sequence . . . . .	162
7.43	Predicted lateral skid ratio: first sequence . . . . .	162
7.44	Predicted input parameters for the risk prediction system: final sequence . . . . .	163
7.45	Predicted vertical force: final sequence . . . . .	164
7.46	Predicted lateral force: final sequence . . . . .	164
7.47	Predicted lateral load transfer ratio: final sequence . . . . .	165
7.48	Predicted lateral skid ratio: final sequence . . . . .	165

# List of Tables

2.1	Speed limit on different road conditions (R- Urban road; T - Rural road; L - Highway) . . . . .	37
4.1	Normalized mean error between different models calculation and simulation data for the vertical force on 18% banked road . . . . .	70
4.2	Normalized mean error between estimated vertical force and simulation output for three typical tests . . . . .	84
5.1	Relevant model parameters of the experimental vehicle . . . . .	92
5.2	Normalized mean error between estimated lateral tire forces/sideslip angle and simulation output for three typical tests . . . . .	111
6.1	The description of the curve identification on the Cartesian coordinate . . . . .	130
7.1	Available parameters from the acquisition system . . . . .	143
7.2	GPS coordinate of the road-side infrastructure . . . . .	155



# Nomenclature

$a_x$	Longitudinal acceleration ( $m/s^2$ )
$a_y$	Lateral acceleration ( $m/s^2$ )
$a_{ym}$	Measured lateral acceleration ( $m/s^2$ )
$C_r$	Total damping coefficient of roll motion ( $N.m.s/rad$ )
$C_{yi}$	Cornering stiffness of the tire ( $N/rad$ )
$d_w$	Tire damping ( $N.s/m$ )
$d_u$	Suspension damping ( $N.s/m$ )
$d_w$	Tire damping ( $N.s/m$ )
$E$	Vehicle track ( $m$ )
$E_1, E_2$	Vehicle front and rear track ( $m$ )
$F_x$	Longitudinal force ( $N$ )
$F_y$	Lateral force ( $N$ )
$F_z$	Vertical force ( $N$ )
$h$	Height of the center of gravity ( $m$ )
$I_{zz}$	Moment of inertial about yaw axis ( $kg.m^2$ )
$i$	Front(1) or rear(2)
$j$	Left(1) or right(2)
$k_u$	Suspension spring ( $N/m$ )
$k_w$	Tire spring ( $N/m$ )
$K_r$	Total spring coefficient of roll motion ( $N.m/rad$ )
$L$	Wheel base ( $m$ )
$L_1, L_2$	Distance from the cog to the front and rear axles respectively ( $m$ )
$m$	Vehicle total mass ( $kg$ )
$m_s$	Vehicle sprung mass ( $kg$ )
$M_x$	Roll moment ( $N.m$ )
$M_y$	Pitch moment ( $N.m$ )
$M_z$	Yaw moment ( $N.m$ )
$r_i$	Effective tire radius ( $m$ )
$R$	Radius of curvature ( $m^{-1}$ )
$s$	Slip ratio
$V_g$	Vehicle speed at COG ( $m/s$ )
$V_x$	Vehicle longitudinal speed ( $m/s$ )
$V_y$	Vehicle lateral speed ( $m/s$ )
$\alpha_i$	Slip angle ( $rad$ )
$\delta_i$	Steering angle at each wheel ( $rad$ )
$\omega_i$	Wheel angular velocity at each wheel ( $rad/s$ )
$\beta$	Sideslip angle at COG ( $rad$ )
$\psi$	Yaw angle ( $rad$ )

$\dot{\psi}$	Yaw rate ( <i>rad/s</i> )
$\theta$	Roll angle ( <i>rad</i> )
$\dot{\theta}$	Roll rate ( <i>rad/s</i> )
$\gamma$	Camber angle ( <i>rad</i> )
$\mu_x$	Longitudinal friction coefficient
$\mu$	Friction coefficient
$\phi_r$	Road inclined angle ( <i>rad</i> )
$\theta_r$	Road bank angle ( <i>rad</i> )
$\rho_{ij}$	Suspension position ( <i>m</i> )

# Glossary

<b>ADAS</b>	Advanced Driver Assistance System
<b>ACC</b>	Adaptive Cruise Control
<b>COG</b>	Center of Gravity
<b>CWS</b>	Curve Warning System
<b>ECU</b>	Electronic Control Unit
<b>ESC</b>	Electronic Stability Control
<b>INS</b>	Inertial Navigation System
<b>LDW</b>	Lane Departure Warning
<b>LTR</b>	Lateral Load Transfer
<b>PSM</b>	Porsche Stability Management
<b>RMF</b>	Rollover Mitigation Functions
<b>ROR</b>	Run Of Road
<b>SIS</b>	Sequential Importance Sampling
<b>SIR</b>	Sequential Importance Resampling
<b>TCS</b>	Traction Control System
<b>TTC</b>	Time To Collision
<b>VSC</b>	Vehicle Stability Control



# Publications

## *Journal papers*

B. Wang, A. C. Victorino and A. Charara, “Embedded Real-Time Estimation of Vehicle Dynamics: Experimental Implementation and Validation Applied with Nonlinear Observers”, IEEE Transactions on Transport. (submitted)

## *International conference papers*

B. Wang, A. C. Victorino and A. Charara, “State observers applied to vehicle lateral dynamics estimation: a comparison between Extended Kalman filter and Particle filter”, 39th Annual Conference of the IEEE Industrial Electronics Society, Austria, Nov, 2013.

B. Wang, A. C. Victorino, A. Charara, K. Augsborg and K. Hopping, “Assessment of Rollover Stability Based on Risk Indicator”, 2013 IEEE Symposium Series on Computational Intelligence, Singapore, Apr, 2013.

B. Wang, Q. Cheng, A. C. Victorino and A. Charara, “Nonlinear Observers of Tire Forces and Sideslip Angle Estimation Applied to Road Safety: Simulation and Experimental Validation”, 2012 IEEE Conference on Intelligent Transportation Systems, USA, Sep, 2012.

B. Wang, Q. Cheng, A. C. Victorino and A. Charara, “Real-Time Experimental Validation of Nonlinear Observer for Vehicle Dynamics Parameters Estimation: A Laboratory Vehicle Description”, 2012 IEEE International Conference on Vehicular Electronics and Safety, Turkey, Jul, 2012.

Q. Cheng, B. Wang, A. C. Victorino and A. Charara, “A real time observer of sideslip angle and lateral tire road forces with experimental validation”, 2012 IEEE Conference on Intelligent Transportation Systems, USA, Sep, 2012.

## *National conference papers*

B. Wang, A. C. Victorino and A. Charara, “Estimation des variables de la dynamique latérale sur chaussée mouillée : validation expérimentale sur véhicule démonstrateur”, 2013 JD-JN-MACS, Strasbourg, July, 2013.

G. Dherbomez, T. Monglon, P. Crubillé, B. Wang, A. C. Victorino and A. Charara, “DYNA, véhicule expérimental pour la Dynamique du Véhicule”, 4èmes Journées Démonstrateurs, Angers, June, 2013.



# Introduction

## Contents

<b>1.1</b>	<b>Motivation</b>	<b>1</b>
<b>1.2</b>	<b>Objective and contribution</b>	<b>2</b>
<b>1.3</b>	<b>Work frame</b>	<b>3</b>
<b>1.4</b>	<b>Thesis structure</b>	<b>4</b>

## 1.1 Motivation

Automobile, one of the most fundamental inventions in human history, has been greatly renovated during the last hundred years. The quantity of automobiles emerges explosive growth. However, the increasing worldwide use of automobiles has brought an argument in total numbers of accidents. According to the latest statistics report in ONISR (Observatoire National Interministriel de la Sécurité Routière), 60,437 accidents occurred in France in 2012, 3,653 fatalities that were projected. 75,851 people were injured in accidents, 27,142 were in hospital [ONISR 2012]. Moreover, an official report of the motor vehicle traffic from NHTSA (National Highway Traffic Safety Administration) manifests that traffic fatalities for the first quarter of 2013 shows that an estimated 7,200 people died in motor vehicle traffic crashes. The actual counts of the motor vehicle traffic in 2012 are totally 33,780, with an increase of 4.4% on a year-on-year basis [NHTSA 2013].

These road crash statistics reports reflect that road accident becomes a leading cause of people's death. Actually, these fatalities and injuries were associated with three principal types: single-vehicle crashes, multi-vehicle crashes, and rollovers. The crash information also states that over 90% of all accidents are caused by human errors. Therefore, the high accident rate and its primary cause in human error engender the requirement to improve the road safety. Except for some passive safety systems, for example the seat belts, loadspace barrier-nets, airbags, another approach has been proposed as an active safety system, this system can effectively help avoid accidents and reduce the effect of the crash. Although various approaches can be chosen to increase road safety, Advanced Driver Assistance Systems (ADAS) can be assumed as a cost-effective way on enhancing road safety.

Recently, some electronics and control systems like ABS (Anti-lock Brake System), ESC (Electronic Stability Control) are equipped in the automobiles scale to avoid the road accidents which are caused by losing of the vehicle control. ESC is integrated with the vehicle braking system, and it is designed to automatically assist drivers in dangerous situations to guarantee vehicle stability. These systems principally deal with the already happened danger, they get involved to help minimize the loss of control. Meanwhile, any other sensor-based ADAS like lane

departure warning system, collision avoidance system are designed to predict the appearance of road crashes.

Actually, these systems rely on the inexpensive sensors such as steering wheel angle sensor, yaw rate sensor, roll rate sensor and so on. But further developed system needs more information about the vehicle dynamics state like tire/road forces. Since current vehicle control algorithms are limited by available vehicle state information. They rely on the integration of inertial sensors to estimate information about vehicle's state, which may be prone to error and uncertainty. If we own the reorganization of tire forces, sideslip angle, and even the friction coefficient, these data can effectively improve the vehicle control performance. But in reality, these sensors are very expensive or inexistent to install in ordinary cars. It must be observed or estimated. The aim of the observer or virtual sensor is to estimate certain particular immeasurable variables from these available measurements. Otherwise, in the future, ADAS is applied not only in current instant where the danger has happened but also in future instant that helps predict the potential risk to improve the vehicle safety.

## 1.2 Objective and contribution

The mentioned-above motivation brings us tremendous interests in exploring the method of improving road safety in the external environment. Stability control is an essential topic in the modern industrial automobile society. Driving safety is widely concerned in the passenger cars to prevent potential risk. More and more electronic active safety systems are fitted out as a standard option. These safety systems are efficient in helping the driver maintain control of the car and also are considered highly cost-effective. However, for the future development trend of these systems, more complex and integrated control units require more information about the vehicle dynamics. Some fundamental parameters like tire road force and sideslip angle are effective in describing vehicle dynamics. Nevertheless, they are lacking an effective and low-cost sensor to measure directly.

Therefore, as noted in this context, the primary goal of this work is to develop a method for acquiring vehicle maneuvering dynamics, a significant capability required to achieve this mission is the ability to estimate the vehicle state. We are willing to estimate these parameters using observer technologies and low-cost sensors which are available on the passenger cars under different road conditions. In a real environment, the road condition is complex, our target is to obtain the knowledge of vehicle dynamics parameters in all terrain, in particular concerning tire force and sideslip angle. Observer technique is preferred due to its universal and robust characteristics. The employed observer should be adapting to different road conditions, meanwhile the complexity of the system is also an important issue in our objective. The balance of system performance and computing time should be cautiously regulated.

Another significant issue is focused on the risk prediction in the future upcoming road condition. Actually, due to the analysis of run-off-road crashes, accidents are caused by a variety of factors, the primary high frequency accident reason is excessive speed, particularly during the upcoming curve. Consequently, we put research emphasis on the application aimed at evaluating the potential risk in a short term and denoting the advisory curve speed to the driver.

The scope of the dissertation is restricted to the estimation of vehicle dynamics and forecasting of risk assessment in a real road environment using proprioceptive sensors. In addition, experimental implementation is also significant in this work. As the requirement of the doctoral responsibility, the new contribution should enhance the state-of-the-art of knowledge in this

field. It is important to enumerate clearly the expected contributions in this dissertation:

- Development of an observer to estimate individual vertical tire forces in real road condition without the constraint of flat road. The road disturbance can influence directly on vehicle dynamics, the tire force model should be reconstructed in order to provide an exact estimation of vertical tire force and relevant influences on the vehicle dynamics instead of giving a precise road bank angle estimation. The Kalman filter is applied to estimate the parameters including in the state vector instead of the open-loop method.
- Development of an application conducted to estimate the lateral tire force and sideslip angle in real-time. Two nonlinear observers are addressed to solve the nonlinearity of vehicle model. The Extended Kalman filter is widely discussed in the previous literature, while we firstly use the Particle filter to estimate vehicle dynamics parameters. Two different observer technologies are proposed and compared with the experimental test. Particularly, the real-time sampling and process system is presented, the estimation with EKF and PF has been developed as a real-time application. The optimized real-time system can meet the requirement of the computational cost of PF. Experimental validations demonstrate the performance of these two estimation methods in various road environments.
- Development of risk prediction system and advisory curve speed system. We adopt previous method for estimating lateral tire force to complete the prediction procedure which is able to forecast vehicle dynamics parameters in future instant. The risk evaluation is proposed to detect whether danger situation will occur or not. A new curve speed warning system basing on vehicle dynamics assessment is developed to denote a safe negotiating speed before entering the approaching curve.
- Implementation of software modules consisting of data processing and embedded application. Experimental data are processed to take off-line test. It should be highlighted that vehicle dynamics parameters estimation algorithm and curve speed procedures are realized and validated through on-line real-time test.

### 1.3 Work frame

The entire work is completed at the HeuDiaSyc (“Heuristic et Diagnostic des Systèmes Complexes”) UMR 7253 CNRS Laboratory at the Computer Science Department of Université de Technologie de Compiègne (UTC) in France, under the supervision of Prof. Ali Charara and A.P. Alessandro Victorino. This Ph.D funding is provided by China Scholarship Council (CSC).

This dissertation is associated with French national ANR project PERCOIVE (Perception coopérative inter-véhicules pour la sécurité routière), which is addressed in increasing traffic safety within a group of motor vehicles through the observation and evaluation of vehicle dynamics parameters. The system acquires information from the interaction with the external environment and neighboring vehicle. Particularly, this project aims to propose solutions to the problem taking account of the environment (exteroceptive) for the estimation of vehicle dynamics, the estimation approach is also considered in the context of multi-vehicle cooperation. This work contributes to the project of PERCOIVE by estimating the vertical tire force taking account of the environment influence, as well as a robust method for estimating lateral tire force in real environment.

The second project related to this work is the Picardie-region project SEDVAC (Système embarqué d'évaluation de la dynamique du véhicule et d'aide à la conduite). The project proposes to develop a system that takes into account information from the environment surrounding the vehicle (e.g., cartographic information, contact forces tire/road ...) to evaluate the dynamic behavior of the vehicle and its relevant impact, as well as alert the driver of potential risk in future instant. The project is assisted by the development of risk prediction and curve speed warning systems presented in this work.

The latest European Project VERVE (Novel Vehicle Dynamics Control Technique for Enhancing Active Safety and Range Extension of Intelligent Electric Vehicles) presents an international joint research project between UTC in Compiègne (Picardie, France) and UT Ilmenau (Thuringia, Germany). Its global scientific objective is to develop a new concept of "Intelligent Electric Vehicles (IEV)", and the development of intelligent and environmentally safe new transportation systems in Thuringia and Picardie regions. One task related to this work is prototyping of an IEV concept with demonstration of intelligent functions of active safety. In addition, a collaboration experimental test at CERAM in France was performed for experimental validation from both sides. In particular, we have published a joint international article [Wang 2013] under the frame of this project.

The overall experimental validation relies on both simulator and experimental vehicle. Certain theoretical tests are performed by using Simulator CALLAS/PROSPER 4.3 and SCANeR Studio 1.2 software developed by OKTAL society. The experimental vehicle is fully developed by our laboratory Heudiasyc. The equipped sensors and in-vehicle system conduct to vehicle dynamics research and real-time application test.

In this work, Matlab environment is used for theoretical development and off-line validation. Real-time applications are implemented in C++ language combining with Qt cross-platform development framework.

## 1.4 Thesis structure

The remainder of this dissertation is divided into four principal parts. The organization structure is elucidated as follows:

### *State of the art review concerning vehicle and tire model, observer technique*

- **Chapter 2: State of the art** principally denotes a review of the vehicle and tire theory. We first present some applied road safety systems. Afterwards, we present pneumatic tire/road interaction characteristics. Primarily, we analyze the vertical load at each tire in three cases: level road, inclined road and banked road. Concerning lateral tire force, the well-known tire model Magic tire model and Dugoff tire model are compared with its own features. Then the vehicle model concerning vertical, longitudinal and lateral axes is introduced. The classic bicycle and four wheel vehicle model are explained as the main modeling in longitudinal and lateral dynamics. Some road-traffic risk assessment methods are reviewed at the end of this chapter.
- **Chapter 3: Observer theory** introduces the principal observer design concept that includes linear/nonlinear system and the observability for each type of system. The Kalman

filter is presented to provide an effective solution for the estimate of linear system, otherwise Extended Kalman filter and Particle filter techniques are respectively elucidated in this chapter for the solution of nonlinear systems.

#### *Vehicle vertical and lateral dynamics estimation*

- **Chapter 4: Vehicle vertical dynamics estimation** firstly validates the existing model developed with an assumption of zero bank angle and analyzes its limitation on banked road. Some parameters e.g. accelerometer and gyrometer outputs need to be reconstructed. In particular, two new vertical force models are proposed with theoretical physical derivation. The Kalman filter is intervened for estimating vertical force instead of open-loop calculation. Finally, we compare the performance of the developed algorithm through some simulation tests.
- **Chapter 5: Vehicle lateral dynamics estimation** focuses on the description of the vehicle lateral dynamics estimation. The double track vehicle model is applied to describe the dynamics parameters, while Dugoff tire model combined with the dynamics tire force relation is adopted in the construction of the tire force. Two nonlinear observers with respect to Extended Kalman filter and Particle filter techniques are complemented as a real-time application. The developed algorithms are validated with real-time acquisition data in real environment.

#### *Risk prediction and curve speed warning*

- **Chapter 6: Prediction system for curve negotiation** explores a hot issue about the risk prediction. Some existing method of risk prediction is presented at the beginning of this section. The forecast method of vehicle dynamics state in the future instant is presented in this section. We also highlight our developed method for predicting the potential risk and denoting the curve warning speed before entering the approaching curve. In the end, the evaluation of the risk occurrence and safe curve speed is validated by using simulated data.

#### *Experimental validation of real-time application*

- **Chapter 7: Implementation of embedded system and experimental validation** gathers the spotlight on the experimental performance of the previous developments. On-board sensors, acquisition system as well as application modules concerning vehicle dynamics parameter estimation, evaluation of potential risk and advisory speed on curves are respectively elaborated in this section. The combined system architecture is validated through real-time experimental test in professional test track and open-road.



# State of the art

---

## Contents

---

<b>2.1</b>	<b>Introduction</b>	<b>7</b>
<b>2.2</b>	<b>Road safety and safe system approach</b>	<b>8</b>
2.2.1	Electronic Stability Control	9
2.2.2	Active Rollover Prevention	11
<b>2.3</b>	<b>Tire model</b>	<b>12</b>
2.3.1	Basic tire characteristics	12
2.3.2	Tire axis frame and terminology	13
2.3.3	Tire forces and moments	14
2.3.4	Steady-state tire model	18
2.3.5	Wheel ground vertical contact forces	25
<b>2.4</b>	<b>Vehicle model</b>	<b>28</b>
2.4.1	Vehicle vertical dynamics model	29
2.4.2	Vehicle longitudinal and lateral dynamics model	31
<b>2.5</b>	<b>Road-traffic risk assessment</b>	<b>35</b>
2.5.1	Excessive driving speed	36
2.5.2	Time to collision	37
2.5.3	Lateral load transfer	38
2.5.4	Lateral acceleration appraisal	39
2.5.5	Vehicle yaw stability	39
2.5.6	Lane departure indicator	39
<b>2.6</b>	<b>Conclusion</b>	<b>40</b>

---

## 2.1 Introduction

In the past decade, vehicle is fully developed by the industrial enterprises and plenty of research and development organizations. Mechanical, electronic and concept design elements are part of the vehicle components. Vehicle structure can be principally divided into three parts: vehicle body, suspensions and tire. All these elements should be considered under the concept of the vehicle dynamics. Recently, some electronic and control systems like ABS, ESP and TCS are equipped in the modern automobiles to avoid the road accidents which are caused by losing of the vehicle control. With these implementations of the advanced driving assistant system, the road safety is obviously improved. These safety systems or any other vehicle stability control systems need accurate dynamics information about the vehicle motion, such as vehicle velocity,

steering wheel angle, acceleration, which are measurable by cheap sensors and accessible on the CAN bus. Actually, as the development of the advanced stability control system (ASCS), some parameters needed for a precise description for the motion of the vehicle, which are inputs for these ASCS, are not available by the current standard production cars due to the reason of the technical limit and cost-effective. Besides, we need to make clear that the dynamics of ground vehicles is often described in terms of performance, handling, and ride. The term handling is often used interchangeably to turning or directional response [Thomas 1997]. The performance of a vehicle is the response to imposed longitudinal forces under acceleration or braking and lateral forces in cornering. Thus, it is necessary to develop a complete understanding of the behavior of tires, characterized by the forces and moments which are generated by the driver command.

Actually, vehicle dynamics has been widely developed for a hundred years, the understanding can be principally divided into two levels: the empirical and the analytical cognition. The empirical understanding is based on plenty of driver trails, it did not include the mechanistic analysis in vehicle design. Therefore, it is limited to the existed experiences, it may lead to hazardous results which are influenced by new unknown factors. Due to the aforementioned reasons, vehicle engineers and researches prefer the analytical approach, which is based on the known laws of physics model. These models can be presented by algebraic or differential equations that give a detailed illustration of the relationship between the tire forces or vehicle motion as well as tire or vehicle physical properties. However, the analytical approach is limited to the mathematical problem. The existence of large numbers of components, subsystems and especially nonlinearity made comprehensive modeling impossible. Thus, we need to simplify the vehicle modeling with the reasonable assumption in order to find the mathematical solutions and satisfy our requirement of computational power.

Many references concentrate on this issue. We can refer to [Rajamani 2012] [Thomas 1997] [Schiehlen 2009] [Popp 2010] [Kiencke 2005] [Milliken 2003] [Reza 2007] and [Wong 2008]. This chapter briefly presents some developed advanced safety applications and vehicle dynamics theory. The section of vehicle model and tire model mainly furnishes a review of the several propositions of the vehicle modeling, and several well-known tire models are introduced respectively based on physical theory model and empirical model. Some concepts of the road-traffic risk assessment are also explained in the final part of this chapter.

## 2.2 Road safety and safe system approach

Road safety is an essential discussion issue on the vehicle development. The ratio of the cost of traffic unsafety compared to the economical and societal cost of traffic congestion is very high [Louwerse 2004]. Some approaches are chosen to improve the road safety, ADAS (Advanced Driver Assistance System) can be considered as an effective and low-cost method to avoid the potential accidents. Figure 2.1 represents a catalog of ADAS applied in accident prevention and collision avoidance.

These systems are structured around some risk estimation methodologies based on probabilistic or deterministic functions, which are defined by previous theoretical and experimental test. These estimation functions can provide a potential hazard probability of car accident at certain moments or situations. When the risk index exceeds to a defined threshold, some alarms such as signal light or buzzer will be activated to inform the driver about the nature of his driving behavior. Some active safety systems can directly change the vehicle dynamics state,

## Advanced Driver Assistance System

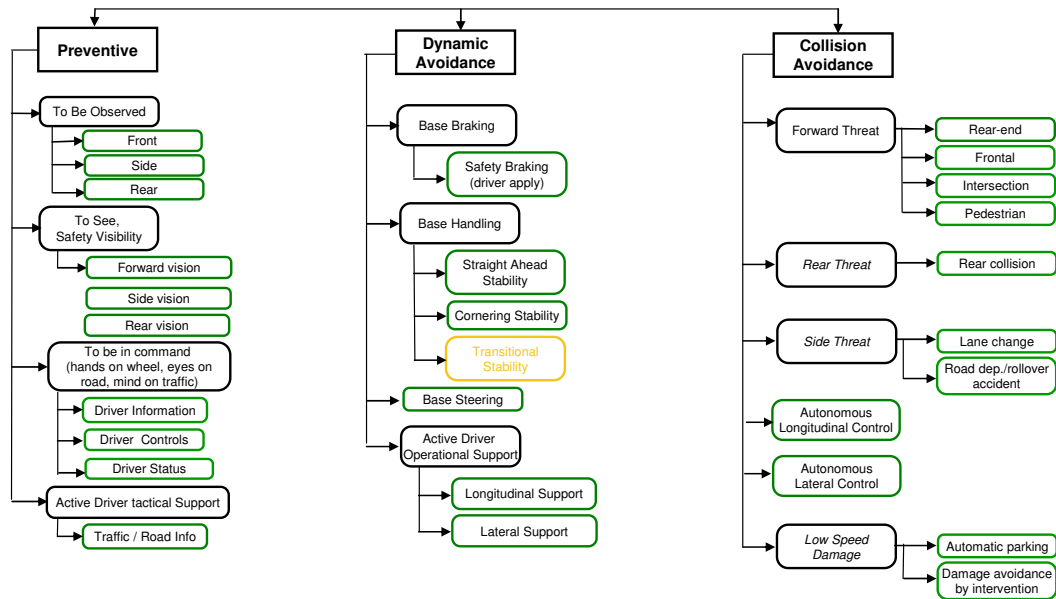


Figure 2.1: The catalogue of Advanced Driver Assistance System [Gunia 2008]

with the intervention of the ECU command on the integrated actuator to give better control during critical situation.

As mentioned above, the high number of accidents and the fact that, human errors are the fundamental source of many of them, resulting in the motivation of developing active safety control systems. A variety of driver assistance systems such as electronic stability control (ESC), traction control system (TCS), rollover prevention, lane departure warning (LDW) systems, collision avoidance systems, and adaptive cruise control (ACC) are being developed to reduce driver burden, partially automate normal driving operations, and reduce accidents [Phanomchoeng 2011]. Typical systems, focused on the lateral skid and rollover, are discussed in the next subsections.

### 2.2.1 Electronic Stability Control

Electronic Stability Control (ESC) is an active safety system that has been developed and commercialized by many automotive manufacturers to effectively prevent vehicles from spinning, drifting out, and rolling over, particularly at the limits where the vehicle may lose control. Based on the system components, it is also called by other names such as Vehicle Stability Control (VSC), Electronic Stability Program (ESP), Dynamic Stability Control, Porsche Stability Management (PSM) under different marketing.

The ESC is defined as a system that has all of the following attributes [NHTSA 2006] [ZANTEN 2000]:

- Adjust the vehicle brakes individually to induce correcting yaw torques to the chassis in order to augment vehicle stability.

- Use a close-loop algorithm to limit understeer and oversteer of the vehicle when appropriate, it is applied as a computer-controlled system (see Figure 2.2).
- Estimate vehicle yaw rate and its sideslip. Yaw rate means the rate of change of the vehicle's heading angle about a vertical axis through the vehicle center of gravity. Sideslip is the arctangent of the ratio of the lateral velocity to the longitudinal velocity of the center of gravity.
- It is able to monitor driver steering input.
- It is operational over the full speed range of the vehicle.

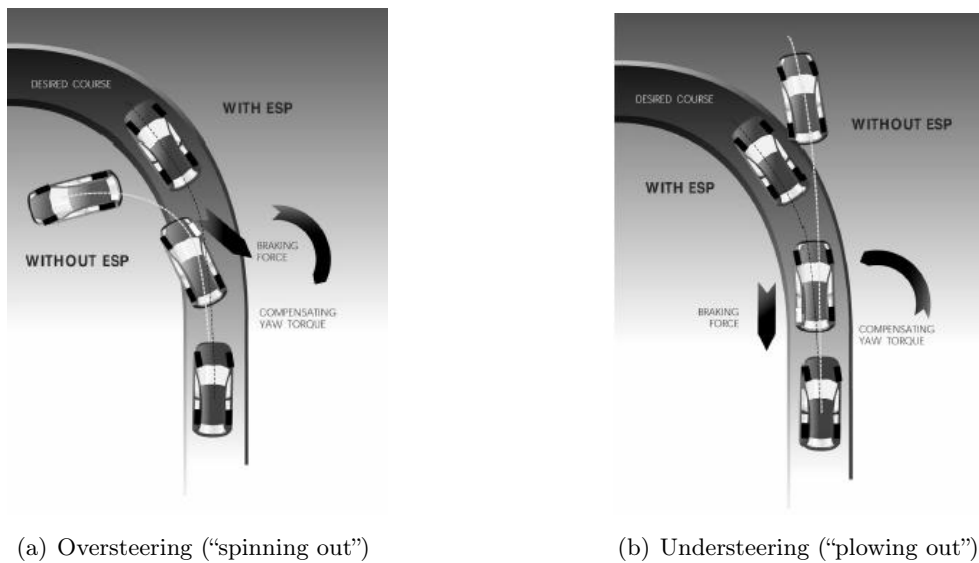


Figure 2.2: ESC interventions for understeering and oversteering [NHTSA 2006]

The basic principle control theory of ESC is considered as the yaw stability control, which employs state feedback control strategy. It can determine the driver's intended heading, measure the vehicle response actual and turn the vehicle if the vehicle's reaction does not match the driver's intend.

When the ESC system detects an imbalance between the measured yaw rate of a vehicle and the path defined by its speed and lateral acceleration (as measured by the steering angle), it automatically intervenes to turn the vehicle. The automatic turning of the vehicle is accomplished by counter torques from the brake system at each tire rather than by steering wheel input. If only one wheel is braked, the uneven brake force will cause the vehicle's heading to change. Figure 2.2 shows the action of ESC using single wheel braking to correct the effect of oversteering or understeering.

Figure 2.2(a) shows the oversteering situation, the vehicle enters a left curve with an extreme travelling speed, the rear of the vehicle begins to slide which would lead to a non-ESC vehicle turning sideways. On the contrary, if the vehicle is equipped with ESC, the system is able to detect the vehicle heading is changing with a steering angle greater than the driver's intended input from steering wheel. ESC can intervene quickly and smoothly, and thus most of the time will go undetected by the drivers, it applies the right front brake to turn the heading of the vehicle back to the correct path.

Market group	n licensed vehicles	Overall n crash	Overall crash rate*	Multi-vehicle crash rate*	Rollover crash rate*	Injury rate per vehicle
Overall	2,995,906	23,826	0.80%	0.48%	0.06%	1.15%
4WD Compact	91,345	640	0.70%	0.44%	0.07%	0.99%
4WD Large	53,462	304	0.57%	0.35%	0.06%	0.83%
4WD Medium	137,530	940	0.68%	0.41%	0.12%	1.02%
Large	261,572	2,041	0.78%	0.46%	0.04%	1.13%
Light	150,655	1,237	0.82%	0.50%	0.05%	1.14%
Luxury	177,151	1,298	0.73%	0.45%	0.04%	1.03%
Medium	467,273	4,003	0.86%	0.51%	0.05%	1.25%
People Mover	70,545	592	0.84%	0.54%	0.05%	1.32%
Small	649,779	5,910	0.91%	0.56%	0.06%	1.30%
Sport	115,690	1,136	0.98%	0.58%	0.07%	1.43%
Van/Ute	252,791	1,854	0.73%	0.43%	0.10%	1.07%
Unknown	568,113	3,871	0.68%	0.42%	0.05%	1.00%

\*Rates are per licensed vehicle

Figure 2.3: Number of currently licensed passenger cars and vans analyzed (n) and number matched to crash data

Figure 2.2(b) shows the understeering situation, the vehicle enters a similar situation. If the road has a small friction coefficient or the vehicle speed is too fast, it reaches the limits of road friction. Then the vehicle would not be able to follow the nominal trajectory required by the driver. Under this condition, ESC can rapidly detect that the vehicle's heading is changing less quickly than the driver's intention. It applies the left rear brake to turn the heading of the vehicle back to the correct path which is similar to the above oversteering situation.

Agency study showed that ESC can effectively reduce single-vehicle crashes by 34% for cars and 59% for SUV (Sport Utility Vehicle). The Insurance Institute for Highway Safety estimates that ESC reduces the risk of fatal single-vehicle wrecks by 56% and fatal multiple-vehicle crashes by 32% [NHTSA 2006] [ZANTEN 2000]. Because of its proven effectiveness, the US government has mandated that all new cars must be equipped with ESC by the 2012 model year.

### 2.2.2 Active Rollover Prevention

As far as we know, rollover is another fatal accident according to the statistical accident report. Figure 2.3 illustrates the percentage of overall crash, multi-vehicle crash and particularly rollover crash. From this table, we can find that Medium 4WD had the highest rollover rate (0.12%), followed by the Vans/utilities (0.10%) [Keall 2007].

Theoretically, the vertical force generates a large enough moment around the vehicle longitudinal axis for an instant, the lateral load transfer from one side to other side leads to the rollover occurrence.

However, in a real situation, the critical lateral forces are generated under some different special conditions. They can be defined as tripped rollover and un-tripped rollover. This so called tripped rollover is due to the vehicle gets in contact with a mechanical obstacle like curb or guardrail from external input. The sudden bounce yields a large roll moment after a driver lost control over the vehicle. On the other hand, an un-tripped rollover happens because severe steering maneuvers generate a high lateral acceleration during emergence situations

[Liebemann 2004].

Active roll prevention is aimed at improving the vehicle stability from un-tripped rollover at emergence situation. Several automotive manufacturers have been trying to find a better available solution, the significant method is to reduce the vehicle velocity and yaw rate from the braking system [Phanomchoeng 2011]. Besides above mentioned ESC, Active Roll Control and Electronic Damper Control can be used as well to ameliorate vehicle stability and avoid critical situations.

Bosch has developed Rollover Mitigation Functions (RMF) indirectly help to reduce the rollover risk. The system is based on the standard ESP sensor settings and provides a scalable structure concerning the determination of rollover critical situations and brake/engine control (Figure 2.4).

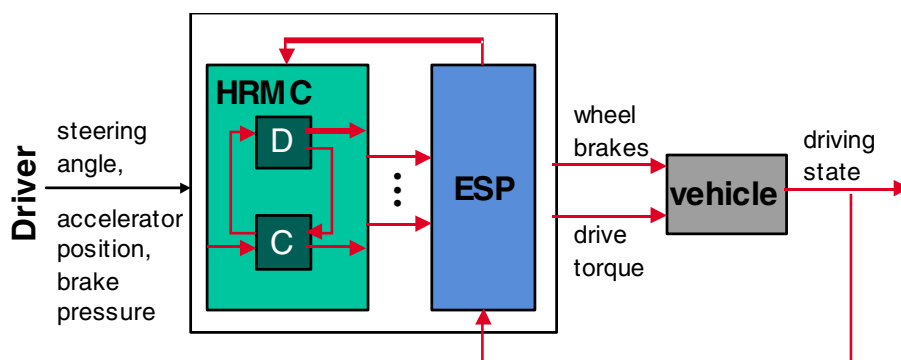


Figure 2.4: Integration of the basic Electronic Stability Program ESP and the Hybrid Rollover Mitigation Controller(HRMC) in the structure of the entire vehicle stabilizing system from Bosch [Liebemann 2004]

## 2.3 Tire model

Firstly, the essential vehicle component pneumatic tire is presented in this section. A tire is a complex technical component of current passenger cars as well as the trucks. Their characteristics are of crucial importance for the dynamic behavior of the road vehicle, it has to cushion, dampen, assure good directional stability, and provide long-term service. The most important capability is to guarantee optimal and reliable road holding quality under strong tire/road contact longitudinal and lateral forces during braking, accelerating and cornering maneuvers in particular the road condition is with low friction such as wet and ice road surface.

In this section, we will present some tire basic characteristics like tire forces and moments that influence vehicle handling as well as the effects of various shape factors of tire characteristics. Two typical tire models: theory model and empirical model will be respectively introduced by the physical and mathematical expressions.

### 2.3.1 Basic tire characteristics

Pneumatic tire is an advanced engineering product composed of rubber and a series of synthetic materials. Generally, it consists of body plies, bead bundle, belts, sidewalls and tire inner liner

(combined with fiber, textile, and steel cords), these components have different functions for providing strength to stay seated, supporting the tension forces generated by tire air pressure and generating forces for turning and going forward. The mentioned interior components are illustrated in Figure 2.5 which gives an exploded view of the apparatus [Reza 2007].

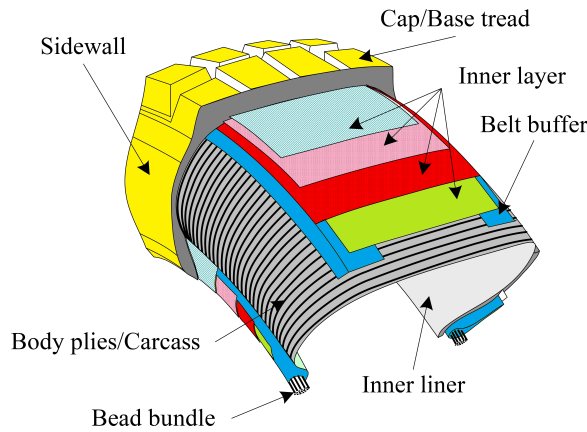


Figure 2.5: The exploded view of sample radial tire interior components

### 2.3.2 Tire axis frame and terminology

SAE has defined the axis system to denote a precise description of the operation conditions, forces and moments experienced by a tire in [SAE 2008]. The axis system is illustrated in Figure 2.6 which includes tire technical terminologies.

The X-axis is defined by the intersection of the wheel plane and the road plane with the positive forward direction. The Y-axis is parallel to the road plane and right-hand. The Z-axis is perpendicular to the road plane with a positive direction upward. For the following presentation of tire model, some major parameter definitions are itemized, the tire moments should be distinguished with the above vehicle moments.

- Wheel plane: Central plane of the tire normal to the axis of rotation.
- Slip angle: Slip angle is the angular difference between the direction of tire contact patch with the road is pointing and the direction of the wheel. Positive slip angle delegates right orientation as it moves in the forward direction.
- Camber angle: Camber angle is the measurement in degrees of the difference between wheel vertical alignment perpendicular to the surface. Positive camber angle corresponds to the top of the tire leaned outward from the vehicle.
- Loaded Radius: The distance between wheel center and the tire contact center of the road plane. The effective tire radius relates the rotational angular velocity of the wheel and the linear longitudinal velocity.
- Longitudinal force: The force acting on the tire which is in the plane of the road and parallel to the intersection of the wheel plane with the road plane.

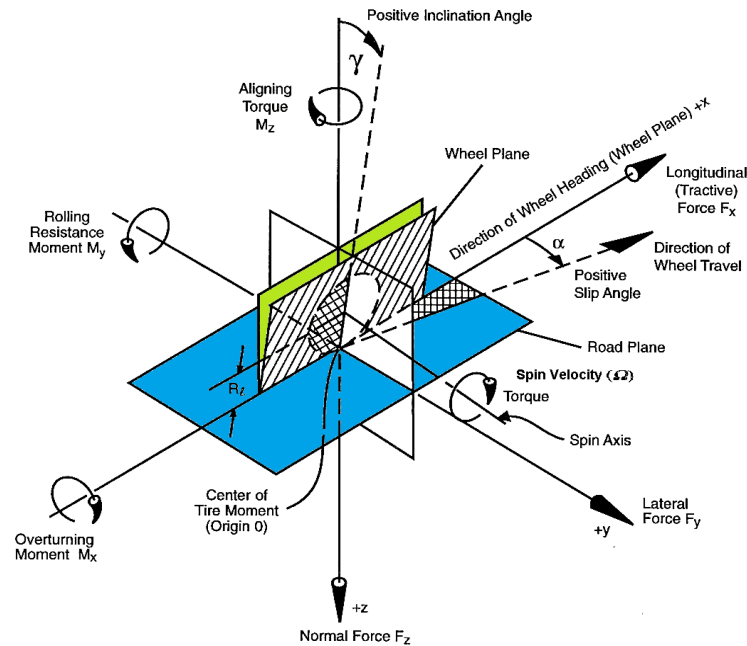


Figure 2.6: SAE tire axis coordinate frame [Smith 2004]

- Lateral force: The force acting on the tire which is in the plane of the road and orthogonal to the intersection of the wheel plane with the road plane.
- Vertical force: The force acting on the tire which is perpendicular to the plane of the road.
- Overturning moment: The moment acting on the tire which is in the plane of the road and parallel to the intersection of the wheel plane and the road plane.
- Rolling resistance moment: The moment acting on the tire which is perpendicular to the plane of the road.
- Aligning moment: The moment acting on the tire which is parallel to the plane of the road.

### 2.3.3 Tire forces and moments

Tires could be considered as a physical system with input and output. Actually, the vertical force also called wheel load  $F_z$  is one of the inputs of the force generator, sideslip  $\alpha$ , longitudinal slip  $s$ , and the camber angle  $\gamma$  are also the components of the input variables. The major outputs are longitudinal force  $F_x$  and lateral force  $F_y$  and three minor outputs: overturning moment  $M_x$ , rolling resistance moment  $M_y$  and aligning moment  $M_z$ . Therefore, this section focuses on the presentation of the relationship model of input and output variables.

#### 2.3.3.1 Longitudinal force and slip ratio

During vehicle accelerating and braking, the deformation of the rubber elements in the tire tread brings an additional slip in order that the tire deflects to develop and sustain the friction force.

In [Thomas 1997], the author explains clearly the reason of the generation of longitudinal force resulted by the deflection of the tire tread elements. As the tread element proceeds back through the contact patch, its deflection builds up concurrently with vertical load and it develops even more friction force. However, when the tread element first enters the contact patch and approaches the rear of the contact patch, they can respectively bend to sustain a force and drop off the friction force until zero as it leaves the road.

Therefore, the accelerating and braking forces are generated by producing a differential between the tire rotational velocity ( $\omega$ ) and longitudinal velocity ( $V_{\omega x}$ ). The essential factor is the production of slip in the contact patch. Slip is defined non-dimensionally, which is defined as:

$$\begin{cases} s(\%) = \left(\frac{r\omega}{V_{\omega x}} - 1\right) \times 100 & \text{accelerating} \\ s(\%) = \left(\frac{r\omega}{V_{\omega x}} - 1\right) \times 100 & \text{braking} \end{cases} \quad (2.1)$$

where  $r$  is the unloaded radius. The slip ratio is positive for accelerating and is negative for braking. The longitudinal force is developed between the tire and the ground to accelerate or brake a vehicle, which is proportional to the vertical force:

$$F_x = F_z \mu_x(s) \quad (2.2)$$

We call  $\mu_x$  the longitudinal friction coefficient and the relationship respects to slip ratio  $s$  during a vehicle movement is given in Figure 2.7. As we can see from this figure, the friction coefficient  $\mu_x(s)$  is proportional to slip ratio  $s$  where the longitudinal slip ratio is small:

$$\mu_x(s) = C_s s \quad s < 0.1 \quad (2.3)$$

where  $C_s$  is called the longitudinal slip coefficient. However, the relation becomes nonlinear where the value  $s$  exceeds the peak value 0.1. The complete tire model that can describe nonlinear region will be discussed hereinafter.

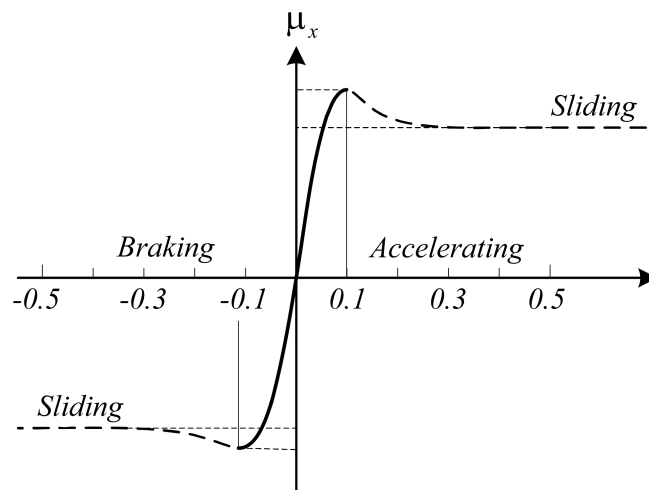


Figure 2.7: Relation between longitudinal friction coefficient and slip ratio

### 2.3.3.2 Lateral force and slip angle

Another essential function of the tire is to generate the lateral force to control the vehicle direction in negotiating the corner or changing the lane. These lateral forces are generated by lateral tire slip (slip angle  $\alpha$ ) and lateral inclination (camber angle  $\gamma$ ).

Slip angle plays an essential role in generating lateral force. The effect of slip angle is clarified in [Thomas 1997]. When a rolling pneumatic tire is subjected to lateral force, the tire will drift to the side. Currently, an angle is created between the direction of the tire contact patch and the direction of the wheel velocity. During a longitudinal movement, there is no lateral tire deflection from its normal position, therefore it sustains no lateral force. However, when the tire is actuated with the orientation angle different from its initial trajectory, the tread elements remain in the original contact position with the road. The intent of orientation change will deflect sideways with respect to the tire. Based on above phenomenon, lateral force builds up as the element moves rearward in the contact patch up to the point where the lateral force acting on the element overcomes the friction available and slip occurs. This mechanism is not an instant phenomenon of the time lags of deflecting the tire sidewalls in the lateral direction. The time lag phenomenon can be judged under low-speed steering angle change. As the steering angle changed, the distance for lateral deflection and force generation is often referred to relaxation length.

Slip angle  $\alpha$  is defined as the arc tangent of division of the lateral and the forward velocity of the wheel:

$$\alpha = \arctan\left(\frac{V_y}{|V_x|}\right) \quad (2.4)$$

The lateral force  $F_y$  is initially proportional to the tire slip angle which is similar to the definition of longitudinal force:

$$F_y = -C_\alpha \alpha \quad (2.5)$$

where  $C_\alpha$  is called the tire cornering stiffness, which is calculated by:

$$C_\alpha = -\lim_{\alpha \rightarrow 0} \frac{\partial(F_y)}{\partial \alpha} \quad (2.6)$$

Figure 2.8 illustrates the relation between lateral force and tire slip angle. As we discussed above, when the slip angle is 0, the correspondent lateral force is 0. It is usually used to analyze the vehicle lateral dynamics and stability behavior in the linear region of the lateral force curve. The curve slope at small slip angle can be considered as the value of cornering stiffness. As the slip angle grows, the lateral force reaches to the maximum where the lateral force is equal to the product of friction coefficient  $\mu$  and the wheel vertical load  $F_z$ , we call this region as a force saturation. It approaches the behavior of loss of the vehicle control at large slip angle, which means that the wheel is approximately locked, the steering input cannot any more affect the lateral dynamics.

Usually, tire characteristic is discussed only in the steady state. The tire model presented in the subsequent section is entirely under the steady state.

### 2.3.3.3 Vertical force

The load on each wheel give basic vehicle data and operating conditions. The load on each wheel are extremely important in determining a car's maximum steady-state cornering capability. The vehicle performance highly depends on the wheel loads. In the real situation the vertical loads

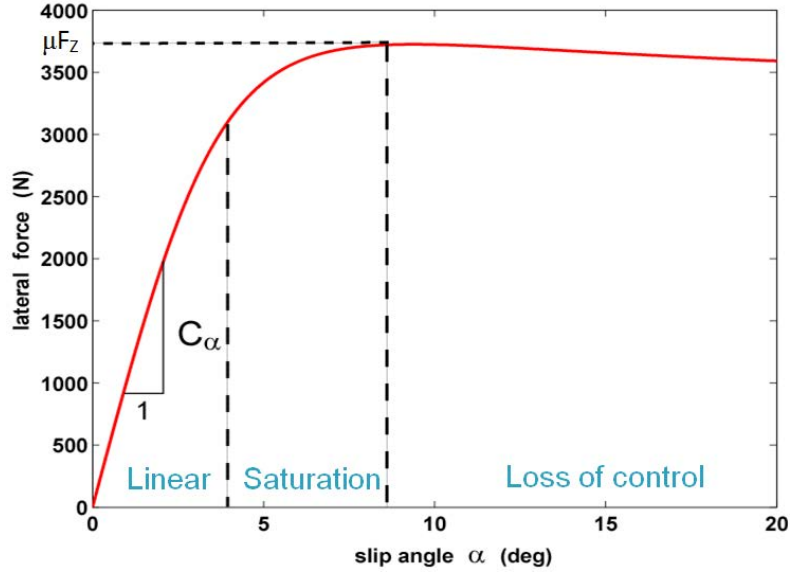


Figure 2.8: Relation between lateral force and slip angle [Hsu 2007]

at each tire is continually changing, when the vehicle accelerates or brakes, the load can be transferred from rear to front tires or reverse. Similarly, as the vehicle turns or changes the lane, the force can transfer from right side to left side or reverse. All the calculations presented are based on the assumption that the vehicle chassis is rigid. The hypothesis makes the model will not be adapted from the flexible model, the calculation will not be accurate. The simple vertical force model can be derived from the statics analysis. The road geometry is generally divided into three cases:

- **Case 1: Vehicle on a level road**

As the car parked on a level road (see Figure 2.16), we assume that the vehicle is rigid and is modeled as a two-axis vehicle. The vertical force can be calculated on front and rear tires as:

$$\begin{aligned} F_{z1} &= \frac{1}{2}mg \frac{L_2}{L} \\ F_{z2} &= \frac{1}{2}mg \frac{L_1}{L} \end{aligned} \quad (2.7)$$

where  $L$  is the wheel base,  $L = L_1 + L_2$ .

- **Case 2: Vehicle on a inclined road**

When a car is on an inclined pavement, the vertical force under each tire is:

$$\begin{aligned} F_{z1} &= \frac{1}{2}mg \frac{L_2}{L} \cos(\phi_r) - \frac{1}{2}mg \frac{h}{L} \sin(\phi_r) \\ F_{z2} &= \frac{1}{2}mg \frac{L_1}{L} \cos(\phi_r) + \frac{1}{2}mg \frac{h}{L} \sin(\phi_r) \end{aligned} \quad (2.8)$$

where  $\phi_r$  is the road inclined angle with respects to the horizontal road,  $h$  is the height of center of gravity.

- **Case 3: Vehicle on a banked road**

A banked road changes the wheel load distribution, the load acting on the lower tires increases, and the load on the upper tires decreases (see Figure 2.17).

$$\begin{aligned} F_{zl} &= \frac{1}{2}mg \frac{E_2}{E} \cos(\theta_r) - \frac{1}{2}mg \frac{h}{E} \sin(\theta_r) \\ F_{zr} &= \frac{1}{2}mg \frac{E_1}{E} \cos(\theta_r) + \frac{1}{2}mg \frac{h}{E} \sin(\theta_r) \end{aligned} \quad (2.9)$$

where  $F_{zl}$  and  $F_{zr}$  respectively represent the vertical force on the left and right side.  $E$  is the vehicle's track that contains the semi-track  $E_1$  and  $E_2$ .  $\theta_r$  stands for the road bank angle.

It is noted that all the presented vertical force model is under the statics situation, however kinematic motion contains longitudinal and lateral acceleration changing the dynamic behavior of the vehicle. This fact is considered by the vertical model in the subsequent section.

### 2.3.4 Steady-state tire model

For vehicle dynamics, tire is one of the most important factors that charge the vehicle's behavior. It plays an essential role in connecting vehicle chassis and road in order to transmit longitudinal, lateral and vertical forces. To give a clear description about tire characteristics and analyzing the effect on certain driving situations, several tire modelings have been proposed during these last decades. These models describe the physical characteristic of tires so that they can be analyzed and evaluated in a mathematical way. Among all the works that have been done in this field, we identify a first class of models based on the physical complex tire model that gives an overall description of tire dynamics state, and a second class based on simplistic expressions obtained by plenty of experimental tests and summarized by empirical way, and a recently third class which is based on advanced finite-element methods that predict the important states at any point of the tire. The initial tire model could be traced in the 1940's by the vehicle and aircraft industry, nowadays for most of the developed system, the empirical equation structures that could be not only easily adjusted to fit the measurements from the tire tests increased due to the complex nature of the tire, but also availably reduce the complexity of calculation are adopted instead of the descriptions of the tire characteristics were derived from physical modeling. In addition, large amount of computer power enables the possibility to solve the physical differential equations related to the tire deformation that focus on the dynamical aspects of the tire behavior.

In our research, all the models intervened are with the steady-state relation. The tire steady-state model describes the tire sliding and sideslip properties in the tire steady motion process. The steady-state model can be divided into theoretical model, the semi-empirical model and the empirical model in Figure 2.9. In this section, we will present mostly used linear model and Dugoff model for the theoretical model and the Magic tire model for semi-empirical model. The performance of each model will be compared.

#### 2.3.4.1 Linear model

The tire model description could be commenced by the most simple tire model. As we have presented in the section of tire force and moment, when the slip ratio and slip angle is small, the force is approximately proportional to these variables. The dynamic properties of the tire are

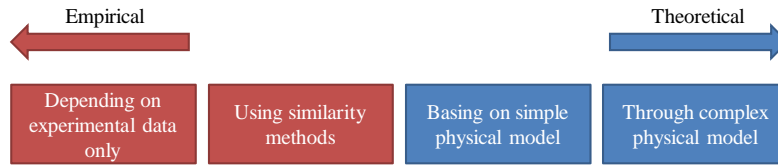


Figure 2.9: Classification of tire models

analytically derived as functions of the slip, slip angle, normal force, and road friction coefficient, so we can easily get the linear relation to the longitudinal force:

$$\begin{aligned} F_{x1} &= C_{s1}s_1 \\ F_{x2} &= C_{s2}s_2 \end{aligned} \quad (2.10)$$

where  $C_{s1}$  and  $C_{s2}$  respectively represent the longitudinal tire stiffness that are depended on the wheel load and the tire-road friction. For the lateral force:

$$\begin{aligned} F_{y1} &= C_{\alpha1}\alpha_1 = C_{\alpha1}(\delta - \theta_{v1}) \\ F_{y2} &= C_{\alpha2}\alpha_2 = C_{\alpha2}(-\theta_{v2}) \end{aligned} \quad (2.11)$$

where we call the  $C_{\alpha1}$  and  $C_{\alpha2}$  lateral cornering stiffness,  $\delta$  is the steering wheel angle,  $\theta_{v1}$  and  $\theta_{v2}$  are the angle between the front/rear wheel velocity vector and the vehicle longitudinal velocity. The linear model is limited by the region of force saturation, where the relation of the slip angle and force is nonlinear (Figure 2.8). The analysis of this nonlinear region is fundamental to describe more precisely the tire dynamics characteristics. This nonlinear region is taken into account in the Dugoff model, presented in the next section.

### 2.3.4.2 Dugoff tire model

The tire model with steady-state relation between slip and generated force were physically derived from variants of the brush model. Some typical brush models had been discussed based on different assumptions since a long time. However the common point among these models is that the polynomial expression should include at least two parameters: the cornering stiffness and friction coefficient. Usually, there are three models referred to as the HSRI-models developed at the Highway Safety Research Institute (US), one of them is the Dugoff tire model. The Dugoff tire model is proposed by providing a method for calculation of forces under combined lateral and longitudinal tire force generation in [Dugoff 1969]. It assumes a uniform vertical pressure distribution on the tire contact patch.

Compared with other tire models, the advantage of the Dugoff model is listed as follows:

- The Dugoff tire model presents the nonlinear dynamics and combined-slip forces.
- Independent values of tire stiffness in the lateral and longitudinal directions.
- Advantage of being an analytically derived model developed from force balance calculations.
- Lateral and longitudinal forces are directly related to the tire road friction coefficient in more transparent equations.

Hence, it is widely used when the tire forces are intervened in the vehicle control or estimation system. In extensive literatures such as [Zhang 1998] [Dakhlallah 2008] [Boyden 1994] [Smith 1995], the Dugoff model is adopted for its simplicity and efficiency. The Dugoff tire model can certainly also be used for calculation of lateral and longitudinal forces, either for pure-slip or combined-slip conditions [Ding 2010]. The tire model is elaborated by the formulas:

The longitudinal force:

$$F_x = C_s \frac{s}{1+s} f(\lambda) \quad (2.12)$$

the lateral force is given as:

$$F_y = C_\alpha \frac{\alpha}{1+\alpha} f(\lambda) \quad (2.13)$$

where  $s$  and  $\alpha$  are respectively the longitudinal slip ratio and slip angle.  $f(\lambda)$  can be expanded as:

$$f(\lambda) = \begin{cases} \lambda(2-\lambda) & \lambda \leq 1 \\ \lambda & \lambda > 1 \end{cases} \quad (2.14)$$

where

$$\lambda = \frac{\mu F_z (1+s)}{2\sqrt{(C_s s)^2 + (C_\alpha \tan(\alpha))^2}} \quad (2.15)$$

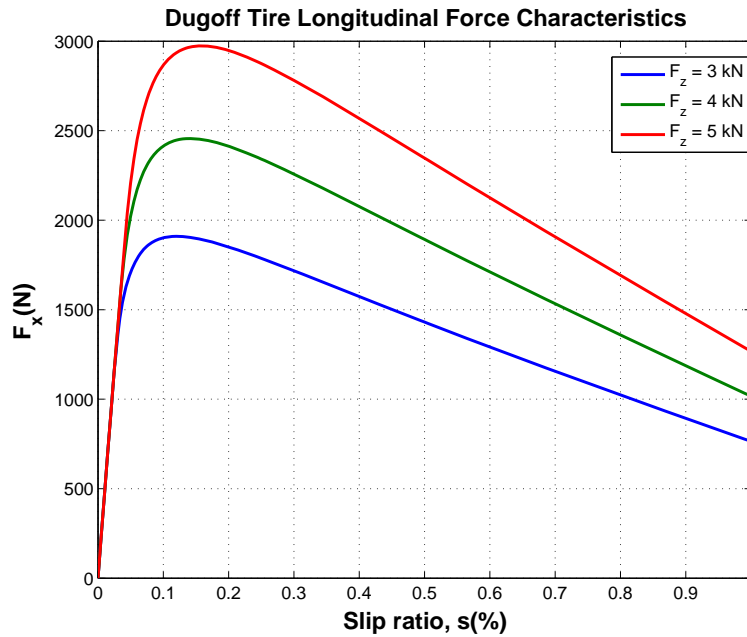


Figure 2.10: Dugoff longitudinal force model characteristics

From these formulas, we can conclude that all the tire properties are synthesized into two parameters: the longitudinal stiffness  $C_s$  and lateral stiffness  $C_\alpha$ . The friction coefficient  $\mu$  is assumed to be constant in this model, which disables its ability to also characterize the longitudinal force accurately for longitudinal slips. The performance of the Dugoff model is represented in Figure 2.10 and 2.11. However, one of its drawbacks is the inaccuracy at large slip ratios, and this will be explained using a pure-slip condition.

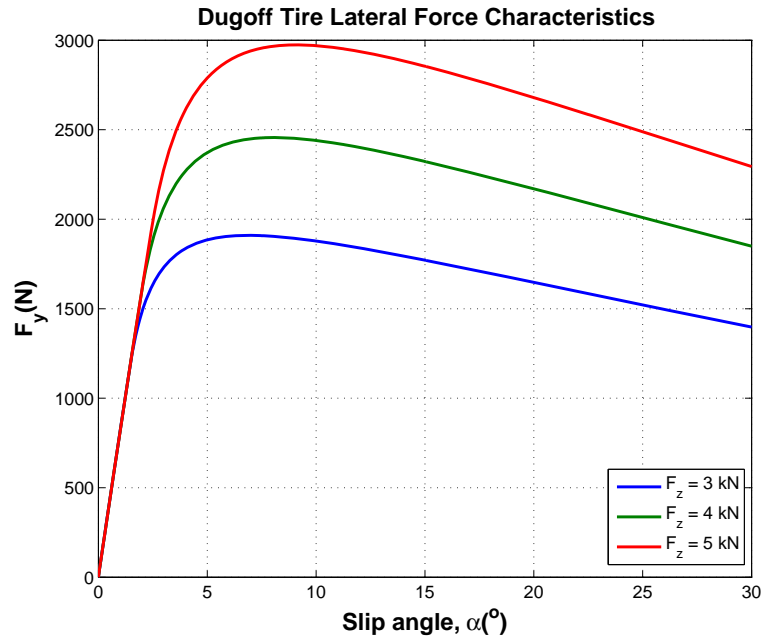


Figure 2.11: Dugoff lateral force model characteristics

Actually, the longitudinal and lateral forces are coupled, hence the longitudinal force can affect the lateral force generated in the contact patch. It is noted that the Dugoff model generates lateral forces with positive slopes in the large slip angles region. Therefore, we introduce the Magic tire model which has slight negative slopes in the nonlinear region [Ding 2010] [Jacob 2007].

### 2.3.4.3 Magic tire model

Following with the preceding section that the tire and moment generations are based on the physical tire model, this subsection will deal with the model that is designed especially with empirical summary. Pacejka firstly proposes the semi-empirical model in [Pacejka 1987] in 1987. This model is termed “semi-empirical” due to the fact that its formulations are not derived from a physical tire model but rather are mathematical approximations of curve that were explored in experiments. In spite of several mathematical functions intervene in the construction in order to describe the characteristic of the cornering force, the explored experimental equations are always restricted to the steady-state situations. Actually, the mathematical representations of longitudinal force and aligning moment were included in the empirical description, in this way, the formulas can be proved suitable in terms of the accuracy requirement. The detailed model and expansion description can be found in [Pacejka 2006]. The development of the model was in a cooperative effort TU-Delft and Volvo for several versions.

The basic form of the formula that holds for given values of vertical load and camber angle is expressed as:

$$y = D \sin [C \arctan \{Bx - E (Bx - \arctan Bx)\}] \quad (2.16)$$

with

$$\begin{aligned} Y(X) &= y(x) + S_v \\ x &= X + S_h \end{aligned} \quad (2.17)$$

where the output  $Y$  represents the assemble of the variables: longitudinal force  $F_x$ , lateral force  $F_y$ , aligning moment  $M_z$  and the input  $X$  stands for the longitudinal slip ratio  $s$  and lateral slip angle  $\alpha$ . Hence, the expansion expression for each variable is listed as follows:

$$\begin{aligned} F_x(s + S_{hx}) &= D_x \sin [C_x \arctan \{B_x s - E_x (B_x s - \arctan B_x s)\}] + S_{vx} \\ F_y(\alpha + S_{hy}) &= D_y \sin [C_y \arctan \{B_y \alpha - E_y (B_y \alpha - \arctan B_y \alpha)\}] + S_{vy} \\ M_z(\alpha + S_{hz}) &= D_z \sin [C_z \arctan \{B_z \alpha - E_z (B_z \alpha - \arctan B_z \alpha)\}] + S_{vz} \end{aligned} \quad (2.18)$$

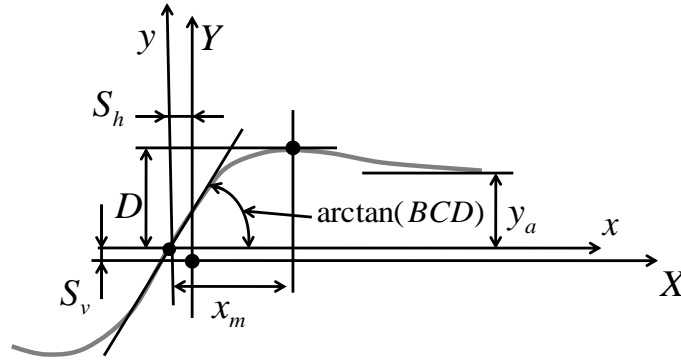


Figure 2.12: Magic formula factors

The alphabet in the formulas are explained by the following items:

- $B$ : the stiffness factor, which determines the slope at the origin.
- $C$ : the shape factor, which controls the limits of the range of the sine function and thereby determines the shape of the resulting curve.
- $D$ : the peak value, which respects to the central x-axis and for  $C \geq 1$ .
- $E$ : the curvature factor, which controls the curvature at the peak and at the same time the horizontal position of the peak.
- $S_h$ : the horizontal shift, which appears when the ply-steer and conicity effects and possibly the rolling resistance cause the  $F_y$  curves not to pass through the origin.
- $S_v$ : the vertical shift, which appears when the ply-steer and conicity effects and possibly the rolling resistance cause the  $F_x$  curves not to pass through the origin.
- $BCD$ : the product corresponds to the slope at the origin ( $x = y = 0$ ).

The longitudinal force with slip ratio is given as:

$$\begin{cases} C_x &= b_0, \\ D_x &= F_z(b_1 F_z + b_2), \\ B_x &= \frac{1}{C_x D_x} (b_3 F_z + b_4) F_z \exp(-b_5 F_z), \\ E_x &= (b_6 F_z^2 + b_7 F_z + b_8)(1 - b_9 \text{sign}(g_l + S_{hx})), \\ S_{hx} &= b_{10} F_z + b_{11}, \\ S_{vx} &= b_{12} F_z + b_{13}. \end{cases} \quad (2.19)$$

The lateral force with slip angle is given as:

$$\begin{cases} C_y &= a_0 \\ D_y &= F_z(a_1 F_z + a_2)(1 - a_3 \gamma^2), \\ B_y &= \frac{1}{C_y D_y} a_4 \sin(2 \arctan(\frac{F_z}{a_5}))(1 - a_6 \|\gamma\|), \\ E_y &= (a_7 F_z + a_8)(1 - (a_9 \gamma + a_{10} \text{sign}(\beta_r + S_{hy}))), \\ S_{hy} &= a_{11} F_z + a_{12} + a_{13} \gamma, \\ S_{vy} &= a_{14} F_z + a_{15} + \gamma(a_{16} F_z^2 + a_{17} F_z). \end{cases} \quad (2.20)$$

The aligning moment is given as:

$$\begin{cases} C_z &= c_0, \\ D_z &= F_z(c_1 F_z + c_2), \\ B_z &= -\frac{1}{C_z D_z} c_3 \|\gamma\| (c_4 F_z^2 + c_5 F_z) \exp(-c_6 F_z), \\ E_z &= -c_2 \|\gamma\| (c_7 F_z^2 + c_8 F_z + c_9), \\ S_{hz} &= c_{10} \gamma, \\ S_{vz} &= (c_{11} F_z^2 + c_{12} F_z) \|\gamma\|. \end{cases} \quad (2.21)$$

The parameters  $a_i$ ,  $b_i$  and  $c_i$  are considered constant in the formulas, which are assigned by the empirical values.  $\gamma$  is the camber angle which is able to lead to a considerable offset of the lateral force versus the slip angle curve. The empirical constants appeared are decided for the road conditions and surface (dry asphalt, ice road...) as well as the tire technical characteristics (pressure, tread...). The illustration of the Pacejka tire model for longitudinal force, lateral force and aligning moment is shown receptively in the following figures.

According to this tire modeling, longitudinal and lateral forces are represented in Figure 2.13 and 2.14, they are independent from each other. This description of the force is valid only when the solicitation is pure. To overcome this problem, other pneumatic models are introduced that provide the coupling of longitudinal and lateral motion. This model will allow us to properly represent the realistic behavior of the tire when solicitation is coupled.

The relation of aligning moment and slip angle is represented in Figure 2.15. Obviously, the aligning moment in the saturation region that is the analogy of Figure 2.8 shows that the aligning moment augments with the slip angle, but it converges to 0 where the slip angle is large. Therefore, it may be interesting to conscious the reason of the unexpected phenomenon at large angles. More complements of other factors' influences and model improvement are explained in [Pacejka 2006].

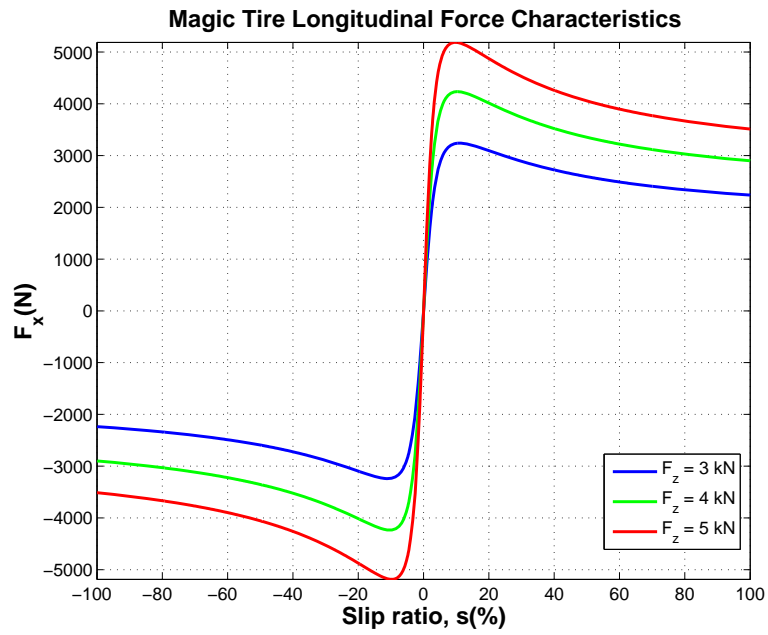


Figure 2.13: Magic longitudinal force model characteristics

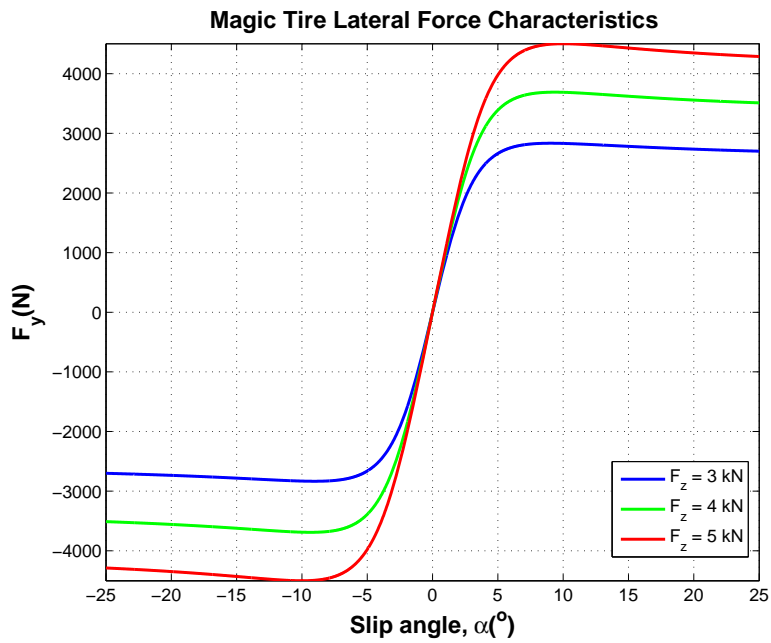


Figure 2.14: Magic lateral force model characteristics

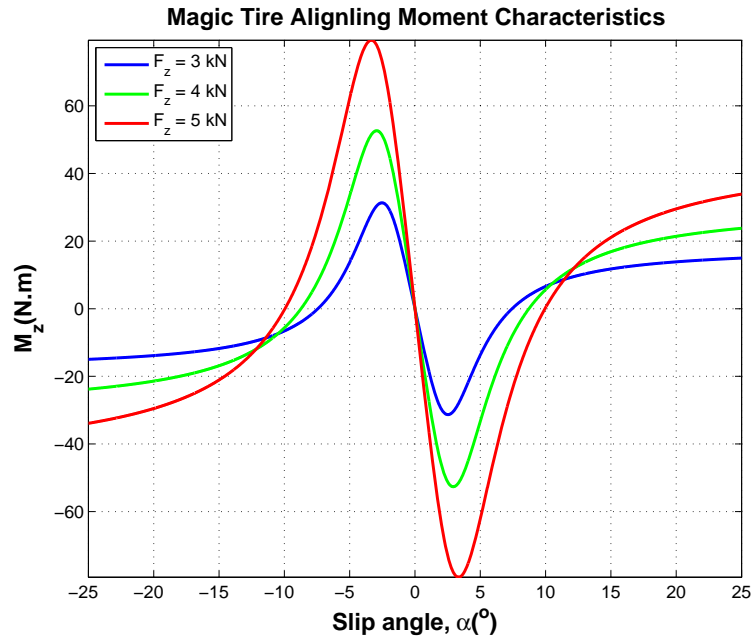


Figure 2.15: Magic aligning moment model characteristics

### 2.3.5 Wheel ground vertical contact forces

The total vertical force is caused by the earth gravitation, but it is distributed at each tire by various factors, the passengers' location, vehicle kinematic motion, road geometry, etc. However, if all these influences are considered into the model design, the model complexity will be augmented rapidly. The high non-linearity also brings the difficulty for the entire description of real system. Hence, some reasonable simplifications are adopted to reduce the complexity. The vertical force model could be supposed to be approximated to the complete physical model. Afterwards, we will present the different road conditions leading to various tire vertical force distributions.

#### 2.3.5.1 Wheel vertical planar dynamics

Firstly, we provide wheel vertical model on the plane road, it is the most simple and generally discussed situation. The road geometry is neglected, furthermore the effect of wheel camber angle ( $\gamma$ ), roll and pitch accelerations ( $\ddot{\theta}$  and  $\ddot{\varphi}$ ) are not considered in this model. All these assumptions are aimed to reduce the complexity of the vertical force model.

The longitudinal and lateral acceleration ( $a_x$  and  $a_y$ ) are only introduced to represent the inertia of vehicle chassis. The wheel load will shift according to the acceleration variation. The vertical force on each tire can be separately decided under the condition that the roll and pitch movement is uncoupled. When the vehicle moves forward, the positive acceleration causes load shift from front to rear axle for the pitch motion of the vehicle body due to its inertia. The complete formula derivation is presented in [Kiencke 2005].

For instance, the front wheel vertical force can be obtained from the formula of torque balance

at rear axle, we can analyze the torque balance presented in Figure 2.16(a):

$$F_{z1}L = mgL_2 - ma_x h \quad (2.22)$$

where  $F_{z1}$  is the total vertical force that includes right and left wheels  $F_{z1} = F_{z11} + F_{z12}$ , thus:

$$F_{z1} = m\left(\frac{L_2}{L}g - \frac{h}{L}a_x\right) \quad (2.23)$$

The front and rear axle are considered to be decoupled. The decoupled virtual mass is resulted of the longitudinal motion, vehicle accelerating and braking can give significant effect on the virtual mass variation. The vehicle mass can be transformed by the front axle load which we also call the virtual mass  $m^*$ :

$$m^* = \frac{F_{z1}}{g} = m\left(\frac{L_2}{L} - \frac{a_x h}{gL}\right) \quad (2.24)$$

At the moment, the virtual mass is thought as the coupling of the lateral and longitudinal motion on front wheels. Consequently, we can consider that the lateral motion is due to the inertia of virtual mass that results in the load transfer from transverse wheel side to another side. The torque balance formula is developed on the contact point of front right wheel in Figure 2.16(b).

$$F_{z11} = m^*g\frac{E_1}{2} - m^*a_y h \quad (2.25)$$

then we can combine equation 2.24 and 2.25 to get  $F_{z11}$ :

$$F_{z11} = \underbrace{\frac{1}{2}mg\frac{L_2}{L}}_{\text{Statics}} - \underbrace{\frac{1}{2}ma_x\frac{h}{L} - ma_y\frac{L_2 h}{LE_1}}_{\text{Individual}} + \underbrace{ma_x a_y\frac{h^2}{LE_1 g}}_{\text{Coupling}} \quad (2.26)$$

This equation can be separated into three parts: the statics load distribution as we have discussed in case 1 of section 2.4.3.3. The middle part is respectively the individual longitudinal and lateral acceleration effect. The final part is the coupling between the pitch and roll dynamics. The wheel forces for other wheels can be derived from the same way:

$$\begin{aligned} F_{z11} &= \frac{1}{2}mg\frac{L_2}{L} - \frac{1}{2}ma_x\frac{h}{L} - ma_y\frac{L_2 h}{LE_1} + ma_x a_y\frac{h^2}{LE_1 g}, \\ F_{z12} &= \frac{1}{2}mg\frac{L_2}{L} - \frac{1}{2}ma_x\frac{h}{L} + ma_y\frac{L_2 h}{LE_1} - ma_x a_y\frac{h^2}{LE_1 g}, \\ F_{z21} &= \frac{1}{2}mg\frac{L_1}{L} + \frac{1}{2}ma_x\frac{h}{L} - ma_y\frac{L_1 h}{LE_2} - ma_x a_y\frac{h^2}{LE_2 g}, \\ F_{z22} &= \frac{1}{2}mg\frac{L_1}{L} + \frac{1}{2}ma_x\frac{h}{L} + ma_y\frac{L_1 h}{LE_2} + ma_x a_y\frac{h^2}{LE_2 g}. \end{aligned} \quad (2.27)$$

The above model neglects the effect of suspension and camber angle. The suspension can reduce the vibration on a bumpy road, however this model can provide accurate calculation result which is enough to meet the requirements of our system. This model not only considers the individual effect at longitudinal and lateral axis but also the coupling of lateral and longitudinal load transfer. Three parts of the formula can produce the vertical loads that are valid for operating conditions.

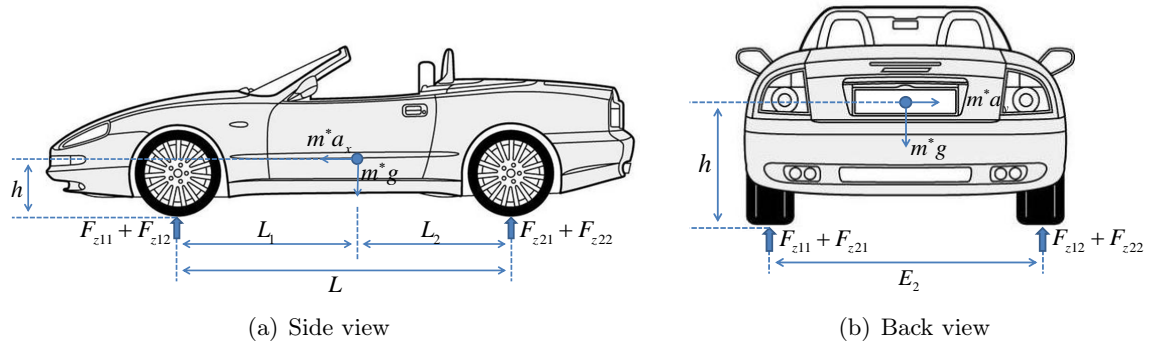


Figure 2.16: Vertical load distribution

### 2.3.5.2 Wheel vertical dynamics on banked road

Road bank angle has a direct influence on the vehicle load distribution and lateral acceleration measurement. To minimize possible modeling and estimation error of vehicle states, it is important for a vehicle dynamics analysis to know the effect of road bank angle experienced by the vehicle. The major challenge in both the estimation of the road bank angle and the determination of vehicle vertical load is to differentiate the road disturbance component (road bank angle) from vehicle vertical dynamics component. Some literatures [Kawashima 2010] [Tseng 2001] and [Ryu 2004] have analyzed the influence of bank angle on the vehicle dynamics. Usually it is important to differentiate between road bank angle ( $\phi_r$ ) and chassis roll angle ( $\phi$ ) relative to the environment coordinate system. The most important parameters when calculating the vertical load distribution is the lateral acceleration, since the normal forces due to gravity and road bank angle are affecting the lateral accelerometer when the vehicle is tilted around the x-axis [Nilsson 2011].

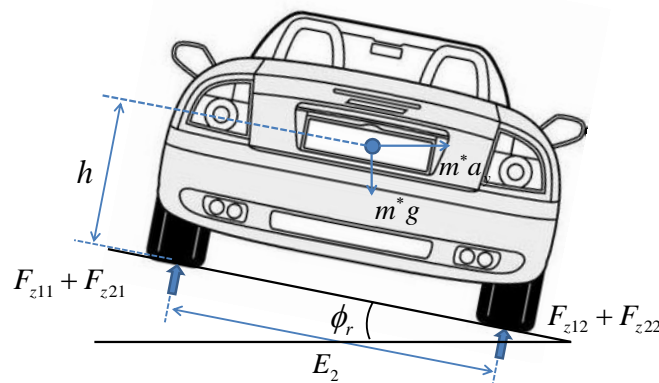


Figure 2.17: Vertical load distribution on banked road

Hence, another extension of the above tire vertical model is developed under the banked road condition that represented in Figure 2.17. The longitudinal and lateral motion is decoupled,

however the vehicle roll motion is considered separately in this model to deflect the vehicle lateral dynamics. It is assumed that an accelerometer and gyroscope sensors are attached at the CG of vehicle mass and the unsprung mass keeps contact with the ground is same. Combined with the above torque balance derivation formulas, we can easily get the relations as follows [Menhour 2010]:

$$\begin{aligned}
F_{z11} &= \frac{1}{2}mg \frac{L_2}{L} \cos(\phi_r) - \frac{1}{2}ma_x \frac{h}{L} - ma_y \frac{L_2 h}{LE_1} - \frac{K_{\phi 1} \phi + C_{\phi 1} \dot{\phi}}{E_1}, \\
F_{z12} &= \frac{1}{2}mg \frac{L_2}{L} \cos(\phi_r) - \frac{1}{2}ma_x \frac{h}{L} + ma_y \frac{L_2 h}{LE_1} + \frac{K_{\phi 1} \phi + C_{\phi 1} \dot{\phi}}{E_1}, \\
F_{z21} &= \frac{1}{2}mg \frac{L_1}{L} \cos(\phi_r) + \frac{1}{2}ma_x \frac{h}{L} - ma_y \frac{L_1 h}{LE_2} - \frac{K_{\phi 2} \phi + C_{\phi 2} \dot{\phi}}{E_2}, \\
F_{z22} &= \frac{1}{2}mg \frac{L_1}{L} \cos(\phi_r) + \frac{1}{2}ma_x \frac{h}{L} + ma_y \frac{L_1 h}{LE_2} + \frac{K_{\phi 2} \phi + C_{\phi 2} \dot{\phi}}{E_2}.
\end{aligned} \tag{2.28}$$

This method does not consider the earth gravitation component on the banked angle, the centrifugal force has a very important influence on lateral and vertical acceleration. Therefore, the force may not be accurate when the vehicle is turning on a banked angle. Consequently, this issue will become an exploration interest in our work.

We have presented above basic tire characteristics and different tire models which will be the foundation of our following research explanations in this chapter.

## 2.4 Vehicle model

Following with the previous presentation of tire model in the previous section, the detailed vehicle body dynamics which has an important role for the understanding of vehicle motion will be discussed in this section.

A full passenger vehicle model consists of sprung mass and unsprung mass. The sprung mass is related to pitch, roll and yaw movement in the longitudinal, lateral and vertical axis. The unsprung mass is composed by the suspension, wheels or tracks and other components which are allowed to bounce vertically with respect to the sprung mass. The definition of the mechanics equations is expressed under the frame of vehicle body coordinate in Figure 2.18.

The vehicle motion is separated by longitudinal axis, lateral axis and vertical axis [Reza 2007]. The 3D individual component is presented as follows:

- Longitudinal force  $F_x$ : It is also called forward force or traction force,  $F_x > 0$  if the vehicle is accelerating that is contrary to braking while  $F_x$  is negative.
- Lateral force  $F_y$ : Lateral force is usually affected by the steering wheel input, it is the principle reason for the vehicle to turn on the road.
- Vertical Force  $F_z$ : Vertical force is an orthogonal force to both  $F_x$  and  $F_y$ , it is also called wheel load or normal force.
- Roll moment  $M_x$ : The roll moment is the product of the sprung mass and the square of the distance between the vehicle's roll center and its center of mass. It is also called bank moment.

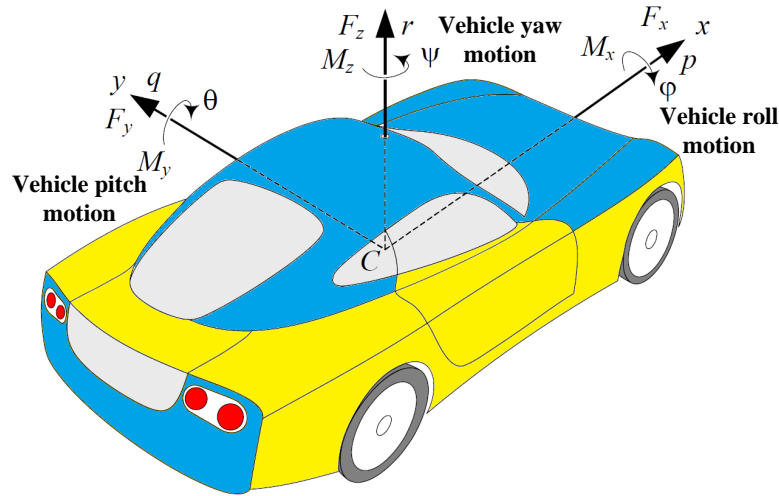


Figure 2.18: Vehicle body coordinate frame

- Pitch moment  $M_y$ : Pitch moment is caused by the up and down movement of different angles of vehicle at  $y$  axis towards the road.
- Yaw moment  $M_z$ : Yaw moment is generated around the yaw axis of a vehicle that changes the direction the vehicle to left or right. It is also called the aligning moment.

In this section, the paragraph is emphasized in the simplified vehicle dynamics model description. The evaluation of vehicle model is more and more complex, however considering the mathematical solution and the hardware computation cost, the simple and effective model is interesting to us. In the subsequent content, some typical and extensive used vehicle dynamics models will be presented.

### 2.4.1 Vehicle vertical dynamics model

Vehicle vertical dynamics is mainly influenced by the suspension system, it reflects the basic vertical vehicle movement. In addition, it has a great impact on the performance of modern vehicles. In order to reduce the transference of vibration and noise, and to improve the comfort of the vehicle, some literatures applied the suspension control to improve the driver comfort sense [Zhan 2000] [Kim 2004]. Some suspension control algorithms are developed to analyze vehicle vertical dynamics [Halfmann 1999] [Emmanuel 2003] and [Milanese 2004]. For further complete information, we can refer to [Reza 2007] [Kiencke 2005] [Rajamani 2012] and [Milliken 2003].

#### 2.4.1.1 Suspension model

The suspension system is a mechanical system of springs and shock absorbers that connect the wheels and axles to the chassis of a wheeled vehicle, it is charged the function of:

- Carrying the static weight of the vehicle,
- Maximizing the friction between the tires and the road surface,
- Providing steering stability with good handling (minimize body roll),

- Ensuring the comfort of the passengers (ability to smooth out a bumpy road).

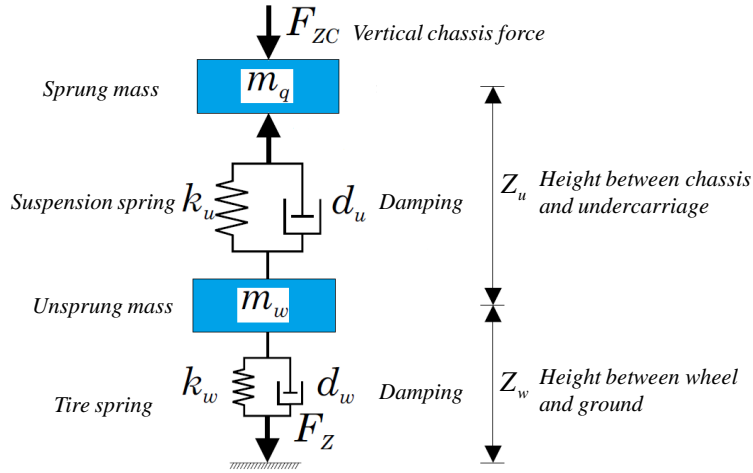


Figure 2.19: A quarter vehicle suspension system

The simplified suspension system is shown in Figure 2.19. According to the function and mechanical structure, the suspension system is classified by the following catalogs:

- Passive suspension,
- Semi-Active suspension: Orifice Based Damper and MR fluid based Damper,
- Active suspension: Slow Active, Active and Fully Active.

The classical suspension model has been discussed in the previous literatures. Particularly, full, half and quarter vehicle suspension models are typically used in the suspension control theory. As far as we know, a quarter vehicle model can be used to predict ride quality and pavement loading very well. The quarter vehicle model is based on several assumptions, there is no vehicle body or axle roll, vehicle velocity is constant, vehicle body is rigid, the suspension and tire characteristics are considered to be linear and the pitch angle is not obvious [Sun 2007]. The quarter vehicle model is employed to characterize vehicle vertical dynamics, which is illustrated in Figure 2.19. It is a model with two degrees of freedom of a suspension moving on a rough pavement, however it can effectively reflect the basic vehicle motion caused by up and down movement despite its simplicity. A parallel spring and damper with constant coefficient is used to model the tire in order to reduce the complexity of the suspension system.

According to the D'Alembert's principle, the vehicle's suspension system is governed by the following relations:

$$\begin{aligned} m_w \ddot{Z}_w + d_u (\dot{Z}_w - \dot{Z}_u) + d_w (\dot{Z}_w - \dot{\xi}) + k_u (Z_w - Z_u) + k_w (Z_w - \xi) &= 0 \\ m_q \ddot{Z}_u - d_u (\dot{Z}_w - \dot{Z}_u) - k_u (Z_w - Z_u) &= 0 \end{aligned} \quad (2.29)$$

Where  $m_w$  and  $m_q$  respectively represent the vehicle unsprung mass and sprung mass and  $m_q$  is one-fourth of the body mass, which is suspended by the main suspension of the vehicle spring  $k_u$  and damping  $d_u$ . The main suspension system are mounted on a wheel of the vehicle

that is named unsprung mass, we consider that for each wheel the springing stiffness  $k_w$  and viscous damping coefficient  $d_w$  are similar.

The quarter car model is a simple form of the 1/4 body of the vehicle, which does not include the representation of the geometric effects of the full car as well as the possibility of longitudinal and lateral coupling. Nevertheless, it composes of the most basic features of the real problem and includes a proper representation of the problem of controlling wheel and wheel-body load variations.

### 2.4.2 Vehicle longitudinal and lateral dynamics model

This section will focus on the representation of vehicle planar dynamics, especially about the longitudinal and lateral motion of vehicle in a plane. Longitudinal dynamics is a forward moving motion of the vehicle, it is mainly influenced by the acceleration and brake of the vehicle. Lateral dynamics is related to the vehicle sideways moving direction, researchers often find this direction more interesting than the longitudinal one since extreme values of lateral acceleration or lateral velocity can decrease vehicle stability and controllability. The following section will mainly present two simply vehicle models: bicycle vehicle model and complete four wheel model.

#### 2.4.2.1 Bicycle vehicle model

The bicycle model is a simplification of four-wheel vehicle model shown in Figure 2.20, it is a common expression of basic vehicle lateral dynamics. This model ignores the influence of the roll and pitch dynamics motion. It largely simplifies the derivation of the equations of motion of the vehicle and easily reduces the complexity of implementation of equations. The model can be found in many literatures, some detailed derivations are given in [Wong 2008] [Milliken 2003] and [Rajamani 2012]. Generally, the simplified bicycle model is formulated by the following relationship:

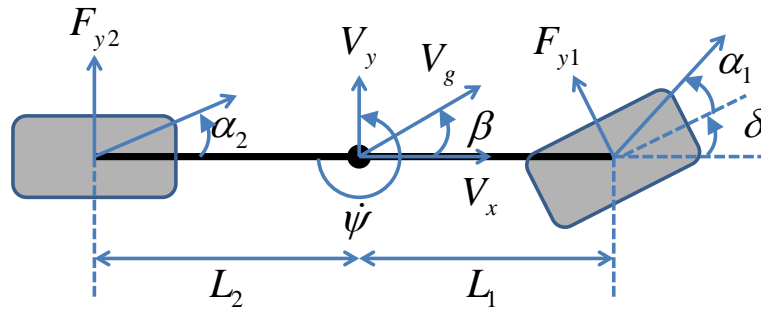


Figure 2.20: Bicycle model

$$\begin{cases} \dot{\beta} &= \frac{1}{mV_g} [F_{x1}\sin(\delta - \beta) + F_{y1}\cos(\delta - \beta) - F_{x2}\sin(\beta) + F_{y2}\cos(\beta)] - \dot{\psi} \\ \dot{V}_g &= \frac{1}{m} [F_{x1}\cos(\delta - \beta) + F_{y1}\sin(\beta - \delta) + F_{x2}\cos(\beta) + F_{y2}\sin(\beta)] \\ \dot{\psi} &= \frac{1}{I_z} [L_1(F_{y1}\cos(\delta) + F_{x1}\sin(\delta)) - L_2F_{y2}] \end{cases} \quad (2.30)$$

The assumption of small angle is to linearize the system, the left and right wheels are regarded as one single wheel. The front left and right steering angles are assumed equal,  $\delta = \delta_{11} = \delta_{12}$ , the

rear steering angle is normally null  $\delta_{21} = \delta_{22}$ . The longitudinal force and lateral forces presented in the formulation are the sum of correspondent axle force,  $F_{x1} = F_{x11} + F_{x12}$ ,  $F_{x2} = F_{x21} + F_{x22}$  and  $F_{y1} = F_{y11} + F_{y12}$ ,  $F_{y2} = F_{y21} + F_{y22}$ .

The slip angle  $\alpha_1$  and  $\alpha_2$  appeared in Figure 2.20 are defined between the sideslip angle and the steering angle. On account of the different velocity direction between chassis and tire, the sideslip angle for each tire is different from the one at the center of gravity. The tire slip angles of the rear and front tires can be easily computed by kinematic equations:

$$\begin{aligned}\alpha_1 &= \beta_1 - \delta_1 \approx \frac{V_y + L_1\dot{\psi}}{V_x} - \delta_1 = \beta + \frac{L_1\dot{\psi}}{V_x} - \delta_1 \\ \alpha_2 &= \beta_2 \approx \frac{V_y + L_1\dot{\psi}}{V_x} = \beta - \frac{L_2\dot{\psi}}{V_x}\end{aligned}\quad (2.31)$$

where longitudinal and lateral velocity are replenished:

$$\begin{aligned}V_x &= (L_1(\dot{\psi} + V_g \sin(\beta))) \sin(\delta) + V_g \cos(\beta) \cos(\delta) \\ V_y &= (L_1(\dot{\psi} + V_g \cos(\beta))) \sin(\delta) - V_g \cos(\beta) \sin(\delta)\end{aligned}\quad (2.32)$$

Obviously, the difference of left and right tire dynamics is not considered in the above equations, especially on the front tires. A more complete vehicle model contains four wheels will be introduced in the following section, which can give a more precise description of vehicle dynamics.

#### 2.4.2.2 Four wheels vehicle model

The four wheels vehicle model is discussed in [Stéphant 2004] [Baffet 2007] [Wenzel 2006] [Doumiati 2009] [Ray 1997]. Since it can give an accurate description of the vehicle planar dynamics, it can be found in plenty of applications aimed for vehicle state estimation and control strategy. The state and parameter estimator presented in our research is based on a four-wheel vehicle model represented in Figure 2.21. The pitch motion and suspension deflections are neglected in this model. The model proposed in [Ray 1997] is formulated as follows:

$$\begin{aligned}\ddot{\psi} &= \frac{1}{I_z} \{ I_{xz} \ddot{\theta} + L_1 [F_{x11} \sin(\delta_{11}) + F_{x12} \sin(\delta_{12}) + F_{y11} \cos(\delta_{11}) + F_{y12} \cos(\delta_{12})] \\ &\quad - L_2 [F_{x21} \sin(\delta_{21}) + F_{x22} \sin(\delta_{22}) + F_{y21} \cos(\delta_{21}) + F_{y22} \cos(\delta_{22})] + M_z \\ &\quad + \frac{E_1}{2} [F_{y11} \sin(\delta_{11}) - F_{y12} \sin(\delta_{12}) + F_{x12} \cos(\delta_{12}) - F_{x11} \cos(\delta_{11})] \\ &\quad + \frac{E_2}{2} [F_{y21} \sin(\delta_{21}) - F_{y22} \sin(\delta_{22}) + F_{x22} \cos(\delta_{22}) - F_{x21} \cos(\delta_{21})] \}, \\ \dot{V}_x &= V_y \dot{\psi} + \frac{1}{m} [F_{x11} \cos(\delta_{11}) + F_{x12} \cos(\delta_{12}) + F_{x21} \cos(\delta_{21}) + F_{x22} \cos(\delta_{22}) \\ &\quad - F_{y11} \sin(\delta_{11}) - F_{y12} \sin(\delta_{12}) - F_{y21} \sin(\delta_{21}) - F_{y22} \sin(\delta_{22}) - m_s h \dot{\psi} \dot{\theta}], \\ \dot{V}_y &= -V_x \dot{\psi} + \frac{1}{m} [F_{x11} \sin(\delta_{11}) + F_{x12} \sin(\delta_{12}) + F_{x21} \sin(\delta_{21}) + F_{x22} \sin(\delta_{22}) \\ &\quad + F_{y11} \cos(\delta_{11}) + F_{y12} \cos(\delta_{12}) + F_{y21} \cos(\delta_{21}) + F_{y22} \cos(\delta_{22}) + m_s h \dot{\theta}], \\ \ddot{\theta} &= \frac{1}{I_{xs}} [m_s h (a_y + V_x \dot{\psi}) + I_{xzs} \ddot{\psi} + m_s h g \theta + M_{\theta 1} + M_{\theta 2}].\end{aligned}\quad (2.33)$$

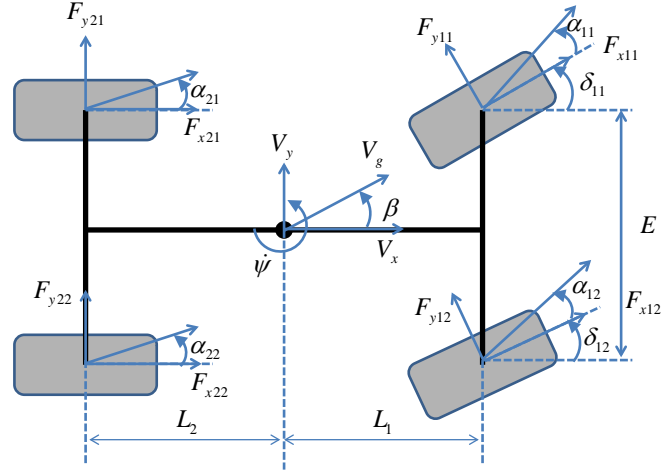


Figure 2.21: Four wheel vehicle model

The motion in longitudinal direction  $V_x$ ; the motion in lateral direction  $V_y$ ; yaw around vertical axis  $z$ , described by the yaw rate  $\dot{\psi}$  and roll motion with regard to longitudinal axis  $\theta$  are considered in this model, the angular velocity of each wheel can be derived as:

$$\begin{aligned}
 \omega_{11} &= -\frac{1}{I_w}(r_{11}F_{x11} - T_{11}), \\
 \omega_{12} &= -\frac{1}{I_w}(r_{12}F_{x12} - T_{12}), \\
 \omega_{21} &= -\frac{1}{I_w}(r_{21}F_{x21} - T_{21}), \\
 \omega_{22} &= -\frac{1}{I_w}(r_{22}F_{x22} - T_{22}).
 \end{aligned} \tag{2.34}$$

where  $\psi$  and  $\theta$  denote respectively the vehicle yaw and roll motion, the vehicle total mass and sprung mass is identified by  $m$  and  $m_s$ . The torque at each wheel can be modulated independently with the assumption that exactly the requested wheel torque can be applied instantaneously to the respective wheel.  $I_{zz}$  represents the moment of inertia about yaw axis,  $I_{xz}$  and  $I_{xzs}$  respectively represent the product of inertia about roll and yaw axis of vehicle mass as well as the vehicle sprung mass,  $I_{xxs}$  means the moment of inertia about the roll axis,  $I_w$  is the wheel moment of inertia. The wheel velocity at each tire is determined by tire radius  $r_{ij}$ , longitudinal force for each wheel  $F_{xij}$  and the wheel torque  $T_{ij}$ .

The four wheel vehicle model is evolved and simplified in order to meet the real application requirement, the lateral dynamics is represented in [Baffet 2007] [Doumiati 2009] with Newton projection on the axis of vehicle velocity ( $V_g$ ) and sideslip angle ( $\beta$ ) at the center of gravity, in which the wheel roll motion is not considered. The simplified lateral dynamics equations are denoted as follows:

$$\begin{aligned}
\dot{\beta} &= \frac{1}{mV_g} [-F_{x11}\sin(\beta - \delta_{11}) + F_{y11}\cos(\beta - \delta_{11}) - F_{x12}\sin(\beta - \delta_{12}) + F_{y12}\cos(\beta - \delta_{12}) \\
&\quad - F_{x21}\sin(\beta - \delta_{21}) + F_{y21}\cos(\beta - \delta_{21}) - F_{x22}\sin(\beta - \delta_{22}) + F_{y22}\cos(\beta - \delta_{22})] - \dot{\psi}, \\
\ddot{\psi} &= \frac{1}{I_z} \{L_1[F_{x11}\sin(\delta_{11}) + F_{x12}\sin(\delta_{12}) + F_{y11}\cos(\delta_{11}) + F_{y12}\cos(\delta_{12})] \\
&\quad - L_2[F_{x21}\sin(\delta_{21}) + F_{x22}\sin(\delta_{22}) + F_{y21}\cos(\delta_{21}) + F_{y22}\cos(\delta_{22})] \\
&\quad + \frac{E_1}{2}[F_{y11}\sin(\delta_{11}) - F_{y12}\sin(\delta_{12}) + F_{x12}\cos(\delta_{12}) - F_{x11}\cos(\delta_{11})] \\
&\quad + \frac{E_2}{2}[F_{y21}\sin(\delta_{21}) - F_{y22}\sin(\delta_{22}) + F_{x22}\cos(\delta_{22}) - F_{x21}\cos(\delta_{21})]\}, \tag{2.35} \\
\dot{V}_g &= \frac{1}{m} [F_{x11}\cos(\beta - \delta_{11}) + F_{y11}\sin(\beta - \delta_{11}) + F_{x12}\cos(\beta - \delta_{12}) + F_{y12}\sin(\beta - \delta_{12}) \\
&\quad + F_{x21}\cos(\beta - \delta_{21}) + F_{y21}\sin(\beta - \delta_{21}) + F_{x22}\cos(\beta - \delta_{22}) + F_{y22}\sin(\beta - \delta_{22})], \\
\dot{V}_x &= V_y\dot{\psi} + \frac{1}{m} [F_{x11}\cos(\delta_{11}) + F_{x12}\cos(\delta_{12}) + F_{x21}\cos(\delta_{21}) + F_{x22}\cos(\delta_{22}) \\
&\quad - F_{y11}\sin(\delta_{11}) - F_{y12}\sin(\delta_{12}) - F_{y21}\sin(\delta_{21}) - F_{y22}\sin(\delta_{22}) - m_s h \dot{\psi} \dot{\theta}], \\
\dot{V}_y &= -V_x\dot{\psi} + \frac{1}{m} [F_{x11}\sin(\delta_{11}) + F_{x12}\sin(\delta_{12}) + F_{x21}\sin(\delta_{21}) + F_{x22}\sin(\delta_{22}) \\
&\quad + F_{y11}\cos(\delta_{11}) + F_{y12}\cos(\delta_{12}) + F_{y21}\cos(\delta_{21}) + F_{y22}\cos(\delta_{22}) + m_s h \dot{\theta}].
\end{aligned}$$

To develop the observer which adopted for the consideration of observability and complexity, a further simplification can be assumed that the left and right front steering angles are equal, while the rear steering wheel angles are null. The expanded form of vehicle wheels velocity vector can be derived as:

$$\begin{cases} V_{x11} = V_g \cos(\beta) - \frac{E}{2} \dot{\psi} \\ V_{y11} = V_g \sin(\beta) + L_1 \dot{\psi}, \end{cases} \tag{2.36}$$

$$\begin{cases} V_{x12} = V_g \cos(\beta) + \frac{E}{2} \dot{\psi} \\ V_{y12} = V_g \sin(\beta) + L_1 \dot{\psi}, \end{cases} \tag{2.37}$$

$$\begin{cases} V_{x21} = V_g \cos(\beta) - \frac{E}{2} \dot{\psi} \\ V_{y21} = V_g \sin(\beta) - L_2 \dot{\psi}, \end{cases} \tag{2.38}$$

$$\begin{cases} V_{x22} = V_g \cos(\beta) + \frac{E}{2} \dot{\psi} \\ V_{y22} = V_g \sin(\beta) - L_2 \dot{\psi}. \end{cases} \tag{2.39}$$

The sideslip angle at each wheel ( $\alpha_{ij}$ ) as well as the body slip angle at COG ( $\beta$ ) is related

to vehicle longitudinal and lateral velocity ( $V_x$  and  $V_y$ ) and yaw rate ( $\dot{\psi}$ ):

$$\begin{aligned}
\beta &= \arctan\left(\frac{V_y}{V_x}\right), \\
\beta_{11} &= \delta_{11} - \arctan\left[\frac{V_y + L_1\dot{\psi}}{V_x - \frac{E}{2}\dot{\psi}}\right], \\
\beta_{12} &= \delta_{12} - \arctan\left[\frac{V_y + L_1\dot{\psi}}{V_x + \frac{E}{2}\dot{\psi}}\right], \\
\beta_{21} &= \delta_{21} - \arctan\left[\frac{V_y - L_1\dot{\psi}}{V_x - \frac{E}{2}\dot{\psi}}\right], \\
\beta_{22} &= \delta_{22} - \arctan\left[\frac{V_y - L_1\dot{\psi}}{V_x + \frac{E}{2}\dot{\psi}}\right].
\end{aligned} \tag{2.40}$$

This section mainly recalls two vehicle models for longitudinal and lateral dynamics, bicycle model has been developed in the field of automobiles since 1956, it is simple but it can generally describe the vehicle dynamics motion. Nevertheless, it is limited to the assumption that the left and right wheels are the same, meanwhile the roll motion is ignored in the bicycle model. The four wheel vehicle model proposed by [Ray 1997] is approached to give a relatively overall description of vehicle dynamics. The four wheels are distinguished for different properties related to its mounting locations, yaw and roll motion are both considered in this model. When the vehicle is in front-wheel-drive model, an assumption that the left and right steering wheel angles are equal and the rear steering wheel is null can be made to denote a further simplified model. This point is essential for our research for providing a possibility to develop a real-time vehicle dynamics parameter estimation method with more stable performance and less computation cost. The next section will focus on the global risk assessment description.

## 2.5 Road-traffic risk assessment

The entire above sections principally present the vehicle and tire basic physical properties. Particularly, [Doumiati 2009] has presented an effective way to estimate the vehicle dynamics parameters, as well as [Ghandour 2011] proposed an risk evaluation approach. Hence, we are desirable to find an intersection from these two previous works. In this section, we concentrate on the discussion of vehicle safety on the road. Road safety is related to vehicle dynamics, conductor maneuver and road infrastructure, the road security analysis should be investigated in different road geometry and traffic conditions. Therefore, several cross-sectional studies such as psychology, sociology, road engineering, vehicle technology are intervened in the issue of road safety in order to recognize a better understanding of this phenomenon and provide a much effective solution for this issue. Usually, the accidents are analyzed by accident frequency and severity rates. A famous statistic aspect of road safety called Smeed's law [Smeed 1949] which can give an empirical evidence of the relation of relate accidents and the number of deaths.

$$\frac{D}{P} = 0.00030\left(\frac{N}{P}\right)^{\frac{1}{3}} \quad \text{and} \quad \frac{D}{N} = 0.00030\left(\frac{N}{P}\right)^{-\frac{2}{3}} \tag{2.41}$$

which present respectively the death per unit of population ( $D/P$ ) and the second one relates the death per registered vehicle ( $D/N$ ) to motorization ( $N/P$ ) [Baruya 1997]. Later on some models

have been researched and certain exceptional factors offer the possibility of the extension form for accident modeling. Solomon in [Solomon 1964] reported the relationship between average speed and collision rates. From the statistical analysis, we can conclude that the number of deaths has quite close relation with the traffic velocity.

The likelihood of traffic accidents is distinctly augmented with a higher cruise speed. In addition, the traffic accidents are due to the driver inattention as well as the loss of vehicle control. The loss of vehicle control is generally caused by the lateral skid and rollover. From the professional viewpoint, the lateral skid and vehicle rollover phenomenon is substantially engendered by the excessive speed, which means that the vehicle dynamics performance cannot sustain the predetermined trajectory. Consequently, we will introduce some risk assessments in the subsequent subsection.

### 2.5.1 Excessive driving speed

Vehicle driving speed is always a hot issue of the road safety, the positive relationship is disclosed by plenty of research and statistical reports that the higher the speed, the more injury accidents occur. The analysis of a wide range of accident studies suggested that 5% accident reduction might be expected for each 1.6km/h reduction in average speed. Allowing for sampling variability in the data, we can be 95% confident that the true value lies between 3.2% and 6.7% [Taylor 2000]. The accident caused by excessive speed usually relates to the condition of road geometry and layout, the road geometry structure principally consists of straight path and curve. The type of road is divided into three groups according to the road measurement function and the speed limit and also in terms of their roadside development.

- Highway
- Suburban link roads
- Typical inner city link roads

Road limited speed is set on the basis of maximum curvature, the additional factors like inclination angle and bank angle give an effect on the regulation of limited speed. Moreover, driver comfort is generally reflected by limiting variation of acceleration during transient maneuver. The relation of radius of curvature ( $R$ ) and vehicle velocity ( $V$ ) is defined by the following equation:

$$R = \frac{V^2}{(\phi_r + f(V))g} \quad (2.42)$$

where  $\phi_r$  is the road bank angle,  $f(V)$  is a predefined function that reflects mobilized adherence. This function is an empirical model used by the SETRA (Road and Motorway Technical Studies Department) for road construction [Sentouh 2007]. The following approximate formula is used for the definition of speed in the interval [40, 140]km/h:

$$f(V) = 0.059 + 30354 \frac{1}{V} + 170.51 \frac{1}{V^2} \quad (2.43)$$

The different speed limits on road condition are represented in the following Table 2.1:

In particular, traffic accidents happened during a cornering, conductors have a bad visual field for the prediction of the forthcoming road geometry condition. In addition, they have little knowledge about the actual road geometry condition, the road maximum friction cost-efficient,

Road type	R60	R80 or T80	T100	L80	L100	L120
Speed limit (km/h)	90	90/110	110/90	110/90	130/110	110

Table 2.1: Speed limit on different road conditions (R- Urban road; T - Rural road; L - Highway)

curve radius as well as the road bank angle are hard to be accessed and to be supplied to them. Therefore, some researchers and societies focus on the development of the curve speed warning application, which allows connected vehicles to receive information that it is approaching a curve along with the recommended speed for the curve (CWS: Curve Warning System). This application offers the capability to supply a warning (visual, sound or tactile signal) to the driver regarding the curve and its recommended speed. In [Ibrahim 2010] [Glaser 2007] [Sayer 2005], they attempt to integrate a system to provide a safe negotiation speed warning to the driver, when the vehicle is approaching a curve. The previous computation would be available for the improvement of road safety and reduction of potential risk probability. Furthermore, more advanced system could perform additional warning actions if the actual speed through the curve exceeds the recommended speed.

[Sentouh 2007] proposes a novel approach to calculate the critical speed in a curve. The road geometry of inclination and bank angle are considered as a factor in this method. Equations are given in two cases:

- In the case  $\theta_r < 0$  :

$$\begin{cases} V_1^2 = \frac{mgEL_2(1 + \frac{h}{L_2}\theta_r - \frac{2h}{E}\phi_r) - \eta_1}{EL_2[\frac{h}{L_2}(C_x - m\rho\beta) + \frac{2h}{E}(2m\rho + C_y\beta^2)]} \\ V_2^2 = \frac{mgEL_2(1 + \frac{h}{L_2}\theta_r + \frac{2h}{E}\phi_r) - \eta_2}{EL_2[\frac{h}{L_2}(C_x - m\rho\beta) - \frac{2h}{E}(2m\rho + C_y\beta^2)]} \end{cases} \quad (2.44)$$

- In the case  $\theta_r > 0$  :

$$\begin{cases} V_3^2 = \frac{mgEL_1(1 - \frac{h}{L_1}\theta_r - \frac{2h}{E}\phi_r) - \eta_3}{EL_1[-\frac{h}{L_1}(C_x - m\rho\beta) + \frac{2h}{E}(2m\rho + C_y\beta^2)]} \\ V_4^2 = \frac{mgEL_1(1 - \frac{h}{L_1}\theta_r + \frac{2h}{E}\phi_r) - \eta_4}{EL_2[-\frac{h}{L_1}(C_x - m\rho\beta) - \frac{2h}{E}(2m\rho + C_y\beta^2)]} \end{cases} \quad (2.45)$$

Finally, the global critical speed in the curve is the minimum value of four restrict velocity:  $V_c = \min(V_1, V_2, V_3, V_4)$ . The complete derivation can be found in the thesis [Sentouh 2007].

### 2.5.2 Time to collision

The analysis of driver behavior in crucial collision is able to provide a precise understanding of the reason why accidents occur as well as provide knowledge on drivers' reaction of turning a severe situation into a controllable one. However, an essential topic is how to recognize and identify the scenario of potential dangerous situations as well as the normal driving conditions. The analysis of several traffic accident studies reveals that the direct use of time-related measures has the ability to execute the decision to avoid collision. In research on traffic conflicts techniques, Time To Collision (TTC) has proven to be an effective measure for rating the severity of conflicts [Van der Horst 1994]. The conception of time-to-collision (TTC) was firstly introduced in 1971 by the US researcher Hayward [Hayward 1971]. [Lee 1976] [Wang 1992] [Minderhoud 2001] and other research laboratories develop different sensor based systems to improve the accuracy of TTC estimation.

In general, this system is based on the vehicle real-time information of the distance to objects, the steering angle, vehicle instantaneous velocity as well as the acceleration. In [Minderhoud 2001], the time to collision of vehicle-driver combination  $i$  at instant  $t$  with respect to a leading vehicle  $i - 1$  could be noted with:

$$TTC_i = \frac{X_{i-1}(t) - X_i(t) - L_i}{\dot{X}_i(t) - \dot{X}_{i-1}(t)}, \quad \forall \dot{X}_i(t) > \dot{X}_{i-1}(t) \quad (2.46)$$

where  $X_i$  and  $\dot{X}_i$  respectively the position and speed of the identification of vehicle  $i$ .  $L_i$  denotes the vehicle length.

The developed application of time to collision indicators could be applied at the assessment of the potential safety support system which would be appeared at some advanced cruise control systems for safe characteristics.

### 2.5.3 Lateral load transfer

Vehicle rollover accident takes up 33% of overall passenger vehicle crashes in terms of the report of the National Highway Traffic Safety Administration (NHTSA) [NHTSA]. Therefore, the active rollover warning system is brought in by the motivation of reduction of the incidents involving vehicle rollover. Many researchers have a developed rollover assessment architecture to detect vehicle rollover [Xu 2007] [Hac 2004a] [Gertsch 2003], the index of lateral load transfer ration [Doumiati 2009] [Kamnik 2003] and time to rollover [Chen 1999] are frequently used in the vehicle accident detection. The LTR (Lateral Load Transfer) defines the wheel load transfer from left or right side due to lateral acceleration. It offers a snapshot of vehicle lateral dynamics by detecting the instantaneous roll dynamics. The lateral load transfer is defined by using four wheel vertical loads:

$$LTR = \frac{F_{z11} + F_{z21} - F_{z12} - F_{z22}}{F_{z11} + F_{z21} + F_{z12} + F_{z22}} \quad (2.47)$$

LTR index uses principally four wheel vertical forces  $F_{zij}(i, j = 1, 2)$ , LTR varies from  $-1$  to  $1$ , which means that the left or right tire losing the contact with ground,  $0$  refers to no load transfer. The definition of threshold for determination of risk is evaluated by analytical calculations and experimental data, the choice of the threshold decides the sensibility of rollover prevention. When the threshold is initialized too high, the LTR index cannot give effective evaluation of prediction of the potential prediction. On the contrary, when the threshold is set too small, the active rollover prevention system will send false signal to the conductors. The LTR can also be deduced from the following equation by replacing the vertical forces:

$$LTR = \frac{2}{E} \frac{h(\cos\phi(V_y + \psi V_x) + hV_x^2 \sin\phi + g \sin\phi)}{g} \quad (2.48)$$

The simplified assumption could be applied to get the expression as follow:

$$LTR_s = \frac{2h}{gE} (a_{ym} + g \sin\phi) \quad (2.49)$$

[Tsourapas 2009] gives a proposition of predictive LTR, the further PLTR derivation can be expressed as:

$$PLTR_s(\Delta t) = LTR(t_0) + \frac{2h}{gE} (a_{ym} + g \sin\phi) \Delta t \quad (2.50)$$

The detailed explanation and validation could be found in this literature.

### 2.5.4 Lateral acceleration appraisal

The lateral acceleration indicator is intended to be used as an early alert system to assist drivers in recognizing when they are exceeding set maximum maneuvering limits of the vehicle. The zone of stability and comfort in terms of lateral acceleration for passengers is defined between  $0.2g$  and  $0.4g$ , however the driving handling will become uncomfortable and critical and the rate of vehicle collision risk where the acceleration is beyond  $0.4g$ . In this situation, several levels of risk warnings could be set according to the rank of dangerous collision. This indicator is able to provide useful information about the limit of vehicle stability.

### 2.5.5 Vehicle yaw stability

Vehicle lateral stability is extremely essential for the road safety of the driver and passengers during excessive lateral maneuver or during lateral maneuver under adverse environmental conditions such as snowy or ice road, sudden tire pressure loss, or sudden side wind. The influential elements of lateral stability are in relation to lateral acceleration and yaw rate, the lateral acceleration effect has been presented in the previous subsection. Moreover, yaw rate is the fundamental vehicle variable to the vehicle stability control system, especially appeared in ESC. On account of the facility of applying yaw rate in the vehicle stability or control system, some developments have been brought in some literatures [Shino 2001] [Mokhiamar 2002]. [Sentouh 2007] analyzed the distinction between measured yaw rate and the modeled one, the notation of these two parameters are defined receptively  $\dot{\psi}_{mea}(t)$  and  $\dot{\psi}_{mod}(t)$ , the disparity between the two can be labeled as  $\Delta\dot{\psi}$ :

$$\begin{cases} \dot{\psi}_{max}(t) &= \dot{\psi}_{mod}(t) + \Delta\dot{\psi} \\ \dot{\psi}_{min}(t) &= \dot{\psi}_{mod}(t) - \Delta\dot{\psi} \end{cases} \quad (2.51)$$

where  $\Delta\dot{\psi} = \dot{\psi}_{mea}(t) - \dot{\psi}_{mod}(t)$ , the threshold  $\Delta\dot{\psi}_n$  is regarded as the level of normal alarm when it is fixed at  $\pm 0.05 rad/s$ , alternatively the threshold  $\Delta\dot{\psi}_s$  is limited at  $\pm 0.08 rad/s$ , which reflects it is under the severe driving condition. The threshold  $\Delta\dot{\psi}$  is tested by plenty of experimental tests, and summarized by empirical regularity.

### 2.5.6 Lane departure indicator

As far as we have presented some risk assessments in the previous subsections, this part will concentrate on another particular type of accident, Run-Off-Road (ROR) crash that occurs when a single vehicle departs the road border. To prevent the ROR accidents, Lane Departure Warning Systems (LDWS) are widely adopted in passenger cars to prevent crashes. The LDWS is usually a vision-based processing system detecting the lane marker and alarm the driver that the vehicle is slowly drifting off the road. Roadside Rumble Strips and Time to Lane Crossing (TLC) are exploited to warn the drivers to take corrective action. Godthelp first proposes the Time to Lane Crossing metric in [Godthelp 1984], it offers a way to predict the remaining time at the established trajectory will depart the road border. Recently, [Ghandour 2011] has predicted the crash accident using risk assessments, like lateral load transfer and lateral skid ratio. [Dahmani 2010] proposes a method of lane departure detection based on road curvature estimation. The author employs a nonlinear model basing on vehicle lateral dynamics and a vision system represented by a T-S fuzzy uncertain model with unknown inputs to estimate vehicle state and road curvature. Moreover, more and more applications are evolved in [Mammar 2004] [Chih-Li 2012] [Suzuki 2003] [Batavia 1999] by using multi-sensors and other detection technologies. TLC is

derived by using a kinematic model of the car and trigonometric formulas in [Mammar 2006a]. The position of vehicle located on the roadway lane marker is identified by kinematic parameters such as: actual vehicle lateral displacement, vehicle geometry, and relevant yaw angle. The relative position from left lane marker assumes that  $y_l$  is the distance between left lane marker and vehicle CG,  $y_{11}$  and  $y_{21}$  respectively represent the left front and rear tire distance from the left lane boundary.

$$\begin{cases} y_{11} &= y_1 - L_1 \sin\psi - \frac{E}{2} \cos\psi \\ y_{21} &= y_1 - L_1 \sin\psi + \frac{E}{2} \cos\psi \end{cases} \quad (2.52)$$

Alternatively, the right side is given with the same form of left one.

$$\begin{cases} y_{12} &= y_2 + L_1 \sin\psi + \frac{E}{2} \cos\psi \\ y_{22} &= y_2 + L_1 \sin\psi - \frac{E}{2} \cos\psi \end{cases} \quad (2.53)$$

TLC is obtained by dividing the distance to collision with vehicle velocity  $v$ . For the time of a vehicle leaving on the left side of the lane, it is expressed as:

$$TLC = \frac{y_{11}}{v \sin\psi} \quad (2.54)$$

TLC seems to be a good indicator in order to predict the potential run off road risk, in particular encountering the upcoming curve in a road.

## 2.6 Conclusion

This chapter provides a brief description of the physical conception in terms of the vehicle dynamics. It outlines the physical tire model as well as the vehicle dynamics model. Many active safety approaches are elaborated as technical applications. In addition, the risk assessments are included as the final part of the organization of this chapter.

In the first instance, we discuss the hot issue around the vehicle safety system. Some commercialized advanced driver assistance systems like electronic stability control system and active rollover prevention systems are elaborated. These two systems respectively supply the solution for the prevention of vehicle drifting out and rollover accidents. Theoretically, more precise and complex electronic system needs more sorts of data acquisition. Therefore, we need to explore vehicle dynamics properties to meet these requirements.

Second, we focus on the presentation of pneumatic tire/road interaction characteristics, the theory model and semi-empirical model are introduced to denote detailed physical elements about tire forces and moments. Primarily, the vertical load on each tire is analyzed in three cases: level road, inclined road and banked road. The vertical force could be considered as the generation factor in the expression of tire longitudinal and lateral force. The simplest linear model represents the basic knowledge of longitudinal and lateral force that is related to the slip ratio and slip angle. Nevertheless, the linear tire model is limited by the region of force saturation appeared in Figure 2.8. Moreover, the Magic tire model has been largely employed in the exploration of vehicle estimation or control systems. Actually, this model is the so-called semi-empirical tire model that summarized by physical model as well as plenty of experimental tests. The shortcoming of this model is the number of tuning parameters which are usually unknown. Finally, we propose to use the Dugoff tire model which is not so accurate as magic tire model, however it synthesizes all parameters into two cornering stiffness. The Dugoff tire model is considered as a reasonable solution in the subsequent research.

---

Afterwards, different types of vehicle models are presented, as far as concerned the vehicle motion, the discussion are separated by vertical, longitudinal and lateral axis. Suspension mechanical system could be regarded as the principal influencing factor for vehicle dynamics motion. In terms of the longitudinal and lateral dynamics model, the classic bicycle and four wheel vehicle models are explained as the main modeling applied in our research. As the basic consideration of different elements, the four wheel vehicle is the optimal model which is adapted to our system requirements of accuracy, reliability and rapidity.

In the end part of this chapter, we put the emphasis on road risk assessment. Several assessments for evaluation and prediction of potential risk are brought in to improve road safety and reduce traffic accident ratio. The entire chapter lays a solid theoretical foundation for the ensuing vehicle dynamics parameter estimation. The following chapters will explain the estimation methodologies and observer techniques.



# Observer theory

## Contents

<b>3.1</b>	<b>Introduction</b>	<b>43</b>
<b>3.2</b>	<b>Observer design</b>	<b>44</b>
3.2.1	Linear system	45
3.2.2	Nonlinear system	46
<b>3.3</b>	<b>Kalman filter</b>	<b>47</b>
<b>3.4</b>	<b>Extended Kalman filter</b>	<b>48</b>
<b>3.5</b>	<b>Particle filter</b>	<b>50</b>
3.5.1	Sequential importance sampling (SIS)	51
3.5.2	Sequential importance resampling (SIR)	52
3.5.3	Particle filter algorithm	52
<b>3.6</b>	<b>Conclusion</b>	<b>53</b>

## 3.1 Introduction

In the real world, different technical fields arise assorted systems for the set of interaction or interdependent components forming a whole combined relationship, so we need certain internal information from external measurements. Actually, it is unrealistic to employ as many sensors as signals of interest describing the system's behavior. The principal reason is given rise to the cost reasons and technological constraints for the access of these signals. In addition, such systems are required to extract signals from noisy measurements which are influenced by errors evolving from constraints of the sensors employed, by random disturbances and noises, and probably the most common, by the lack of precise knowledge of the underlying physical phenomenology generating the process in the first place [Candy 2007].

Vehicle control system partially depends on the accuracy of the measurement inputs, the feedback is denoted according to the comparison of measurement and ideal state. The knowledge of these essential parameters of a vehicle control system can improve the stability of vehicle motion in the emergence situation, however some variables like tire road force, slip angle and vehicle transverse velocity are really rough to be obtained with physical sensors for economic reasons. Moreover, with the complex control system, the number of required input variables is limited by the realistic equipments. It is necessary for us to consider a better way to solve the above difficulty. How can we acquire the information from technical innovation instead of employing physical sensors and applied commercial sensors within multiple systems offering input singles? The solution provided by engineers is the observer technology that is substantially applied in industrial and aviation field.

The observer technology is also called the “virtual sensor”, it is regarded as the heart of a general problem for the purpose of variable identification, fault detection and control. Usually, the observer relies on a model of the real system, the model is a state-space representation. The required information is reconstructed by state variables defined in the state vector. The observer can offer an estimation of dynamical system for actual state of the considered model at each instant. In general, the system can be divided into linear system and nonlinear system. For the linear system, the solution was proposed by Kalman and Luenberger for the simple linear model. However for the nonlinear system, because of the difficulties involved in dealing with nonlinear system, in encountering the problem of offering available results for a very restricted class of nonlinear systems and proving the global convergence analytically, the extended Kalman filter (EKF), unscented Kalman filter (UKF), particle filter (PF), sliding-mode filter etc. are developed for the nonlinear characteristics.

This chapter is organized as follows: at the beginning, we introduce the principal observer design concept that includes linear/nonlinear system and the observability for each type of system. The following section, the Kalman filter and state-space representation is presented to provide an effective solution for the estimate of linear system. To extend to a larger field, the nonlinear system, the theory of extended Kalman filter is expounded with the complete operation steps. Moreover, considering the highly nonlinearity system and non-Gaussian noises perturbed within the system, the particle filter is presented in section 5. Finally, it presents the conclusion of the observer theory description.

## 3.2 Observer design

Observer technology offers an effective way to supply sufficient information on the process state in the control or monitoring system, because in practice system, the on-line measurement is not always available for providing reliable information. Therefore, the state observer is employed to reconstruct the inaccessible but essential measurements for deterministic or stochastic dynamics systems. Mathematical model is designed to replace the sensors, state observers play a fundamental role in process control or monitoring component in an entire system. The principal schema is represented in Figure 3.1, as far as an explicit dynamical system is designed, the state variables are an estimate of the actual state of the considered model, ordinarily the model is in a state-space representational form.

The state of dynamics system is a set of physical quantities appeared in the system which specially give a complete determination of the transient evolution of system. The system order is defined uniquely, however the physical variables appeared in the state of system is not limited to the unique form. In many cases, the choice of the state variables is clear. However, there are also many cases in which the choice of state variables is not quite obvious.

A series of initial conditions are required to be determined for the solution of the system expressed by normal differential equations. The quantity of initial conditions should be compatible with the system order, therefore the number of first order differential equations modeled in mathematical expression is equal to the system order. We call the dynamic variables that shown in the expression of first order equations as the state variables.

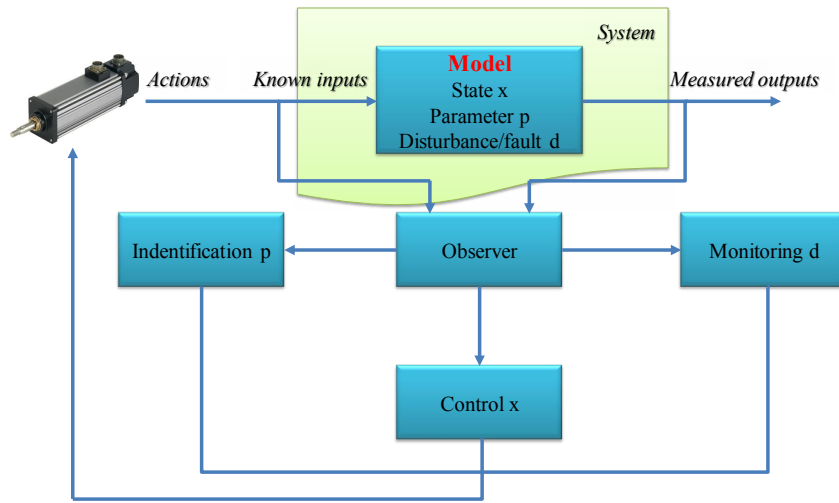


Figure 3.1: Observer employed in control system

### 3.2.1 Linear system

Firstly, we begin the discussion about the system with the simple case: linear system, which is used essentially in the important applications of automatic control and signal processing. It is a mathematical model in which the output vector is equal to the value of a linear operator applied to the input vector. In the first instance, a linear time invariant continuous time system is considered as the form:

$$\begin{cases} \dot{x}(t) = A_c x(t) + B_c u(t) \\ y(t) = C_c x(t) \end{cases} \quad (3.1)$$

for the discrete time system, the state space can be expanded as:

$$\begin{cases} x(k+1) = Ax(k) + Bu(k) \\ y(k+1) = Cx(k) \end{cases} \quad (3.2)$$

where  $x \in \mathfrak{R}^n$  is the state vector,  $y \in \mathfrak{R}^p$  is the measure,  $u \in \mathfrak{R}^m$  is the input vector. Matrix  $A$  and  $C$  respectively represent the state evaluation and observation matrix. The validation of observability of such discrete time system is given in the matrix as follows:

$$\begin{pmatrix} C \\ CA \\ CA^2 \\ \vdots \\ CA^{n-1} \end{pmatrix} \quad (3.3)$$

The system is observable with the condition that the rank of above observability matrix is  $n$  that is equal to the dimension of state vector  $x$ , and it is noted that there are some similar ways to test the observability like: the observability Gramian [Guermah 2008].

$$W_{o,T} := \sum_{k=0}^{T-1} A^{*k} C * C A^k \quad (3.4)$$

is full rank  $n$ . The observer design for linear time invariant system is considered by using the Luenberger observer and Kalman observer.

### 3.2.2 Nonlinear system

Actually, in many cases, the dynamics system cannot be still precisely described by a class of finite dimensional, time invariant linear systems [Moraal 1995], hence the system with some degrees of nonlinearity is considered by a method of reconstructing the state variables with a mathematical model, considered in a continuous-time nonlinear system, of the form:

$$\begin{cases} \dot{x}(t) = f(x(t), u(t)), & x(0) = x_0 \\ y(t) = h(x(t)) \end{cases} \quad (3.5)$$

similarly, we give a discrete-time nonlinear form on  $\mathfrak{R}^n$  at instant  $k$ :

$$\begin{cases} x(k+1) = f(x(k), u(k)) \\ y(k) = h(x(k)) \end{cases} \quad (3.6)$$

where  $f$  and  $h$  respectively represent the evaluation and observation equations with  $f \in \mathfrak{R}^n$  and  $h \in \mathfrak{R}^p$ .

We used to consider the observability of the linear system with observability matrix. However, currently we consider the observability of nonlinear system is presented with local observability. The global consideration [Hermann 1977] [Khalil 2002] is not refereed in this section. The nonlinear system could be though as weakly observable at the consequence  $x_0$  under the condition that if at the instant  $t_1$  that any initial state  $x(t_0)$  in a neighborhood  $X_0$  of  $x_0$  can be distinguished from any other state  $x_1 \in X_0$  using the input variable  $u(t)$  and output variable  $y(t)$  over the time interval  $t_0 \leq t \leq t_1$ . Therefore, the nonlinear system is called locally weakly observable if it is weakly observable and there exists a neighborhood  $X_1 \subset X_0$  of such that  $x(t) \in X_1$ , for  $t_0 \leq t \leq t_1$  [Hermann 1977] [Khalil 2002].

Local observability can be verified by using the same matrix, that the Lie derivative is used to constitute the observable matrix.

With definition  $L_f^0(h) = h$ , we can also define the higher-order Lie derivatives:

$$L_f^2(h) = \frac{\partial}{\partial x} [L_f^1(h)].f \quad (3.7)$$

It is noted that if  $\dot{x} = f(x)$ , then  $\dot{h} = \frac{\partial h}{\partial x} \frac{\partial x}{\partial t} = \frac{\partial h}{\partial x} \cdot f = L_f^1(h)$ . For the single measure, the observability matrix is given as:

$$W_o(x) = \begin{pmatrix} dh(x) \\ dL_f h(x) \\ \vdots \\ dL_f^{n-1} h(x) \end{pmatrix} \quad (3.8)$$

The system is observable with the condition that the rank of matrix  $W_o(x)$  is  $n$  that is equal to the dimension of state vector  $x$ . In this case, the system can be considered to be local observable with the satisfaction of the observability rank condition. For the expansion form of

multi measures  $[h_1, \dots, h_p]$ , the observability observer can be modified as:

$$W_o(x) = \begin{pmatrix} dh_1(x) \\ \dots \\ dh_p(x) \\ dL_f h_1(x) \\ \dots \\ dL_f h_p(x) \\ dL_f^{n-1} h_1(x) \\ \dots \\ dL_f^{n-1} h_p(x) \end{pmatrix} \quad (3.9)$$

Usually, the nonlinear system is approached to the real dynamics system, consequently the nonlinear observer design has been largely discussed for the specific structures of nonlinear system. The extended Luenberger and Kalman observers are used in the uniformly observable systems, some other observer techniques are developed with particle filter and sliding mode observer.

In the subsequent section, we will focus on the explanation of different observer structures: the linear Kalman filter, the extended Kalman filter applied to nonlinear system and the particle filter with Monte-Carlo method.

### 3.3 Kalman filter

R. E. Kalman first published his famous statistical estimation theory in 1960 [Kalman 1960], it is essential for the control of a dynamics system in the continuous manufacturing process like aircraft, spacecraft and navigation. It is described as a recursive solution to estimate the instantaneous state of the process, in a way that the mean squared error could be minimized. The Kalman filter is incipiently discovered in the linear dynamics system perturbed by white noise, the advantage is that it not only provides the past, current and future instant, but also performs well when the nature of the system is not quite precise. Some introductions can be cited in [Grewal 1993] [Sorenson 1960] and [Welch 1995] to give an elaborate presentation of the greatest discovery of control application in the twentieth century. [Welch 1995] gives a clear explanation about the discrete-data linear system.

The Kalman filter is employed to estimate the state of a discrete-time system which expressed with a linear stochastic difference equation. The state vector  $x \in \mathbb{R}^n$  and measurement  $y \in \mathbb{R}^p$  is indicated in state-space representation:

$$\begin{cases} x_k = Ax_{k-1} + Bu_{k-1} + w_{k-1} \\ y_k = Hx_k + v_k \end{cases} \quad (3.10)$$

where  $w_k$  and  $v_k$  represent receptively the process and measurement noise. The noise is assumed to be white noise, which are independent from each other, especially with normal probability distributions:

$$\begin{aligned} p(w) &\sim N(0, Q) \\ p(v) &\sim N(0, R) \end{aligned} \quad (3.11)$$

where matrix  $Q$  and  $R$  stand for the process noise covariance and measurement noise covariance that change at each iteration of the estimation process.

The Kalman filter process uses a recursive method, it is generally divided into two steps: time update equations and measurement update equations. The time update equations is also called prediction phase in which the current state and error covariance are obtained to prepare a priori estimate for the next step. Measurement update equations can be also regarded as correction phase, which is responsible for updating the estimate as well as the error covariance. This feedback step is able to improve a posteriori estimate using measurement in the previous priori estimate. The complete operation of Kalman filter is realized by the following steps:

- **Time update (Prediction)**

- (1) Predict the state estimate

$$\hat{x}_{k|k-1} = A_k \hat{x}_{k-1|k-1} + B_k u_{k-1} \quad (3.12)$$

- (2) Predict the error covariance estimate

$$P_{k|k-1} = A_k P_{k-1|k-1} A_k^T + Q_k \quad (3.13)$$

- **Measurement update (Correction)**

- (4) Compute the Kalman gain

$$K_k = P_{k|k-1} H_k^T (H_k P_{k|k-1} H_k^T + R_k)^{-1} \quad (3.14)$$

- (5) Update state estimate with measurement  $y_k$

$$\hat{x}_{k|k} = \hat{x}_{k|k-1} + K_k (y_k - H_k \hat{x}_{k|k-1}) \quad (3.15)$$

- (6) Update the error covariance

$$P_{k|k} = (I - K_k H_k) P_{k|k-1} \quad (3.16)$$

The choice of the process and measurement noise covariance is tuned off-line. The well tuned  $Q$  and  $R$  matrix could make estimation error covariance  $P_k$  and Kalman gain  $K_k$  stabilize quickly and remain constant.

### 3.4 Extended Kalman filter

In a real situation, the physical model or quantities of interest cannot always stay in the linear manner, with the complex dynamics system, it is more likely evolved to nonlinear form. The nonlinear system is more interesting to us, however if the process and observation model are nonlinear in practice situation, the required probability density function is impossible to give the exact form and could easily to be calculated through extensive numeric integration [Durrant-Whyte 2001].

Therefore, with Taylor series, suitable linearization of the nonlinear state and observation equations could be found around the current estimate. In this way, it could provide same basic form as the linear Kalman filter to the nonlinear system. Partial derivation of the process and measurement function offers the linearization form to the nonlinear relationship. Consequently, it is another extended form of normal Kalman filter. The extended Kalman filter is proved that

can provide extremely good estimate of the states of a nonlinear system, that is the reason why plenty of applications are developed with a variety of estimation problems, for example some applications and tutorials are in [Ljung 1979] [Haykin 2001] and [Wenzel 2006]. The state model is also assumed to have a state vector  $x \in \mathfrak{R}^n$  and a measurement vector  $y \in \mathfrak{R}^p$ .

$$\begin{cases} x_k = f(x_{k-1}, u_{k-1}) + w_{k-1} \\ y_k = h(x_k) + v_k \end{cases} \quad (3.17)$$

Initially, we just have the available information of the mean  $\mu_0$  and the covariance  $P_0$  during the initial phase, with these optimal estimate  $x_0^a$  and error covariance can be derived as:

$$\begin{aligned} x_0^a &= \mu_0 = E[x_0] \\ P_0 &= E[(x_0 - x_0^a)(x_0 - x_0^a)^T] \end{aligned} \quad (3.18)$$

The complete operation is elaborated by the following steps:

- **Time update (Prediction)**

- (1) Predict the state estimate

$$\hat{x}_{k|k-1} = f(\hat{x}_{k-1|k-1}, u_{k-1}) \quad (3.19)$$

- (2) Predict the error covariance estimate

$$P_{k|k-1} = F_{k-1}P_{k-1|k-1}F_{k-1}^T + Q_{k-1} \quad (3.20)$$

- **Measurement update (Correction)**

- (4) Compute the Kalman gain

$$K_k = P_{k|k-1}H_k^T(H_kP_{k|k-1}H_k^T + R_k)^{-1} \quad (3.21)$$

- (5) Update state estimate with measurement  $y_k$

$$\hat{x}_{k|k} = \hat{x}_{k|k-1} + K_k(y_k - h(\hat{x}_{k|k-1})) \quad (3.22)$$

- (6) Update the error covariance

$$P_{k|k} = (I - K_kH_k)P_{k|k-1} \quad (3.23)$$

where  $F_{k-1}$  and  $H_k$  are respectively the Jacobian of  $f(\cdot)$  and  $h(\cdot)$  around the current state estimate and they are defined as:

$$F_{k-1} = \begin{bmatrix} \frac{\partial f_1}{\partial x_1} & \frac{\partial f_1}{\partial x_2} & \cdots & \frac{\partial f_1}{\partial x_n} \\ \vdots & & \ddots & \vdots \\ \frac{\partial f_n}{\partial x_1} & \frac{\partial f_n}{\partial x_2} & \cdots & \frac{\partial f_n}{\partial x_n} \end{bmatrix} \quad H_k = \begin{bmatrix} \frac{\partial h_1}{\partial x_1} & \frac{\partial h_1}{\partial x_2} & \cdots & \frac{\partial h_1}{\partial x_n} \\ \vdots & & \ddots & \vdots \\ \frac{\partial h_p}{\partial x_1} & \frac{\partial h_p}{\partial x_2} & \cdots & \frac{\partial h_p}{\partial x_n} \end{bmatrix} \quad (3.24)$$

Although EKF is largely opted to solve the nonlinear dynamics system due to its simple conception and fast operation, it is also subjected to perform badly with estimates deviating from the true state even becoming unstable so that the observer cannot be convergent. The principal reason is due to the uncertain of the model of sensors and environment as well as the limitation

of the original algorithm. The state distribution is approximated by a Gaussian random variable which is propagated analytically through the “first-order” linearization of the nonlinear system, such propagation may lead to errors in the true posterior mean and covariance of the transformed (Gaussian) random variable [Wan 2000]. Furthermore, the Jacobin matrices of the derivation of the process and measurement function do not always exist when the nonlinear model is complex. Therefore, some other estimation methods based on different statistical solutions are proposed afterwards, a good estimate can be found by Monte Carlo simulation. The methodology of particle filter for the estimation of nonlinear system is presented in the subsequent section.

### 3.5 Particle filter

Actually, the accuracy of estimation of the designed system is affected by the constraints of the sensors applied in the system, the process random noise also generates errors that cause deviation from the real data. Most important analysis of the performance depends on the precise and overall consideration of system modeling. Therefore, it has attracted much attention from worldwide researchers to find an approach to capture all the information available in the process schema. The process design evolves from the realm of statistical signal processing using a Bayesian approach [Candy 2007]. Bayesian nonlinear statistical signal processing technique was involved to make the simulation-based methods by using sampling theory and Monte Carlo method, hence system model and noise are not limited to the condition of nonlinear approximations and Gaussian processes noises. In addition, growing current computer computational capacity makes the Bayesian approach be applicable in real time.

With recent research evolution, a method called “importance sampling”, that is based on Markov models, is discussed and implemented in certain applications (verification, probabilistic reasoning...). With the importance sampling theory basis, a particle filter (PF) is proposed for the concept of different observer techniques which supply a way to describe probability distribution. It is expanded to be with discrete non-parametric representation and implemented in a bootstrap mode. A tutorial of particle filter will be interesting to be presented in the following paragraphs.

To introduce the application of the sequential Monte Carlo method, using particle filter, to solve the problem of estimating the state of a dynamic system, let’s consider the discrete-time nonlinear state-space representation in the following form as:

$$\begin{aligned}x_k &= f(x_{k-1}, v_{k-1}) \\y_k &= h(x_k, n_k)\end{aligned}\tag{3.25}$$

where  $x_k$  is the representation of the state vector and  $y_k$  is the measurement vector. The process noise  $v_k$  and measurement noise  $n_k$  are assumed to be white noise and independent.  $f$  and  $h$  are respectively the nonlinear process and measurement function.

This state-space representation can equivalently be formulated with an infinite dimensional hidden Markov model (HMM), defined by:

$$p(x_0), p(x_k|x_{k-1}), p(y_k|x_k)\tag{3.26}$$

The definition of hidden Markov chain is initialized with probability density function  $p(x_0)$ , the likelihood of current time is given based on the state at previous time  $p(x_k|x_{k-1})$ , the probability distribution of measurement is expressed by  $p(y_k|x_k)$  [Hol 2004].

A principal problem associating to this filter technique is how to estimate the state vector at sequence  $k$ , simultaneously with the measurement denoted from the initial instant of the time  $k$  included. As far as we know the theoretical foundation of Bayesian method, the problem is able to be solved by  $p(x_k|y_{1:k})$ . The probability density can be obtained by two steps. These two steps work in a recursive framework, just like the operation of Kalman filter: the prediction step and the update step. In the prediction step, the probability density function  $p(x_{k+1}|y_{0:k})$  is determined by  $p(x_k|y_{0:k})$  at previous time  $k$  which is assumed already known in the history phase.

$$p(x_{k+1}|y_{0:k}) = \int p(x_{k+1}|x_k)p(x_k|y_{0:k})dx_k \quad (3.27)$$

In addition, the update step is formulated by the equations as follows:

$$\begin{aligned} p(x_k|y_{0:k}) &= \frac{p(y_k|x_k)p(x_k|y_{0:k-1})}{p(y_k|y_{0:k-1})} \\ p(y_k|y_{0:k-1}) &= \int p(y_k|x_k)p(x_k|y_{0:k-1})dx_k \end{aligned} \quad (3.28)$$

Obviously, the prior distribution is updated during the recursive operation, at each iteration a new measurement  $y_k$  is brought in to obtain the posterior over  $x_k$  by making use of the Bayes' theorem.

Since the integral operation involved in the recursion, the computation of prediction and update step is quite difficult to obtain an analytical solution. Hence the Monte Carlo method is introduced to numerically approximate the probability density function  $p(x_{0:k}|y_{0:k})$  in particle filter.

### 3.5.1 Sequential importance sampling (SIS)

As we have discussed above, when the prediction and update steps cannot be realized directly with analytical method, we use the Monte Carlo method to solve the estimation problem. In particular, the sequential importance sampling is the fundamental usage applied with Monte Carlo theorem. In this technique, the prior distribution at time  $k$  can be factorized to update the particles and their weights for the next time step, as follows:

$$\begin{aligned} q(x_{0:k}|y_{0:k}) &= q(x_k|x_{0:k-1}, y_{0:k})q(x_{0:k-1}|y_{0:k-1}) \\ &= q(x_0) \prod_{i=1}^k q(x_i|x_{0:i-1}, y_{0:i}) \end{aligned} \quad (3.29)$$

$$\begin{aligned} p(x_{0:k}, y_{0:k}) &= p(x_k, y_k, x_{0:k-1}, y_{0:k-1}) \\ &= p(y_k|x_k, x_{0:k-1}, y_{0:k-1})p(x_k|x_{0:k-1}, y_{0:k-1})p(x_{0:k-1}, y_{0:k-1}) \\ &= p(y_k|x_k)p(x_k|x_{k-1})p(x_{0:k-1}|y_{0:k-1}) \end{aligned} \quad (3.30)$$

To update the weight, we can use the definition of importance weight  $w(\cdot)$  in terms of the importance sampling.

$$w(x_{0:k}) = \frac{p(x_{0:k}, y_{0:k})}{q(x_{0:k}|y_{0:k})} \quad (3.31)$$

The equations (3.29), (3.30) and (3.31) are combined to obtain a recursive expression for the importance weight:

$$w(x_{0:k}) = w(x_{0:k-1}) \frac{p(y_k|x_k)p(x_k|x_{k-1})}{q(x_k|x_{0:k-1}, y_{0:k})} \quad (3.32)$$

If we assume that  $q(x_k|x_{0:k-1}, y_{0:k}) = q(x_k|x_{k-1}, y_k)$ , the update step can be simplified as:

$$\begin{aligned} x_k^i &\sim q(x_k|x_{k-1}^i, y_k) \\ w_k^i &= w_{k-1}^i \frac{p(y_k|x_k^i)p(x_k^i|x_{k-1}^i)}{q(x_k^i|x_{k-1}^i, y_k)} \end{aligned} \quad (3.33)$$

where  $i \in [1, N]$  is the sequential number of  $N$  particles. The sequential importance sampling offers an approach to update the state vector and the importance weights, however, this method has some obvious shortcomings. The importance function form causes the augmentation of variance of importance weights, which means that the normalized importance weights are approximated to zero. The observer will become unstable as  $k$  increase due to the discrepancy between the weights. This phenomenon is defined as a degeneracy problem. To avoid few particles have significant weight and diverge the filter, an effective solution was found in the resampling method.

### 3.5.2 Sequential importance resampling (SIR)

The sequential importance resampling algorithm (SIR) can be considered as the extension of sequential importance sampling (SIS), the state transition distribution takes place of the proposed distribution  $q(x_k|x_{k-1}, y_k)$  at every iteration and resampling is modified at the entire operation steps. A simple way to express the reduced update equations is given by:

$$\begin{aligned} x_k^i &\sim p(x_k|x_{k-1}^i) \\ w_k^i &\propto p(y_k|x_k^i) \end{aligned} \quad (3.34)$$

Resampling is concentrated on the selection of new particles position and weights, nevertheless it engenders some other disadvantages. The proposal distribution is then not relied on the observation  $y_k$ , its influence is not considered in the state estimate process. Otherwise, during a resampling period, large weight particles are drawn with higher probability than the small weights, the so-called sample impoverishment problem could reduce the diversity of the particles. The resampling step introduces much more computation load into the filter operation cost.

An appropriate choice of resampling method relating to the system is able to reduce the complexity of calculation and improve the quality of resampling for importance weights in the corresponding system design. Several methods are discussed in some literature. Typically, multinomial resampling [Gordon 1993], residual resampling [Liu 1998], stratified resampling [Doucet 2001] [Kitagawa 1996], systematic resampling [Kitagawa 1996] [Arulampalam 2002] are some common encountered means of resampling. The choice of resampling schema and comparison of performance will be elaborated in the section of design of observers which is suitable for our requirements of system frame.

### 3.5.3 Particle filter algorithm

To summarize the theorem of particle filter, which is also called bootstrap filter in some literatures, the algorithm includes three principal step: initialization, importance sampling and

resampling. In the part of importance sampling step, the state vector and importance weights are updated at each iteration. Resampling process is implemented to avoid the degeneracy problem. Hence, the particle filter algorithm is concluded as following recursive steps:

1. Initialization,  $k = 0$  : for  $i = 1, \dots, N$ ,
  - Sample  $x_0^i$  from a prior density  $p(x_0)$ .
  - Set weights  $\omega_0^i = \frac{1}{N}$ .
2. Importance sampling: at time  $k \geq 1$ , for  $i = 1, \dots, N$ ,
  - Sample  $x_k^i \sim q(x_k | x_{k-1}^i, y_k)$ .
  - Compute the weights  $\tilde{\omega}_k^i = \tilde{\omega}_{k-1}^i \frac{p(y_k | x_k^i) p(x_k^i | x_{k-1}^i)}{q(x_k^i | x_{k-1}^i, y_k)}$
  - Normalise the weights  $\omega_k^i = \frac{\tilde{\omega}_k^i}{\sum_{i=1}^N \tilde{\omega}_k^i}$
3. Resampling: at time  $k \geq 1$ , for  $i = 1, \dots, N$ , if  $N_{eff} < n_k$ 
  - Resampling particles  $\tilde{x}_k^i$  from the  $x_k^i$  according to the weights  $\omega_k^i$ .
  - Set  $\omega_k^i = \frac{1}{N}$ .

## 3.6 Conclusion

This chapter denotes a summary of the linear/nonlinear observation techniques for the dynamics systems where it is unrealistic to employ all the necessary sensors. Some essential measurement sensors are limited by technical reasons as well as the expense budget in the designed system. Therefore, some statistical theorems are intervened to find an effective solution of estimating the underlying system state perturbed by noise.

To give an explicit observer design of a system, a mathematical model should be precise to describe the entire system. This model needs overall consideration of the system features to avoid the potential observer divergence in real applications. The state variables should give an estimate of the actual state of the considered model which is able to be expressed as a state-space representation. In order to identify the system model, the linear model and nonlinear model are separately introduced to describe two general cases of dynamics system. The observability analysis has to be verified in the scheme of observer design. The observability of linear system is easy to be insured with observation matrix, while the observability of nonlinear system is defined by local observability with intervention of Lie derivative.

Especially in this chapter, the Kalman filter and particle filter are proposed to solve the estimation problem applied respectively to linear and nonlinear system. The Kalman filter describes a recursive solution to the linear system. However in real situations, the physical model maybe change to nonlinear manner, another extension form of Kalman filter with linearization of the nonlinear state and observation can provide an acceptable estimate performance, it is appointed to be extended Kalman filter. The drawback of extended Kalman filter is mainly reflected on the “first-order” linearization of the nonlinear system, on account of the existence of Jacobian matrices and the deviation of differential calculus. Based on these shortcomings, we introduce the particle filter, which using Bayesian approach. The particle filter is available for highly nonlinear approximations and non-Gaussian noise disturbing the system. The elements

of sequential importance sampling (SIS) are deduced with a brief description of Monte-Carlo method. To avoid the degeneracy problem, the sequential importance resampling (SIR) can be considered to be the variant form of SIS, which the state transition distribution is modified according to the resampling operation at every iteration.

The application of these different observers will be integrated with the vehicle and tire dynamics model in the entire contribution of this thesis. The Kalman filter and particle filter will be embedded in the real-time system and the performance will be compared through copious experimental validations.

# Vehicle vertical dynamics estimation on banked road

---

## Contents

---

<b>4.1</b>	<b>Introduction</b>	<b>55</b>
<b>4.2</b>	<b>Analysis of existing method limitation</b>	<b>57</b>
4.2.1	Validation of existing vertical tire model	57
4.2.2	Analysis of model limitation	59
<b>4.3</b>	<b>Vertical tire force model on banked road</b>	<b>60</b>
4.3.1	Acceleration measurement	61
4.3.2	Roll dynamics of the vehicle body	61
4.3.3	Pitch angle calculation	64
4.3.4	Vertical force modeling	65
<b>4.4</b>	<b>Observer design <math>O_{F_z}</math></b>	<b>71</b>
4.4.1	Discrete time state-space representation	71
4.4.2	Observability analysis	73
<b>4.5</b>	<b>Simulation validation</b>	<b>74</b>
4.5.1	Simulation environment	74
4.5.2	Observer regulation	74
4.5.3	Validation test	76
<b>4.6</b>	<b>Conclusion</b>	<b>84</b>

---

## 4.1 Introduction

Vehicle dynamics is concerned with the movement of vehicles. Generally, the vehicle movements are summarized with braking, accelerating and cornering. The static wheel load is generated by the earth gravity force. The braking and accelerating movements cause the longitudinal load transfer between front wheels and the rear ones, the pitch angle reflects this phenomenon along the longitudinal axis. Cornering movement is generated by the steering wheel angle input from driver and the lateral acceleration affects the transverse load transfer on each side of the vehicle.

Knowing the distribution of vertical load at each wheel is essential for the vehicle handling, helping to improve the road safety, especially reducing the rate of occurrence of vehicle rollover accident. As far as we know, longitudinal and lateral dynamics also depend on the input variables that comprise vehicle vertical force. However, the vertical force at each tire is not simply distributed by average, they are influenced by the center of gravity, suspension characteristics, road geometry and so on.

Besides the fact that the complex environment elements yield the difficulty to the modeling, nowadays there is no low cost sensor which is capable to offer the effective measurement of the load developed on each wheel. The wheel force transducer has recently been purchased by some laboratory or automobile industry research centers for the aim of validation and experimental test. Because of its stiff price, these sensors are impossible to be equipped with production cars. Therefore, it is necessary to use other techniques to obtain this fundamental information which may be required by some advanced vehicle control or stability systems.

Since the precise vertical force can give impact on the determination of other variables and the performance of stability control system, plenty of researches are exploited on this issue. Some books about vehicle dynamics present some vertical force models, in [Milliken 2003], the tire force is dealing with steady-state operating conditions, the lateral and longitudinal load transfer are considered in the modeling, the roll term is added to the formula. In [Reza 2007], author provides several conditions of load variation, the parked car on level pavement, the parked car on an inclined road, the wheel load is affected by the decomposition of gravity on the inclined road. Similarly, the wheel load is constructed with parked car on a banked road. [Imine 2008] deals with a heavy vehicle model with an appropriate wheel road contact model in order to estimate vertical forces using sliding mode observers. The influence of the road profile is applied as an input of the evaluation of wheel loads. [Wenzel 2006] proposes to use DEKF (Dual extended Kalman filter) to estimate a series of vehicle dynamics parameters that comprise of vertical force. The load distribution is calculated due to the longitudinal and lateral acceleration. Except in some works considering static wheel load distribution, the suspension model is also considered having an essential influence on the tire vertical force behavior. [Prem 1998] investigate a “quarter-truck” models that feature complex non-linear multi-leaf steel springs, air springs, and hydraulic dampers to evaluate the dynamic wheel load performance. [Kiencke 2005] and [Doumiati 2009] couple the longitudinal and lateral dynamics to give a precise vertical tire force model on flat road. Nevertheless, all these contributions are based on the basic hypothesis, the road geometry is neglected which means that the vehicle is always on the ideal plane road. [Menhour 2011] estimates the road bank angle as the input variable of the sliding mode observer, which is used as fundamental input variables in the vehicle stability control strategy. [Ryu 2004] and [Tseng 2001] concentrate on the estimation of the road bank angle and the analysis of the influence on vehicle dynamics, however, the bank angle is not considered directly in the vehicle vertical tire force models. In [Yu 2013], they present a method of bank angle estimation applied to bus rollover prediction. A 2-DOF vehicle model and Dugoff tire model are used, however the vertical forces that are necessary in the Dugoff tire model are constructed with the effect caused by roll motion of sprung mass in the derivation of wheel load transfer equations.

In this chapter, we will first focus on the analysis of the limit of existing methods that developed for vertical load distribution. Actually in real environment, the road bank angle may lead to higher accident rate of rollover during a curved road. Hence, a vertical tire force model taking into account the constraints of road geometry condition is quite necessary in such case. Our objective is to provide an exact estimation of vertical tire force and relevant influences on the vehicle dynamics instead of giving a precise road bank angle estimation, differently of other literatures, the road bank angle will not appear explicitly in our formulations of the mathematical equations. The motivation of this section is the fact that we could estimate vertical forces considering the environmental effect, what give more precision on other dynamic parameters/variables estimation, as described in the following chapters.

The organization of this chapter is presented as follows: section 2 validates the existing

model developed with an assumption of zero bank angle, analyzing its limitation on banked road. Section 3 concerns the analysis of the accelerometer and gyrometer outputs, the signals should be reconstructed since it contains a gravity term by the inclination of the sprung mass. Two new vertical force models are proposed with theoretical physical derivation, these equations are validated and compared with open-loop method. In section 4, we present an observer design aimed at estimating the vertical forces with Kalman filter. Section 5 presents various evaluations of different simulation tests, the performance is compared with figures and statistics report. Finally, it is the conclusion and some perspectives in the future work.

## 4.2 Analysis of existing method limitation

### 4.2.1 Validation of existing vertical tire model

The wheel vertical load is affected by various elements, in the commonly used model, the road geometry is neglected, roll and pitch dynamics motions are not considered. These assumptions are proposed to reduce the complexity of the vertical tire force model. [Kiencke 2005] introduces a vertical force model that contains two input variables: longitudinal and lateral acceleration ( $a_x$  and  $a_y$ ). When vehicle moves forward, the positive acceleration causes load shift from front to rear axle for the pitch motion of the vehicle body due to its inertia. On the contrary, the load shifts from rear to front axle during braking. The lateral acceleration gives rise to the load transfer from left side to the other side. A nonlinear formula expressing the vertical load distribution is given as follows:

$$\begin{aligned}
 F_{z11} &= \frac{1}{2}mg \frac{L_2}{L} - \frac{1}{2}ma_x \frac{h}{L} - ma_y \frac{L_2 h}{LE_1} + ma_x a_y \frac{h^2}{LE_1 g}, \\
 F_{z12} &= \frac{1}{2}mg \frac{L_2}{L} - \frac{1}{2}ma_x \frac{h}{L} + ma_y \frac{L_2 h}{LE_1} - ma_x a_y \frac{h^2}{LE_1 g}, \\
 F_{z21} &= \frac{1}{2}mg \frac{L_1}{L} + \frac{1}{2}ma_x \frac{h}{L} - ma_y \frac{L_1 h}{LE_2} - ma_x a_y \frac{h^2}{LE_2 g}, \\
 F_{z22} &= \frac{1}{2}mg \frac{L_1}{L} + \frac{1}{2}ma_x \frac{h}{L} + ma_y \frac{L_1 h}{LE_2} + ma_x a_y \frac{h^2}{LE_2 g}.
 \end{aligned} \tag{4.1}$$

A slalom test is performed to analyze the property of the above equations with experimental data. The maneuver time history of the slalom test is given in Figure 4.1. The initial speed reaches to  $50km/h$ , following with a slalom maneuver with the acceleration  $-5m/s^2 < a_y < 5m/s^2$  at constant speed  $40km/h$ . The slalom test with high value of lateral acceleration is able to create more lateral load transfer from one side to the other side.

As the result shown in Figure 4.2, the vertical force at front wheels during the slalom period, the load shift from right tire to left tire can make the left tire vertical force reaches up to  $6500N$ . We can conclude that the calculated vertical force matches well with the measurement of wheel force transducers (This sensor for the measurement of wheel forces and moments in three dimensions will be presented in the section of description of experimental vehicle). According to the analysis of the results in this figure, we conclude that, the open-loop model proves its efficiency without using observer technique. Especially in the fast transient period, for instance during the time interval  $7s < t < 8s$ , the red line representing model values can tightly follow the measurement in blue.

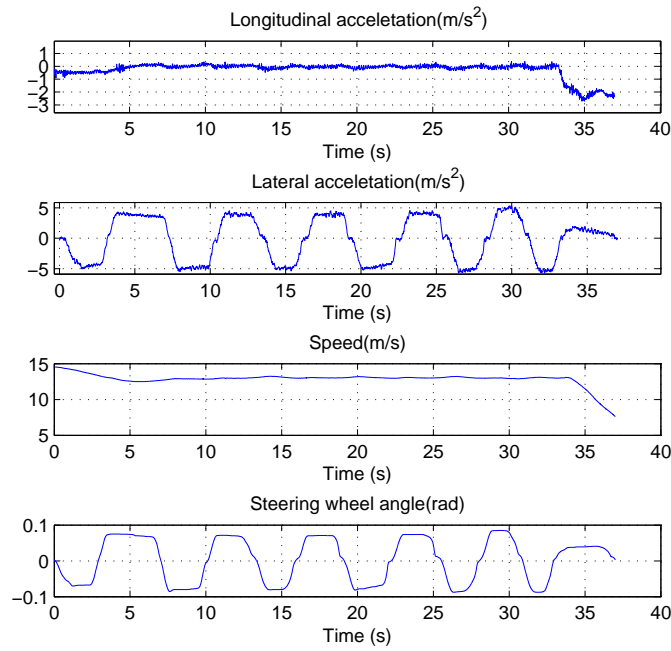


Figure 4.1: Maneuver time history of the slalom test

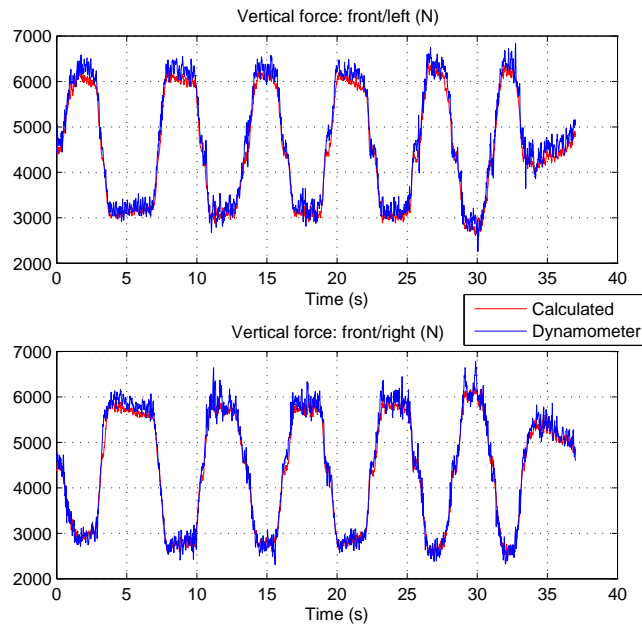


Figure 4.2: Vertical forces at front wheels calculated with open-loop

### 4.2.2 Analysis of model limitation

As we use the open-loop method to obtain the wheel load, we can find some obvious limitation in the figure, the difference between estimates and measurements, in some parts of the trajectory, can be explained by the negligence of lateral load transfer accompanied by the lateral movement, in addition, the tire camber angle and suspension kinematic characteristic is not considered in this model. Consequently, the mentioned open-loop method reflects some limitations because of these complicated and unconsidered variables. In particular, the interest of the environment effect is not presented in this sort of model. Therefore, we will analyze the variation of road geometry with some simulation tests, particularly for the road bank angle.

To verify such phenomenon described in the above paragraph, we will introduce some simulation tests. We propose to use vehicle simulation software PROSPER/CALLAS, developed by OKTAL society, it is an advanced vehicle simulation software that has been validated by many research laboratories and automobile industry. The detailed configuration of the simulator will be explained in the section 4.5.1. The following test uses the simulator to consider the effects of the variation of the road geometry. Here we will provide a test during a double lane change (DLC) mode. The initial speed is about  $70\text{km/h}$ , the road bank angle is set at 10%. Analyzing Figures 4.3 and 4.4, that show the front wheel vertical force, we can conclude that the model bias is significant. The model is not valid any more, during the lane change maneuver, the deviation between the simulator output and the calculated vertical force is important. It is noted that in the modeling, the suspension kinematic and roll dynamics are ignored. Furthermore, during the period of keeping moving straight, even though there is no dynamics movement along the longitudinal and lateral axis, there is a constant shift between the values. This phenomenon could be explained by the lack of terms that contains the road geometry disturbance.

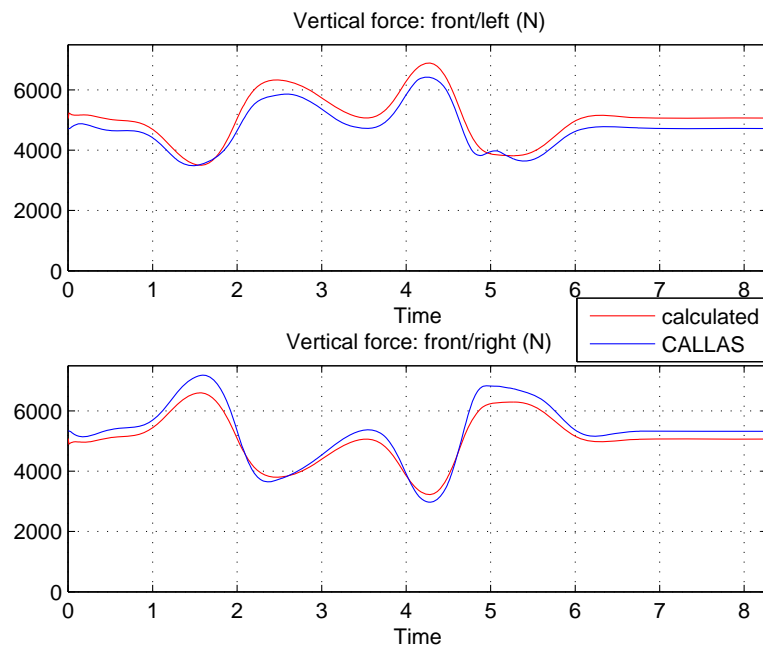


Figure 4.3: DLC test with 10% bank angle: vertical force at front wheels

The road bank angle as one of the essential effect of road geometry that has a direct influence

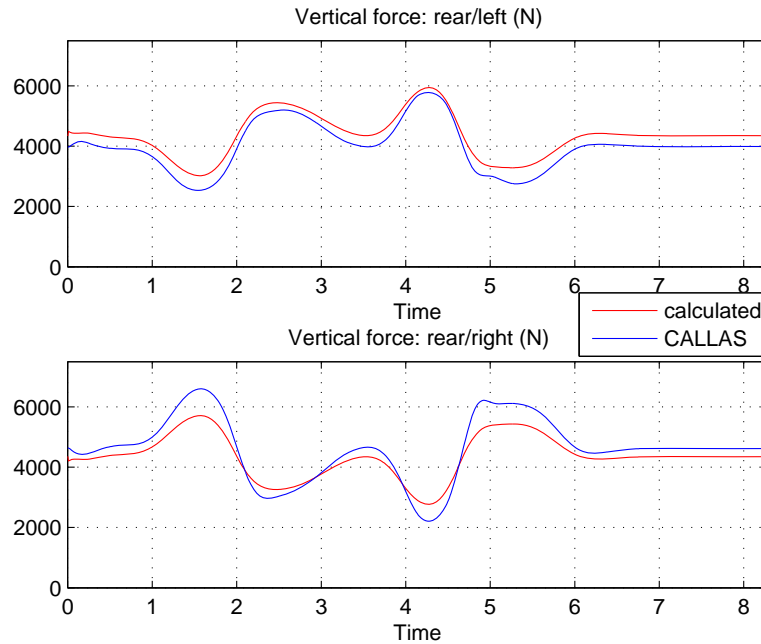


Figure 4.4: DLC test with 10% bank angle: vertical force at rear wheels

on vehicle dynamics and lateral accelerating measurement. If we understand the impact of road bank angle experienced by the vehicle on the vehicle stability controller, it is benefit to minimize the estimation deviation and improve the system accuracy. As far as we know, the suspension roll angle and road bank angle are different. The road angle is the geometric characteristic of the road external environment, on the contrary, the suspension roll angle is produced by road bank angle and the suspension deflection, affected by vehicle dynamics. Nevertheless, the lateral accelerometers are fixed on the vehicle body frame, these two variables are not distinguished.

Therefore, a lot of researchers develop the estimation method to obtain this bank angle, separating it with suspension roll angle [Tseng 1999] [Kawashima 2010] [Dahmani 2010]. Compared with existing contribution, our objective is to find an effective way to obtain the vehicle roll angle, the precise value of road bank angle is not the focus of our research intention, hence the approach of complex rotation of the vehicle frame given by the Euler angles about vehicle-frame-fixed axes could be avoided.

### 4.3 Vertical tire force model on banked road

The road disturbance can influence directly on vehicle dynamics, since vehicle is no longer running on a quasi-flat road, certain effects on the acceleration measurements, including the gravity component, may lead to incorrect estimation of the vehicle states or even misleading the vehicle stability system. The gyro sensor similarly is affected by the banked road. Almost all the mathematical models designed for the flat road is not suitable for the current situation. Hence, we need to exploit more robust dynamics model with the consideration of road perturbation. Before presenting the developed vertical force formulation, we would like to analyze the acceleration, roll and pitch dynamics components in the first instance.

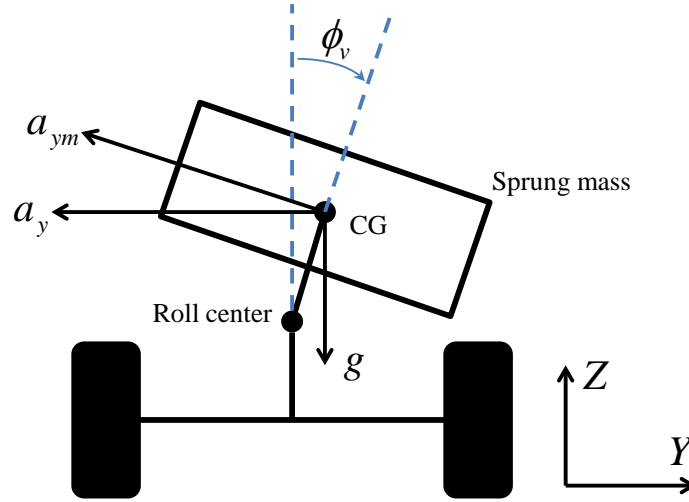


Figure 4.5: Lateral acceleration measurement on flat road

### 4.3.1 Acceleration measurement

The lateral acceleration plays a fundamental role in affecting the lateral load transfer on the wheel level. Let's consider the figure 4.6, the output of accelerometer on quasi-flat road attached to the CG of vehicle sprung mass contains the gravity component and the acceleration force component, it can be formulated as:

$$\begin{aligned} a_{ym} &= a_y \cos \phi_v + g \sin \phi_v \\ a_{zm} &= -a_y \sin \phi_v + g \cos \phi_v \end{aligned} \quad (4.2)$$

when the vehicle roll angle  $\phi_v$  is small, the lateral acceleration and vertical acceleration could be approximated by  $a_{ym} = a_y$  and  $a_{zm} = g$ . The illustration of the decomposition of lateral acceleration is denoted in Figure 4.5.

In the case of the modeling on the banked road in Figure 4.6, the roll angle contains the suspension roll angle and road bank angle, hence  $\phi_v$  in equation (4.2) should be replaced by  $\phi = \phi_v + \phi_r$ . The acceleration measurement can be updated by the following equations employed in [Kawashima 2010] [Piyabongkarn 2009]:

$$\begin{aligned} a_{ym} &= a_y \cos \phi + g \sin \phi \\ a_{zm} &= -a_y \sin \phi + g \cos \phi \end{aligned} \quad (4.3)$$

### 4.3.2 Roll dynamics of the vehicle body

The roll motion of the vehicle body is mainly generated due to the lateral inertial force caused by the lateral maneuver. The force acts at the center of gravity, it is assumed to create a roll moment in terms of the roll axis, called roll center. The center of roll motion is distinguished from the center of gravity with respect to the vehicle body. The roll center is in the transverse vertical plane through any pair of wheel center and equidistant from them. The determination of the center position is due to the suspension kinematic and vehicle sprung mass distribution.

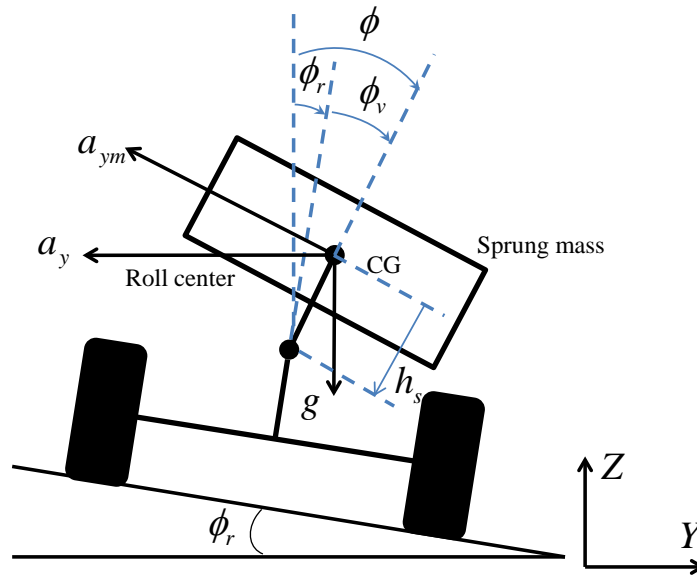


Figure 4.6: Lateral acceleration measurement and roll dynamics on banked road

Usually, the roll center changes according to the vehicle movement that defects on the suspension deflection, here we assumed that the vehicle roll center keeps constant and it is coincident with the center of gravity [Milliken 2003].

Considering the roll dynamics in Figure 4.6, a differential equation that based on the torque balance can be summarized as follows:

$$I_{xx}(\ddot{\phi}_v + \ddot{\phi}_r) = -C_r(\dot{\phi}_v + \dot{\phi}_r) - K_r\phi_v + m_s h_s a_y \cos(\phi_v + \phi_r) + m_s h_s g \sin(\phi_v + \phi_r) \quad (4.4)$$

Where  $I_{xx}$  is the inertia moment of the sprung mass  $m_s$  with respect to the roll axis,  $C_r$  and  $K_r$  denote respectively the total damping and spring coefficients of the roll motion of the vehicle system,  $h_s$  is the height of the sprung mass about the roll axis. To simplify this model, we suppose that the mass of four wheels and part of the mass of the suspension system is not intervened in such model. According to the description of the decomposition of the measured lateral acceleration  $a_{ym} = a_y \cos \phi + g \sin \phi$  in previous subsection, the equation 4.4 can be simplified as:

$$I_{xx}(\ddot{\phi}_v + \ddot{\phi}_r) + C_r(\dot{\phi}_v + \dot{\phi}_r) + K_r\phi_v = m_s h_s a_{ym} \quad (4.5)$$

Presented in plenty of research related to vehicle roll stability control or rollover prevention system, vehicle roll angle is a fundamental input variable as required in these sorts of systems. Therefore, some studies propose assorted methods to calculate or estimate the vehicle roll angle, [Ryu 2002] uses GPS signals to estimate the roll and pitch attitude angles of a vehicle when the vehicle moves on the ground. [Kawashima 2009] and [Carlson 2003] respectively present the roll angle intervened method to realize the rolling stability control and rollover prevention systems for passenger cars. Except for the integration of the roll rate to estimate the roll angle, [Hac 2004b] provides an effective way to obtain the roll angle both under transient and steady-state cornering maneuvers performed on smooth road.

The suspension relative position sensors offer a simple approach to access these variables, which is also not sensitive to the vehicle parameters variations. At some extent, this estimation method of the vehicle roll angle is robust to the road disturbance, especially with bank angle. [Hac 2004b] proposes a roll angle model expressed with suspension deflection, with which the pitch dynamics affection is decoupled from the roll motion. The suspension mechanical part compressed and extended with respect to the lateral maneuver during the turning. The model equation is given as:

$$\begin{aligned}\phi &= \frac{\Delta_{11} - \Delta_{12} + \Delta_{21} - \Delta_{22}}{2E} - \frac{ma_{ym}h}{k_{tr}} \\ &= \frac{(\rho_{11} - \rho_{s1}) - (\rho_{12} - \rho_{s1}) + (\rho_{21} - \rho_{s2}) - (\rho_{22} - \rho_{s2})}{2E} - \frac{ma_{ym}h}{k_{tr}} \\ &= \frac{\rho_{11} - \rho_{12} + \rho_{21} - \rho_{22}}{2E} - \frac{ma_{ym}h}{k_{tr}}\end{aligned}\quad (4.6)$$

where  $\Delta_{ij}(i, j = 1, 2)$  is the suspension deflection at each wheel.  $E$  is the effective track's width. Usually the relative position sensors are not facile to install on the suspension, hence they could be replaced by the chassis height sensors at each corner,  $\rho_{ij}(i, j = 1, 2)$  is the suspension position sensors,  $\rho_{s1}$  and  $\rho_{s2}$  are respectively the initial suspension positions at static steady state. The evaluation test is given with simulation data, the road bank angle is set at 10% as the same as the previous DLC test for the vertical force. The performance of this model is illustrated in Figure 4.7.

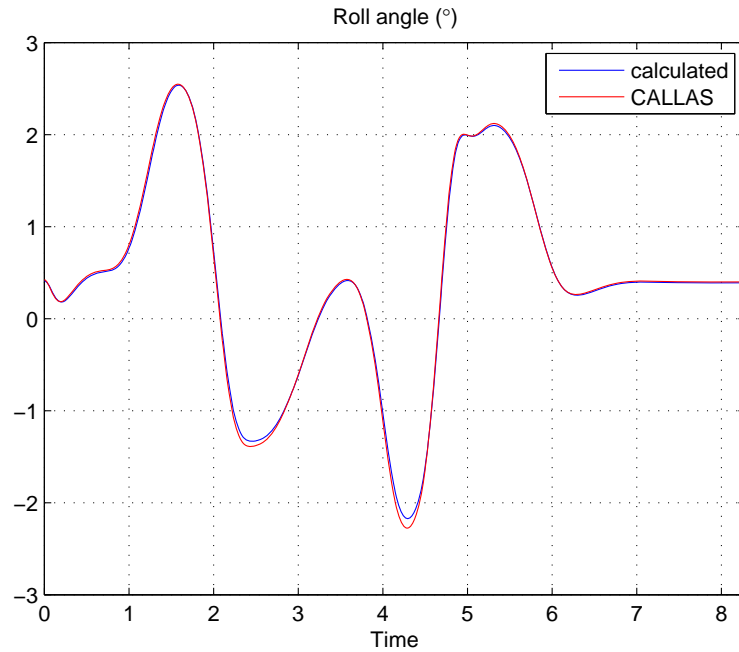


Figure 4.7: Comparison of the calculated roll angle from suspension deflection and the simulation with 10% bank angle

In practice situation, the term  $\frac{ma_{ym}h}{k_{tr}}$  can be considered to be constant, since it has weakly influence in the equation. Therefore, we could multiply a factor within this formulation to take

place of this additional term. We can conclude from the figures that the calculation related to the suspension deflection denotes satisfying result. The computed roll angle is quite close to the simulation reference both during the transient period ( $0s < t < 6.5s$ ) and the steady state period ( $6.5s < t < 8s$ ) where the roll angle is not equal to 0 due to the disturbance of road bank angle. The model performance is limited on rough road and large roll angle, however the efficacy and facility characteristics of this model are interesting for us.

### 4.3.3 Pitch angle calculation

Concerning the vehicle pitch angle with respect to the longitudinal axis, is also one of the essential variables in vehicle dynamics control and suspension kinematic design. The further development of electronic components requires a precise value that may be obtained using estimate method due to economical reasons. Some researchers develop certain methods to estimate the vehicle pitch angle. [Oh 2013] employs a cost-effective six-dimensional inertial measurement unit. They compare the performance of the pseudointegral estimation and the kinematic angle observer form. [Eric Tseng 2007] roughly estimates the vehicle pitch angle using the sensors which are available for electronic stability control, the expression of the roll angle is presented in this article, the lateral velocity is neglected due to the current available sensors on production vehicles. [Ding 2006] explains an estimation method of vehicle pitch angle applying the measurement of longitudinal and vertical acceleration and vehicle velocity.

Similarly to the roll angle calculation, we can also deduce the pitch angle calculation using the suspension deflection. Accelerating and braking maneuvers make the suspension deflection compress and extend differently at front and rear wheels. To distinguish from the roll angle calculation, the effect of weight distribution should be considered especially in the pitch angle calculation, because the center of mass is usually equidistant from the left and right wheels. In most cases of the weight distribution of the front-driven car, front-engine design has the advantage of permitting a more practical engine-passenger-baggage layout, hence the weight distribution is designed between “40/60” and “35/65” (written in the form  $X/Y$ , where  $X$  is the percentage of load distribution at front axle, and  $Y$  is the percentage at rear axle). In other words, the vehicle inclination angle at static state is not equal to zero, this angle  $\theta_s$  is represented in Figure 4.8.

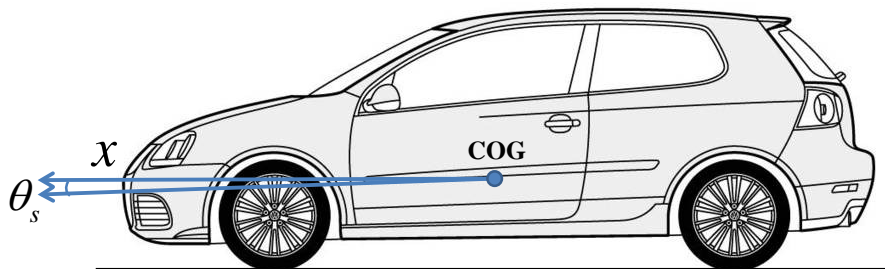


Figure 4.8: Vehicle lateral view

According to the vehicle body coordinate frame, the longitudinal axis is parallel to the horizontal line and it is perpendicular to the gravity. The inertial measurement unit offers the pitch angle that includes the initial statics pitch angle  $\theta_s$ , hence it is necessary to add a term

that express this phenomenon. The pitch angle calculation is formulated as follows:

$$\begin{aligned}
 \theta &= \frac{\Delta_{11} - \Delta_{21} + \Delta_{12} - \Delta_{22}}{2(L_1 + L_2)} - \frac{ma_{xm}h}{k_{tr}} + \theta_s \\
 &= \frac{(\rho_{11} - \rho_{s1}) - (\rho_{21} - \rho_{s2}) + (\rho_{12} - \rho_{s1}) - (\rho_{22} - \rho_{s2})}{2(L_1 + L_2)} - \frac{ma_{xm}h}{k_{tr}} + \theta_s \\
 &= \frac{(\rho_{11} - \rho_{21} + \rho_{12} - \rho_{22}) + 2(\rho_{s2} - \rho_{s1})}{2(L_1 + L_2)} - \frac{ma_{xm}h}{k_{tr}} + \theta_s
 \end{aligned} \tag{4.7}$$

where  $L_1$  and  $L_2$  are the distance between center of gravity and front/rear axle.  $\rho_{ij}(i, j = 1, 2)$  is the suspension position sensors,  $\rho_{s1}$  and  $\rho_{s2}$  are respectively the initial suspension positions at static steady state. A DLC test is simulated by the simulator CALLAS, the evaluation of the model's equation is validated with the configuration of 10% road bank angle. The comparison of calculated pitch angle in red line and the simulator software output in blue line is given out in Figure 4.9.

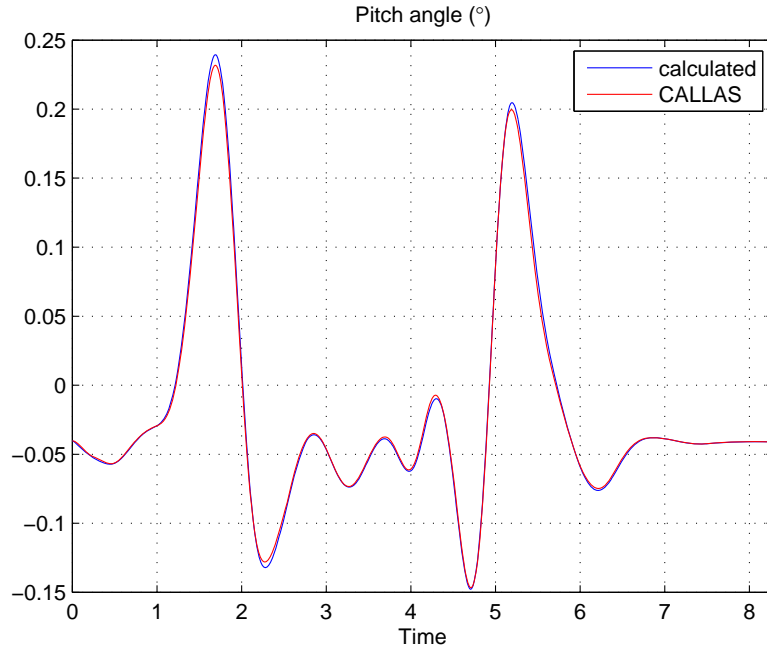


Figure 4.9: Vehicle model on inclined road

The result of the pitch angle presents that the model is valid even with accelerating or braking maneuver. The method employing suspension deflection could effectively give a precise and sensible description of the pitch motion with road disturbance. This model is operative with the assumption that the vehicle roll and pitch dynamics are neglected, besides the road pavement is smooth since the suspension deflection is directly affected by the condition of road surface. The calculated result may not be accurate where the road is rough.

#### 4.3.4 Vertical force modeling

In this section, we will introduce the vertical force modeling developed in our work to supply a precise estimation where the road is no longer flat. Ignoring the suspension dynamics and

coupling of pitch and roll dynamics, the vertical force model is firstly deduced in the following parts.

From the vehicle load distribution illustrated in Figure 2.16(a), and according to the torque balance about the wheel ground contact point of the rear axle, we have:

$$F_{z1}L = mgL_2 - ma_x h \quad (4.8)$$

where  $F_{z1}$  is the vertical load on the front tires and  $m$  is the vehicle mass. In addition,  $g$  and  $a_x$  can be measured respectively by the IMU (Inertial Measurement Unit) as  $a_{zm}$  and  $a_{xm}$ , the above formulation can be replaced by:

$$F_{z1}L = ma_{zm}L_2 - ma_{xm}h \quad (4.9)$$

then, we have:

$$F_{z1} = m\left(\frac{L_2}{L}a_{zm} - \frac{h}{L}a_{xm}\right) \quad (4.10)$$

Actually, it is assumed that not only the sprung mass but also the whole vehicle including sprung mass and unsprung mass rotate around the front wheel contact point. That is the reason why the equations above use the complete vehicle mass instead of the vehicle body mass. Hence, in order to decouple the front and rear axles, a virtual mass  $m^*$  is used. We firstly consider the case of the front axle, the virtual mass can be derived as:

$$m_f^* = \frac{F_{z1}}{a_{zm}} = m\left(\frac{L_2}{L} - \frac{h}{L} \frac{a_{xm}}{a_{zm}}\right) \quad (4.11)$$

The deduced virtual mass takes into account of the mass transfer during accelerating. Consequently, this mass will be used as a coupling term between longitudinal and lateral dynamics. The subsequent explanation of vehicle vertical tire force derivative process using physical model employs this vehicle virtual mass.

### **Method 1:**

Analyzing the front part of vehicle model located on a banked angle, the analysis of forces and moments components is represented in Figure 4.10.

Applying the torque balance equations on the vehicle body around the virtual roll axis, we can get the equations:

$$\begin{cases} F'_y = m_f^* a_y \cos\phi + m_f^* g \sin\phi \\ F'_z = -m_f^* a_y \sin\phi + m_f^* g \cos\phi \\ I_{xxf}(\ddot{\phi}_v + \ddot{\phi}_r) = M + F'_y h_s \end{cases} \quad (4.12)$$

where  $F'_y$  and  $F'_z$  are respective the lateral and vertical force at the point of roll center.  $M(C_r \dot{\phi}_v + K_r \phi_v)$  is treated as the summarized rotation force generated due to the roll motion of suspension and tires,  $\dot{\phi}_r$  is omitted. Combining the acceleration measurement in 4.2, torque balance equations are transformed as:

$$\begin{cases} F'_y = m^* a_{ym} \\ F'_z = m^* a_{zm} \\ I_{xxf}(\ddot{\phi}_v + \ddot{\phi}_r) = M + F'_y h_s \end{cases} \quad (4.13)$$

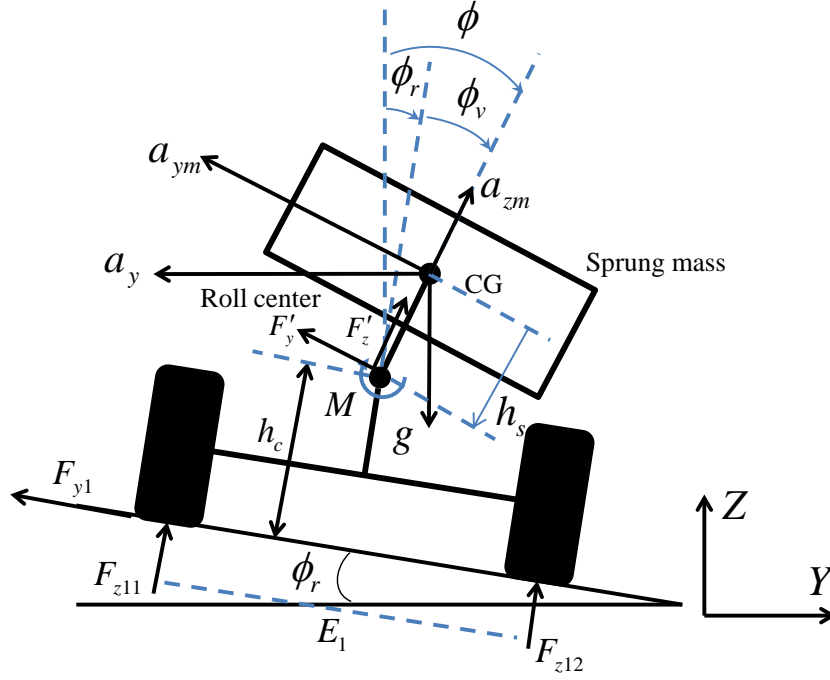


Figure 4.10: Vehicle and suspension model on banked road

As far as the torque balance is applied to the contact point of vehicle wheel, we can obtain the lateral and vertical force related to the contact point of the front wheels.

$$\begin{cases} F_{z11} + F_{z12} = F'_y \sin \phi_v + F'_z \cos \phi_v \\ F_{y1} = m_f^* (a_{ym} \cos \phi_v - a_{zm} \phi_v) \\ M = F_{y1} h_c + \frac{E_1}{2} (F_{z11} - F_{z12}) \end{cases} \quad (4.14)$$

In this case, we take some assumptions to simplify the model [Song 2013]. The vehicle mass is considered as the same as the vehicle sprung mass, the affection of the suspension and tire is omitted here.  $F_{y1}$  can be simplified as the same as  $F'_y$ , equaling to  $m_f^* a_{ym}$ . In addition,  $\ddot{\phi}_v$  and  $\ddot{\phi}_r$  are considered very small, which could be ignored. Consequently, the term  $I_{xxf}(\ddot{\phi}_v + \ddot{\phi}_r)$  representing the moment of inertia of the sprung mass could be approximated to zero due to the negligence of  $\ddot{\phi}_v$  and  $\ddot{\phi}_r$ . The vertical force of front wheels is able to be derived basing on the above assumptions. The final deduced vertical force expression is described as:

$$\begin{aligned} F_{z11} &= \frac{1}{2} m_f^* (a_{ym} \sin \phi_v + a_{zm} \cos \phi_v) - m_f^* a_{ym} \frac{h_s + h_c}{E_1} \\ F_{z12} &= \frac{1}{2} m_f^* (a_{ym} \sin \phi_v + a_{zm} \cos \phi_v) + m_f^* a_{ym} \frac{h_s + h_c}{E_1} \end{aligned} \quad (4.15)$$

To make the equations more clear,  $a_{ym} \sin \phi_v + a_{zm} \cos \phi_v$  is replaced by  $a_z$ :

$$a_z = a_{ym} \sin \phi_v + a_{zm} \cos \phi_v \quad (4.16)$$

Taking place of  $m_f^*$  in equation 4.11 and by analogy for the other rear wheels, vertical force at

four wheels can be formulated as:

$$\begin{aligned}
F_{z11} &= \frac{1}{2}ma_z \frac{L_2}{L} - \frac{1}{2}ma_{xm} - ma_{ym} \frac{L_2 h}{LE_1} + m \frac{a_{xm} a_{ym}}{a_z} \frac{h^2}{LE_1} \\
F_{z12} &= \frac{1}{2}ma_z \frac{L_2}{L} - \frac{1}{2}ma_{xm} + ma_{ym} \frac{L_2 h}{LE_1} - m \frac{a_{xm} a_{ym}}{a_z} \frac{h^2}{LE_1} \\
F_{z21} &= \frac{1}{2}ma_z \frac{L_1}{L} + \frac{1}{2}ma_{xm} - ma_{ym} \frac{L_1 h}{LE_2} + m \frac{a_{xm} a_{ym}}{a_z} \frac{h^2}{LE_2} \\
F_{z22} &= \frac{1}{2}ma_z \frac{L_1}{L} + \frac{1}{2}ma_{xm} + ma_{ym} \frac{L_1 h}{LE_2} - m \frac{a_{xm} a_{ym}}{a_z} \frac{h^2}{LE_2}
\end{aligned} \tag{4.17}$$

### Method 2:

Vehicle roll motion does not directly appear in the first method, it is replaced by other form concerning lateral force applied to the roll center. The second method is based the representation of vehicle roll motion in the formulations. The sprung system activates a torque to vehicle body around the roll center corresponding to different roll angle  $\phi_v$ , which can be described by the following equation:

$$M = K_r \phi_v + C_r \dot{\phi}_v \tag{4.18}$$

Where  $C_r$  and  $K_r$  are respectively the total damping and spring coefficients of the roll motion of the vehicle system. The suspension kinematic movements generate additional force at the same time, but it is noted that these forces have no effect on the load transfer between left and right wheel.

Analyzing the physical model of vehicle simplified chassis and suspension in Figure 4.11, the Newton's third law of motion is applied to receive a torque balance from the suspension system in the opposite direction with respect to the wheel and axle force. The torque balance around the roll center is formulated as:

$$M + F_{z11} \frac{E_1}{2} - F_{z12} \frac{E_1}{2} + F_{y1} h_c = 0 \tag{4.19}$$

$F_{y1}$  is supposed to be calculated using vertical force, it is obvious that  $F_{y1} h_c$  is not significant compared with other parts in the equation. That reason allows  $F_{y1} h_c$  to be ignored, hence the above equations can be rewritten as:

$$F_{z12} - F_{z11} = \frac{2}{E_1} (K_r \phi_v + C_r \dot{\phi}_v) \tag{4.20}$$

The first method has the relations of tire force  $F_{z1}$ ,  $F_{z12}$ , lateral force  $F'_y$  and vertical force  $F'_z$  at the point of roll center as well as the vertical acceleration combined with measured acceleration and vertical acceleration.

$$\begin{cases}
F_{z11} + F_{z12} = F'_y \sin \phi_v + F'_z \cos \phi_v \\
F'_y = m_f^* a_{ym} \\
F'_z = m_f^* a_{zm} \\
a_z = a_{ym} \sin \phi_v + a_{zm} \cos \phi_v
\end{cases} \tag{4.21}$$

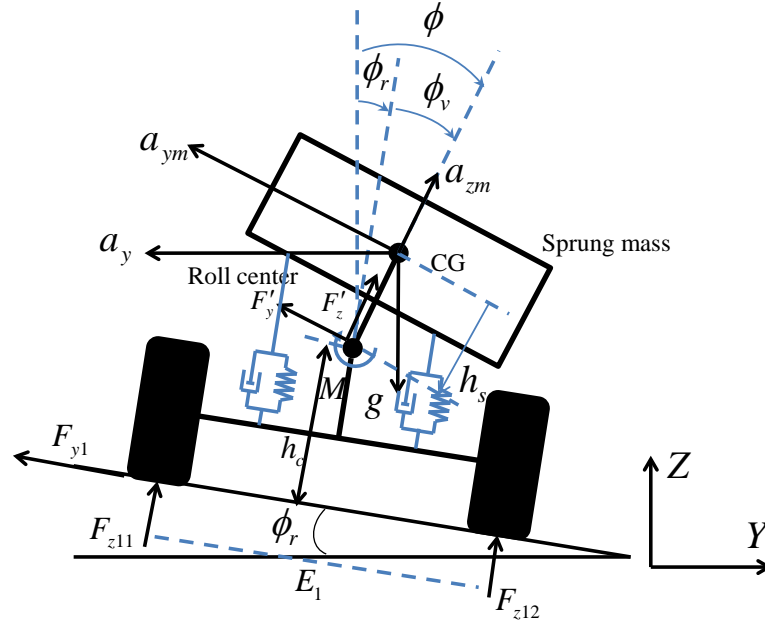


Figure 4.11: Vehicle and suspension model with banked angle

Finally, the vertical force at each wheel could be deduced by following expressions that contain vehicle roll motion:

$$\begin{aligned}
 F_{z11} &= \frac{1}{2}ma_z \frac{L_2}{L} - \frac{1}{2}ma_{xm} - \frac{K_r}{E_1}\phi_v - \frac{C_r}{E_1}\dot{\phi}_v \\
 F_{z12} &= \frac{1}{2}ma_z \frac{L_2}{L} - \frac{1}{2}ma_{xm} + \frac{K_r}{E_1}\phi_v + \frac{C_r}{E_1}\dot{\phi}_v \\
 F_{z21} &= \frac{1}{2}ma_z \frac{L_1}{L} + \frac{1}{2}ma_{xm} - \frac{K_r}{E_2}\phi_v - \frac{C_r}{E_2}\dot{\phi}_v \\
 F_{z22} &= \frac{1}{2}ma_z \frac{L_1}{L} + \frac{1}{2}ma_{xm} + \frac{K_r}{E_2}\phi_v + \frac{C_r}{E_2}\dot{\phi}_v
 \end{aligned} \tag{4.22}$$

#### 4.3.4.1 Analysis of two models with open-loop method

Before the step of observer design, it is necessary to validate the model with open-loop method. The precision of the model description can effectively improve the performance of the observer. In this section, the objective is to find an available model which can be employed with the road disturbance, particularly our research is focused on the road rank angle perturbations. We have presented the common vertical force model (so-called  $Fz_m$ ) with the formulation presented in equations (4.1) applying longitudinal and lateral acceleration, this model is assumed totally based on the hypothesis of flat road. The model designed for the condition of banked road disturbance ( $Fz_{m1}$ ) applies the torque balance to vehicle body around the virtual roll axis, the roll motion is not considered in this model, such model is deduced and denoted by the final expressions in equation (4.17). On the contrary, it is replaced by the lateral force and vertical force applied at the point of roll center. In order to introduce the kinematic roll motion in the model, we propose an overall model ( $Fz_{m2}$ ) considering the roll motion dynamics due to the lateral load transfer. The detailed equation of physical model is derived in (4.22).

The simulation test is given out with the DLC maneuver where the road bank angle is initialized at 18%, and presented in figures 4.12 and 4.13. It is obvious from these figures that the previous common vertical tire force model is not able to provide a precise approximation with the reference data. On the other hand, the new deduced vertical tire force model adapted to the disturbance of road bank angle evidently improves the accuracy of the models in different road environments.

To evaluate the performance of the open loop calculation, the output lines of different models and simulation data are drawn. However, the figures are not enough for making precise analysis. As a result, the normalized mean error proposed in [Stéphane 2004] is introduced in this study. This variable is calculated as follows:

$$\varepsilon_y = 100 * \frac{\text{mean}(|y_{\text{mod}} - y_{\text{meas}}|)}{\text{max}(|y_{\text{meas}}|)} \quad (4.23)$$

where  $y_{\text{mod}}$  is the value calculated by the observer,  $y_{\text{meas}}$  is the measured value and  $\text{max}(|y_{\text{meas}}|)$  is the absolute maximum value of the measured data.

To provide a complementary approach to analyze the performance of different force models, Table 4.1 explains the statistical difference among these three vertical tire force models. The minimum of ancient model widely used is 15.55, while the normalized mean error of method 1 is 3.53 and the one of method 2 is about 2.44.

	$F_{zm}$	$F_{zm1}$	$F_{zm2}$
$F_{z11}$	12.28	1.08	1.33
$F_{z12}$	7.45	2.01	1.94
$F_{z21}$	15.55	3.53	2.44
$F_{z22}$	8.69	1.62	1.79

Table 4.1: Normalized mean error between different models calculation and simulation data for the vertical force on 18% banked road

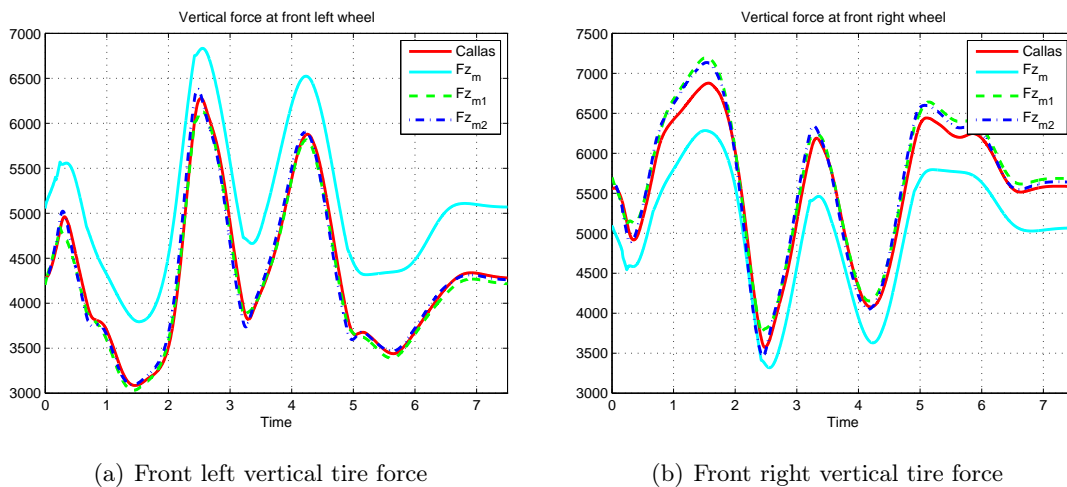


Figure 4.12: Comparison of multi-models of vertical front tire force with 18% bank angle

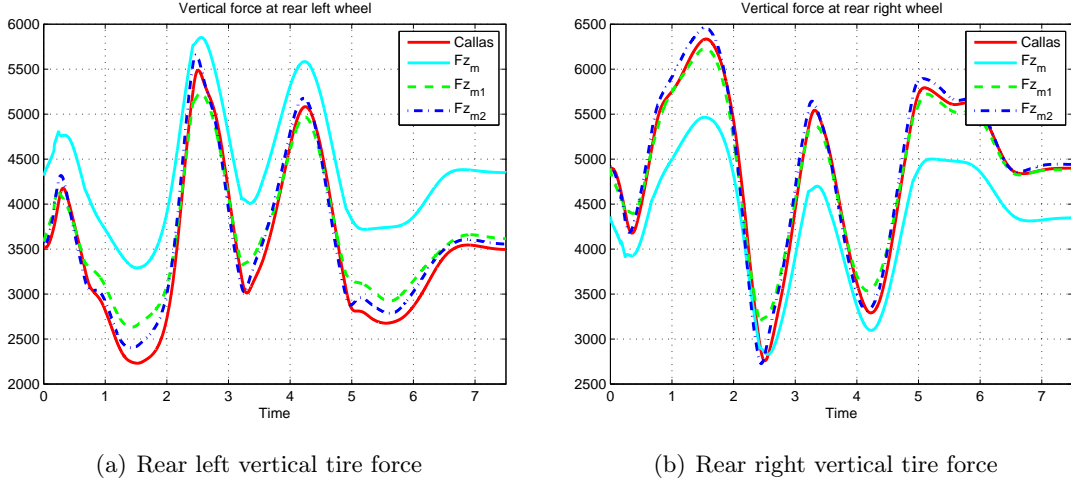


Figure 4.13: Comparison of multi-models of vertical rear tire force with 18% bank angle

Although the open-loop calculation of vertical tire force models can denote satisfactory performance on the banked road, it is limited due to the variation of certain parameters and assumptions that aimed at simplifying the model. Actually, for some parameters considered as constant is changing during the different maneuver, especially on the banked angle. The center of gravity is not the same as it is on the quasi-flat road, and in a real situation, the roll center and track's width are flexible during the lateral movements. In addition, the assumption of negligence of the components of suspensions and tires as well as the roll dynamics leads to complicated and unmodelled variations to be added into the model.

Consequently, in the next section, the observer technique is introduced to be used instead of the open-loop calculation, the estimation results are could be respected more robust to the variations of certain parameters and more accurate compared with respect to the measured data.

## 4.4 Observer design $O_{F_z}$

### 4.4.1 Discrete time state-space representation

As the roll motion is presented within the relation of the vertical tire force, we choose this model ( $F_{zm2}$ ) presented in equations 4.22. The linear Kalman filter is intervened to estimate the required variables, the system model is represented in a discrete state-space form:

$$\begin{cases} x_k = Ax_{k-1} + Bu_{k-1} + w_{k-1} \\ y_k = Hx_k + v_k \end{cases} \quad (4.24)$$

where matrix  $A$  is the state evolution matrix,  $H$  is the observation matrix.  $w_k$  and  $v_k$  are assumed to be Gaussian, temporally uncorrelated and zero-mean noises.

The vehicle state vector  $x \in \mathfrak{R}^{12}$  at instant  $k$  is presented as:

$$x_k = [\phi_{vk}, \dot{\phi}_{vk}, F_{z11k}, F_{z12k}, F_{z21k}, F_{z22k}, a_{xmk}, \dot{a}_{xmk}, a_{ymk}, \dot{a}_{ymk}, a_{zk}, \dot{a}_{zk}]^T \quad (4.25)$$

The state vector is initialized as:

$$x_k = [0, 0, 0.25mg, 0.25mg, 0.25mg, 0.25mg, 0, 0, 0, 0, 0, 0]^T \quad (4.26)$$

Here, we assume that  $a_{xm}'' = a_{ym}'' = \ddot{a}_z = 0$ , it is called ‘‘random walk model’’ from [Doumiati 2009]. This model is used under the assumption that the vehicle is dealing with quasi steady-state operating conditions. It requires that there are no abrupt changes in acceleration signals from gyro, otherwise it is also useful to reduce the noise of output signals from gyro.

The fundamental variables are presented in the state vector, there is no input vector  $u_k$ , hence the matrix  $B$  is null in such system.

The observation vector  $y_k \in \mathfrak{R}^9$  at instant  $k$  is defined as:

$$y_k = [\phi_{vk}, \dot{\phi}_{vk}, F_{z11k}, F_{z12k}, F_{z21k}, F_{z22k}, a_{xmk}, a_{ymk}, a_{zk}]^T \quad (4.27)$$

The particular linear system is first given in continuous-time state-space:

$$\dot{x} = \begin{cases} \dot{\phi}_v & = \dot{\phi}_v \\ \ddot{\phi}_v & = -\frac{K_r}{I_{xx}}\phi_v - \frac{C_r}{I_{xx}}\dot{\phi}_v + \frac{mh_c a_{ym}}{I_{xx}} \\ \dot{F}_{z11} & = \frac{1}{2}m\dot{a}_z \frac{L_2}{L} - \frac{1}{2}m\dot{a}_{xm} - \frac{K_r}{E_1}\dot{\phi}_v - \frac{C_r}{E_1}\ddot{\phi}_v \\ \dot{F}_{z12} & = \frac{1}{2}m\dot{a}_z \frac{L_2}{L} - \frac{1}{2}m\dot{a}_{xm} + \frac{K_r}{E_1}\dot{\phi}_v + \frac{C_r}{E_1}\ddot{\phi}_v \\ \dot{F}_{z21} & = \frac{1}{2}m\dot{a}_z \frac{L_1}{L} + \frac{1}{2}m\dot{a}_{xm} - \frac{K_r}{E_2}\dot{\phi}_v - \frac{C_r}{E_2}\ddot{\phi}_v \\ \dot{F}_{z22} & = \frac{1}{2}m\dot{a}_z \frac{L_1}{L} + \frac{1}{2}m\dot{a}_{xm} + \frac{K_r}{E_2}\dot{\phi}_v + \frac{C_r}{E_2}\ddot{\phi}_v \\ \dot{a}_{xm} & = \dot{a}_{xm} \\ \ddot{a}_{xm} & = 0 \\ \dot{a}_{ym} & = \dot{a}_{ym} \\ \ddot{a}_{ym} & = 0 \\ \dot{a}_z & = \dot{a}_z \\ \ddot{a}_z & = 0 \end{cases} \quad (4.28)$$

We employ a Kalman filter to estimate the linear time-invariant system with stochastic discrete-time state space representation. To transform from continuous-time system, the first order approximation of Euler is used.

$$\dot{x}_{k-1} = \frac{x_k - x_{k-1}}{t_s} \quad (4.29)$$

$t_s$  is the sampling time, Euler discretization gives the same result as a first-order approximation to the matrix exponential in the conversion of a continuous time signal to a discrete time signal. However, it is noted that the output of the discretization using the Euler method depends on the sampling time (discretization time), usually the choice of the sampling interval is very short. Therefore, the discrete-time state-space system can be defined as the form:

$$x_k = x_{k-1} + t_s \dot{x}_{k-1} \quad (4.30)$$

The presentation of each variables in the measurement vector is listed as:

- $\phi_v$  concerns the identified vehicle roll angle, separated from the gyro measurement that also contains road bank angle. This angle is calculated by using the suspension deflection in  $\phi_v = \frac{\rho_{11} - \rho_{12} + \rho_{21} - \rho_{22}}{2E} - \frac{m a_{ym} h}{k_{tr}}$ .
- $\dot{\phi}_v$  is the roll rate measured by gyrometer.

- $F_{zij}$  represents vertical force at four wheels calculated in model formulated in 4.22.
- $a_{xm}$  and  $a_{ym}$  measured by accelerometer directly or may be accessed from the CAN bus.
- $a_z$  can be treated as the vertical force which composed by lateral and vertical acceleration measured from accelerometer, the formulation of mentioned vertical acceleration is given as  $a_z = a_{ym}\sin\phi_v + a_{zm}\cos\phi_v$ .

According to the adopted discrete-time state-space representation, the state evaluation  $A$  and observation matrix  $H$  are given respectively as:

$$A = \begin{pmatrix} 1 & t_s & 0 & 0 & 0 & 0 & 0 & 0 & 0 & 0 & 0 & 0 \\ -\frac{K_r t_s}{I_{xx}} & 1 - \frac{C_r t_s}{I_{xx}} & 0 & 0 & 0 & 0 & 0 & 0 & mh \frac{t_s}{I_{xx}} & 0 & 0 & 0 \\ -\frac{K_r t_s}{E_1} & -\frac{C_r t_s}{E_1} & 0 & 0 & 0 & 0 & -0.5mt_s \frac{h}{L} & 0 & 0 & 0 & 0.5mt_s \frac{L_2}{L} & 0 \\ \frac{K_r t_s}{E_1} & \frac{C_r t_s}{E_1} & 0 & 0 & 0 & 0 & -0.5mt_s \frac{h}{L} & 0 & 0 & 0 & 0.5mt_s \frac{L_2}{L} & 0 \\ -\frac{K_r t_s}{E_2} & -\frac{C_r t_s}{E_2} & 0 & 0 & 0 & 0 & 0.5mt_s \frac{h}{L} & 0 & 0 & 0 & 0.5mt_s \frac{L_1}{L} & 0 \\ \frac{K_r t_s}{E_2} & \frac{C_r t_s}{E_2} & 0 & 0 & 0 & 0 & 0.5mt_s \frac{h}{L} & 0 & 0 & 0 & 0.5mt_s \frac{L_1}{L} & 0 \\ 0 & 0 & 0 & 0 & 0 & 0 & 1 & t_s & 0 & 0 & 0 & 0 \\ 0 & 0 & 0 & 0 & 0 & 0 & 0 & 1 & 0 & 0 & 0 & 0 \\ 0 & 0 & 0 & 0 & 0 & 0 & 0 & 0 & 1 & t_s & 0 & 0 \\ 0 & 0 & 0 & 0 & 0 & 0 & 0 & 0 & 0 & 1 & 0 & 0 \\ 0 & 0 & 0 & 0 & 0 & 0 & 0 & 0 & 0 & 0 & 1 & t_s \\ 0 & 0 & 0 & 0 & 0 & 0 & 0 & 0 & 0 & 0 & 0 & 1 \end{pmatrix},$$

$$H = \begin{pmatrix} 1 & 0 & 0 & 0 & 0 & 0 & 0 & 0 & 0 & 0 & 0 & 0 \\ 0 & 1 & 0 & 0 & 0 & 0 & 0 & 0 & 0 & 0 & 0 & 0 \\ 0 & 0 & 1 & 0 & 0 & 0 & 0 & 0 & 0 & 0 & 0 & 0 \\ 0 & 0 & 0 & 1 & 0 & 0 & 0 & 0 & 0 & 0 & 0 & 0 \\ 0 & 0 & 0 & 0 & 1 & 0 & 0 & 0 & 0 & 0 & 0 & 0 \\ 0 & 0 & 0 & 0 & 0 & 1 & 0 & 0 & 0 & 0 & 0 & 0 \\ 0 & 0 & 0 & 0 & 0 & 0 & 1 & 0 & 0 & 0 & 0 & 0 \\ 0 & 0 & 0 & 0 & 0 & 0 & 0 & 1 & 0 & 0 & 0 & 0 \\ 0 & 0 & 0 & 0 & 0 & 0 & 0 & 0 & 1 & 0 & 0 & 0 \\ 0 & 0 & 0 & 0 & 0 & 0 & 0 & 0 & 0 & 1 & 0 & 0 \end{pmatrix}$$

As we have presented the variables in the state vector and measurement vector, it is obvious that some of them are reduplicate in both vectors, so the state-space model does not completely represent the physical system since certain estimated variables are already accessible from measurements. The observer could perform much stably and precisely due to the more accurate measurements included in the system.

#### 4.4.2 Observability analysis

The analysis of observability is an essential process in designing observers. Before applying Kalman filter as an application related to the modeling of vertical tire force on banked road, it is obligatory to check the system observability. The observability is considered as the extent of the internal states of a system could be inferred from knowledge of its external outputs. For time-invariant linear system, a convenient method making use of the observability matrix is able

to validate whether the system is observable according to the state space representation. The observability matrix is defined as:

$$O = [H \quad HA \quad HA^2 \quad \dots \quad HA^{n-1}]^T \quad (4.31)$$

If the row rank of the observability matrix is equal to the dimension of state vector  $n$ , the system is observable. In our case, the observability matrix is verified using MATLAB function that computes the observability matrix for state-space systems, the matrix is with full rank of 12. Therefore, we can conclude that our system is observable at any instant  $k$ .

## 4.5 Simulation validation

So far, we have presented two novel models considering the road disturbance, particularly about the road bank angle and compared them with ancient model. Analyzing the limitation of the open-loop calculation, the Kalman filter for linear system is introduced to enable the vehicle model be robust to the variation of certain parameters and the negligence of unmodelled elements. This section will present the validation of performance of an observer using simulation data, some comparisons will be given to different open-loop models.

### 4.5.1 Simulation environment

As far as the real road condition is concerned, it is usually difficult to find and have the knowledge of the precise geometry information about the slope road, except for some professional test tracks. For the convenience of our research, we use a simulator CALLAS created by society OKTAL, which is an advanced vehicle simulation software that has been validated by many research laboratories and automobile enterprises.

### 4.5.2 Observer regulation

As discussed in section 3.3 about the Kalman filter, in this point we need to ask a question. What can be considered as a good behavior of the Kalman filter and how can good behavior be observed? The response is related to the adjusting covariance matrices in the Kalman operation process. Actually, there are two matrices need to be regulated in the Kalman filter, the system process noise covariance matrix  $Q$  and measurement noise covariance matrix  $R$ .  $Q$  is usually regulated depended on the accuracy of the modeling, while  $R$  is related to the quality of measured signals. In the actual implementation of the filter, tuning  $R$  is relatively easier since we are able to take some off-line sample measurements in order to determine the variance of the measurement noise. This is done in a learning phase prior to the operation of the filter. Comparing with  $R$ , The determination of the process noise covariance  $Q$  is usually more difficult. The reason is due to the fact that we are not able to access directly the information from the process which we are estimating. Sometimes if the selection of  $Q$  is suitable, even though the modeling is not complex or comprehensively described with all features of the system,  $Q$  can inject enough uncertainty into the process to obtain an acceptable estimation results [Welch 1995]. Hence in real regulation of the parameters of Kalman filter, we need make more effort to set an optimal regulation of the process noise covariance matrix  $Q$ .

Considering the simulated implementation of our observer  $O_{F_z}$ , because we use the simulator in our validations, the output signals of such professional vehicle dynamics software is considered



$$R = \begin{pmatrix} 0.1 & 0 & 0 & 0 & 0 & 0 & 0 & 0 & 0 \\ 0 & 0.5 & 0 & 0 & 0 & 0 & 0 & 0 & 0 \\ 0 & 0 & 10^2 & 0 & 0 & 0 & 0 & 0 & 0 \\ 0 & 0 & 0 & 10^2 & 0 & 0 & 0 & 0 & 0 \\ 0 & 0 & 0 & 0 & 10^4 & 0 & 0 & 0 & 0 \\ 0 & 0 & 0 & 0 & 0 & 10^2 & 0 & 0 & 0 \\ 0 & 0 & 0 & 0 & 0 & 0 & 1 & 0 & 0 \\ 0 & 0 & 0 & 0 & 0 & 0 & 0 & 1 & 0 \\ 0 & 0 & 0 & 0 & 0 & 0 & 0 & 0 & 1 \end{pmatrix}$$

### 4.5.3 Validation test

In this subsection, we will focus on the performance validation applying above-mentioned theoretical development. The tests will be realized with different road geometry disturbances concerned with bank angle: 0%, 10% and 18%, while different typical test maneuvers are taken to solicit the dynamics characteristics of the developed model. Some nomenclatures are explained here for a clearer description between different methods. For the representation of roll angle in the figure, the calculated value is derived from the deflection of suspension mechanical part during the cornering in equation (4.6). The symbol of  $F_{z_m}$  and  $O_{F_z}$  respectively delegate the ancient common used model in [Doumiati 2009] and the Kalman filter applying our original vertical tire force model.

#### 4.5.3.1 Steering wheel alternation slalom test on leveled road

First, a steering wheel alternation test on leveled road is performed in the simulator. The new developed model should be validated not only on the banked road but also on the normal flat road. The overall trajectory record of vehicle movement is illustrated in Figure 4.15. The choice of the test must maximally reflect the dynamics characteristics of the longitudinal and lateral movements. The relevant maneuver time history is represented in Figure 4.16. During the test, the initial velocity is  $40\text{km/h}$ , then the vehicle begins to brake and accelerate alternately during each 10s, the longitudinal acceleration can reach up to  $-6.6\text{m/s}^2 < a_x < 3.7\text{m/s}^2$ . Meanwhile, the steering wheel changes from one side to another side at the moment of vehicle accelerating and braking, the lateral acceleration can attain  $-7.8\text{m/s}^2 < a_y < 7\text{m/s}^2$ . These two movements along longitudinal and lateral axes are simultaneous at instant 5s and 15s.

Figure 4.17(a) and 4.17(b) illustrate the vertical force variations at front tires, while Figure 4.18(a) and 4.18(b) describe the reconstruction of rear vertical tire force. The elaborate description can be divided by several periods:

- $0\text{s} < t < 10\text{s}$ : the first period of steering wheel alternation with severe brake, a sudden change of steering wheel occurs at instant 5s and undergoes with a rough brake that leads to the longitudinal acceleration attains  $-7\text{m/s}^2$ . The front wheels are with more loads and rear wheels are relieved due to the braking. At the same time, the right wheels become overloaded comparing with the left ones.
- $10\text{s} < t < 20\text{s}$ : the second period of steering wheel alternation with severe brake, which is similar to the first period.

- $20s < t < 35s$ : vehicle moves at a constant velocity with a slight steering wheel alternation maneuver. The left wheels are loaded due to the inertial force created by the lateral acceleration.

We can conclude from the figures illustrating the vertical tire forces, our observer  $O_{F_z}$  in blue dashdot performs well, there is some small difference compared with the simulated data represented in red line. Even though the virtual vehicle was driven in critical situations (where  $a_x = -7m/s^2$ ,  $a_y = 6m/s^2$ ), the estimated vertical tire force can always follow with the reference data and the load of front right wheel can attain at  $8500N$ . Analyzing the ancient model  $F_{z_m}$ , it can be found to have some limitation, because of the negligence of the vehicle roll motions generated by the lateral load transfer of the sprung mass. It is noted that the difference can be found in the vertical force of rear left wheel at instant  $5s$  and  $15s$  due to the negligence of lateral load transfer. This steering wheel alternation test on leveled road with rough braking demonstrates the performance of the constructed observer and the ancient open-loop model, longitudinal and lateral dynamics are greatly solicited during critical situations.

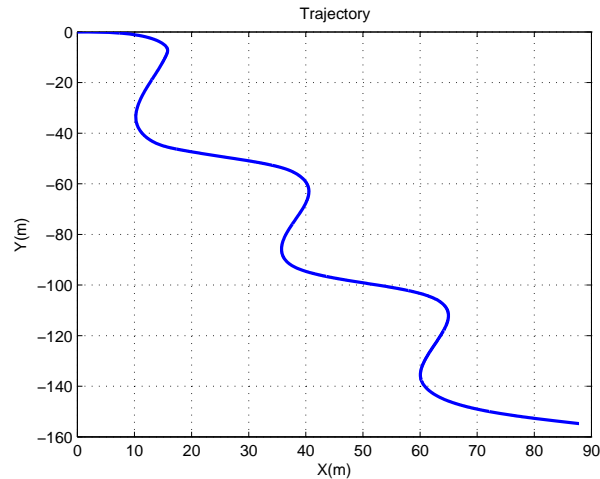


Figure 4.15: The trajectory of vehicle body movement: steering wheel alternation test on leveled road

#### 4.5.3.2 Steering wheel alternation test on 10% banked road

The second test is quite similar to the first steering wheel alternation test, however the road geometry disturbance is added into this scenario. The road bank angle is initialized at 10%. The longitudinal and lateral are combined, the trajectory of vehicle movement is represented in Figure 4.20, while the vehicle maneuver is illustrated in Figure 4.19. The vehicle begins to brake roughly from an initial velocity, the range of longitudinal acceleration during all maneuvers is  $-8m/s^2 < a_x < 5.5m/s^2$ , during the first braking period, the maximum deceleration can reach up to  $-8m/s^2$ , which can be considered as an emergency brake. Simultaneously, the variation of lateral acceleration is between  $-6.4m/s^2 < a_y < 9.4m/s^2$ , particularly the maximum lateral acceleration  $a_y = 9.4m/s^2$  means intense lateral load transfer caused by transverse movement. The test is negotiated on the banked road at a constant inclined angle 10%, the left road

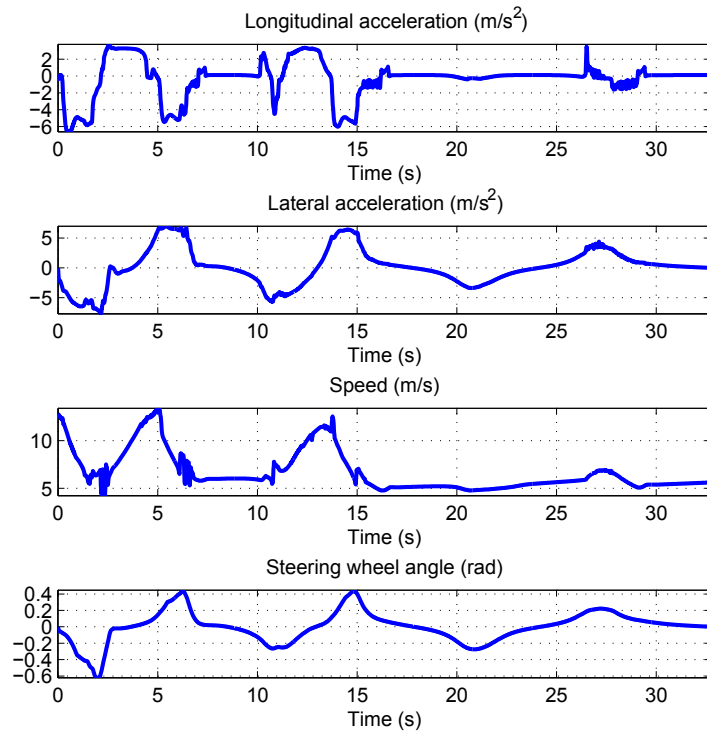
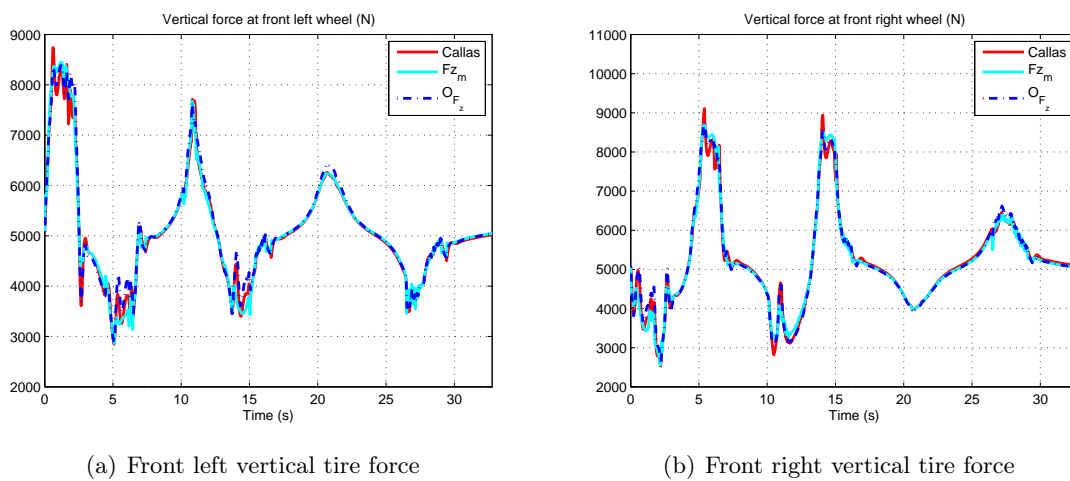


Figure 4.16: Maneuver time history: steering wheel alternation test on leveled road



(a) Front left vertical tire force

(b) Front right vertical tire force

Figure 4.17: Comparison of front vertical tire forces: steering wheel alternation test on leveled road

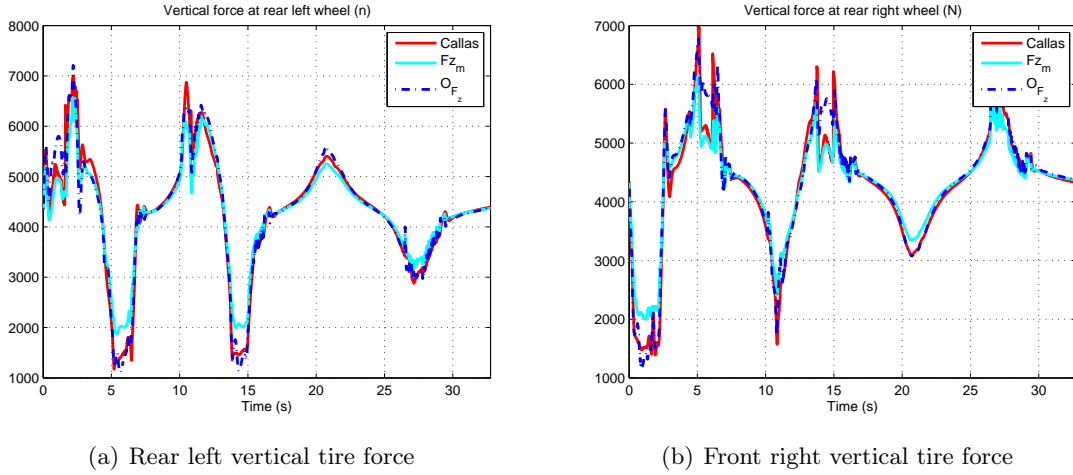


Figure 4.18: Comparison of rear vertical tire forces: steering wheel alternation test on leveled road

boundary is higher than the right one, hence the gravity decomposition generates much more load at right tires.

The roll angle model is validated on the banked road. Even though the parameter of road bank angle  $\phi_r$  is not presented in the model, it can follow well with the measurement of vehicle roll angle according to the deduced relation of suspension deflection. Figure 4.21 represents the performance of the calculated roll angle compared with simulation output. It tracks well with the measurement during the transient period, particularly where the lateral acceleration up to 9.4%. This effective and simple method is convenient for our requirement.

Figure 4.22(a) and 4.22(b) represent the vertical tire force estimation at front tires on 10% banked angle, while Figure 4.23(a) and 4.23(b) illustrate the rear ones. Obviously, the ancient model  $F_{z_m}$  in cyan line using only longitudinal and lateral acceleration is no longer available, we can see a significant bias between the model and CALLAS data. However the reconstructed observer  $O_{F_z}$  demonstrates its efficacy, it is able to track well with the simulation output signals even with the situation where the vehicle was put in critical driving maneuver ( $a_y > 4m/s^2$ ), the observer performance is satisfactory. Some slight derivations can be noticed in these figures due to the negligence of the drift of the center of gravity, as well as the disregard of the suspension kinematic motion and the camber angle affection.

#### 4.5.3.3 ISO lane change on 18% banked road

The final maneuver is shown in Figure 4.25, the trajectory is presented within an ISO lane change at a constant velocity  $60km/h$ . The maneuver time history is represented in Figure 4.24. The longitudinal acceleration is tiny, while the interval of the variation of the lateral acceleration is  $-4m/s^2 < a_y < 4m/s^2$ . Hence, the vehicle is typically affected by the lateral movement. The road bank angle is set at 18% in the configuration of the road environment of the simulator.

- $0s < t < 1s$  and  $6s < t < 7.5s$ : vehicle moves straight forward, there is no typical movement on longitudinal and lateral axis. The vehicle is considered to be at steady state.
- $1s < t < 6s$ : the transverse transient period is presented in this section, the lateral load transfer from one side to the other side due to the steering command, the ISO double lane

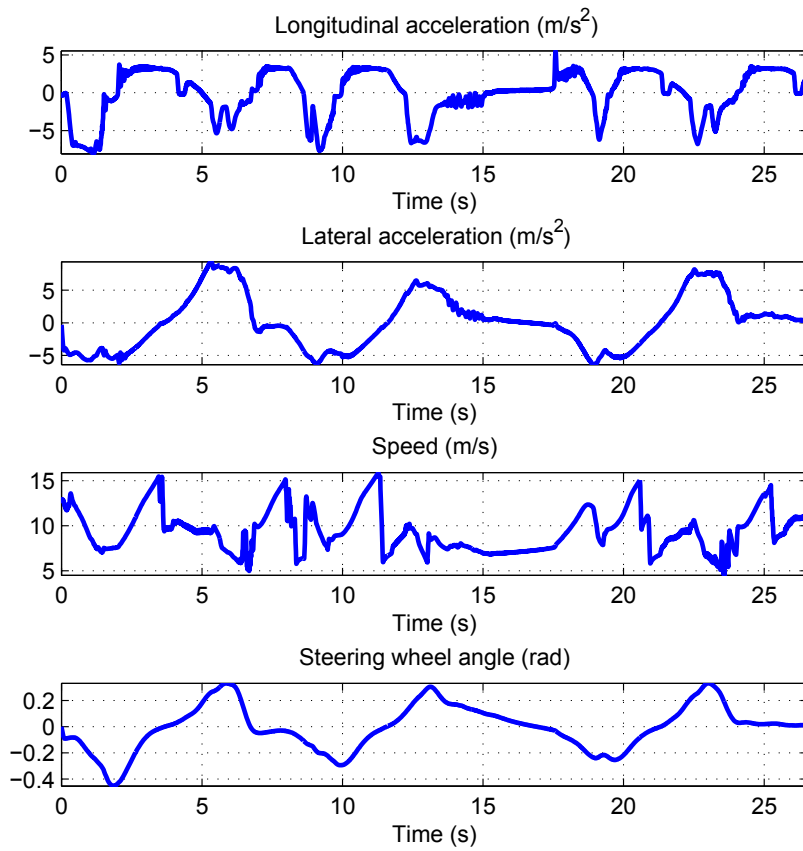


Figure 4.19: Maneuver time history: steering wheel alternation test on 10% banked road

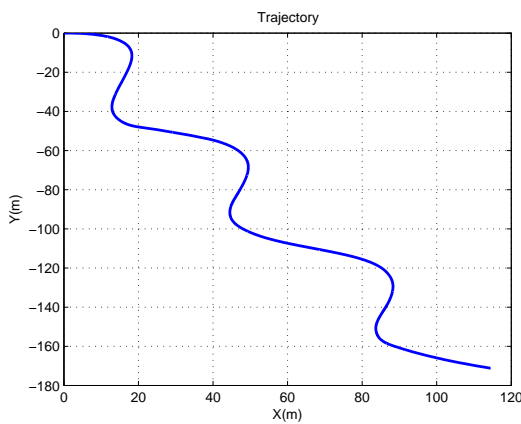


Figure 4.20: The trajectory of vehicle body movement: steering wheel alternation test on 10% banked road

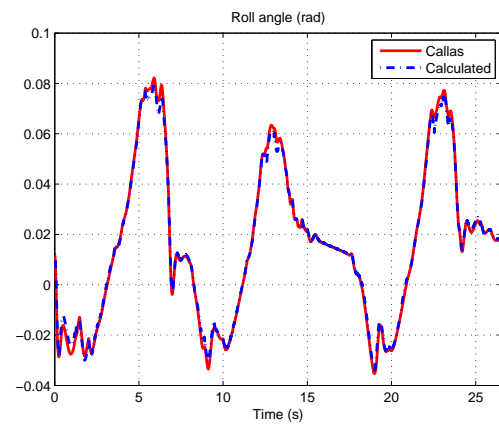
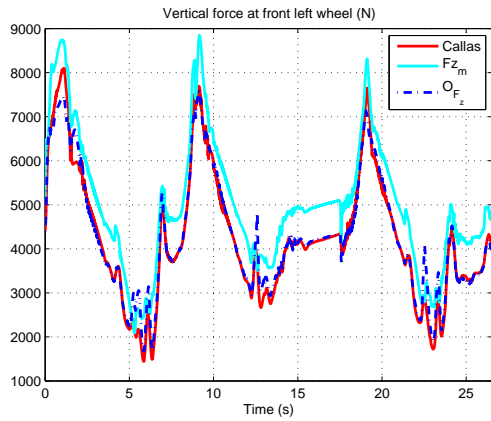
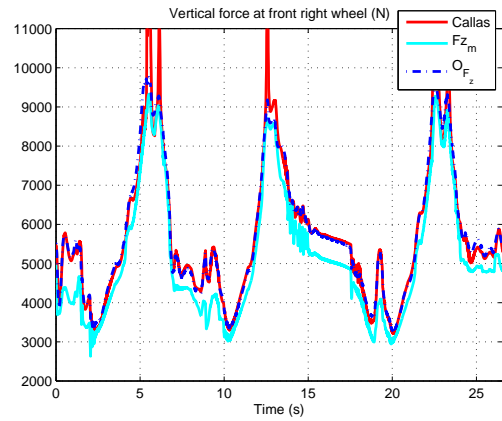


Figure 4.21: Roll angle model: steering wheel alternation test on 10% banked road

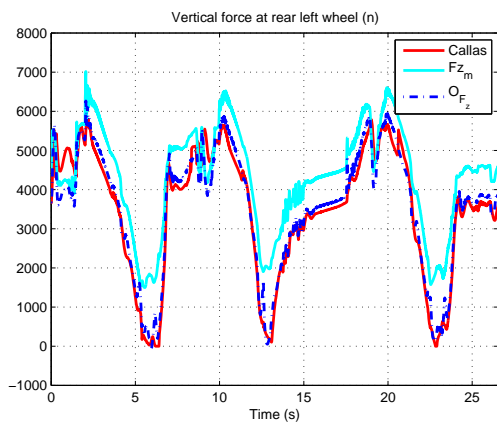


(a) Front left vertical tire force

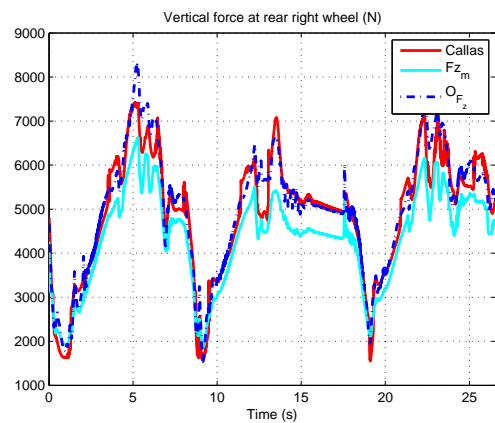


(b) Front right vertical tire force

Figure 4.22: Comparison of front vertical tire forces: steering wheel alternation test on 10% banked road



(a) Rear left vertical tire force



(b) Rear right vertical tire force

Figure 4.23: Comparison of rear vertical tire forces: steering wheel alternation test on 10% banked road

change is used to evaluate the handling performance of a vehicle and is an integral part of the vehicle design procedures and assessment.

Shown in Figure 4.26, the vehicle roll angle is calculated according to the suspension deflection, as we have discussed above, the method applying suspension variations provides an accurate result with road inclined disturbance. The roll dynamics of the vehicle body during the transient and steady state is precisely drawn during such test.

Figure 4.27(a), 4.27(b), 4.28(a) and 4.28(b) show the variations of the wheel loads at each tire. The phenomenon of the model  $F_{z_m}$  is similar to the previous test, the vertical forces are totally shifted due to the lateral inclination angle during both transient and steady-state periods. The observer performs very well during the steady-state, the estimated vertical force are quite close to the simulation output. However, we can find some bias between them during the lane changing instant ( $4s < t < 5s$ ) when the vehicle is turning right. The load transfer from right side to the left wheels, we can see that the estimated load distribution on left tires is kind of overloaded, while the value of the left ones is smaller than the reference data. These disharmonious results can be explained by the assumption of simplification of roll dynamics and the unconsidered dynamics influences within the vehicle tire force model. Besides, the suspension kinematic affection and tire camber angle over big bank angle disturbance are also neglected in our research.

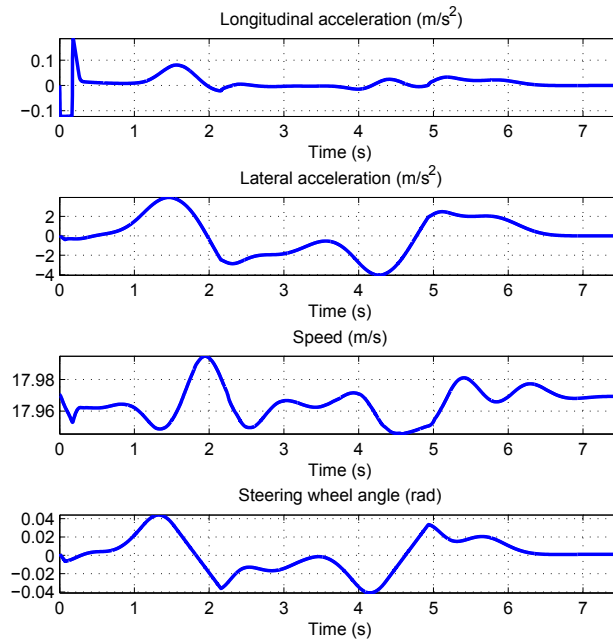


Figure 4.24: Maneuver time history: ISO lane change on 18% banked road

#### 4.5.3.4 Summary

Three different simulation tests are used to validate the performance of our reconstructed model and observer. The comparative tests with different road disturbances clearly identify the limi-

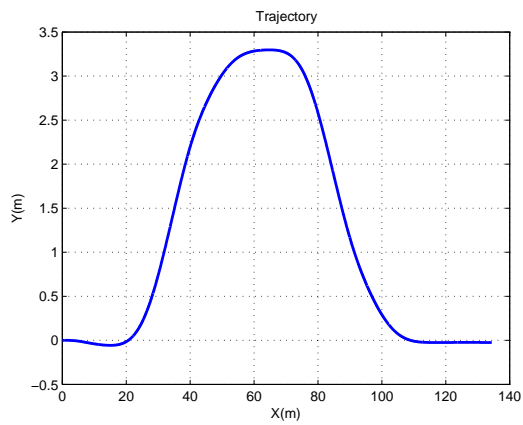


Figure 4.25: The trajectory of vehicle body movement: ISO lane change on 18% banked road

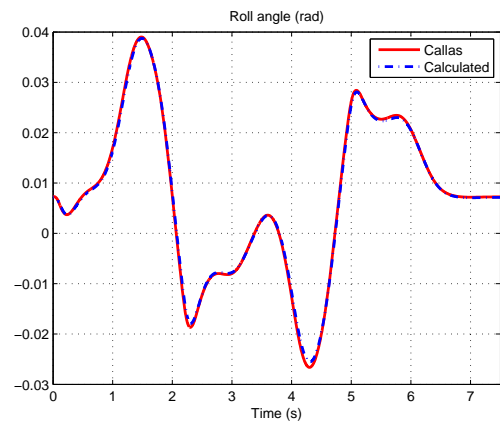
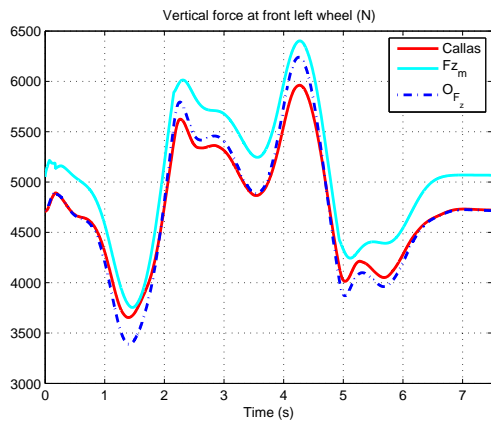
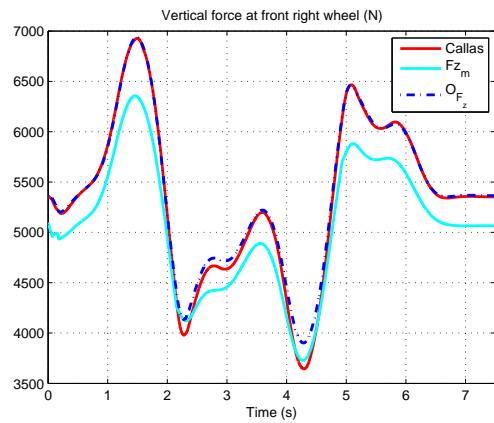


Figure 4.26: Roll angle model: ISO lane change on 18% banked road

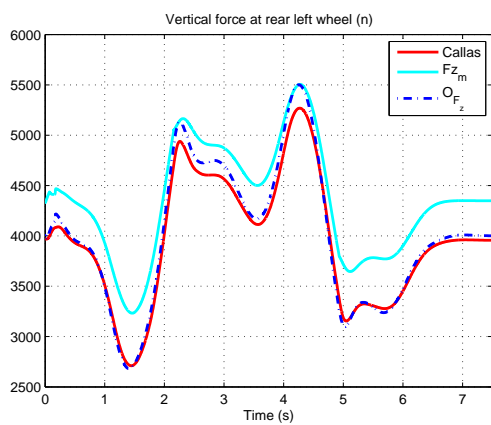


(a) Front left vertical tire force

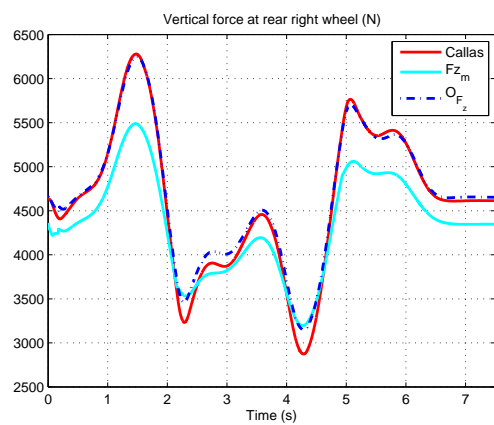


(b) Front right vertical tire force

Figure 4.27: Comparison of front vertical tire forces: ISO lane change on 18% banked road



(a) Rear left vertical tire force



(b) Rear right vertical tire force

Figure 4.28: Comparison of rear vertical tire forces: ISO lane change on 18% banked road

tation of each method. Except for the illustration using MATLAB plot, the statistics analysis of normalized mean error is also employed to provide an overall comparison between different tests in Table 4.2.

	Test 1		Test 2		Test 3	
	$F_{z_m}$	$O_{F_z}$	$F_{z_m}$	$O_{F_z}$	$F_{z_m}$	$O_{F_z}$
$F_{z11}$	0.97	0.94	9.42	1.90	5.54	1.47
$F_{z12}$	1.09	0.82	3.31	1.14	4.13	0.67
$F_{z21}$	2.70	1.75	16.46	4.72	7.41	1.41
$F_{z22}$	2.56	1.90	7.90	3.83	5.01	1.11

Table 4.2: Normalized mean error between estimated vertical force and simulation output for three typical tests

Comparing with the normal model based on the assumption of flat road and the observers considering road disturbance in the first test (steering wheel alternation test on leveled road). Two methods are quite similar, however the observer performs a little better than the ancient model. The difference is embodied especially in the second test and the third test where the road bank angle is presented respectively with 10% and 18%. In fact, a heavily longitudinal and lateral movement simultaneously occurred in the test on the banked angle leads to the ancient assumptions are not available. Therefore the new features need to be considered in the vertical tire force model. The statistics values demonstrated that the performance of the new load distribution model applied at four wheels are evidently improved. It is noted that the rough longitudinal deceleration at  $-8m/s^2$  and lateral acceleration at  $9.4m/s^2$  appeared in test 2, the performance is affected by the intense movement due to the assumption of the unmodelled dynamics and some parameter variations, some work is still needed to be consummated in the future.

## 4.6 Conclusion

This chapter mainly deals with the problem of vertical tire force estimation on banked road. We firstly validate the common model [Kiencke 2005] [Doumiati 2009] with the assumption of flat road as well as the limitation of such model. To extend the estimation method to general environment, road disturbance should be considered in the renovated model. It is noted that vertical force is an input variable in the prediction system of vehicle rollover, the road angle is prone to cause the augmentation of such accident rate, especially for high COG cars. The road disturbance can influence directly on vehicle dynamics as well as the gyro sensor, some fundamental variables are analyzed with the road banked condition. We introduce the acceleration decomposition, vehicle roll angle and pitch angle are exploited with the consideration of banked road perturbation, an effective method using suspension deflection at four wheels is validated. The suspension roll angle is separated from the road bank angle from the gyrometer's measurement.

With the knowledge of the separated vehicle roll angle, we are able to reconstruct an adequate model providing a precise description of the vehicle dynamics on banked road. The first model is deduced by using accelerometer in three axes ( $a_{xm}, a_{ym}, a_{zm}$ ), the lateral and vertical acceleration are due to the gravity term at the output of the accelerometer attached to the inclined vehicle sprung mass. The second deduced model adds a roll dynamics term in the for-

---

mulation of the vertical load distribution at each tire. These two new derived models and the ancient one are compared with an open-loop method, we finally choose the second deduced model employing accelerometer and roll dynamics to develop an observer, the Kalman filter technique is intervened for a linear system. Several critical tests are performed to compare and validate our new algorithm, the observer gives convenient results even when high longitudinal/lateral accelerations act simultaneously. It is also interesting for us to apply this method in real-time system, however we also encounter some challenges. The variation of road bank angle is not considered in this model, and the suspension deflection is heavily affected on bumpy road in real situations. All these elements are still waiting to be solved in a future work.

In the subsequent chapter, we will focus on the research of lateral dynamics, a robust method of lateral force estimation will be presented to supply more precise vehicle dynamics information, in order to develop more robust embedded ADAS and improving the road safety in the future. This is the ultimate object of our research.



# Vehicle lateral dynamics estimation

---

## Contents

---

<b>5.1</b>	<b>Introduction</b>	<b>87</b>
<b>5.2</b>	<b>Retrospection of estimation of lateral dynamics parameters</b>	<b>89</b>
5.2.1	Estimation of lateral force	89
5.2.2	Estimation of sideslip angle	90
5.2.3	Analysis of relationship between lateral force and slip angle	90
<b>5.3</b>	<b>Vehicle and tire model</b>	<b>91</b>
5.3.1	Double track vehicle model	91
5.3.2	Tire force modeling	92
<b>5.4</b>	<b>Estimation process in real-time</b>	<b>94</b>
<b>5.5</b>	<b>Nonlinear observer modeling</b>	<b>95</b>
5.5.1	State-space representation	95
5.5.2	Implementation of filter technique	96
5.5.3	Observer tuning	98
<b>5.6</b>	<b>Experimental validation</b>	<b>100</b>
5.6.1	Slalom test on dry pavement	101
5.6.2	Slalom test on wet pavement	102
5.6.3	Closed circle test on bumpy road	107
5.6.4	Summary	111
5.6.5	Robustness with respect to vehicle parameters	112
<b>5.7</b>	<b>Conclusion</b>	<b>112</b>

---

## 5.1 Introduction

In the previous chapter, we have discussed the braking and accelerating impact on the vehicle vertical load distribution, this chapter will focus on the lateral dynamics that charged by the cornering movement. To reduce the lateral skid accident, and improve the vehicle safety handling, we need to analyze the relation of some fundamental parameters, for example the lateral tire force and sideslip angle.

It is noted that tire generates appropriate lateral forces to support the vehicle along a certain path, when the vehicle is undergoing a turning maneuver. These lateral forces are created by the deformation in the tire tread. As a result of the deformation, the traveling direction of the tire differs from the wheel center plane by the slip angle. The relation between lateral forces and slip angles determines the vehicle lateral dynamics [Dixon 1996].

As far as the lateral tire force is studied and analyzed in some literatures, the general characteristics are divided into two regions. In the normal driving situation, the cornering force remains in the linear region, which means that the cornering force is proportional to the input of tire slip angle. Usually, we can treat that the lateral force is ideal to the drivers' input, the vehicle is well under the control of predicted behavior.

Alternatively, the vehicle is in the nonlinear situation where the handling behavior undergoes an emergency maneuver, for example, the vehicle passes a turning with an excessive velocity. The augmentation of lateral tire force is limited by the maximum adhesion force which is depended on the wheel loads and the coefficient of friction. The lateral force cannot follow with the tire slip angle proportionally like the linear region any more. Therefore, the lateral force is not able to sustain the driver's expected steering input, the vehicle handling is not guaranteed under this situation, the risk of occurrence of skid accidents may be increased on account of the saturation of lateral force.

In common situation, drivers do not always have the ability and experience to deal with the emergency dangerous situation, therefore, some electronics and control systems like ABS, ESP are equipped in the modern automobiles to avoid the road accidents which are caused by losing of the vehicle control. Vehicle stability control systems that prevent vehicles from spinning and drifting out have been developed and recently commercialized by several automotive manufacturers. Such stability control systems are also often referred to as yaw control systems or electronic stability control systems. With these implementations of the advanced driving assistant system, the road safety is obviously improved.

These safety systems or any other vehicle stability control systems need accurate dynamics information about the vehicle motion, such as vehicle velocity, steering wheel angle, acceleration, which are measurable by the cheap sensors and accessible on the CAN bus. Actually, as the development of the advanced stability control system, some parameters of the precise description of the vehicle's motion can't be obtained by the current standard production cars due to the limit of the technique and cost-effective. Therefore, we need to find a solution to make these essential parameters available on the onboard vehicle system.

In this chapter, we treat the problem of estimating the lateral tire/road forces and sideslip angle, but considering it in the following view point:

- (i) the final nonlinear state observer must be robust enough to adapt to high nonlinearities of the system;
- (ii) but in another way, it must be simple enough to work in real-time on the onboard informatics of the vehicle.

Considering the objective in (i), we have constructed a state observer based on the Extended Kalman filter and the Particle filter technique for the comparison of the performance of these two observation techniques in an experimental high soliciting test-drive performed in a professional vehicle test drive site. Considering the objective in (ii), we will focus on the synthesis of our observers, the Dugoff tire model and the plane double track model. These vehicle dynamics models are chosen due to the simplicity of the system. Developing lateral tire/road force and sideslip angle observers, robust to non-linearities, working in real-time during the vehicle displacement and using simple models, is a challenge considered by industrial application objectives. The two nonlinear observers are constructed based on the vehicle and tire nonlinear models. The system complexity is reduced in order to satisfy the real-time application requirement. The performance

of the estimation process will be tested by the experimental vehicle equipped in our laboratory. The research is considered as the extension of the contribution in the thesis of [Doumiati 2009].

The rest chapter is organized as follows: we firstly denote a review of the estimation method of lateral dynamics parameters. Section 3 presents vehicle and tire model which are used in our work. The entire estimation procedures are implemented in real-time on in-vehicle system in section 4. Afterwards, we focus on the presentation of construction of observers in section 5. In section 6, some experimental tests are performed to validate the effectiveness and robustness of proposed method in this chapter. Finally, the conclusion and perspectives are summarized.

## 5.2 Retrospection of estimation of lateral dynamics parameters

Since lateral dynamics is essential for the implementation of the advanced stability control system, hence we can find a large amount of literatures concerning this issue, particularly discussing and analyzing estimation methods of lateral tire force and sideslip angle.

### 5.2.1 Estimation of lateral force

The knowledge of lateral tire force is essential for the future active safety system, [Senger 1989] describes observers for the lateral dynamics of vehicle that work well when tire forces are linear, but fail in the nonlinear range when either the road/tire interface properties or an accurate analytic tire force model is unknown. Normally it is difficult to know either factor, and these observers have limited practical use. [Kim 2009] presents a method for identifying lateral tire force dynamics by studying the vehicle dynamics. The methodology is based on the EKF (Extended Kalman filter) and makes it possible to determine lateral tire force dynamics on the basis of the results obtained from standard on-road handling maneuvers. An empirical tire-terrain model from Pacejka's Magic Formula and Extended Kalman filter is presented to estimate tire force in [Zhu 2011]. Another seven degrees of freedom's vehicle model is described in [Li 2010], the dynamics state can be measured or estimated by using the fusion of information of the DSC sensors. Ray in [Ray 1998] proposes a novel estimation method EKBF for the estimation of tire force, a random walk model is added to determine the force, and a Bayesian approach is used to determine the road friction. Estimated tire force is used to implement unified-chassis-control (UCC) systems in [Cho 2010], the wheel-dynamics model is simplified for the description of tire force. Some other estimation methods are proposed by using unknown input proportional-integral observers for the vehicle lateral dynamics estimation in [Mammar 2006b]. Recently in our laboratory, [Stéphane 2004] estimates the transverse tire force with linear and nonlinear models, the linear observer and three nonlinear observers: extended Luenberger observer, Extended Kalman filter and sliding-mode observer are employed to supply an approach to solve the estimation problem. The bicycle model is adopted in the thesis contribution. Afterwards, [Baffet 2007] propose observers to estimate lateral tire force per axle using Extended Kalman filter and without the input knowledge of torque measurement. The vehicle model described by lateral force per axle is firstly proposed by Ray in [Ray 1997]. Nowadays, [Doumiati 2009] summarizes and renovates the estimation method by per wheel. The shortcoming of negligence of lateral load transfer in previous methods is solved by applying a cascaded observer with estimation of lateral load transfer. The vertical tire force could be more precisely estimated as input variable in the estimation process of lateral tire force. The Extended Kalman filter and Unscented Kalman filter is compared with experimental validation.

### 5.2.2 Estimation of sideslip angle

Another essential parameter considered in the lateral dynamics is the sideslip angle, this angle is defined between the orientation of the vehicle and the direction of travel at the center of gravity. Actually, the direct measurement of such parameter requires expensive equipment such as optical correlation sensor. In normal driving situation, vehicle moves forward safely, the vehicle sideslip angle is small. At this moment, the steering characteristic specifies a tight connection between the steering wheel angle, yaw rate, lateral acceleration, and vehicle sideslip angle. The vehicle sideslip angle can therefore be estimated using a static model or a simple linear, dynamic model. An integration approach is proposed in [Van Zanten 2002], the sideslip angle is attempted to be estimated through sideslip rate integration. The sideslip rate can be accessed by the following relationship:

$$\dot{\beta} = \frac{a_y}{V_x} - \dot{\psi} \quad (5.1)$$

where  $\beta$  is the sideslip angle at the center of gravity,  $a_y$  represents the lateral acceleration,  $V_x$  is the vehicle longitudinal velocity, and  $\dot{\psi}$  is the yaw rate. However, this method is limited by the uncertainty and errors occurring in the integration operation, especially when the vehicle is in the extreme situation that the behavior of vehicle is highly nonlinear. A large number of researchers put the emphasis on the development of an effective approach to estimate the sideslip angle even under critical situation.

A closed-loop estimator is introduced to estimate the dynamics parameters using a kinematic model in [Chen 2008]. Sensor noises are modeled as process noise with a nonlinear disturbance input matrix. The extended Kalman filter is used to design the estimation gain, because the input matrix contains state variables. [Grip 2009] develops a vehicle sideslip observer that considers the nonlinearities of the system in the block of design and theoretical analysis. The research is aimed at reducing the computational complexity compared to the EKF, a new nonlinear vehicle sideslip observer (NVSO) is used to make the observer suitable for implementation in embedded hardware. Extensive and systematic tests in a variety of situations compare the performance of NVSO and EKF. [Stéphane 2004] uses sliding mode observer and Extended Kalman filter on the sideslip angle estimation, the pitch and roll dynamics are neglected. [Baffet 2007] estimates the sideslip angle with the consideration of the friction variation under different road conditions. [Doumiati 2009] uses four-wheel vehicle model and Dugoff tire model to provide an accurate estimation applying the Extended Kalman filter and Unscented Kalman filter. Recently, Particle filter has been involved in the sideslip angle estimation with the simulation results in [Cheng 2011].

[Ryu 2002] and [Bevly 2001] propose other different strategies using Inertial Navigation System (INS) sensors with GPS measurements. A two antenna GPS system can be used to provide vehicle heading. They provide accurate (unbiased) high update estimates of the vehicle and tire sideslip angles.

### 5.2.3 Analysis of relationship between lateral force and slip angle

Since the tight relationship between lateral force and sideslip angle is considered in the kinematic model. Many illustrations can be found in plenty of publications e.g. [Pacejka 2006] [Ray 1997] [Shiang-Lung 2004]. The lateral force and sideslip angle are initially linear, as sideslip angle changed, the lateral force starts to saturate due to the friction limit of the road. The slope of the curve is determined by the cornering stiffness. The nonlinear region is dangerous for the

cause of loss of vehicle control. The saturation value largely depends on the vertical force and coefficient of friction illustrated in Figure 5.1. Our target is to denote an accurate estimation of lateral force and sideslip angle even within the nonlinear region during extreme driving situation.

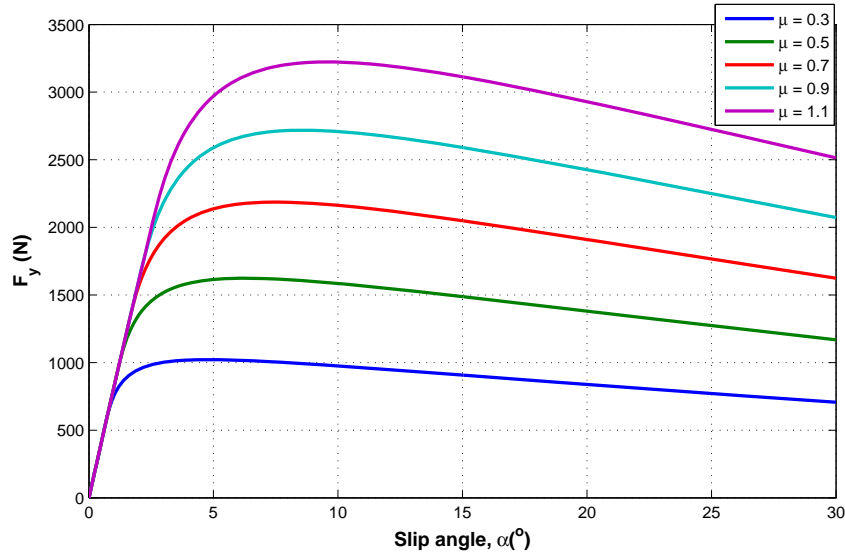


Figure 5.1: Typical lateral force versus slip angle

## 5.3 Vehicle and tire model

### 5.3.1 Double track vehicle model

Some vehicle models had been proposed to describe the vehicle dynamics. We use the four wheels model which presents clearly four wheel instead of the bicycle model which are represented by one single front/rear wheel in [Segel 1956]. A detailed presentation of the double track model can be found in [Von Vietinghoff 2005]. Some hypotheses are given to simplify the dynamics relations:

- Aerodynamic drag force and rolling resistance are ignored;
- Pitch behavior is not presented in this model;
- Camber angle is neglected, especially for the front wheels;
- Front steering angles are assumed to be equal;
- The vehicle model is supposed to be front-wheel drive systems, therefore the longitudinal force at rear wheels is considered null.

Parameter	Value
Total mass of the vehicle $m/kg$	1719
Height of the center of gravity $h/m$	0.57
Distance from the cog to the front axle $L_1/m$	1.116
Distance from the cog to the rear axle $L_2/m$	1.592
Vehicle track $E/m$	1.513
Moment of inertia with respect to the yaw axis $I_{zz}/kg.m^2$	3300

Table 5.1: Relevant model parameters of the experimental vehicle

With these hypotheses, the double track model represented in Figure 2.21 can be reasonably simplified by the formulas as follows:

$$\begin{aligned}
\ddot{\psi} &= \frac{1}{I_z} [L_1(F_{y11}\cos(\delta_{11}) + F_{y12}\cos(\delta_{12}) + F_{x11}\sin(\delta_{11}) + F_{x12}\sin(\delta_{12})) \\
&\quad - L_2(F_{y21}\cos(\delta_{21}) + F_{y22}\cos(\delta_{22})) + \frac{E}{2}(F_{y11}\sin(\delta_{11}) - F_{y12}\sin(\delta_{12}) \\
&\quad + F_{x12}\cos(\delta_{12}) - F_{x11}\cos(\delta_{11}))], \\
\dot{\beta} &= \frac{1}{mV_g} [(F_{x11} + F_{x12})\sin(\delta_{12} - \beta) + F_{y11}\cos(\delta_{11} - \beta) + F_{y12}\cos(\delta_{12} - \beta) \\
&\quad + F_{y21}\cos(\delta_{21}) + F_{y22}\cos(\delta_{22}) + F_{x21}\sin(\delta_{21} - \beta) + F_{x22}\sin(\delta_{22} - \beta)] - \dot{\psi}, \\
\dot{V}_g &= \frac{1}{m} [F_{x11}\cos(\beta - \delta_{11}) + F_{x12}\cos(\beta - \delta_{12}) + F_{x21}\cos(\beta) + F_{x22}\cos(\beta) + \\
&\quad F_{y11}\sin(\beta - \delta_{11}) + F_{y12}\sin(\beta - \delta_{12}) + F_{y21}\sin(\beta) + F_{y22}\sin(\beta)].
\end{aligned} \tag{5.2}$$

where  $F_{y11}$ ,  $F_{y12}$ ,  $F_{y21}$  and  $F_{y22}$  are the lateral forces at the front left, front right, rear left and rear right wheel, respectively. The  $F_{xij}$ , ( $i, j = 1, 2$ ) is the corresponding longitudinal force at each wheel, where  $F_{x2j}$  is null according to the above hypothesis.  $\dot{\psi}$  is the yaw rate and  $\delta_{ij}$  ( $i, j = 1, 2$ ) are the steering angles at each wheel.  $L_1$  is the distance between the front axle and the center of gravity, while  $L_2$  is the one between the rear axle and the center of gravity.  $E$  is the vehicle track.  $V_g$  is the velocity at the center of gravity.  $\beta$  is the sideslip angle at the center of gravity.  $\alpha_{ij}$  ( $i, j = 1, 2$ ) is the sideslip angle at each wheel.  $a_x$  and  $a_y$  are the longitudinal and lateral acceleration, respectively. The relevant model parameters of the experimental vehicle are listed in Table 5.1.

## 5.3.2 Tire force modeling

### 5.3.2.1 Vertical tire force model

The wheel load is mainly caused by the earth gravity, however when a car is in a steady-state turn, an inertial reaction force is developed to opposite the lateral acceleration. Meanwhile, when a car is under positive or negative acceleration, an inertial reaction is developed which is similar to the car in a turn. Longitudinal or lateral load transfer is discussed in [Milliken 2003]. However, to avoid the complexity of the suspension, damper system and the roll couple distribution, the vertical force is proposed to be calculated by the simple approach which only depends on the longitudinal acceleration and lateral acceleration. Longitudinal acceleration causes a pitch motion due to inertia, the wheel load shifts from front to rear axle. The lateral load transfer

is similar to the longitudinal movement during the vehicle in a turn. When the pitch and roll couple is not considered, the vertical force at each wheel could be calculated independently. This model is presented in [Rajamani 2006]. The static equations deduced by the torque balance on the wheel ground contact point are given as follows:

$$\begin{aligned}
F_{z11} &= m_v \cdot \left( \frac{l_r}{l} g - \frac{h}{l} a_x \right) \cdot \left( \frac{1}{2} - \frac{h}{e_{fg}} a_y \right), \\
F_{z12} &= m_v \cdot \left( \frac{l_r}{l} g - \frac{h}{l} a_x \right) \cdot \left( \frac{1}{2} + \frac{h}{e_{fg}} a_y \right), \\
F_{z21} &= m_v \cdot \left( \frac{l_r}{l} g + \frac{h}{l} a_x \right) \cdot \left( \frac{1}{2} - \frac{h}{e_{fg}} a_y \right), \\
F_{z22} &= m_v \cdot \left( \frac{l_r}{l} g + \frac{h}{l} a_x \right) \cdot \left( \frac{1}{2} + \frac{h}{e_{fg}} a_y \right), .
\end{aligned} \tag{5.3}$$

### 5.3.2.2 Lateral tire force model

The vehicle handling in a turn is mainly based on the lateral forces. These forces are influenced by the tire properties, road condition and vehicle velocity. Several tire mathematical models have been developed by the tire experiments and the theory of the behavior of the physical structure. A well-known empirical model is the Magic Formula tire model (Pacejka model) presented in [Pacejka 1987], it's possible to be used for accurate modeling, however the complexity of this model usually leads to the heavy computation work on the onboard processors. In addition, it requires many special tire parameters to complete the empirical formulas which are usually unknown. Therefore, a proper tire model that can meet not only the requirements of nonlinearity but also the computation efficiency was being perused by many researchers. Dugoff model is widely used for the analysis of non-linear dynamics and combined-slip force in [Dugoff 1969] and [Ding 2010]. Instead of the common linear tire model, the nonlinear Dugoff tire model can be expressed by a simple rational function, which is adopted for developing the vehicle dynamics parameters estimation and control strategies.

$$F_{yij} = -C_{ij} \tan \alpha_{ij} f(\lambda), \tag{5.4}$$

where  $C_{ij}(N/rad)$  is the cornering stiffness assumed to be known,  $\alpha_{ij}$  is the sideslip angle at each wheel given by the following equation:

$$\begin{aligned}
\alpha_{11} &= \delta_{11} - \beta - \frac{L_1 \dot{\psi}}{V_g}, \\
\alpha_{12} &= \delta_{12} - \beta - \frac{L_1 \dot{\psi}}{V_g}, \\
\alpha_{21} &= -\beta + \frac{L_2 \dot{\psi}}{V_g}, \\
\alpha_{22} &= -\beta + \frac{L_2 \dot{\psi}}{V_g}.
\end{aligned} \tag{5.5}$$

and  $f(\lambda)$  is a nonlinear function of the sideslip angle and the vertical force,

$$f(\lambda) = \begin{cases} (2 - \lambda)\lambda & \text{if } \lambda < 1, \\ 1 & \text{if } \lambda \geq 1, \end{cases} \tag{5.6}$$

and

$$\lambda = \frac{\mu F_{zij}}{2C_{ij} \tan \beta_{ij}}, \quad (5.7)$$

with  $\mu$  the friction coefficient between the tire and the road,  $F_{zij}$  is the vertical force on each wheel. The effect of the longitudinal force is ignored because of the simplicity of the model.

When the sideslip angle changes, there is a time lag for lateral force to act. Since the lateral deformation on the tire occurs with a little delay compared with the steer wheel input. Hence the relaxation length is related to the distance needed by the tire to reach a steady state situation after a step change in slip. A dynamic model of tire force has been proposed by [Rajamani 2006]:

$$\dot{F}_{yij} = \frac{Vg}{\sigma_i} (-F_{yij} + \bar{F}_{yij}), \quad (5.8)$$

where  $\sigma_i$  is the relaxation length which is supposed to be known, the  $\bar{F}_{yij}$  is the static force calculated by the Dugoff model (5.4).

## 5.4 Estimation process in real-time

The implementation of estimation process is illustrated in Figure 5.2. A particular module ‘‘CubeClient’’ is developed for the task of communication between data acquisition cube and host computer, sending request, receiving UDP packet and decoding UDP packet. These decoded data will be used as the inputs of the estimation process operated in real-time. All the sensor data are synchronized at the host PC and then send to the shared memory. A more complete explanation of the communication and acquisition architecture will be given in chapter 7.

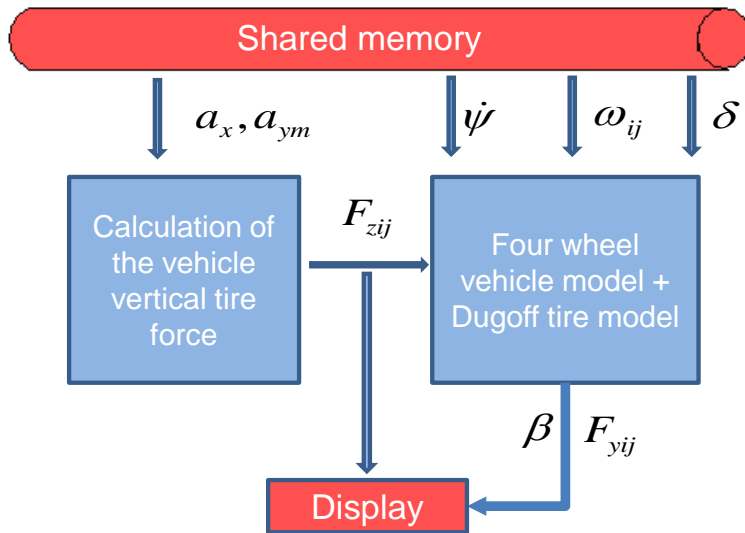


Figure 5.2: Lateral tire force estimation schema

The required measurement in this estimation process is itemized as follows:

- $a_x, a_{ym}$ : longitudinal and lateral accelerations measured by the inertial measurement.

- $\dot{\psi}$ ,  $\omega_{ij}$ ,  $\delta$ : vehicle yaw rate, wheel velocity and steering wheel angle accessed from vehicle CAN bus.

The quality of the required measurement is reduced, in order that the system has more opportunities to be realized in our quotidian vehicle as an additional safety option. In this bloc, the vertical force is calculated directly, it can effectively reduce the complexity of system structure and avoid the augmentation of the dimension of state vector. The vertical force and other measured data are used as the input of the estimator aimed at estimating the lateral force and sideslip angle. Other components which are designed for the management of different equipments are constructed in our work. In the system of the estimation process, observers are developed in .dll form as a real-time application.

## 5.5 Nonlinear observer modeling

As mentioned in the previous section, different observer technologies are used in the estimation process. We propose to use two nonlinear observers which are adapted to the nonlinear vehicle and tire model explained in the second section.

### 5.5.1 State-space representation

Considering current estimation methodologies, the Extended Kalman filter (EKF) and the Particle filter (PF) are selected in our algorithms. For a general nonlinear model, it can be formulated as follows:

$$\begin{cases} x_t &= f(x_{t-1}, u_t) + \omega_t, \\ y_t &= h(x_t) + v_t, \end{cases} \quad (5.9)$$

where  $x_t$ ,  $y_t$ ,  $u_t$  give respectively state space, measurement vector and input vector. The function  $f$  and  $h$  represent the process and measurement function, the random variables  $\omega_t$  and  $v_t$  represent the process and measurement noise.

The state vector  $x_t$  comprises the yaw rate, sideslip angle, velocity and lateral forces:

$$x = [\dot{\psi}, V_g, \beta, F_{y11}, F_{y12}, F_{y21}, F_{y22}, F_{x1}]. \quad (5.10)$$

Otherwise, the input vector  $u_t$  comprises the steering angle and vertical forces at each tire:

$$u = [\delta, F_{z11}, F_{z12}, F_{z21}, F_{z22}]. \quad (5.11)$$

Usually, we consider that the steering wheel angle of the front tires are equal and these on the rear tires as zero. The measurement vector  $Y_t$  is given as follows:

$$y = [\dot{\psi}, V_g, a_x, a_y]. \quad (5.12)$$

Combined with the model that we have presented in this section 2.4.2.2, the nonlinear system function can be summarized in continuous-time state-space. Moreover, the first order approximation of Euler is used to transform the continuous-time system to the discrete-time system, since the Euler discretization gives the same result as a first-order approximation to the matrix exponential in the conversion of a continuous time signal to a discrete time signal.

$$x_k = x_{k-1} + t_s \dot{x}_{k-1} \quad (5.13)$$

It is noted that  $t_s$  is the sampling time, consequently the nonlinear evaluation function  $f$  is discretized with the state variables at instant  $k$  related to the instant  $k - 1$ :

$$\left\{ \begin{array}{l} x_{1,k} = x_{1,k-1} + \frac{t_s}{I_z} [L_f((x_{4,k-1} + x_{5,k-1}) \cos(u_{1,k}) + x_{8,k-1} \sin(u_{1,k})) \\ \quad - L_r(x_{6,k-1} + x_{7,k-1}) + \frac{E_1+E_2}{4}(x_{4,k-1} \sin(u_{1,k}) - x_{5,k-1} \sin(u_{1,k}))] \\ x_{2,k} = x_{2,k-1} + \frac{t_s}{m}(x_{8,k-1} \cos(x_{3,k-1} - u_{1,k}) + x_{4,k-1} \sin(x_{3,k-1} - u_{1,k}) \\ \quad + x_{5,k-1} \sin(x_{3,k-1} - u_{1,k}) + x_{6,k-1} \sin(x_{3,k-1}) + x_{7,k-1} \sin(x_{3,k-1})) \\ x_{3,k} = x_{3,k-1} + \frac{t_s}{mx_{2,k-1}}(-x_{8,k-1} \sin(x_{3,k-1} - u_{1,k}) + x_{4,k-1} \cos(x_{3,k-1} - u_{1,k}) \\ \quad + x_{5,k-1} \cos(x_{3,k-1} - u_{1,k}) + x_{6,k-1} \cos(x_{3,k-1}) + x_{7,k-1} \cos(x_{3,k-1})) - t_s x_{1,k-1} \\ x_{4,k} = x_{4,k-1} + \frac{t_s x_{2,k-1}}{\sigma_f} (\overline{F_{y11}} - x_{4,k-1}) \\ x_{5,k} = x_{5,k-1} + \frac{t_s x_{2,k-1}}{\sigma_f} (\overline{F_{y12}} - x_{5,k-1}) \\ x_{6,k} = x_{6,k-1} + \frac{t_s x_{2,k-1}}{\sigma_r} (\overline{F_{y21}} - x_{6,k-1}) \\ x_{7,k} = x_{7,k-1} + \frac{t_s x_{2,k-1}}{\sigma_r} (\overline{F_{y22}} - x_{7,k-1}) \\ x_{8,k} = x_{8,k-1} \end{array} \right. \quad (5.14)$$

where  $\sigma_f$  and  $\sigma_r$  represent the front and rear tire relaxation length,  $\overline{F_{yij}}$  is the lateral tire force at four wheels calculated by the Dugoff tire model. Correspondingly, the observation equation  $h$  in discrete-time expression is given as follows:

$$\left\{ \begin{array}{l} y_{1,k} = x_{1,k} \\ y_{2,k} = x_{2,k} \\ y_{3,k} = \frac{1}{m}(x_{8,k} \cos(u_{1,k}) - x_{4,k} \sin(u_{1,k}) - x_{5,k} \sin(u_{1,k})) \\ y_{4,k} = \frac{1}{m}(x_{8,k} \sin(u_{1,k}) + x_{4,k} \cos(u_{1,k}) + x_{5,k} \cos(u_{1,k}) + x_{6,k} + x_{7,k}) \end{array} \right. \quad (5.15)$$

Subsequently, for this nonlinear model, the implementation of two different observers will be presented in the following part:

## 5.5.2 Implementation of filter technique

### 5.5.2.1 Observability analysis

As the nonlinear state-space representation is given in the previous section, an essential condition of the construction of the observer, that is the observability, should be verified. The nonlinear system cannot use the observability matrix any more, the observability of nonlinear system is verified through a concept of local observability, where the Lie derivative is used to constitute the observable matrix. It is difficult to compute the Lie derivative terms in such a complex model even with the support of the mathematical toolbox in MATLAB. A simplification was proposed in [Doumiati 2009] to apply the linear model instead of the Dugoff tire model, the system is local observable except when the vehicle velocity is quite slow.

### 5.5.2.2 EKF algorithm:

The Kalman filter is firstly proposed by R. E. Kalman at 1960 [Kalman 1960], which solves the discrete data linear filtering problem by using a recursive method. The Kalman filter provides an effective method to estimate the state and minimize the mean squared error. The Kalman filter is able to estimate the past, current and future states. However, the Kalman filter is

addressed to solve the linear problem. As we have presented, the vehicle and tire models are nonlinear, therefore we propose to use the Extended Kalman filter (EKF), identified here as  $O_{EF_y}$ , to estimate the process and measurement relationship [Welch 1995].

The state estimation is given by linearizing the process function, using the first element of the Taylor series expansion. Meanwhile Euler discretization for all continuous variables is made to obtain a discrete time system. The EKF is widely used to estimate the vehicle dynamics parameters in [Kim 2009] [Baffet 2007].

The Extended Kalman filter Algorithm:

- Time update equations:

$$\hat{x}_{t|t-1} = f(\hat{x}_{t-1|t-1}), \quad (5.16)$$

$$P_{t|t-1} = F_t P_{t-1|t-1} F_t' + Q, \quad (5.17)$$

- Measurement update equations:

$$K_t = P_{t|t-1} H_t' (H_t P_{t|t-1} H_t' + R)^{-1}, \quad (5.18)$$

$$\hat{x}_{t|t} = \hat{x}_{t|t-1} + K_t (y_t - h(\hat{x}_{t|t-1})), \quad (5.19)$$

$$P_{t|t} = (I - K_t H_t) P_{t|t-1}. \quad (5.20)$$

where  $F_t$  and  $H_t$  are the process and measurement Jacobian at step  $t$ :

$$F_t = \left. \frac{\partial f(x_{t-1})}{\partial x_{t-1}} \right|_{x_{t-1}=\hat{x}_{t-1|t-1}}, \quad (5.21)$$

$$H_t = \left. \frac{\partial h(x_t)}{\partial x_t} \right|_{x_t=\hat{x}_{t|t-1}}.$$

$Q$  and  $R$  are the variance-covariance matrices related to the Gaussian, white and centered noise  $\omega_t$  and  $v_t$  (in equation 5.9), respectively. The detailed observer tuning will be given in the next subsection.

### 5.5.2.3 Bootstrap PF algorithm:

The Extended Kalman filter is the most popular approach to solve the recursive nonlinear state estimation, nevertheless we need to linearize the nonlinear state transition and observation equations for the current state. This local linearization may produce a divergence from the correct state-space trajectory, even when the system and/or observation noises are low. Therefore, we propose to use the Particle filter (PF), identified by  $O_{PF_y}$  on the text, to process the nonlinear model instead of the linearization technique of the EKF to approximate the nonlinear state transition equation.

There are many tutorials for the methods of the Particle filter in [Beadle 1997][Candy 2007], the Particle filter is regarded as an approximation of a Bayesian filter. The Sampling Importance Resampling (SIR) method or bootstrap method is a Monte Carlo method that can be applied to recursive Bayesian filtering problems [Arulampalam 2002]. The principal algorithm has been presented in section 3.5.3.

Actually, we cannot get rid of Gaussian approximations by adopting the Extended Kalman filter. However, Particle filter is a method for discrete approximation of dynamic and non-Gaussian probability distribution, but by using numerous particles with higher computation

cost. Most Particle filter algorithms are variants of the basic SIS (Sampling importance sampling) algorithm. However, a degeneracy problem occurs during the iteration of the update equations. A few particles have significant weight distribution, the other particles will have very small weights. In a common way, we can use the resampling method to deal with the degeneracy problem. A new set of defined particles will replace the degenerative particles. In the real application, the resampling step is always a crucial and computationally expensive part in a Particle filter, therefore the balance between the resampling quality and computational efficiency should be discussed. Several resampling methods are given in [Douc 2005][Hol 2006] and [Bolic 2003].

The optimal choice of resampling method can give the benefits from the reducing of the system complexity and improving the quality of the resampling step. Considering these factors, we opt the residual resampling algorithm among several resampling algorithms by the comparison mentioned in [Douc 2005][Hol 2006]. The residual resampling algorithm has satisfactory computation effort and resampling performance. Moreover, it's not sensitive to the order in which the particles are ordered, with the behavior more like the basic multinomial resampling approach that neglects the numbered particles' order. The residual resampling algorithm is presented as follows [Liu 1998]:

Residual resampling Algorithm:

- Integer part: at time  $t \geq 1$ , for  $i = 1, \dots, N$ ,
  - Apportion the integer part of  $k_t^i = \lfloor N\omega_t^i \rfloor$  to the new distribution.
- Residual number of particles to sample: at time  $t \geq 1$ , for  $i = 1, \dots, m$ , where  $m = N - \sum_{i=1}^N k_t^i$ ,
  - Resample  $m$  particles where the probability for selecting  $\tilde{x}_t^i$  is proportional to  $\tilde{\omega}_t^i = \frac{N\omega_t^i - \lfloor N\omega_t^i \rfloor}{N - \sum_{i=1}^N k_t^i}$ .
  - Generate  $m$  independent ordered random variables  $u_t^i$  uniformly distributed on interval  $[0, 1)$ .
  - Select  $\tilde{x}_t^i$  according to the above mentioned distribution  $\tilde{\omega}_t^i = x_t^i(P^{-1}(u_t^i))$ , for  $u_t^i \in [\sum_{j=1}^{i-1} \tilde{\omega}_t^j, \sum_{j=1}^i \tilde{\omega}_t^j)$ , where the function  $P^{-1}$  express the inverse of the cumulative probability distribution function associated with the normalized weight  $\tilde{\omega}_t^i$ .

### 5.5.3 Observer tuning

The observer tuning is a very important step during the design of the observers. All the model and measurement quality should be considered in the set of the covariance matrices. For the measurement noise covariance  $R$ , it is possible to measure the process, so some off-line measurements of the sensors could be taken in order that we could decide the variance of the measurement noise. The sensors equipped in our experimental vehicle have good accuracy, hence the noise of the measurement is quite small, which means that we have good confidence about the measurements.

On the contrary, the process noise covariance is usually more difficult to be determined, by the reason that the process cannot be observed directly by us. A relatively uncertain process model can even have better estimation results via the selection of covariance matrix  $Q$ . The yaw rate, vehicle velocity at the center of gravity and sideslip angle have a precise model as described in the section II, hence they have a small uncertainty at the average noise. Considering the

dynamics lateral force model with the relaxation length, the uncertainty about the lateral force model is not too much. However, we don't use any longitudinal tire force model here, which means that the longitudinal movement is ignored in our process model. The longitudinal model is totally uncertain, therefore the noise is set to high noise level.

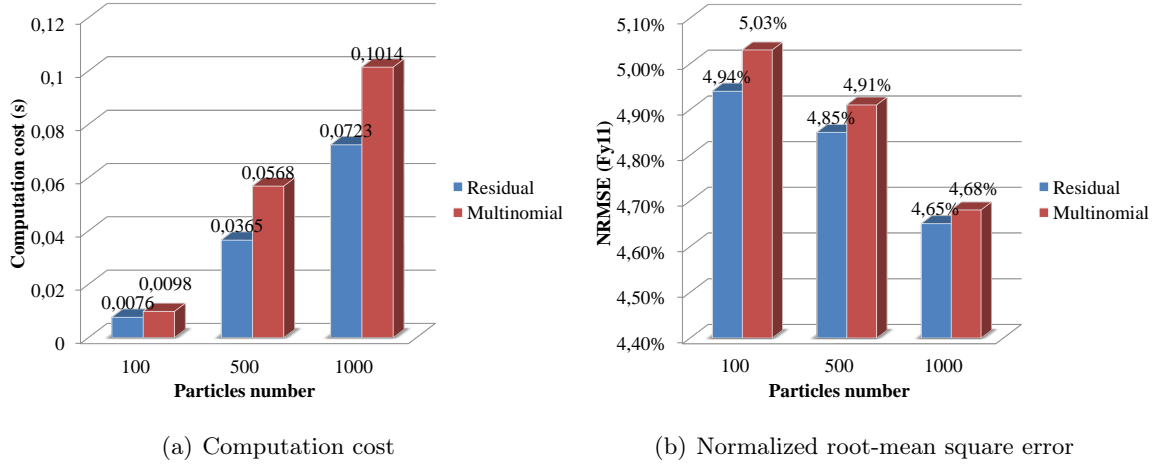


Figure 5.3: Comparison of two resample algorithms

Besides, the measurement covariance  $R$  and the process noise covariance  $Q$  are diagonal, they are respectively considered uncorrelated. After several on-line tests, the optimal noise tuning of EKF is given as the matrices as follows:

$R_{EKF}$  :

$$\begin{pmatrix} 0.005 & 0 & 0 & 0 \\ 0 & 0.001 & 0 & 0 \\ 0 & 0 & 0.01 & 0 \\ 0 & 0 & 0 & 0.06 \end{pmatrix}$$

$Q_{EKF}$  :

$$\begin{pmatrix} 10^{-8} & 0 & 0 & 0 & 0 & 0 & 0 & 0 \\ 0 & 0.001 & 0 & 0 & 0 & 0 & 0 & 0 \\ 0 & 0 & 0.000004 & 0 & 0 & 0 & 0 & 0 \\ 0 & 0 & 0 & 10^3 & 0 & 0 & 0 & 0 \\ 0 & 0 & 0 & 0 & 10^3 & 0 & 0 & 0 \\ 0 & 0 & 0 & 0 & 0 & 10^3 & 0 & 0 \\ 0 & 0 & 0 & 0 & 0 & 0 & 10^3 & 0 \\ 0 & 0 & 0 & 0 & 0 & 0 & 0 & 10^5 \end{pmatrix}$$

Usually, the observer tuning of the PF can use the EKF tuning as a reference, hence the PF tuning is given as follows:

$R_{PF}$  :

$$\begin{pmatrix} 0.04 & 0 & 0 & 0 \\ 0 & 0.08 & 0 & 0 \\ 0 & 0 & 0.05 & 0 \\ 0 & 0 & 0 & 0.01 \end{pmatrix}$$

$Q_{PF}$  :

$$\begin{pmatrix} 0.0008 & 0 & 0 & 0 & 0 & 0 & 0 & 0 \\ 0 & 0.001 & 0 & 0 & 0 & 0 & 0 & 0 \\ 0 & 0 & 0.00001 & 0 & 0 & 0 & 0 & 0 \\ 0 & 0 & 0 & 10 & 0 & 0 & 0 & 0 \\ 0 & 0 & 0 & 0 & 10 & 0 & 0 & 0 \\ 0 & 0 & 0 & 0 & 0 & 10 & 0 & 0 \\ 0 & 0 & 0 & 0 & 0 & 0 & 10 & 0 \\ 0 & 0 & 0 & 0 & 0 & 0 & 0 & 1000 \end{pmatrix}$$

Additionally, another essential parameter for the Particle filter is particle number. The particle number can effectively affect the computation cost and the quality of observer's performance. A simple measure of the computation cost can be given in Figure 5.3, several propositions of particle number are compared w.r.t the iteration cycle time in Figure 5.3(a) and the statistic error analysis of the estimation results in Figure 5.3(b). The precision of the estimator is not well enhanced with the augmentation of the number of particle, however the computation time cannot satisfy the requirement of the real-time process system with a high number of particles. In consequence, the number of the particle is set to be 100 during the experimental validation. Moreover, the comparison between residual resample and multinomial resample algorithm with different number of particles illustrates that the reason of using residual resample algorithm. The strict requirement of the real-time system necessitates better designed observers.

From what has been discussed above, the tuned Extended Kalman filter and Bootstrap Particle filter with residual resample have been respectively implemented as a real-time application running at  $200Hz$  in C++. The performance of these embedded process systems will be demonstrated in the following experimental tests.

## 5.6 Experimental validation

In this section, we present the validation of the performance of the EKF and PF through real data acquired with the experimental vehicle. The tests are operated with our own developed Peugeot 308sw equipped with various sensors. The input measurements of the observer are obtained from CAN bus, accelerometer and gyrometer. To validate the performance of the observer output, the tire forces and torques are measured in three dimensions. These sensors are applied only for the experimental validation, since these sensors are too much expensive to be applied in the passenger cars. The sideslip angle at COG is measured by the optical sensor CORREVIT which aimed at measuring the longitudinal and lateral velocity as well as the sideslip angle. The complete description of the function of sensors and the entire architecture of the acquisition system will be completed in chapter 7.

We would like to provide three different tests to validate the performance of observers in different road conditions, the vehicle transverse dynamics is compared with two different observation techniques presented in chapter 3, which are the extended Kalman filter observer  $O_{EF_y}$  and the particle filter observer  $O_{PF_y}$ . As we have presented and analyzed plenty of tests for the normal road condition in [Baffet 2007] and [Doumiati 2009], here we would like to give out some experimental tests in real common driving situation with typical pavements: dry, wet and bumpy. The first slalom test is performed on the dry plane pavement, which is considered to

validate the basic performance of our two different observers; the second test is a slalom maneuver on the wet urban road; the third test is aimed at validating the observer stability under the bumpy road, where the input variables are much noisier. These tests are distinguished from the smooth simulation test, all the input measurements are acquired from our real-time data acquisition system, and the observers are embedded in the process system. It is noted that all the estimations are completed in real-time, the plots of validation and the comparison results are implemented with MATLAB environment.

### 5.6.1 Slalom test on dry pavement

First, a slalom test is performed with our experiment vehicle DYNA on the Mortefontaine Automobile Testing and Research Centre (CERAM - Centre d'Essais et de Recherche Automobile de Mortefontaine). The test track is set to be dry ( $\mu = 1.0$ ). The experimental test trajectory is given as follows in Figure 5.5. We choose some characteristic segments to analyze the performance of our acquisition system and the observer's output in red area in Figure 5.5. Figure 5.4 shows the maneuver time history, during this test, the lateral acceleration reaches to  $0.6g$ , average speed of the slalom test is about  $50km/h$  and it begins to brake at the end of the test. The slalom maneuver is operated within the time interval ( $5s < t < 35s$ ). The wheel transducers are equipped at front wheels for the validation of tire/road contact point forces, the CORREVIT is used for the sideslip angle measurement.

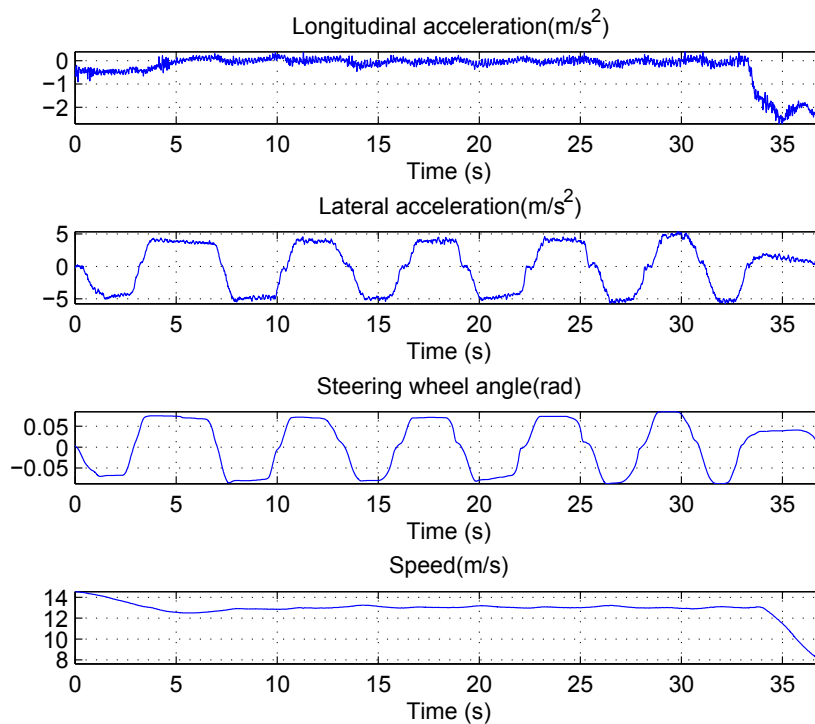


Figure 5.4: Maneuver time history: slalom test on dry pavement

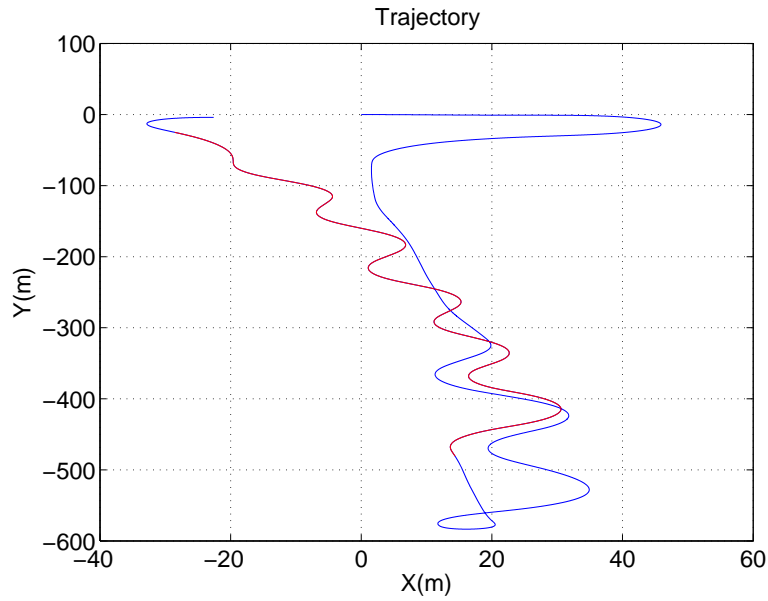


Figure 5.5: The trajectory of vehicle body movement: slalom test on dry pavement

The slalom test is usually considered a difficult maneuver from the estimation viewpoint. The vehicle dynamics characteristics are better solicited in this maneuver, it can better reveal the potential of the observer's performances. Figure 5.6 shows the vertical tire force calculated with open-loop method presented in equation (2.27). The advantage and limitation has been proved in the previous section, several experimental tests validate the feasibility of applying this model in the close-loop estimation of the desired lateral tire force. The calculated results match well with measurement from wheel force transducers. The estimation result of lateral forces is shown in Figure 5.7(a) and 5.7(b), the red lines correspond to the experimental data. Blue and green lines are respectively the results of the EKF ( $O_{EF_y}$ ) and PF ( $O_{PF_y}$ ) state observers.

From the quality analysis, the performance of our observer is quite good. During the transient period, the steering wheel angle changes quickly, it brings server maneuvers on the suspension and tire deformation. Hence even though the lateral tire forces follow tightly with the measurement, some slight deviation can be found at the moment of each peak of the turning.  $O_{EF_y}$  and  $O_{PF_y}$  provide similar performance concerning the slalom test, they are a little over estimated comparing with the measured data, it may be explained by the vehicle camber angle that affects the tire deformation as well as the suspension kinematic. Similarly, the observers provide an accurate estimation of the sideslip angle comparing with the CORREVIT sensor's measurement.

### 5.6.2 Slalom test on wet pavement

A second test is performed on a raining urban road, the parameters of the vehicle and observer configuration is not modified except for the coefficient of friction. According to the real road condition, the coefficient of friction is set at 0.6. Since the observer tuning is not changed in this test, the performance of the observers is able to apply the information about the robustness on different road conditions. The slalom maneuver is realized at an average speed of  $12m/s$  on the wet asphalt, we realized two slalom maneuver tests, the tracked trajectory is shown in

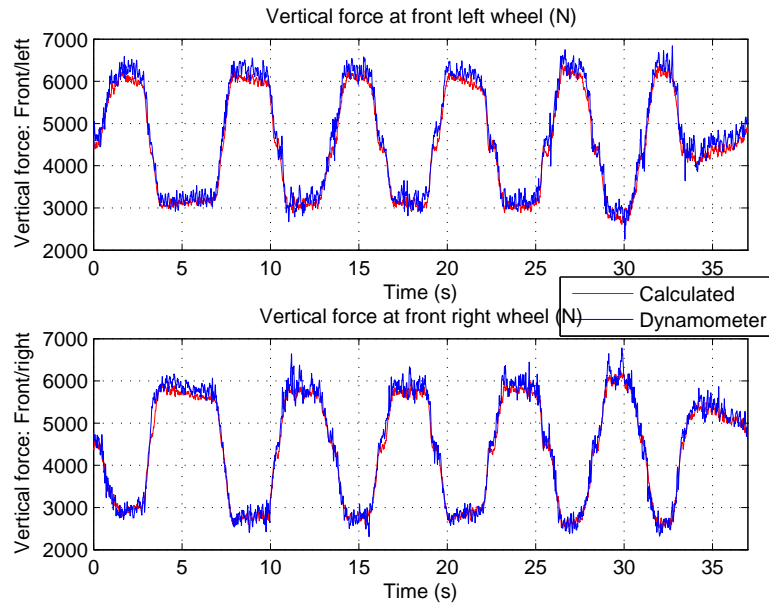
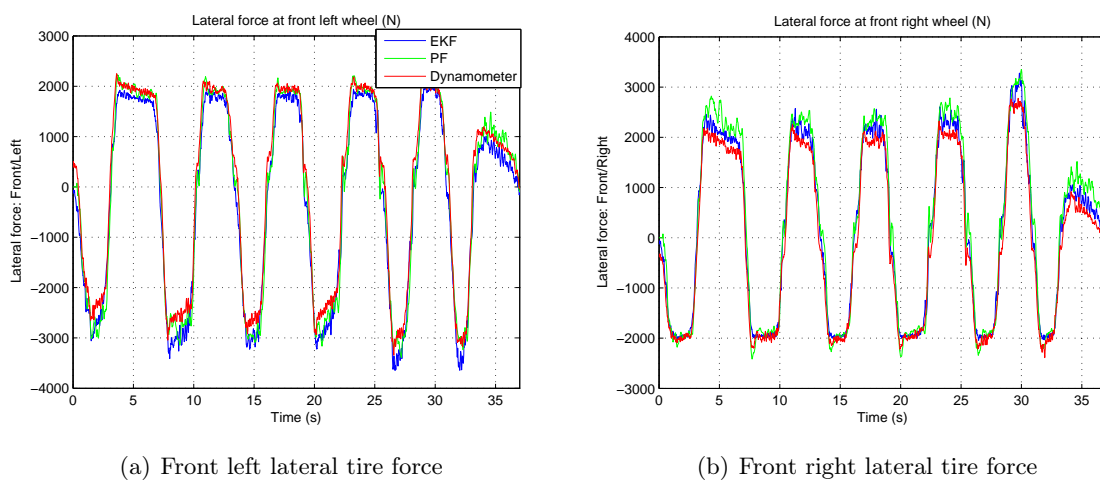


Figure 5.6: Comparison of front vertical tire forces: slalom test on dry pavement



(a) Front left lateral tire force

(b) Front right lateral tire force

Figure 5.7: Comparison of front lateral tire forces: slalom test on dry pavement

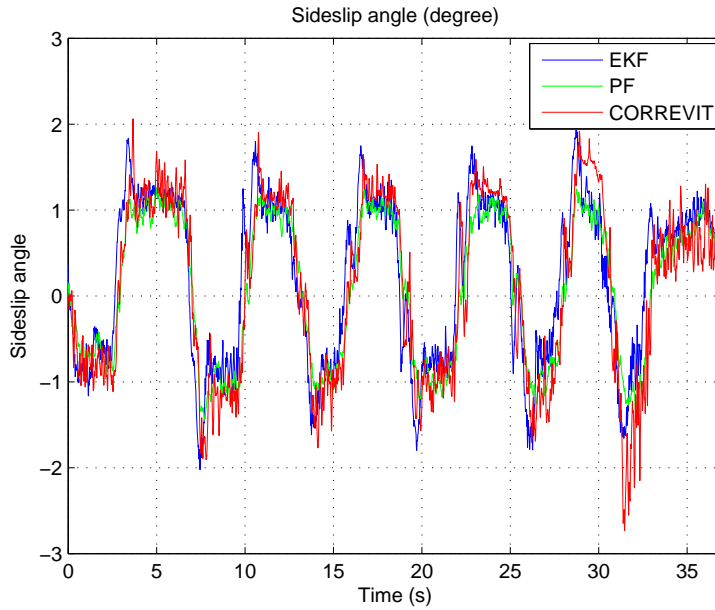


Figure 5.8: Comparison of sideslip angle: slalom test on dry pavement

Figure 5.10. The vehicle starts to accelerate at  $2m/s^2$ , then it begins to negotiate first slalom maneuver with a quasi-constant velocity at  $40km/h$ , the car turns around at the end of the road in order to perform a second test under the same condition. The steering angle was reaching the maximum range angle during the turn. Then the vehicle performs a second slalom test at the constant speed  $50km/h$ . The lateral acceleration can attain at  $-5m/s^2 < a_y < 5m/s^2$  during this experimental test. The detailed maneuver time history is illustrated in Figure 5.9.

Figure 5.11 illustrates the front vertical force distribution. Since the rear wheel force transducers were not installed at this test, we are not able to provide the comparison with respect to the rear ones. This test can be generally divided into three sections: two slalom maneuvers and one transient turning maneuver. The comparison result of two slalom tests is quite close to the first slalom test, the front vertical tire forces track closely with the sensor measured data. For the time period ( $20s < t < 30s$ ), vehicle speed is quite slow however the steering wheel angle input reaches up to  $0.5rad$ , this special movement is out of the constraint of the equations that reveals the vertical tire force related to longitudinal and lateral acceleration. Comparing the plotted estimation results concerned with lateral tire force, the particle filter and Extended Kalman filter are able to provide satisfactory estimation values, the lateral tire force recorded in the right hand and left one arise alternately above  $3000N$  due to the steering wheel handling. The same situation appeared for the lateral tire force, during the time period  $20s < t < 30s$ , the lateral tire force especially on the front right one saturates at about  $3000N$ , however the measured force exceeds  $4000N$ , this phenomenon is more obvious in the sideslip angle estimation. The explanation of this special comportment is due to the unmodeling characteristic of the vehicle model. When the vehicle speed is too slow, while the steering wheel angle is no longer provoke corresponding dynamics response. Currently, we need to explore another model for the case of low-speed comportment. Obviously, the wet road condition largely affects the precision of the sideslip angle estimation applying EKF. The low coefficient friction may much

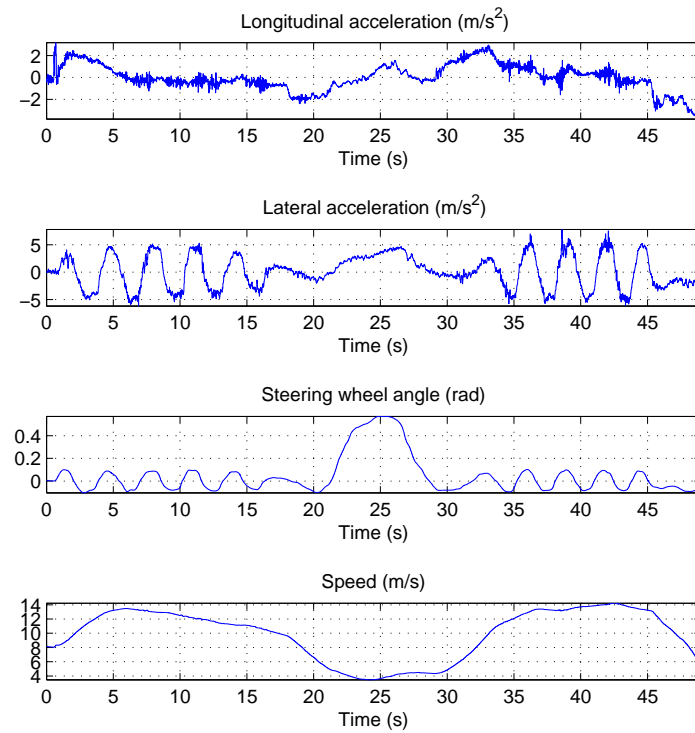


Figure 5.9: Maneuver time history: slalom test on wet pavement

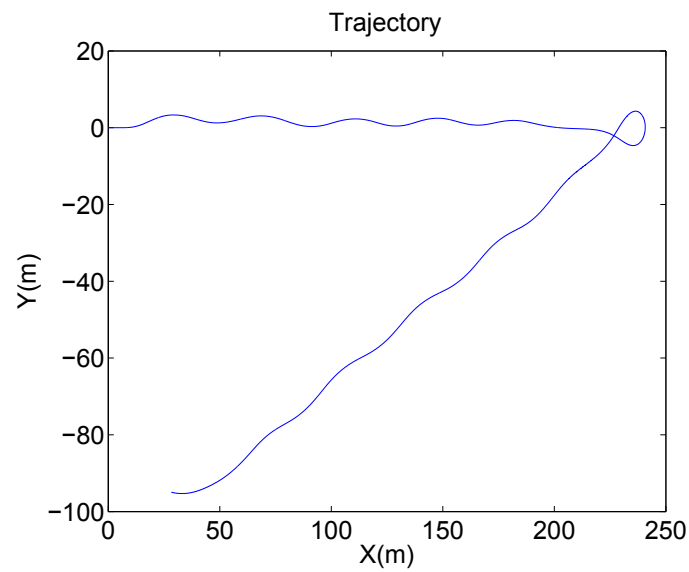


Figure 5.10: The trajectory of vehicle body movement: slalom test on wet pavement

easily take the force into nonlinear region, the EKF appears the risk of the observer divergence in the second slalom test. Therefore, the summarization directly perceived through the figures reveals that the Extended Kalman filter is somewhat feeble for this rainy road condition slalom test. The particle filter performs better for this current driving condition.

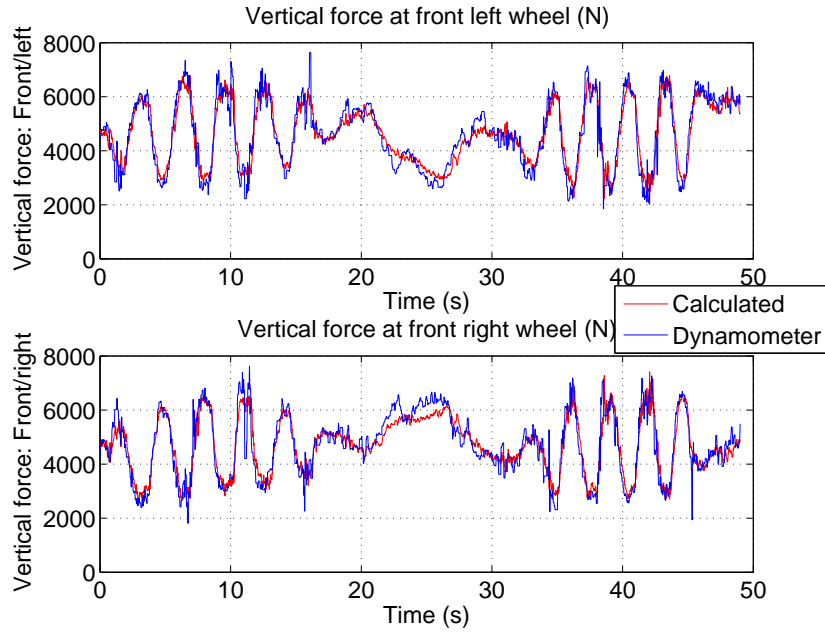
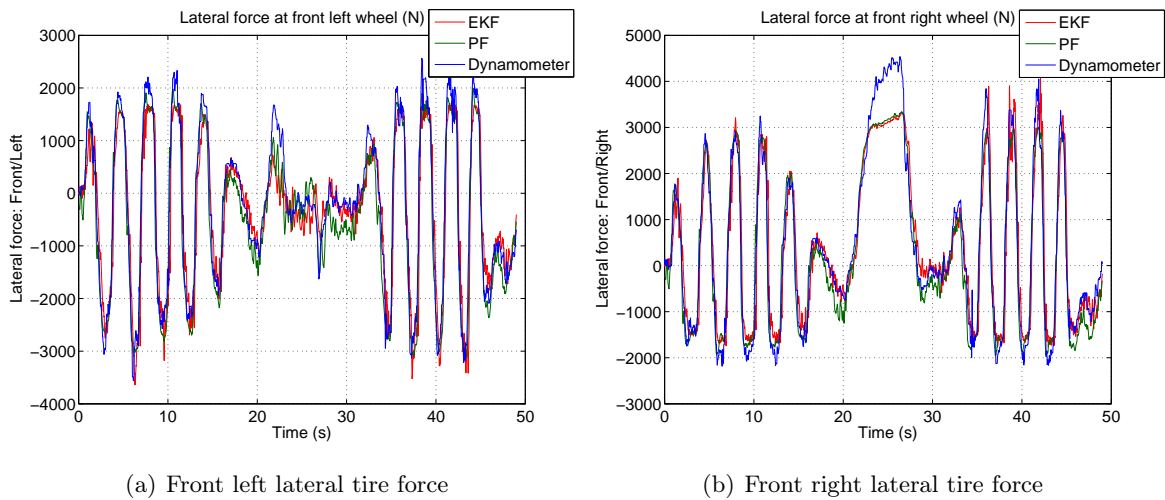


Figure 5.11: Comparison of front vertical tire forces: slalom test on wet pavement



(a) Front left lateral tire force

(b) Front right lateral tire force

Figure 5.12: Comparison of front lateral tire forces: slalom test on wet pavement

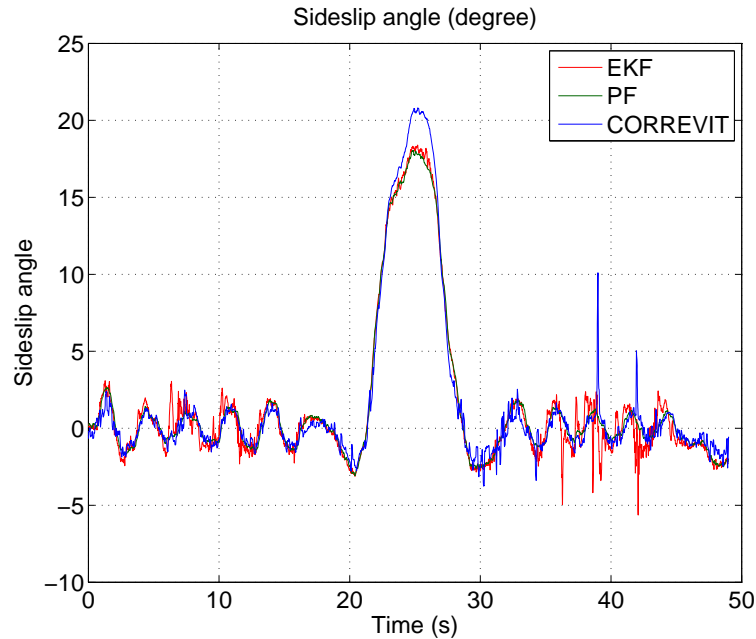


Figure 5.13: Comparison of sideslip angle: slalom test on wet pavement

### 5.6.3 Closed circle test on bumpy road

As we have discussed two typical experimental tests for different road conditions: dry and wet asphalt. This test is considered as a general performance evaluation for two observer technologies. The special point is that the road pavement is not a plane surface, some road bumps and makers can be assumed to be as the disturbances intervened in the observer estimation process. The test was done by taking campus internal lane around our research center, hence the vehicle speed is not allowed to be very fast. As we have presented in Figure 5.15, the vehicle trajectory is tracked within a closed loop, several severe curves can be found in this trace, these sections are expected to provoke the appearance of large sideslip angle. The time history is illustrated in Figure 5.14, this test combines with accelerating-braking and turning compartments, the lateral acceleration is constrained at  $-4m/s^2 < a_y < 4m/s^2$ .

Four vertical tire forces are respectively represented in Figure 5.16 and 5.17. The vertical tire force in open-loop at each tire is relevant and accurate with respect to the measured tire force, the load distribution at each tire is precisely described according to the analysis of torque balance at each tire. Even though the lateral load transfer is not directly affected in our expression, the longitudinal and lateral accelerations take account of the combination of the longitudinal and transverse movement into the modeling. Seen in Figure 5.18 and 5.19, they are dedicated to presenting the lateral tire force. The plotted estimation results follow well with the real values, globally the estimation accuracy is able to meet our requirement to take place of such physical wheel transducers. It is obvious that we could find the consequence of the load transfer produced from right side to the left hand at several time sequences. For example, in Figure 5.18, at time instant 5s, 20s..., the front left lateral tire force is much higher than the right one, this is due to the lateral load transfer affected on the tire. Usually the front tire charges much lateral force than the rear ones, it is explained by the unbalance vehicle load distribution by

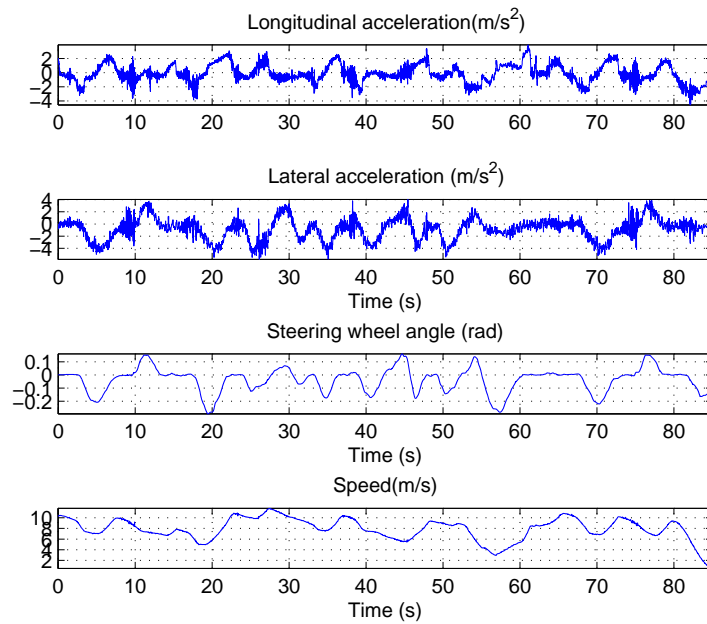


Figure 5.14: Maneuver time history: closed circle on bumpy road

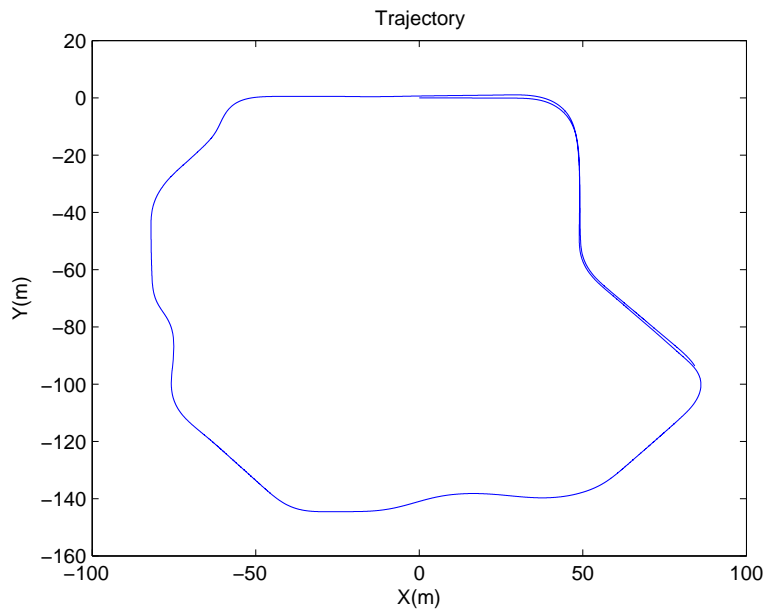


Figure 5.15: The trajectory of vehicle body movement: closed circle on bumpy road

the vehicle chassis design. The powertrain system and other accessory equipments make the front tire generally distributed with more load. Therefore, the lateral tire forces are affected by the tire load distribution. A conclusion can be directly drawn from these figures that the results are global good, and particle filter is much smoother than the red one that illustrated Extended Kalman filter. As far as we have presented the road surface is with bumpy and wave obstacles, the Extended Kalman filter can track well with the trend of the handling, however the disturbance on the input measurement apparently influences the observer's output. Figure 5.20 gives a good match between the estimated sideslip angle and the optical sensor. The particle filter successfully tracks the corresponding measurement, at the instant 20s and 57s where the sideslip angle exceeds  $-8^\circ$ , the corresponding lateral tire force attains at 3540N on front left wheel. Even though the lateral tire forces evidently enter the nonlinear region, the estimation result is satisfactory. The same phenomenon of sideslip angle appeared is similar to the lateral tire force, the result estimated by the particle filter is quite accurate, however the Extended Kalman filter is less convergent, some fluctuation can be detected in red line. Therefore comparing with the Extended Kalman filter, the particle filter is much more robust to the disturbance added into the input measured signals.

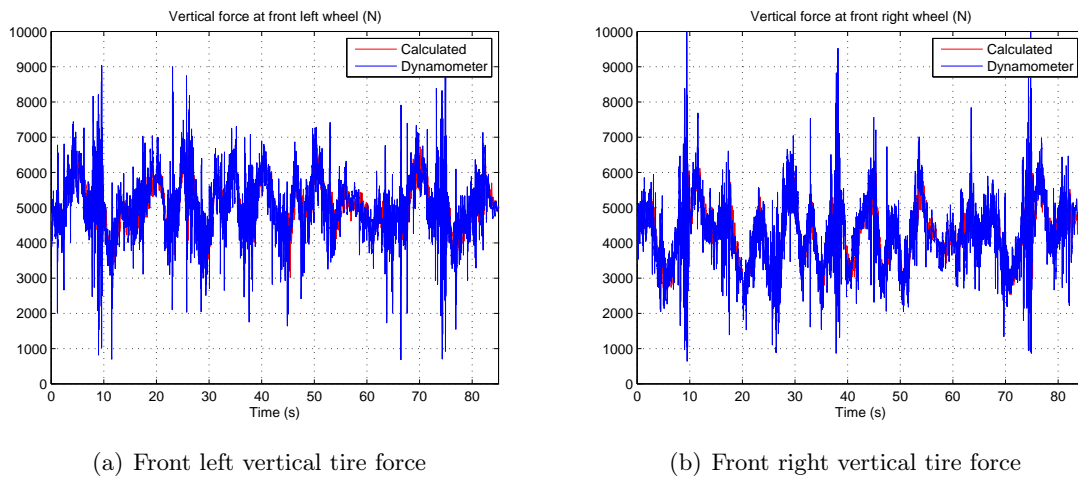


Figure 5.16: Comparison of front vertical tire forces: closed circle on bumpy road

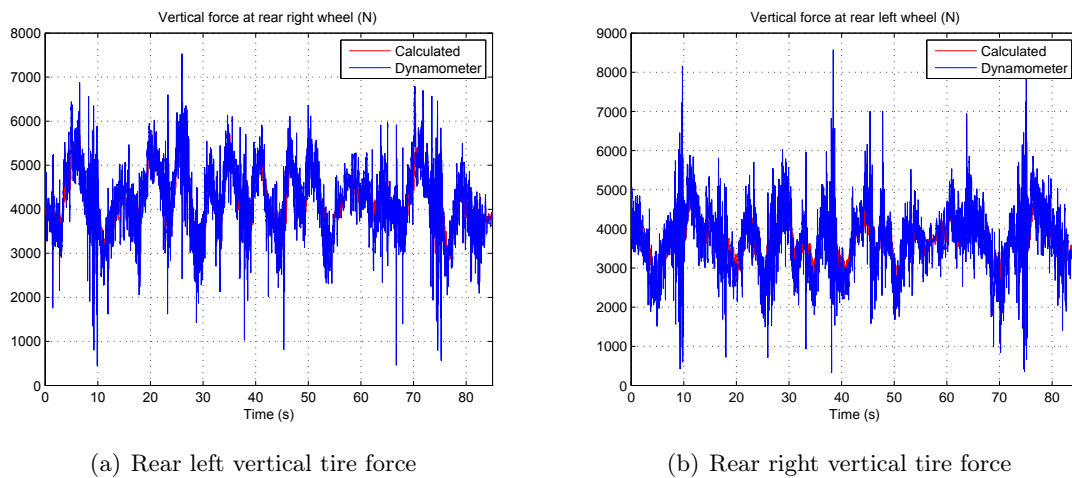


Figure 5.17: Comparison of rear vertical tire forces: closed circle on bumpy road

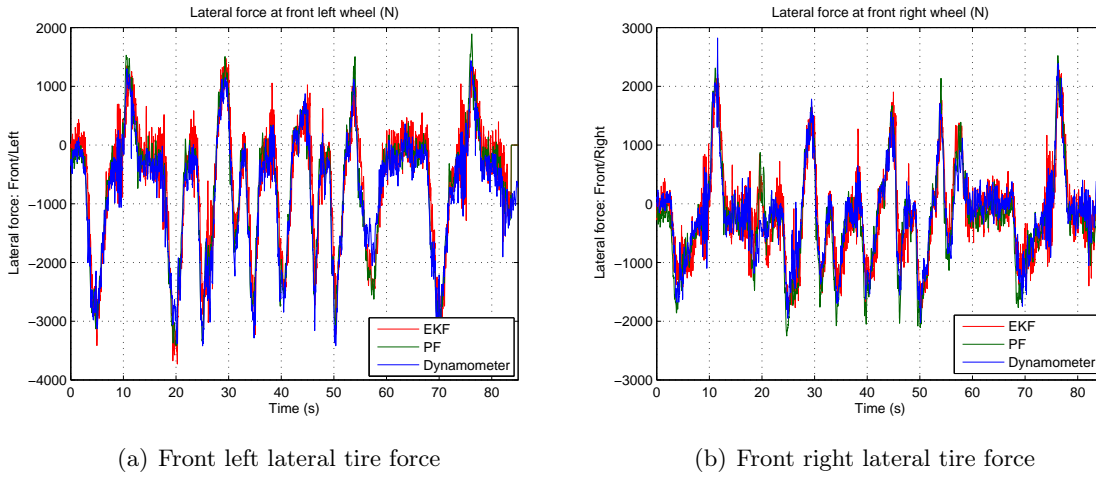


Figure 5.18: Comparison of front lateral tire forces: closed circle on bumpy road

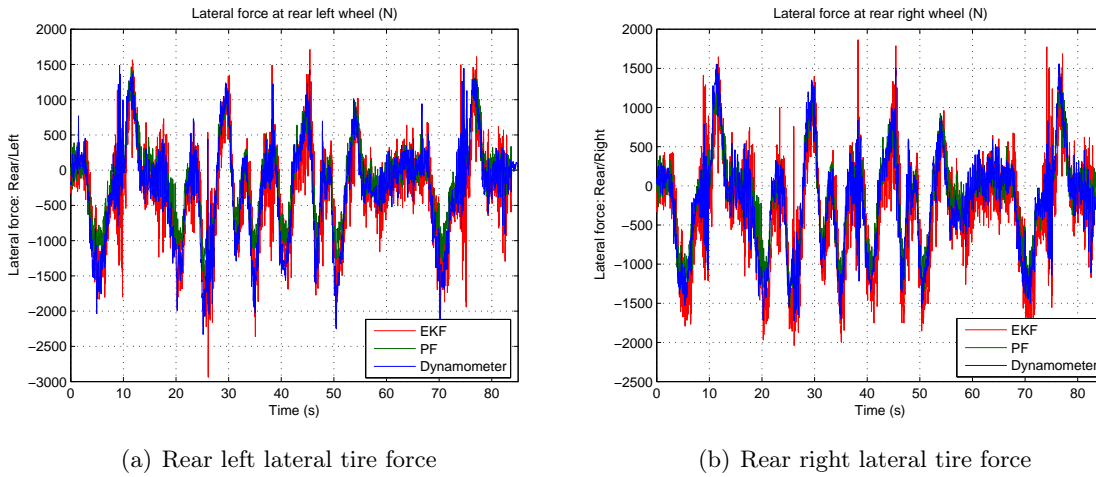


Figure 5.19: Comparison of rear lateral tire forces: closed circle on bumpy road

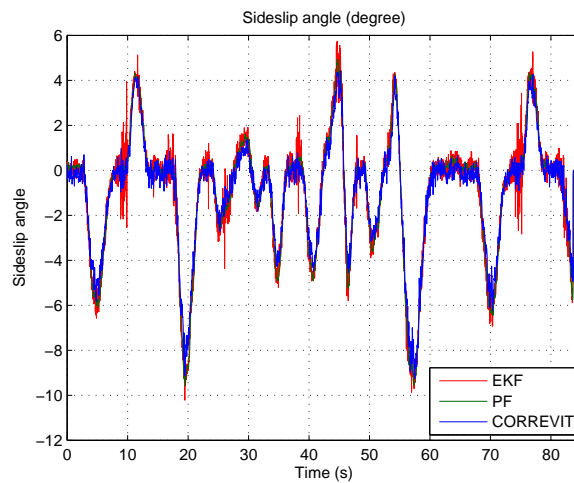


Figure 5.20: Comparison of sideslip angle: closed circle on bumpy road

### 5.6.4 Summary

From the previous figures illustrating estimation performance in the above section, we can easily draw the conclusion globally that  $O_{EF_y}$  and  $O_{PF_y}$  provide a successful estimation of the vehicle lateral dynamics, particularly the essential lateral tire force and sideslip angle are precisely estimated during steady-state and transient period. Except for the method of figure illustration, another statistic approach is employed to explain and compare the performance of each observer in a systemic way. The comparison between two different observers is illustrated by the figures and also analyzed by the statistics report. The normalized root-mean-squared-error is defined as:

$$NRMSE = \frac{\sqrt{\frac{1}{T} \sum_{t=1}^T (x_t - \hat{x}_t)^2}}{x_{max} - x_{min}} \quad (5.22)$$

The observer evaluation is reported in Table 5.2. It is explained that the rear force transducers were not yet equipped in our experimental vehicle in the first and second test, hence unfortunately the comparison data of rear tires is lacked in this table. In the first test (dry pavement),  $O_{EF_y}$  and  $O_{PF_y}$  produce similar results, it is hard to distinct which estimation method is more effective for the tire force, however the NRMSE of the sideslip angle states that  $O_{PF_y}$  is better than  $O_{EF_y}$ . A slight advantage is embodied in this normal slalom test, afterwards a same slalom test is performed on the wet asphalt ( $\mu = 0.6$ ), the parameters of the configuration of the observers are not changed, we expect to evaluate the robustness of the observers. Seen from the statistic report,  $O_{PF_y}$  provides stable and accurate estimation for both the front tire forces and sideslip angle, the NRMSE for  $O_{PF_y}$  is smaller than that for  $O_{EF_y}$ . On the wet pavement, the performance of particle filter is better than the Extended Kalman filter. In test 3 (bumpy pavement),  $O_{PF_y}$  is always less than 8%, while  $O_{EF_y}$  is above 8%, in particular the rear right tire attains 10.22%. Both two observer technologies supply accurate estimation of sideslip angle, with this test condition the particle filter reflects more advantages on the robustness of observation with respect to different real road environments.

	Test 1		Test 2		Test 3	
	$O_{EF_y}$	$O_{PF_y}$	$O_{EF_y}$	$O_{PF_y}$	$O_{EF_y}$	$O_{PF_y}$
$F_{y11}$	6.50	5.12	7.90	6.25	8.26	5.79
$F_{y12}$	5.02	7.96	8.05	6.55	7.68	6.28
$F_{y21}$	-	-	-	-	9.97	7.82
$F_{y22}$	-	-	-	-	10.22	7.85
$\beta$	11.45	8.63	4.52	3.64	3.96	3.27

Table 5.2: Normalized mean error between estimated lateral tire forces/sideslip angle and simulation output for three typical tests

From the figure and statistic report of the comparison representing two observers  $O_{EF_y}$  and  $O_{PF_y}$ , we can deduce that both EKF and PF are able to precisely estimate the variables in the constructed state vector, however PF shows more robust and accurate characteristics in the estimation process. Due to the global performance analysis, PF is less sensitive to the variation of the real environment for the nonlinear system: the road friction and surface condition. However, the computation time is largely augmented on account of the step of sampling and resampling process, this is always a challenge by applying the particle filter in real-time system, hence the particle number cannot be opted with large quantity. EKF is used as a simple and universal

method, even though it is somewhat unreliable in certain situation, however it is also figured out for a satisfactory solution for the estimation of vehicle dynamics parameters.

### 5.6.5 Robustness with respect to vehicle parameters

As we have presented several comparative experimental tests in the previous section, all the vehicle parameters are supposed known before the operation. Actually, in real situations, the vehicle parameters cannot be measured at any time and it is impossible to be initialized at the departure of each itinerary. Therefore, it inspires a great interest for us to study the performance of our observers in the presence of variation of certain parameters. In particular, we take the vehicle mass and the coefficient of friction as the target variables to evaluate the robustness of two different observers  $O_{EF_y}$  and  $O_{PF_y}$ . Since the vehicle is usually changed by the number of passengers and carrying cargoes in the trunk, the variation of vehicle mass may potentially change some other parameters e.g. center of gravity. Another selected parameter is the coefficient of friction, because the road condition changes at every instant, hence it is arduous to keep it constantly in the real driving situation. We choose the final test on the bumpy road, the vehicle mass is varying between  $-30\%$  and  $30\%$ , the variation step is set at  $10\%$ . The behavior of the coefficient of friction is similar to that of the vehicle mass.

First, we give the illustration of the mass variation to evaluate the robustness of the observer from Figure 5.21. The y-axis of figures is calculated according to the NRMSE equation in 5.22. The evaluation results are denoted respectively in Figure 5.21(a) and 5.21(b) applying Extended Kalman filter and Particle filter techniques. The variation from  $-30\%$  to  $30\%$  affects more seriously on the NRMSE, it is clear that the mass variation has a great influence on the precision of EKF and PF for the estimation of lateral tire forces, however  $O_{PF_y}$  is less sensible than  $O_{EF_y}$ . Analyzing the sideslip angle, it is not obviously affected by the change of vehicle mass.

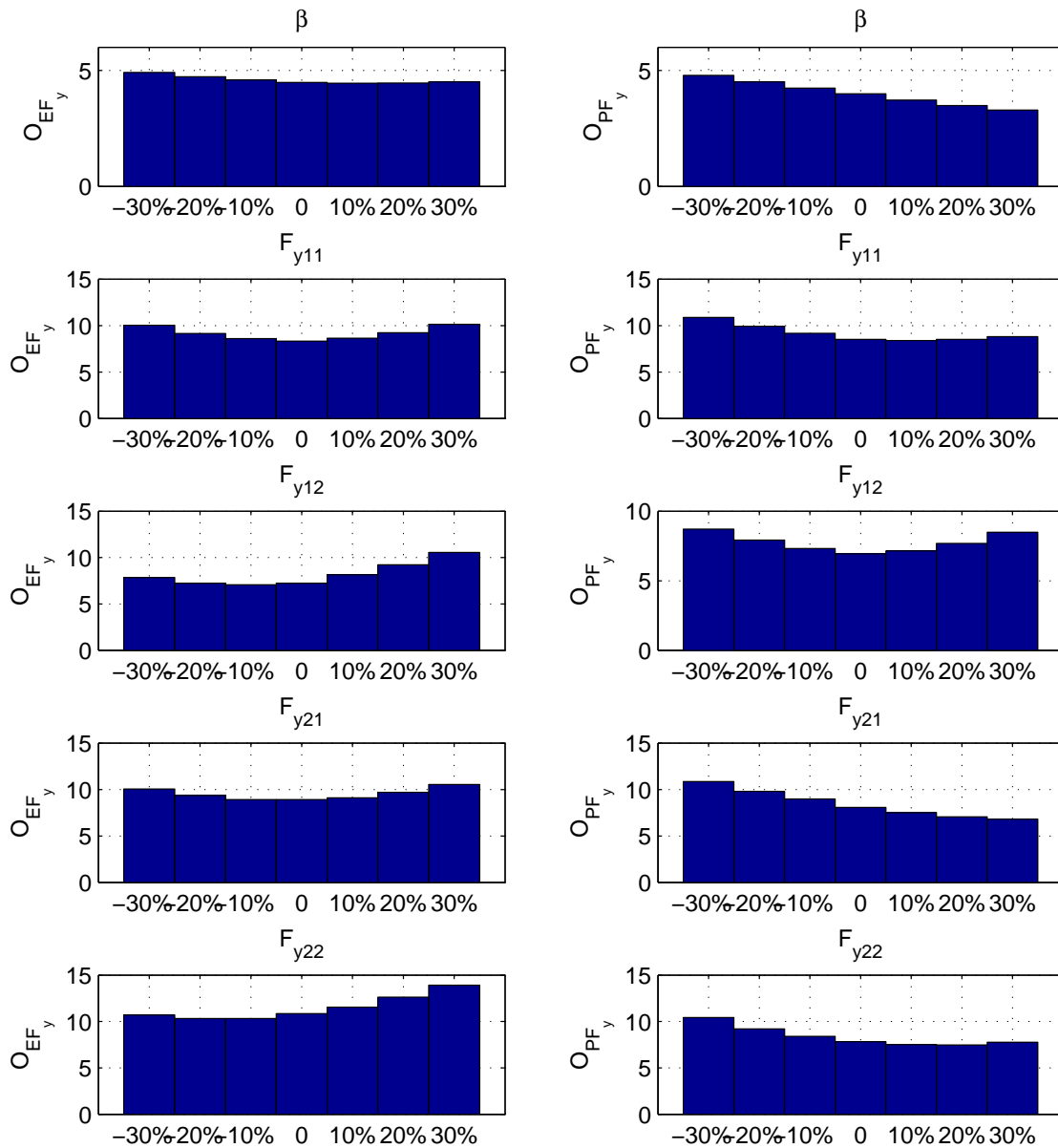
Figure 5.22(a) and 5.22(b) respectively illustrate the influence of the  $\mu$  variation, the sideslip angle is merely affected by the  $\mu$  variation. Besides, the lateral tire forces are also not quite affected by the decreasing of  $\mu$ . It manifests that when the road pavement is no more dry, changing to the wet surface, the two methods are able to provide similar results.

In brief,  $O_{EF_y}$  and  $O_{PF_y}$  are robust to the variation of two selected parameters,  $O_{PF_y}$  is less sensible than  $O_{EF_y}$  in the evaluation in terms of the observer robustness. Therefore, they are reliable to be applied in the common condition in order to estimate the essential vehicle dynamics parameters in the advanced driver assistance system.

## 5.7 Conclusion

This chapter gives a description of the vehicle lateral dynamics estimation, we look back the development about the estimation of the vehicle dynamics parameters concerning lateral tire force and sideslip angle. It is noted that these vehicle dynamics parameters are essential for the evaluation of the vehicle safety and the extension of the vehicle driving assistance system.

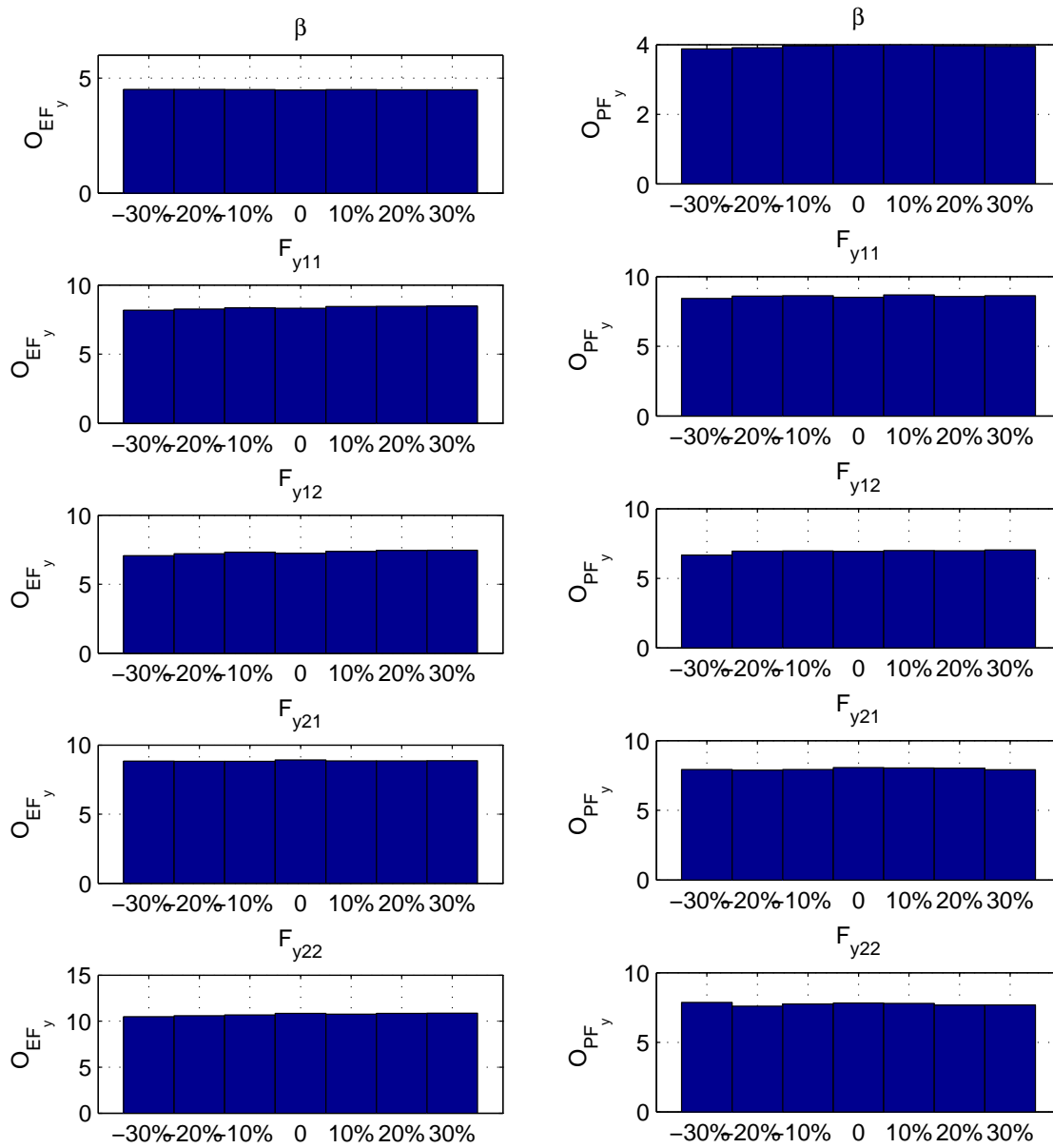
The double track vehicle model is applied to describe the dynamics parameters, we are trying to simplify the model with certain reasonable assumptions in order to make the calculation block easier but still remain at an accurate level. The required vertical force in the lateral tire force equations is calculated directly with a simple open-loop approach which depends on the longitudinal and lateral acceleration. Dugoff tire model combined with the dynamics tire force



(a) The robustnesses of Extended Kalman filter

(b) The robustnesses of Particle filter

Figure 5.21: Closed circle test on bumpy road:  $m : -30\% : 10 : 30\%$ ,  $m$  at  $0\% = 1667kg$



(a) The robustnesses of Extended Kalman filter

(b) The robustnesses of Particle filter

Figure 5.22: Closed circle test on bumpy road:  $\mu : -30\% : 10 : 30\%$ ,  $\mu$  at 0% = 1.0

relation is adopted in the construction of the tire force. All above mentioned solutions are based on the consideration of the balance of computational cost and precision. Since our target is to integrate such system into our experimental vehicle for the further ADAS modules in the passenger cars. The entire system is also complemented with the Extended Kalman filter and the Particle filter techniques. Besides, they are programmed as a real-time application embedded in the vehicle mounted system.

The developed algorithms are validated with real-time acquisition data. As lots of tests had been validated and compared in the previous research in our laboratory, the contribution of this thesis is to develop and extend these systems to be available in the real driving environment as well as to be operated in real-time with onboard data acquisition and information processing system. Several tests performed demonstrate the performance of our developed algorithm and the embedded system. A slalom test on dry and wet pavement respectively shows the evaluation of the capability of Extended Kalman filter and Particle filter techniques. In addition, a general test on bumpy road with high noise input is used to identify two different observer techniques. Although the Monte-Carlo method is always considered to be a heavy cost computation approach, however it is indubitable to be more robust to not only the external environmental condition (road pavement, friction change) but also the vehicle parameters (mass, height of gravity) than the Bayesian-based method with a Gaussian distribution. The detailed presentation of the vehicle embedded system will be given in chapter 7.

For the consideration of future exploration, a similar query may be raised by the readers what the performance will be given where the road is with bank and slope angle or with the coupling of the two conditions. It is interesting to continue this way to solve these questions. Since the real environment is quite complex, how can we deal with it in a simplification approach? The unknown input observer technique may give an effective solution to these uncertain information. Moreover, it will be an attractive study of applying these parameters providing the assessment of vehicle safety and the possibility of the control system development. The next chapter will focus on the development of the application employing these vehicle dynamics parameters, the risk prediction system will be presented with the description of basic theory and the implementation of corresponding system.



# Prediction system for curve negotiation

---

## Contents

---

<b>6.1</b>	<b>Introduction</b>	<b>117</b>
<b>6.2</b>	<b>Existing method of risk anticipation</b>	<b>118</b>
6.2.1	Road departure prediction	119
6.2.2	Vehicle rollover prediction	119
6.2.3	Curve speed prediction	119
6.2.4	Vehicle dynamics state prediction	120
<b>6.3</b>	<b>Methodology of the prediction system for safe curve negotiation</b>	<b>120</b>
6.3.1	Coordinate system and transformation	121
6.3.2	Reconstruction of the vehicle dynamics parameters	122
6.3.3	Methodology of the prediction system	124
<b>6.4</b>	<b>Simulation validation</b>	<b>129</b>
<b>6.5</b>	<b>Conclusion</b>	<b>137</b>

---

## 6.1 Introduction

Nowadays many driver safety assistance and stability control systems, such as lane departure warning system (LDWS), adaptive cruise control (ACC), electronic stability program (ESP), and active rollover prevention (ARP), are often equipped on modern vehicles. These embedded subsystems for the prevention of vehicle accident are demonstrated to be effective and low-cost in order that they are widely adopted in many automobile manufacturers. All the mentioned above systems are developed to reduce the vehicle run-off-road crashes. According to the study report of the United States Insurance Institute for Highway Safety (IIHS), it is issued that if all passenger vehicles were equipped with ESP, up to 10,000 fatal US crashes could be avoided annually. However, these systems rely on basic vehicle information from CAN bus, camera or radar. These systems typically react to an event that has already occurred and correct the driver's decision fault with the intervention of kinds of electronic systems.

The prediction system is different from the current ESP, ACC systems, the idea of such system is to provide driver a warning of the possibility that the accident may be occurred based on current driving maneuver and external road environment. However the question is proposed that how can we obtain the required information from the vehicle in the environment and what system can be exploited with these available information? These questions will become very appealing for us to predict an impending safety event and advise the driver to react in order to avoid potential road-departure accidents. Actually, the more complex and effective systems need more accurate information about the vehicle dynamics. Some parameters can be measured

directly, however some essential vehicle dynamics parameters are difficult to be accessed due to the limited technique reasons as well as the economic reasons. To solve this problem, we need to look back the presentation of previous chapters. The concept of virtual sensor was proposed by introducing the observer technology, the unmeasured variables can be estimated from the reconstruction of corresponding models.

With these estimated variables, we are able to design a prediction system for the lateral drift and rollover warning. In most cases, road departure accidents occurred during the curve negotiation. Therefore, our interest is focused on the safety improvement at the curve, we are willing to design a system to warn drivers when they are drifting out of their lane or about to enter a curve at an unsafe speed. To deal with this problem, we are trying to find a solution basing on the vehicle dynamics characteristics and GPS based positioning system. These two mentioned elements are extended as following considerations:

- (i) Development of a prediction algorithm basing on the vehicle dynamics information;
- (ii) Road geometry identification with the technique of vehicle localization.

To deal with the first proposition, we can use the methodology developed in the previous sections, which provides accurate data about vehicle dynamics. The validated accuracy and efficiency estimation methods supply a solution to the unmeasured data. Besides, other required data could be measured by cheap sensors. The implemented embedded system in real-time can be employed as the input variables of the prediction systems. The second point makes use of the vehicle global position and wireless communication techniques to respectively identify and transfer the information about the road geometry characteristics. In this chapter, we will take these considerations into an integrated system that consists of the subsystem of vehicle dynamics parameter estimation, global localization and vehicle to infrastructure communication. The entire system need to be realized in real-time, some parts of the development are based on the previous research in the thesis of [Ghandour 2011].

This chapter is organized as follows: some existing method of risk prediction is presented in the first section, different types of risk assessment method reflect the most frequent accidents that counted in the vehicle crash statistics report, such as road departure prediction, vehicle rollover prediction and curve speed prediction are respectively retrospected. In addition, a vehicle dynamics state prediction is able to forecast the vehicle state in an instant in the future. Section three principally highlights our innovated method for predicting the potential risk and denoting the curve warning speed before entering the approaching curve. The prediction system components and operation diagram are explained clearly in this section. In section four, the proposed prediction method is firstly realized through a simulation scenario, evaluation of the risk occurrence and curve speed is validated by using simulated data. Finally, some summaries and remarks with respect to the developed method are mentioned in the last section.

## 6.2 Existing method of risk anticipation

The risk anticipation and evaluation methods had been widely discussed in the literature, some studies have been conducted in the assessment of the risk that may be occurred during certain situations.

### 6.2.1 Road departure prediction

For the prediction of the road departure, [Chen 1995] proposes a vision-based method called AURORA, which is a kind of roadway departure warning system, just a simple downward looking vision system is employed at  $60Hz$ . The vehicle's lateral displacement could be accurately estimated applying vision process from the images that taken by color camera with a wide angle lens. The precise lateral displacement provides time-to-lane-crossing (TLC) measurement. When the TLC falls below the pre-initialized threshold, the warning system will be activated. Similar methods can be found in different literatures with [Lee 1999] [Lee 2002] [Jung 2005]. Except for the proposition of the vision-based method, a preview-based control strategy is presented for the prevention of the road departure of heavy vehicles, the DGPS is employed to give information about the heading error and yaw rate in [Morellas 1997].

### 6.2.2 Vehicle rollover prediction

Another principal reason of accidents is explained by the vehicle rollover, hence a lot of researches are aiming at predicting the vehicle rollover phenomenon and preventing it. [Chen 2001] develops an anti-rollover control algorithm based on the Time-To-Rollover (TTR) metric. The index is calculated in real-time with a simple model applying steering and direct yaw moment control inputs. A feedback control of differential braking schema prevents the vehicle rollover trend, the Load-Transfer-Ratio (LTR) is selected to supply the insightful evaluation of the anti-rollover control before starting the optimization process. [Bouton 2007] proposes a rollover indicator dedicated to light all terrain vehicles, it integrates off-road environments specificities. The new designed indicator based on a pure rolling assumption, which is dedicated to parameters identification and tire stiffness estimation. The second model permits to introduce the influence of sliding effects into load transfer. [Takano 2001] uses a three-DOF vehicle model to construct the vehicle lateral acceleration as well as the yaw angle and roll angle acceleration, the rollover risk is assumed to happen when the overturning moment caused by the lateral acceleration acting on the vehicle exceeds a threshold value by static analysis. Some other literatures equally presenting vehicle rollover prediction can be found in [Yu 2008] [Imine 2007] for heavy vehicles.

### 6.2.3 Curve speed prediction

According to the statistics report of the vehicle crash accidents, the curve becomes a black spot for its high ratio of the accident occurrence. The curve speed prediction (CSW: Curve Speed Warning) is designed to address control loss due to excessive speed in curves. Many literatures explore in this issue, [Sentouh 2006] proposes a computational method taking account multiple factors that include vehicle, driver, and infrastructure. The four-wheel model is employed to give information about vehicle dynamics, the road geometry (curvature, slope, and super-elevation) and the maximal friction are considered in generating the speed profile. [Glaser 2007] presents an integrated system providing a safe speed for the upcoming curve, this kind of system has the ability of recognizing the geometric characteristics of the coming road from transponder, computing the safety cruise velocity to an approaching curve as well as controlling vehicle speed in the safe range. Another approach of reconstructing road curvature attributes in real time using digital map data based on the proposed circle center search and circle selection algorithms are presented in [Li 2008]. The characteristics of the vehicle dynamics, road geometry and driver performance index are considered in the decision of the safe speed for negotiating a curve.

### 6.2.4 Vehicle dynamics state prediction

The above mentioned typical vehicle safety prediction and warning systems are proved to be effective in improving vehicle safety, however the vehicle information processing with the models are based on data of current vehicle state. For example, the proposed methods predicting the vehicle rollover index can identify just current potential dangerous situation, we can assume that the methods work at each point on the movement of trajectory, but whether can we extend this on the future instant in a section form instead of a point? To answer this question, we need to forecast the information about the vehicle trajectory and the corresponding dynamics parameters. [Hsu 2009] proposes a vehicle full-state estimation and prediction system to describe overall vehicle dynamics, the steering wheel angle, braking force and tracking force are used as the inputs. The switch observer technique along with three types of sensors (lateral acceleration sensor, longitudinal velocity sensor and suspension displacement sensor) is employed to provide the predicted values. [Jun 2010] develops an on-line measurement and prediction technology for vehicle motion state. The state parameters can be measured by MIMU (Micro Inertial Measurement Unit), in order to improve the precision, Kalman filter is designed to accomplish sensor signals fusion. Yaw rate, longitudinal velocity, yaw angle and roll angle are forecasted by applying auto regressive (AR) modeling prediction. Recently, [Ghandour 2011] describes a new method to forecast the vehicle dynamics parameters including tire forces and sideslip angle which are usually assumed hard to be achieved, the indicators of lateral skid and rollover are applied in order to evaluate the potential risk in the future instant.

## 6.3 Methodology of the prediction system for safe curve negotiation

Basing on the review of previous literatures, we developed a method to provide risk prediction with the normal driving maneuvers. Actually, due to analysis of the run-off-road crashes, accidents are caused by a wide variety of factors. Detailed analysis of 200 NASS CDS crash reports indicat that run-off-road crashes are primarily caused by the following six factors (in decreasing order of importance) [Pomerleau 1999]:

- Excessive speed (32.0%) - traveling too fast to maintain control
- Driver incapacitation (20.1%) - typically drowsiness or intoxication
- Lost directional control (16.0%) - typically due to wet or icy pavement
- Evasive maneuvers (15.7%) - driver steers off road to avoid obstacle
- Driver inattention (12.7%) - typically due to internal or external distraction
- Vehicle failure (3.6%) - typically due to tire blowout or steering system failure

Therefore, our research is focused on the high frequency accident reason: excessive speed, particularly during the upcoming curve. The first question that we encounter is how to decide the vehicle relative position and the location of the approaching curve. Usually, we choose global position system to give an accurate location in the external environment.

### 6.3.1 Coordinate system and transformation

Nowadays, vehicle localization technologies are widely explored in industrial and research area, they are usually applied at the fields of navigation, guidance and control of automobile and aircraft. However, there are several coordinate frames used in the system design. The raw data acquiring from commercial GPS is commonly with the frame of geodetic coordinate. It cannot directly be perceived on the map to identify the target position in the local map. Hence, we are willing to transform the geodetic coordinate system into the earth-centered earth-fixed (ECEF) coordinate system, the detail description of other coordinate systems can be found in [Cai 2011].

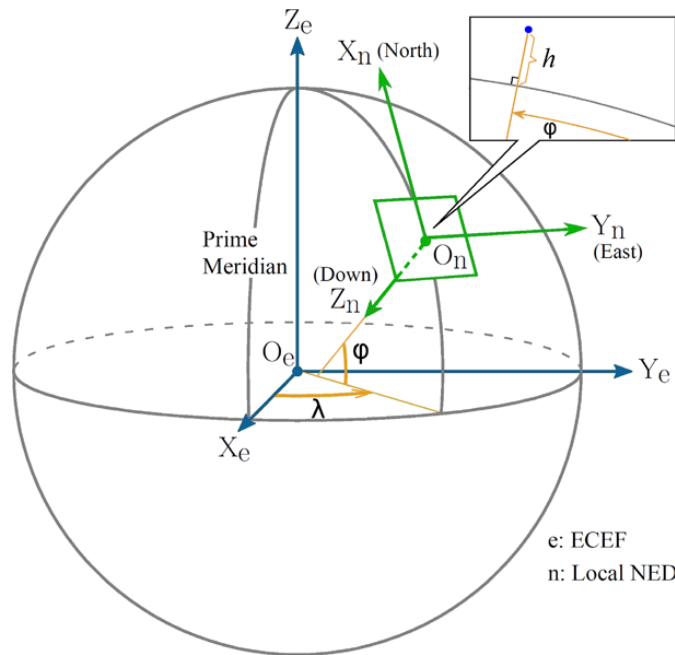


Figure 6.1: Geodetic and ECEF coordinate systems [Cai 2011]

Figure 6.1 illustrates the geodetic coordinate system and the earth-centered earth-fixed (ECEF) coordinate system. The geodetic system characterizes a coordinate point near the earth's surface with three parameters: longitude, latitude and height (or altitude), which are respectively denoted by  $\lambda$ ,  $\varphi$ , and  $h$ . The longitude  $\lambda$  represents the rotational angle between the Prime Meridian and the measured point, the angle variation range changes from  $-180^\circ$  to  $180^\circ$ . The latitude measures the angle (ranging from  $-90^\circ$  to  $90^\circ$ ) between the equatorial plane and the normal of the reference ellipsoid that passes through the measured point. The height  $h$  is the local perpendicular distance between the measured point and the reference sea line. The position vector in geodetic coordinate system is given as:

$$P_g = [\lambda \quad \varphi \quad h]^T \quad (6.1)$$

This geodetic coordinate information does not be used directly in our system, because we are not able to precisely denote the distance between our vehicle and the upcoming curve. The accurate distance in the unit of meter is preferred to be known in the design of our prediction system. Therefore, we employ another coordinate system rotating with the earth around its spin

axis. In this case, a fixed point on the earth's surface has a fixed set of coordinates defined along three axes  $X_e$ ,  $Y_e$  and  $Z_e$ , the origin ( $O_e$ ) for three axes is located at the center of the earth. The transformation from geodetic system to ECEF coordinate system is given as follows:

$$P_e = \begin{bmatrix} x_e \\ y_e \\ z_e \end{bmatrix} = \begin{bmatrix} (N_e + h) \cos \varphi \cos \lambda \\ (N_e + h) \cos \varphi \sin \lambda \\ [N_e(1 - e^2) + h] \sin \varphi \end{bmatrix} \quad (6.2)$$

where the prime vertical radius of curvature  $N_e$  and the first eccentricity  $e$  are derived according to following definitions and equations:

$$\begin{aligned} R_{Ea} &= 6,378,137.0m, \\ f &= 1/298.257223563, \\ R_{Eb} &= R_{Ea}(1 - f) = 6,356,752.0m, \\ e &= \frac{\sqrt{R_{Ea}^2 - R_{Eb}^2}}{R_{Ea}} = 0.08181919, \\ N_e &= \frac{R_{Ea}}{\sqrt{1 - e^2 \sin^2 \varphi}}. \end{aligned} \quad (6.3)$$

These parameters are either defined or derived based on the WGS 84 (world geodetic system 84, which was originally proposed in 1984 and lastly updated in 2004 [212]) ellipsoid model. Applying this coordinate frame, it improves the facility of the localizing the target vehicle in the local maps. The distance between moving forward car and the approaching curve can be estimated precisely in real-time. The geometric characteristics of the curve, described by parameters in equation (6.3), are forwarded to the vehicle embedded system through a communication device installed at the environment near the curve (the road side unit). This is explained in section 6.3.3.1 below.

### 6.3.2 Reconstruction of the vehicle dynamics parameters

In this subsection, we will present some basic formulas concerning vehicle dynamics parameters to be predicted. Before that, we need to explain the approach to calculate an essential parameter which describes the trajectory curvature. The previous description of the coordinate transformation enables us to use the ECEF coordinate system directly. Hence, the GPS trajectory can be accessed in our system with the form of Cartesian coordinate  $(x, y)$ . Afterwards, the curvature  $\kappa$  of a plane curve given by Cartesian parametric equations  $x = x(t)$  and  $y = y(t)$  in two dimensions space is formulated as [Casey 1996]:

$$\kappa = \frac{x'y'' - y'x''}{(x'^2 + y'^2)^{3/2}} \quad (6.4)$$

If trajectory can be expressed by the form  $y=f(x)$ , the equation of curvature becomes:

$$\kappa = \frac{\frac{d^2y}{dx^2}}{[1 + (\frac{dy}{dx})^2]^{3/2}} \quad (6.5)$$

### 6.3.2.1 Lateral acceleration

The first parameter required is the vehicle lateral acceleration in the curve, as we know, the lateral acceleration of the vehicle body at each point of the trajectory comes from the composition of the centrifugal acceleration and the component of the acceleration of the gravity. To simplify the model, road curve surface is assumed without bank angle, so the component of acceleration of gravity is omitted here. The lateral acceleration can be obtained as following form:

$$a_y = \frac{v_x^2}{r} = v_x^2 \kappa \quad (6.6)$$

### 6.3.2.2 Yaw rate

Yaw rate is the vehicle's angular velocity around its vertical axis. Otherwise, yaw rate is also considered as the rate of change of the heading angle. Basing on this understanding, the yaw rate can be simply defined using vehicle trajectory at each point on the curve. [Cunha 2011] employs following equation to obtain vehicle yaw rate, however, this method works only on the short sampling frequency.

$$\dot{\psi} = \frac{d}{dt} [\tan^{-1}(\frac{dy}{dx})] \quad (6.7)$$

### 6.3.2.3 Steering wheel angle

In the structure of the vehicle parameter prediction part, steering wheel angle is fundamental to maneuver a vehicle. We need a steering mechanism to turn wheels, the turning angle controlled by steering angle is individual for each front wheel. During cornering, the inside wheel must turn with a greater angle than the outside one, since the inside wheel undergoes with a smaller radius. For low lateral acceleration, it is common to use Ackermann geometry to describe different steering angles at each wheel, shown in Figure 6.2. The equation describing the Ackermann mechanism is given as follows:

$$\delta_{in/out} = \frac{L}{r \pm E_2/2} = \frac{L}{\kappa^{-1} \pm E_2/2} \quad (6.8)$$

### 6.3.2.4 Wheel velocity

Another parameter should be noted with difference is the wheel velocity, the rear wheels are discussed here to denote different wheel rotation speeds during a curve. The expression is composed by vehicle longitudinal speed, yaw rate as well as the road curvature [Osborn 2006].

$$\omega_{2j} = \frac{v_x \pm \dot{\psi} E_2/2}{r} \quad (6.9)$$

where  $E_2$  is the width of rear axle.

We take a sequence of simulation tests in order to verify models presented in equations (6.4) to (6.9). We recall that the inputs to these calculations are the trajectory of the curve (x, y points characterizing the center of the lane) and the longitudinal velocity  $V_x$  in the curve. The Cartesian form of the curve calculated in a previews learning stage and stocked in a road-side unit, and the  $V_x$  is calculated by the vehicle, when it is approaching the curve, as the mean value of the  $V_x$  during a window before entering the curve. These points are explained below. The

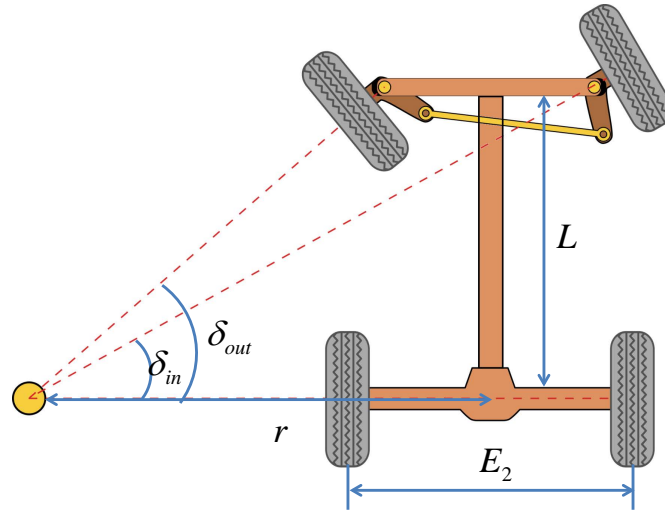
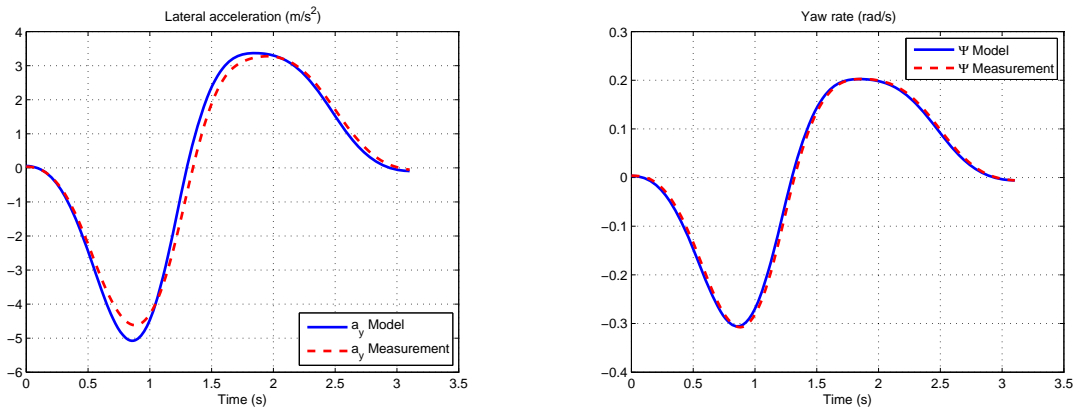


Figure 6.2: Ackermann steering mechanism

reconstructed dynamics parameters comparing with the simulation real output is illustrated in Figure 6.3. The lateral acceleration and yaw rate in Figure 6.3(a) and 6.3(b) can be precisely reconstructed applying the vehicle trajectory and longitudinal speed. In Figure 6.3(c) steering angle of the inner wheel is smaller than the steering wheel angle input, it is reasonable to be accepted due to the reason explained in the mentioned subsection 6.3.2.3. Wheel rotation velocity is represented in Figure 6.3(d), though some bias is found in the figure, it does not greatly affect the global performance with such slight difference. Comparison of reconstructed lateral acceleration and measurement.

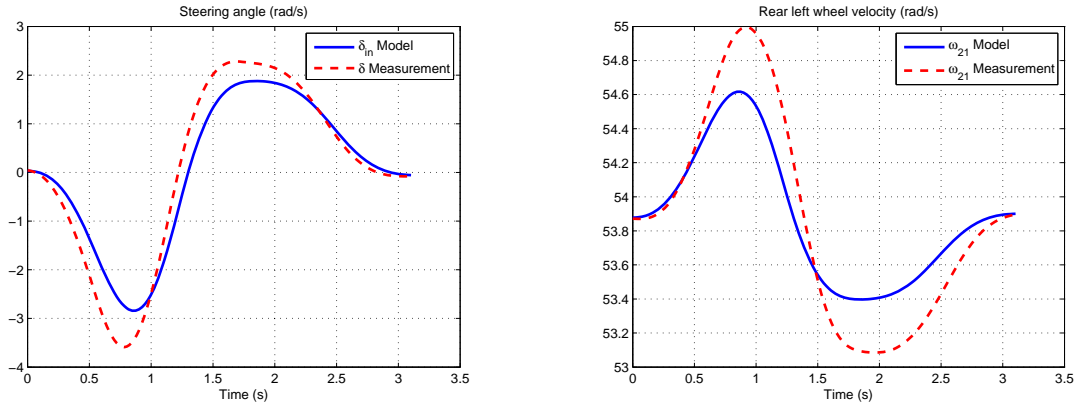


(a) Comparison of reconstructed lateral acceleration and measurement

(b) Comparison of reconstructed yaw rate and measurement

### 6.3.3 Methodology of the prediction system

The prediction system for road curve warning is based on three principal blocks: the global information collection system, risk prediction system and the driver warning part. Before presenting



(c) Comparison of reconstructed steering angle and measurement

(d) Comparison of reconstructed rear left wheel velocity and measurement

Figure 6.3: Reconstruction of the vehicle dynamics parameters

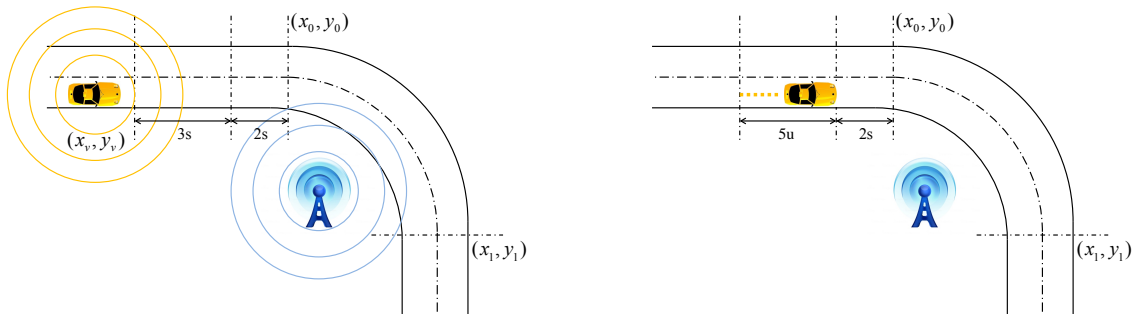
the principle of each block, we need to declare our hypothesis before the modeling. The risk prediction and curve speed warning systems are proposed with the consideration of following assumptions:

- **Hypothesis 1:** *The vehicle moves forward normally within the road bound, and follows its lane during the curve;*
- **Hypothesis 2:** *The prediction system begins to operate only when the distance between the vehicle and curve geometry center is less than the defined threshold, besides the variable trend of the distance must be decreased, which means that the vehicle is approaching the curve;*
- **Hypothesis 3:** *Considering the applying of vehicle-infrastructure wireless communication technologies, only one road side unit is connected with the experimental vehicle. Multiple connected activations are not considered;*
- **Hypothesis 4:** *Vehicle real-time data of longitudinal acceleration and velocity are recorded within a distance gap before approaching the curve, which is so-called "prediction window", the mean value of the longitudinal acceleration and vehicle speed of this distance interval is taken as the input variables for the next block.*

Considering above hypothesis, the prediction system can be principally divided into 5 steps that illustrated in Figure 6.4. The elaborate method will be separately presented in the following parts.

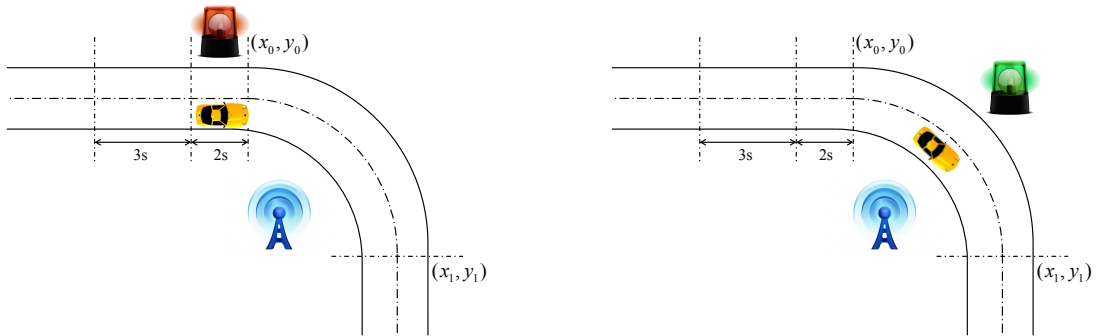
### 6.3.3.1 Global information collection system

The first block is the information collection part. This part consists of two principle functions: collection of the vehicle and curve geometry data and localization of the distance from the upcoming curve. The data collection and the activation of the systems are illustrated in the phase 1 and 2 in Figure 6.4(a) and 6.4(b).



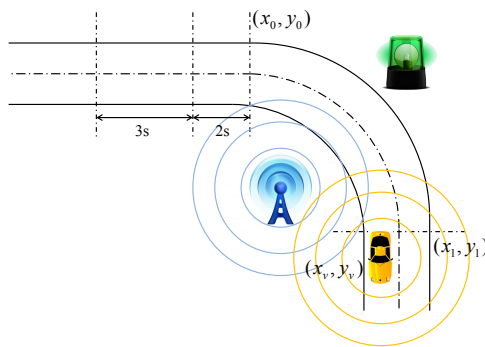
(a) Risk prediction and curve speed warning systems: phase 1

(b) Risk prediction and curve speed warning systems: phase 2



(c) Risk prediction and curve speed warning systems: phase 3

(d) Risk prediction and curve speed warning systems: phase 4



(e) Risk prediction and curve speed warning systems: phase 5

Figure 6.4: Risk prediction and curve speed warning systems

Figure 6.4(a) illustrates the method of receiving road geometry information and vehicle real-time dynamics parameters. First, when the vehicle is approaching the communication range of the road-side unit, the defined communication protocol allows the data transfer between vehicle and infrastructure, a more complete explanation about the V2I communication architecture is given in [El Ali 2010]. All the geometry data is preprocessed from GPS trajectory, the curve beginning and the end coordinate as well as the curvature are stocked in the road-side unit. As soon as vehicle receives the data package sent from the road infrastructure, through the communication network structure, it starts to calculate the distance between vehicle and the beginning of the curve. The distance decreases until the time attains 5s estimated with current speed from the curve, where the first 3s is a time window reserved to for storing the vehicle longitudinal velocity and acceleration in 200Hz in order to calculate its mean value, and the last 2s is reserved to the action of the drive. Basing on the mentioned-above hypothesis 4, the mean vehicle longitudinal acceleration and velocity can be derived as follows:

$$\begin{aligned}\bar{v}_x &= \frac{\sum_{i=1}^N v_x(i)}{N} \\ \bar{a}_x &= \frac{\sum_{i=1}^N a_x(i)}{N}\end{aligned}\tag{6.10}$$

where N is the entire quantity of sampling point during the time interval of 3s. These two variables are essential for the following prediction system. The remaining time of 2s is reserved for the consideration of the system processing time and the driver's reaction time due to the empirical analysis.

### 6.3.3.2 Risk prediction system

The risk prediction system starts to operate where vehicle is approaching the curve with the rest of time of 2s. Prediction system is illustrated by several blocks in Figure 6.5. At the beginning of the system schema, vehicle velocity and acceleration, vehicle current location and road geometry information are received from different data acquisition modules that developed and integrated in our software architecture. The startup condition arises when the time is less than the predefined 2s. This condition allows driver has enough reaction time to adopt corresponding behavior.

First block of the vehicle parameters prediction is able to obtain the necessary input variables which are employed in the subsequent estimation part. Lateral acceleration, rear wheel rotation, steering angle and raw rate are predicted according to the known curvature, the mean longitudinal velocity and longitudinal acceleration. Second block aimed at estimating of the vehicle dynamics parameters as the lateral tire force and sideslip angle has been presented in chapter 5, where the details about these observation processes are given. Since the system action time is quite important to evaluate the effectiveness, we choose Extended Kalman filter due to its simplicity and quickness. The maximum friction is proposed using the method of [Ghandour 2011]. As a result, the maximum friction, coefficient of friction at each tire as well as the vertical tire force provided in the second block offer the possibility to predict and evaluate the future instant based on the driver maneuver, vehicle technical characteristic and the curve geometry. Among these three influence elements, it is noted that only driver maneuver can be changed temporarily, hence the driver can brake the car when the danger is detected before entering the curve.

In order to take the decision of the safe curve negotiation speed, we need to think about some approaches to provide a risk elevation using above estimated variables. Here, we employ two risk

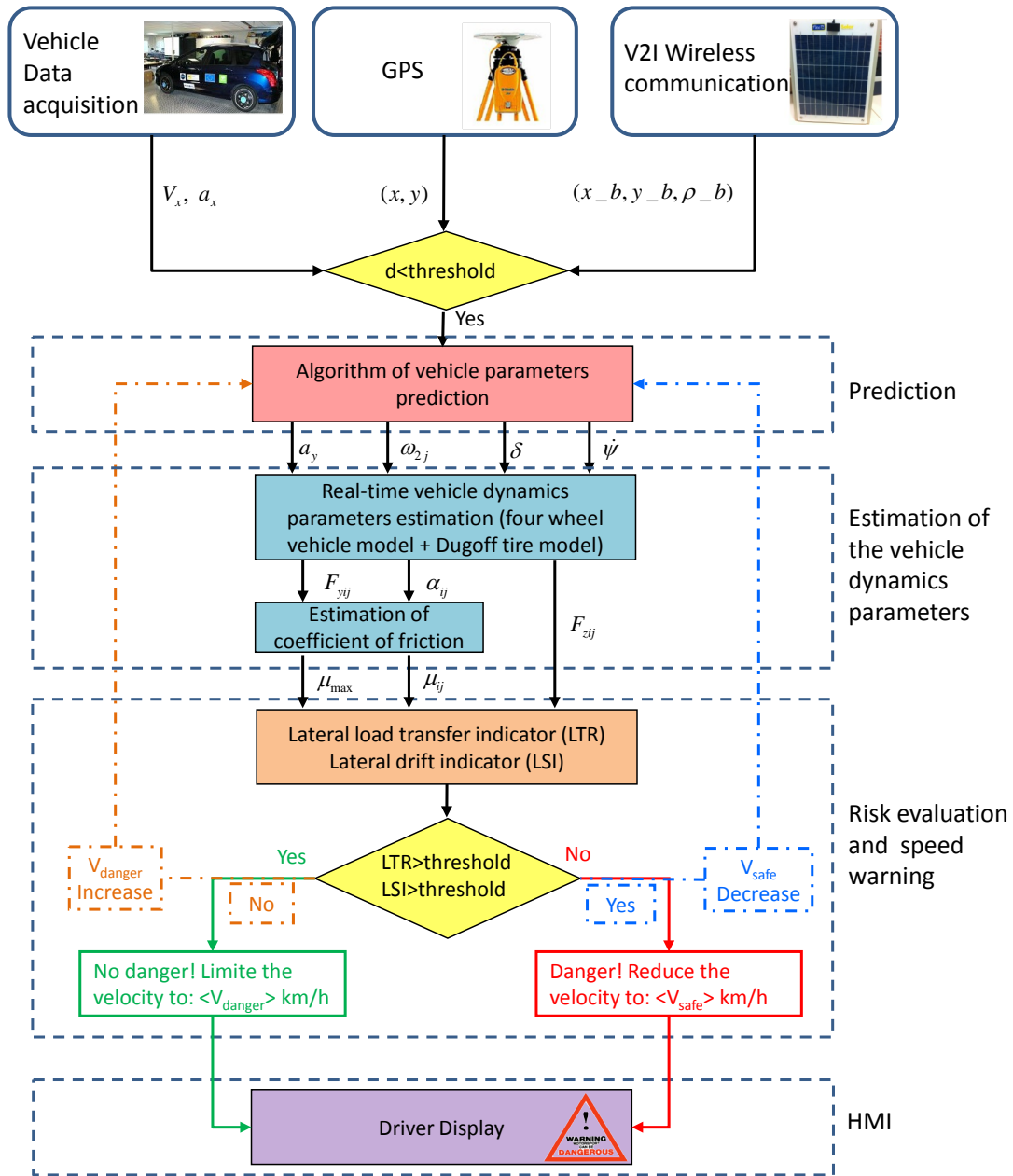


Figure 6.5: The schema of implemented prediction system

assessment indexes: load transfer ratio (LTR) and lateral skid ratio (LSR), which respectively evaluate the risk of vehicle rollover and lateral skid during the movement. [Palkovics 2001] denotes a definition of lateral load transfer ratio that explains the wheel load transfer from left or right side due to lateral acceleration. It offers a snapshot of vehicle lateral dynamics by detecting the instantaneous roll dynamics. Here, the lateral load transfer ration is defined by using four wheel vertical forces which are estimated in the block of estimation of the vehicle dynamics parameters:

$$LTR = \frac{F_{z11} - F_{z12} + F_{z21} - F_{z22}}{F_{z11} + F_{z12} + F_{z21} + F_{z22}} \quad (6.11)$$

In order to denote the assessment representing the loss of adhesion resulting in the lateral drift, [Ghandour 2011] proposes a evaluation method applying the maximum friction coefficient:

$$LSR_{ij} = 1 - \left\| \frac{\mu_{max} - \mu_{ij}}{\mu_{max}} \right\| \quad (6.12)$$

$$\mu_{ij} = \left\| \frac{F_{yij}}{F_{zij}} \right\|$$

The index threshold is defined empirically at 0.8 due to the simulation test, when  $LTR$  and/or  $LSR_{ij}$  are over this threshold, the vehicle is assumed to have a potential risk of rollover and/or lateral drift. Actually, these assessment indexes are not easily comprehensible to vehicle drivers, hence we need to provide a more directly perceived parameter - vehicle velocity to give a warning to driver to adopt corresponding brake behavior.

Two situations are considered at the schema in Figure 6.5. First, there is no risk ratio exceeding the defined threshold, the vehicle speed increases to give a feedback to the beginning of the system. The closed loop is illustrated with orange dash-dot line in Figure 6.5. The conditional expression for the loop will continue to repeat itself until  $LTR/LSR_{ij}$  exceeds the threshold with the augmentation of vehicle speed at each repetition, the final corresponding vehicle speed is assumed as the dangerous speed for the negotiation of the upcoming curve (the green solid line in the diagram). Driver could receive a warning displayed on terminal equipment to avoid exceeding this speed.

Alternatively, when  $LTR/LSR_{ij}$  is detected above the threshold at first time of system operation, the vehicle speed will continue to decrease within the closed-loop as shown in Figure 6.5 represented by blue dash-dot line, until all the risk assessment values are blew the threshold. The vehicle speed for passing the curve safely will be displayed inviting driver to brake the car to slow down. Simultaneously, a red-light alert icon is displayed on the HMI to warn the driver. This step is illustrated in the sequence of Figure 6.4(c). In addition, the system is able to monitor the vehicle real-time speed comparing with the recommended running speed, if driver slows down the vehicle speed less than the threshold before entering and negotiating the curve, the red-light alert icon will turn to green one as illustrated in Figure 6.4(d).

The last step of the entire procedure is represented in Figure 6.4(e). When the vehicle is reaching at the ending of curve, the system is reinitialized and prepared for the subsequent upcoming curve.

## 6.4 Simulation validation

The performance of the risk predication and advisory curve speed negotiation is validated using simulator environment. A primary simulation test is proposed to simulate the scenario, a modified double lane change maneuver is performed with four curves identified on the trajectory.

Figure 6.6 illustrates the global maneuver by the Cartesian coordinate in blue line. Four curves are defined due to the geometry of the entire trajectory. The detail of description for the location of the four curves is given in the following Table 6.1, and it is also marked on the Cartesian coordinate with green line.

	Starting point	End point	Curve length (m)
Curve 1	(10.21, 0.98)	(17.90, 1.23)	8
Curve 2	(40.08, 4.27)	(48.82, 4.61)	9
Curve 3	(62.17, 4.62)	(71.83, 4.33)	10
Curve 4	(95.27, 1.17)	(101.93, 1.04)	7

Table 6.1: The description of the curve identification on the Cartesian coordinate

We simulate the vehicle moving along the trajectory, when it is approaching the first curve. In the simulation environment, the data collection distance is defined of  $2s$  before the start of the curve, the parameters which are required as the input of the subsequent block aimed at predicting the vehicle dynamics parameters (in Figure 6.5) are calculated basing on the mean longitudinal speed and acceleration as well as the storage of the curve geometry information. The predicted lateral acceleration, yaw rate, steering angle and wheel rotation velocity are respectively represented in Figure 6.7, the lateral acceleration and yaw rate precisely following with the measured data during the negotiation of the curve, furthermore the steering angle is reconstructed with reasonable deviation. The difference of the vehicle speed is quite small, which could be ignored. It is noted that the hypothesis of mean speed and longitudinal acceleration is available to provide accurately predicated parameters in a short future instant. Actually, when the starting point of the prediction system is near enough to the curve, the predicted parameters will match more precisely with the real situation while the car will pass the curve. However, the reaction time for the driver to take the corresponding measures should be considered as an essential factor in the definition of this distance. Considering the simulation environment as well as off-line calculation, this distance is set at  $1s$ , which is distinct from the experimental validation in real environment.

Applying these variables in the estimation block, the vertical tire force is firstly calculated and it is illustrated in Figure 6.8. The predicted vertical tire force is practically acceptable at such transient interval, the deviation of  $200N$  at rear wheel is treated as tiny affection on the system. Moreover, Figure 6.9 denotes the estimated lateral tire force, it is concluded that the global comportment between the predicted estimation and measurement is similar, however some bias is detected due to the accumulating of the previous difference, which is brought in by predicted parameters. In fact, the prediction system provides an approach to forecast the vehicle state in the upcoming curve comparing with real driving maneuver. Definitely, the prediction vehicle state in the future instant basing on current vehicle dynamics characteristics cannot always be extremely precise due to the constantly changing from driver, hence some reasonable deviation is acceptable for us. The validation concerning parameter prediction of other three curves is not introduced here.

Figure 6.10(a) and 6.10(b) respectively represent the load transfer ratio and lateral skid ratio at the first sequence of the curve speed proposition (that is the closed loop in orange and in green of Figure 6.5) during the first upcoming curve. The LTR index shows no danger of rollover, LSR is also smaller than the threshold but is quite close to the defined potential dangerous value. As soon as the system firstly forecast the vehicle state in the curve that there is no danger to be

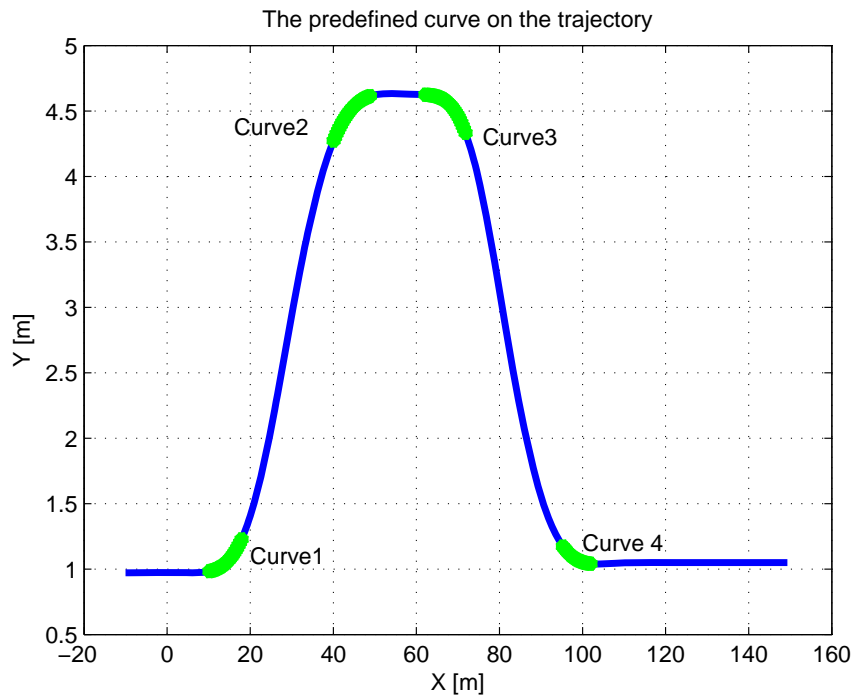


Figure 6.6: The trajectory of modified double lane change maneuver: four curves identified on the Cartesian coordinate

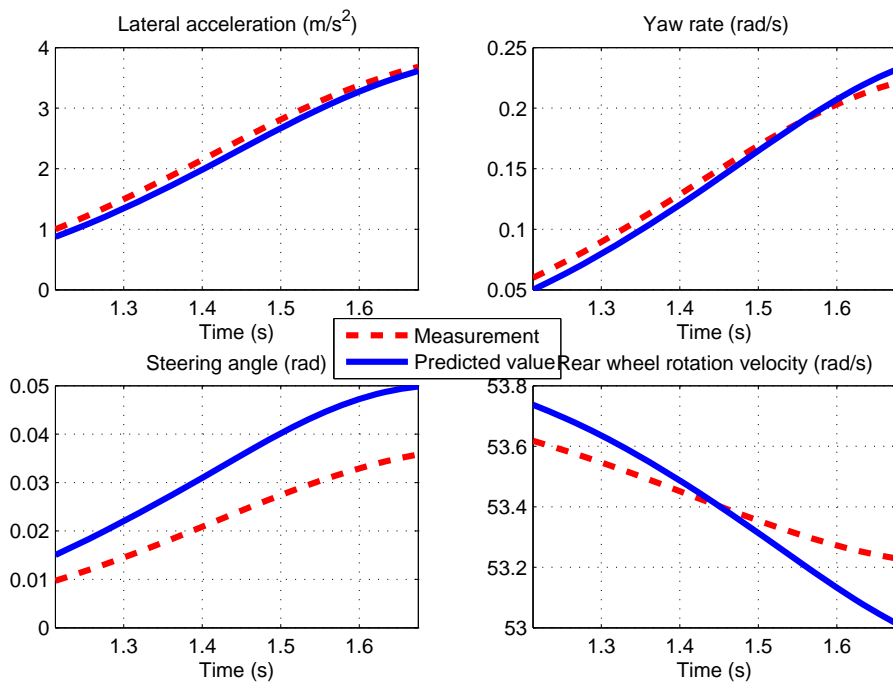


Figure 6.7: The predicted value of vehicle dynamics input parameters in the first curve

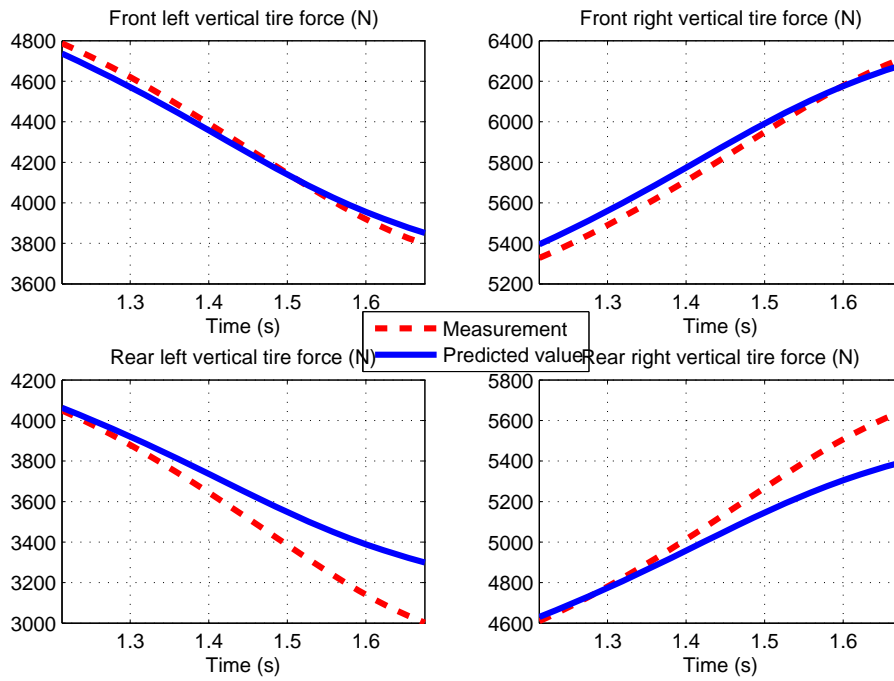


Figure 6.8: The predicted value of vertical tire force in the first curve

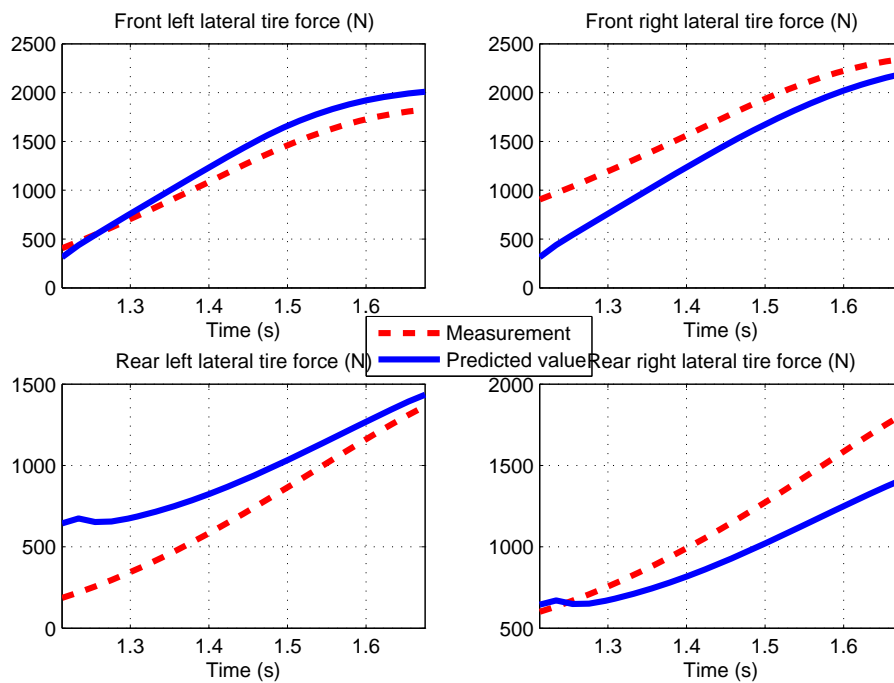


Figure 6.9: The predicted value of lateral tire force in the first curve

appeared, the system itself begins to increase the internal vehicle speed, the dashed orange line) and adopts it as the new vehicle speed in order to obtain the danger speed that can guarantee the vehicle passing this curve without lateral drift (this is the velocity closed loop described in figure 6.5, the dashed orange line). The speed augmentation steps are omitted here, only the final sequence is illustrated in Figure 6.10(c) and 6.10(d). When LSR of front left wheel exceeds the threshold, the circle in prediction system stops and the dangerous speed for passing this curve is informed to the driver to pay attention (green rectangle in Figure 6.5).

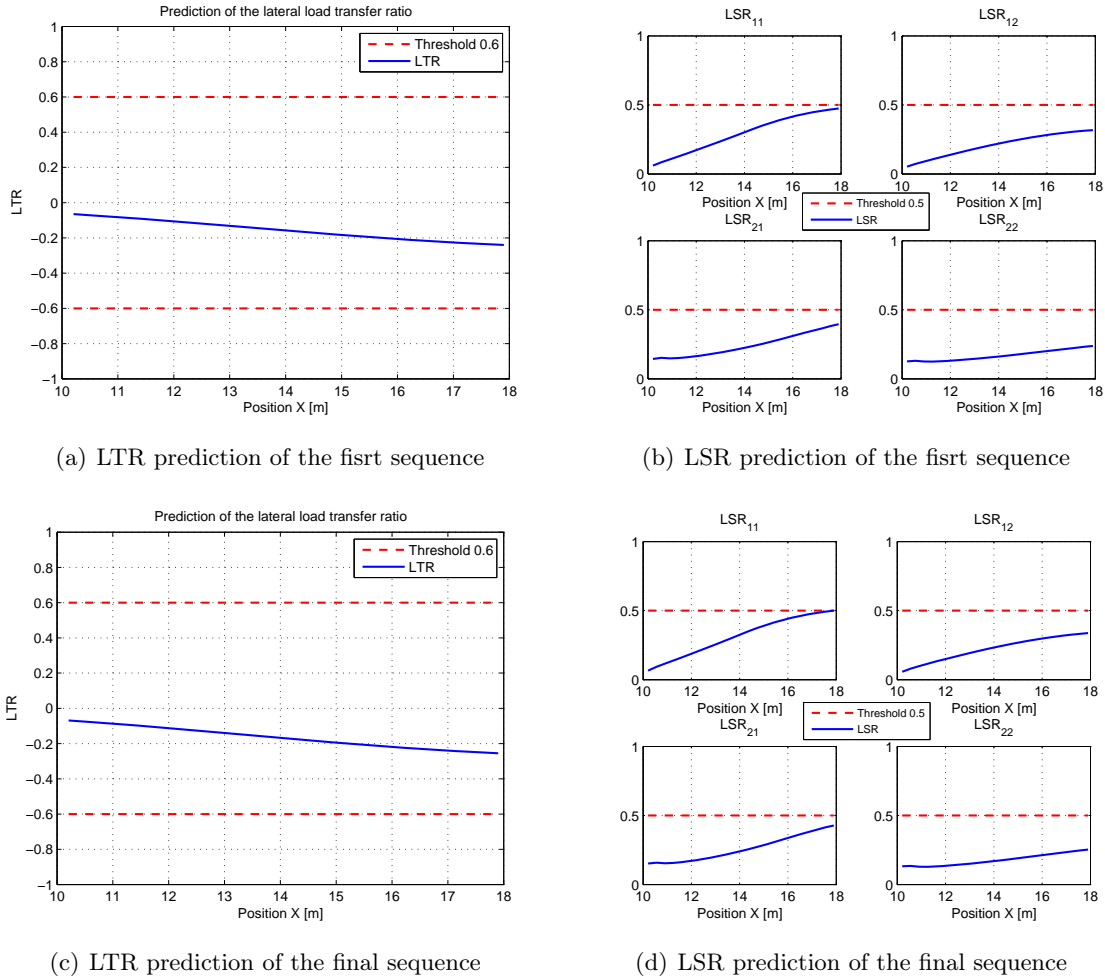


Figure 6.10: The evaluation of potential risk and safe negotiation speed in the first curve

The vehicle continues to move approaching the second curve, the processes are analogue to the first curve. No rollover risk is detected according to the index value represented in Figure 6.11(a), however LSR index at rear left wheel surpasses the risk level a little bit in Figure 6.11(b), vehicle speed is decreased on the velocity closed loop until LSR index decreasing to a lower value than the threshold (Figure 6.11(c) and 6.11(d)).

On the third curve, and considering the LTR index in Figure 6.12(a), one sees that the lateral load transfer from one side to the other side is not excessive. However, LSR index of right wheels exceeds the threshold as seen in 6.12(b). What happens is that a sudden curve at right hand leads to the load transfer from right hand to the left on, i.e. right wheels have less load distribution. Hence right tires possess higher probability of occurrence of lateral drift

phenomenon. Finally, the system recommends a safe speed to the driver to slow down so that the index values are those represented in 6.12(d).

Analyzing the final curve traversed by the vehicle, predicted LTR and LSR index at first sequence are illustrated in Figure 6.13(a) and 6.13(b), the situation is similar to the first curve, there is no predicted risk detected before entering the curve. LSR at rear right wheel increases until it passes the potential risk level in Figure 6.13(d).

Figure 6.14 represents the curve negotiation speed which is able to ensure the vehicle passes the approaching curve with less probability of accidents. The potential risk region is marked with red line in the trajectory, it is illustrated that curve 1 and 4 has no potential danger, however lateral skid risk is predicted in the section of the second and third curve. Therefore, the danger speed of the first and last curve is proposed to the driver, if they continue with current driving speed to pass the curve, there is no risk to be appeared, but it is recommended that they should not exceed this speed. Alternatively, the risk is predicted in the second and third curve where the running speed before these two curves may lead to lateral drift if the driver doesn't take appropriate action to slow down the car. Therefore, our system denotes an advisable speed and reminds the driver of the consideration for their safety, they should brake the car until the alarm is lifted.

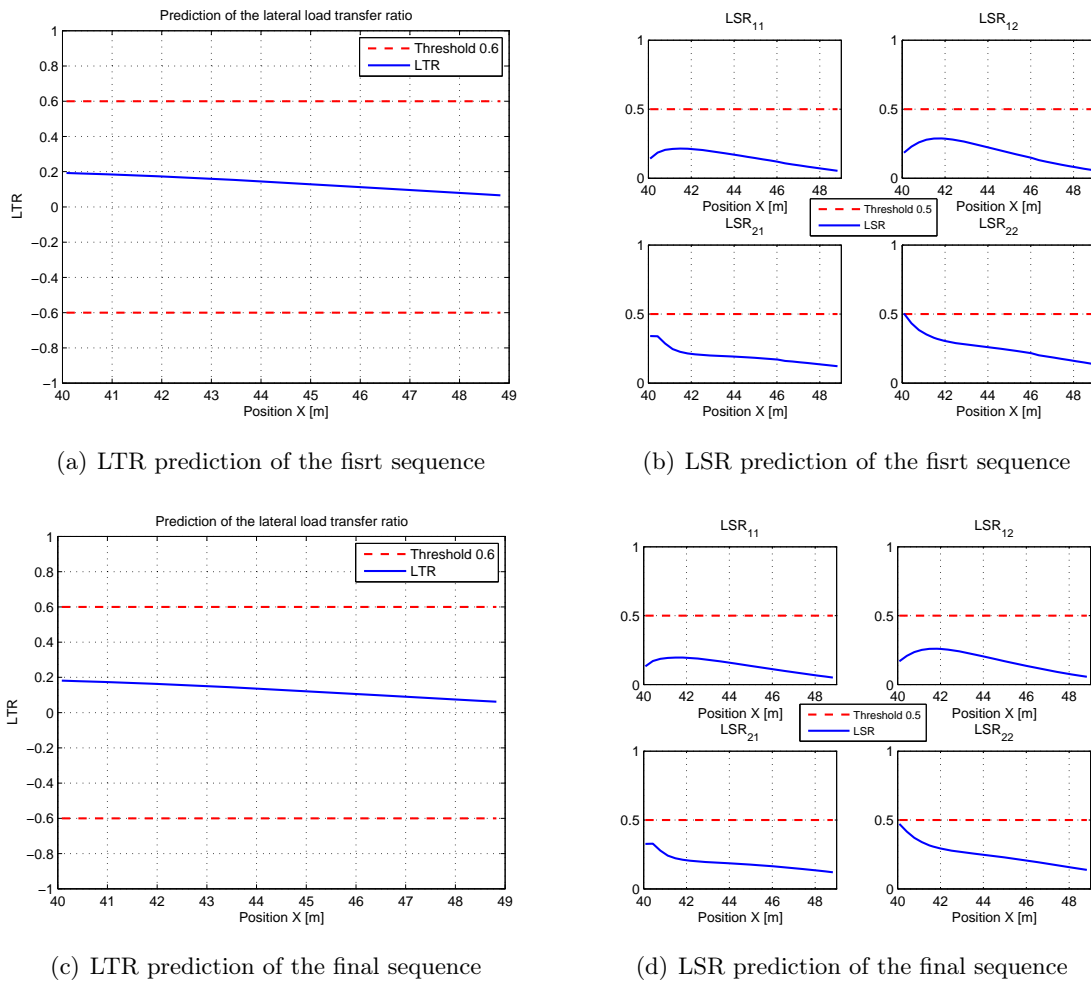
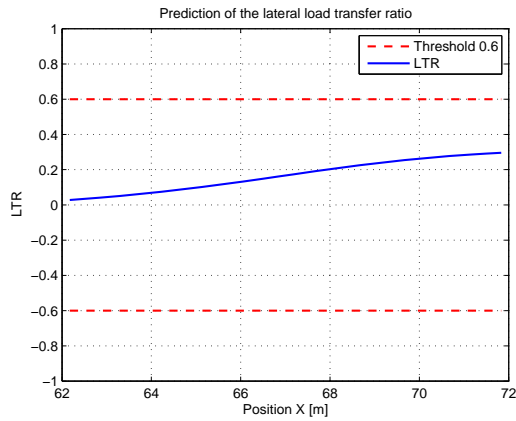
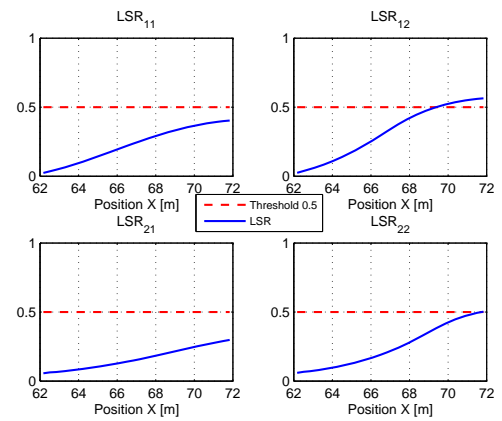


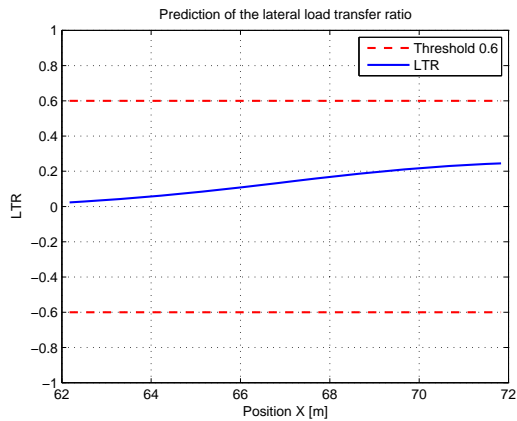
Figure 6.11: The evaluation of potential risk and safe negotiation speed in the second curve



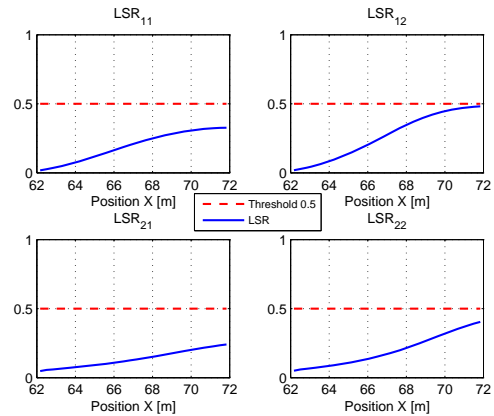
(a) LTR prediction of the first sequence



(b) LSR prediction of the first sequence

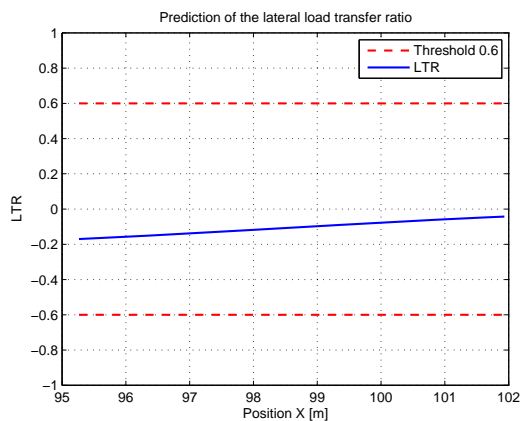


(c) LTR prediction of the final sequence

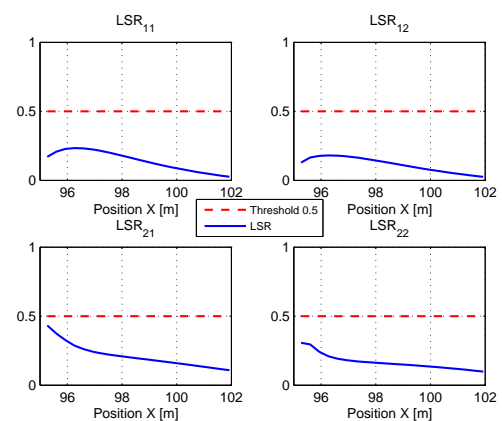


(d) LSR prediction of the final sequence

Figure 6.12: The evaluation of potential risk and safe negotiation speed in the third curve



(a) LTR prediction of the first sequence



(b) LSR prediction of the first sequence

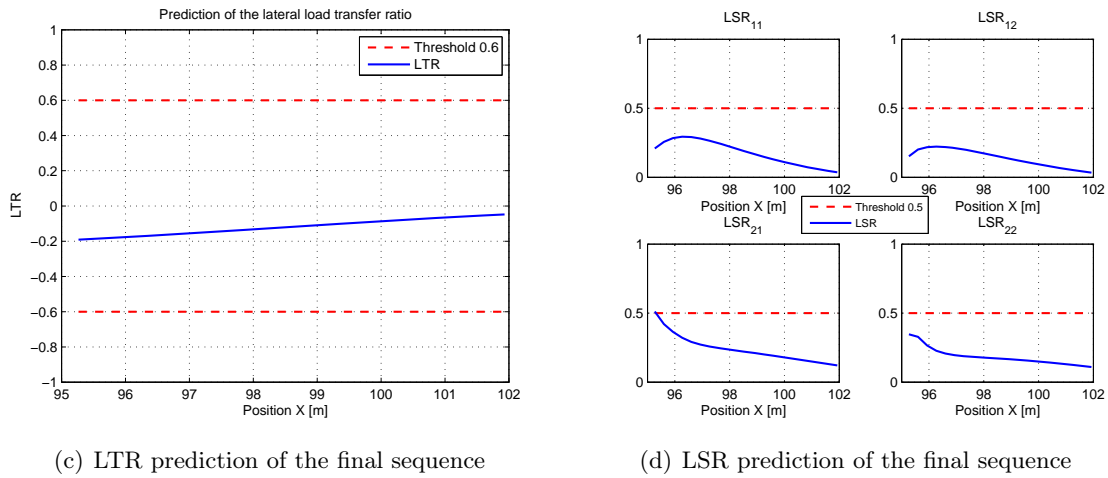


Figure 6.13: The evaluation of potential risk and safe negotiation speed in the fourth curve

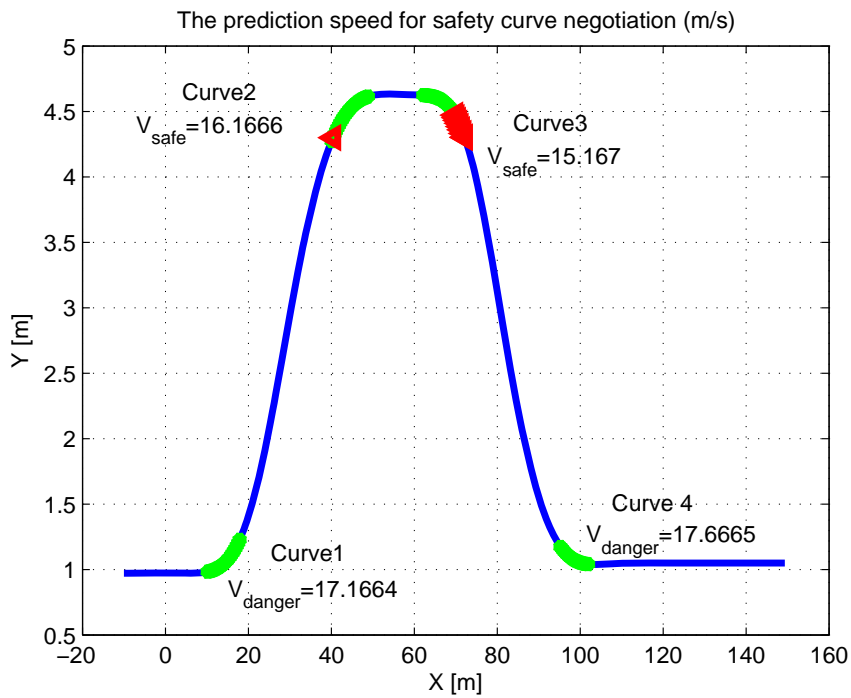


Figure 6.14: The trajectory of modified double lane change maneuver: four curves identified on the Cartesian coordinate

## 6.5 Conclusion

This chapter lays the emphasis on describing an applied method of predicting vehicle dynamics parameters, evaluating potential risk as well as establishing advisory speed on curves. The proposed method in this section is tightly associated with the previous sections that describe the vehicle vertical and lateral dynamics.

In the first part, we epitomize an overview of the existing methods and systems concerning some typical risk evaluation approaches. According to the analysis of vehicle accident statistics report, the accidents are usually happened due to lateral drift and rollover, especially on curves. Therefore, some researches about road departure prediction and rollover prediction are quoted here. The curve speed warning system is directly against the occurrence of excessive speed on curves.

Considering the existing methods being used in the reality, the available information for these methods is still limited. Therefore, our target is to propose a method which is able to forecast the vehicle dynamics parameters in the approaching future, and provide an accurate description of the vehicle state in order to precisely predict and evaluate the potential risk. Some fundamental parameter prediction formulas are validated basing on the proposed hypothesis and road geometry which are easy to be obtained. The procedure for implementing this method consists of three steps. During the first step, the required information is collected by vehicle data acquisition system as well as wireless transmission. During the second step, the prediction algorithm starts to provide risk assessment and advisory speed to pass the upcoming curve. The last step concerns on the modality available to warn drivers of an impending crash threat, the alarm in visual interface will be lifted until vehicle speed is decreased below the advisory speed, the system surveys the vehicle moving speed during the entire trajectory. In the final part, simulation scenario is created to simulate the vehicle passing several defined curves, the procedure is validated using simulation data. It is demonstrated that our prediction system has the ability to predict the future risk assessment basing on current state and recommender drivers to pass the curve with safe speed. This method is able to effectively improve the vehicle safety and help driver avoid accident threat.

Considering the future work, the risk prediction system will be complemented with other functions which are more effective and systematic to evaluate the potential risk. Otherwise, the current method needs road-side infrastructures to provide curve geometry information. It is figured out that the vehicle trajectory should be known before the itinerary, instead some other technical will be integrated to recognize the curve geometry characteristics (from the embedded environment perception, for example) and extend the system to the non-constraint map condition.



# Implementation of embedded system and experimental validation

---

## Contents

---

<b>7.1</b>	<b>Introduction</b>	<b>139</b>
<b>7.2</b>	<b>Experimental vehicle-infrastructure integration</b>	<b>139</b>
7.2.1	Embedded sensors	140
7.2.2	Software modules	143
<b>7.3</b>	<b>Experimental validation</b>	<b>146</b>
7.3.1	Vehicle dynamics parameters estimation	147
7.3.2	Risk predication and curve speed warning system	155
<b>7.4</b>	<b>Conclusion</b>	<b>166</b>

---

## 7.1 Introduction

In the previous chapters, we have presented our theoretical algorithms that aimed at providing vehicle dynamics parameter estimation and predicting vehicle potential risk as well as the curve advisory speed to enhance the vehicle safety. Actually, theoretical development should be validated by applying not only off-line simulator environment but also extensive practice tests. Therefore, this chapter is designed to explain the implementation of the experimental vehicle and in-vehicle embedded systems. The ultimate target is to design and implement real-time distributed ADAS applications which are efficient for improving road safety.

This chapter is principally divided into two parts. The first part globally presents the experimental vehicle architecture, which consists of onboard sensors and software modules. The acquisition system is able to record driver's behavior and the corresponding compartment characteristics. The data acquisition, transmission and processing producers are explained to give to the reader an overall view of the software components.

The second part denotes some validation tests about the vehicle dynamics parameters and the prediction system. These systems will be embedded as an on-line application in order to verify whether they can always provide satisfactory results in the external environment. Moreover, the integration and operation of the entire system will be tested to ensure that it is stable and reliable during real driving conditions.

## 7.2 Experimental vehicle-infrastructure integration

In this section, we will mainly present an important part of the implementation of the experimental vehicle in our laboratory, all the result contributions use the data acquired with this

testbed. Our experimental vehicle DYNA is instrumented by the laboratory HEUDIASYC UMR 7253 CNRS at Compiègne, France in Figure 7.1, we employ a Peugeot 308sw to install all the necessary equipments. The subsequent subsections will focus on the introduction with respect to the hardware and software integration [Dherbomez 2013].



Figure 7.1: Heudiasyc laboratory experimental vehicle: DYNA

### 7.2.1 Embedded sensors

In order to obtain the required data and validate the developed algorithms, plenty of sensors are equipped in our vehicle. The classification of the usage of sensors is listed as follows:

#### *Sensors used for validation:*

- CORREVIT S-400: Non-Contact Optical Sensor for slip free measurement of transversal dynamics at large operating ranges. The sensor is installed at the place of the spare wheel under the car, for the measurement of transversal speed and sideslip angle (see Figure 7.2).
- Kistler RoaDyn S625 wheel force transducers: four wheel force sensors for passenger cars RoaDyn (Kistler) are fixed at each wheel (see Figure 7.3). It's able to measure all the forces and wheel torques in three dimensions, it also offers the accurate measurement of the rotation angle. These sensors are very expensive for ordinary cars. It is noted that they are used for the experimental validation of the observer results for tire forces in the contact point between wheels and ground.
- GPS receiver operating in RTK mode locates the vehicle with centimetric accuracy.

#### *Sensors used for input requirement:*

- CROSSBOW VG700AB: it is designed specifically for automotive test applications. It combines MEMSIC's high performance fiber optic gyros with silicon micro-machined (MEMS) accelerometer technology, in order to provide a highly accurate Vertical Gyro (VG) and Inertial Measurement Unit.



Figure 7.2: The Correvit installed at place of the spare wheel



Figure 7.3: Kistler wheel force transducers at front left wheel

- CORRSYS-DATRON HT500: this height sensor for non contact distance measurement is used to measure the deflection between chassis and ground. They are installed respectively in the front and back of the car body on both sides (see Figure 7.4).
- Sensor WAYCON SX50: sensors are installed with the suspension which can draw accurate wire position (see Figure 7.5). These sensors measure the distance of the deflection between wheels and car body.
- Available data on CAN bus: wheel rotation velocity, engine speed, yaw rate, brake pressure, lateral acceleration from the ESP, steering wheel angle.



Figure 7.4: Laser sensor for chassis height measurement



Figure 7.5: Suspension deflection sensor

### *Exteroceptive sensors:*

- A scenario record camera is used to register the vehicle trajectory.
- Mobileye system: it is able to provide a list of detected obstacles (pedestrians, vehicles, ...) and the position of the vehicle relative to the ground side markings on the vehicle CAN bus in real-time.

- Ibeo Standard (8L) Eight Layer/Multi-Echo LUX Sensor (Ibeo LUX 8L): the sensor is installed at front bumper to track the object on top 4 layers and raw data ground scanning/profiling (see Figure 7.6).



Figure 7.6: Laser sensor installed at front bumper

Figure 7.7: Embedded electronics and computer in the trunk

As it is mentioned above, an essential sensor Correvit is installed at place of the spare wheel under the car. However, the required value should be transformed at the center of gravity from the rear part of the car. Hence, the sideslip angle at the center of gravity is recalculated from the signal measured by a sensor located at the rear part of the chassis by the following formula [Lechner 2002]:

$$\beta_{cog} = \beta_m + L\dot{\psi}/V \quad (7.1)$$

where  $\beta_{cog}$  and  $\beta_m$  respectively represents the sideslip angle at the center of gravity and measured signal from sensor.  $L$  is the distance between the center of gravity and the sensor location.

All the electronics systems and PC are located in the trunk (see Figure 7.7). As well as, Figure 7.8 illustrates all the sensor location on the experimental vehicle. The following list 7.1 presents the available parameters that can be accessed in our acquisition system.

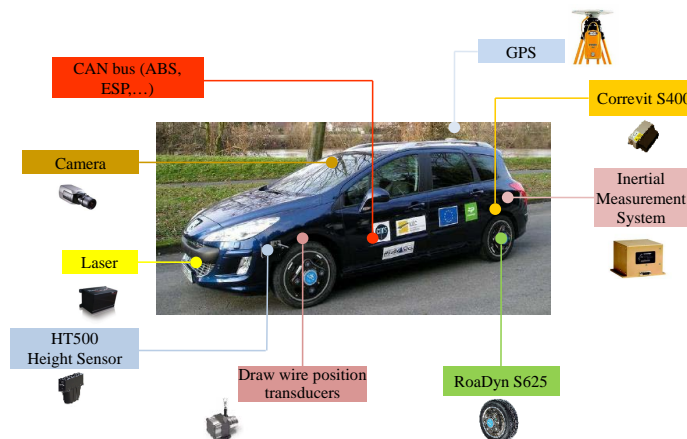


Figure 7.8: Laboratory experimental vehicle equipped with sensors

$T$	Timestamps ( $s$ )	PC
$H_{ij}$	Distance deflection between chassis and the ground at each corner ( $cm$ )	CORRSYS-DATRON HT500
$V_m$	Magnitude speed of the vehicle ( $50mV/kph$ )	CORREVIT S-400
$\beta_m$	Sideslip angle ( $500mv/deg$ )	CORREVIT S-400
$F_{x_{ij}}$	Longitudinal force for each tire ( $N/mv$ )	Kistler RoaDyn S625
$F_{y_{ij}}$	Lateral force for each tire ( $N/mv$ )	Kistler RoaDyn S625
$F_{z_{ij}}$	Vertical force for each tire ( $N/mv$ )	Kistler RoaDyn S625
$M_{x_{ij}}$	Longitudinal moment for each tire ( $N.m/mv$ )	Kistler RoaDyn S625
$M_{y_{ij}}$	Lateral moment for each tire ( $N.m/mv$ )	Kistler RoaDyn S625
$M_{z_{ij}}$	Vertical moment for each tire ( $N.m/mv$ )	Kistler RoaDyn S625
$\theta_{ij}$	Wheel angle for each tire ( $0.036deg/mv$ )	Kistler RoaDyn S625
$\omega_{ij}$	Wheel angular velocity for each tire ( $deg/s/mv$ )	Kistler RoaDyn S625
$a_x$	Longitudinal acceleration ( $g$ )	VG700AB
$a_y$	Lateral acceleration ( $g$ )	VG700AB
$a_z$	Vertical acceleration ( $g$ )	VG700AB
$\dot{\phi}$	Roll rate ( $deg/s$ )	VG700AB
$\dot{\psi}$	Pitch rate ( $deg/s$ )	VG700AB
$\dot{\psi}$	Yaw rate ( $deg/s$ )	VG700AB
$\phi$	Roll angle ( $deg$ )	VG700AB
$\varphi$	Pitch angle ( $deg$ )	VG700AB
$\psi_c$	Yaw rate ( $>0$ in trigonometric direction) ( $deg/s$ )	CAN bus
$a_{y_c}$	Lateral acceleration ( $>0$ to the right) ( $m/s^2$ )	CAN bus
$P_b$	Brake pressure ( $bar$ )	CAN bus
$V_s$	Vehicle speed ( $km/h$ )	CAN bus
$S$	Traveled distance ( $m$ )	CAN bus
$a_{x_c}$	Longitudinal acceleration ( $m/s^2$ )	CAN bus
$\delta$	Steering wheel angle ( $>0$ in trigonometric direction (to the left)) ( $deg$ )	CAN bus
$\dot{\delta}$	Rotation rate of the steering wheel ( $deg/s$ )	CAN bus
$\dot{\delta}_{opt}$	Optimized rotation rate of the steering wheel ( $deg/s$ )	CAN bus
$\omega_{AV}$	Mean speed of the front wheels ( $km/h$ )	CAN bus
$\omega_{ARG}$	Speed of the rear left wheel ( $km/h$ )	CAN bus
$\omega_{ARD}$	Speed of the rear right wheel ( $km/h$ )	CAN bus
$\lambda$	Longitude ( $rad$ )	GPS
$\gamma$	Latitude ( $rad$ )	GPS

Table 7.1: Available parameters from the acquisition system

## 7.2.2 Software modules

### 7.2.2.1 Architecture of the acquisition system

We have developed an acquisition system, which is capable of acquiring 16, 32 or 48 analog channels using a 24-bit converter [Dherbomez 2013]. It consists of a computer UEI powered by a 200 MHz PowerPC processor running a real-time operating system Xenomai. The UEILogger

is a powerful standalone data logger based on the UEI PowerDNA Ethernet DAQ Cube. The Cube is based on the framework of Xenomai with 48 acquisition inputs. The Xenomai is a real-time development framework cooperating with the Linux kernel. It is used to provide a pervasive, interface-diagnostic, real-time support to user-space applications. Some tasks are executed in the framework of Xenomai:

- 1) Task of acquiring the highest priority, periodic frequency and frequency acquisition.
- 2) Task of digital filters function that can be applied to all channels. The software provides data acquisition by using the analog cards AI-217. The DNA-AI-217 Analog Input Board is compatible with cube chassis. The DNA version is a kind of analog input module for using with the PowerDNA Cube.

### *Communication protocol*

Cube runs with the software which can constitute a system of acquisition network incorporating digital filters with different cutoff frequency. Cube returns as UDP frame according to the request from PC. The packet is sent back on a low frequency, which is a divisor of the acquisition frequency. In our embedded data acquisition system, the acquisition frequency is  $4k\text{Hz}$ , however the data packet is sent back in  $200\text{Hz}$ .

### *Digital filter*

In order to deal with the signals, a 5th order Chebyshev filter applied has a cutoff frequency of  $35\text{Hz}$ , no aliasing and loss of information allows it up to  $20\text{Hz}$ . It is applied to process each sample and all channels of the task distributed. In addition, we use a FIR filter with a cutoff frequency of  $145\text{Hz}$ , and no aliasing and loss of information allows it up to  $100\text{Hz}$ . Its calculation is too expensive to make it possible to calculate systematically. Hence we adopt one sample takes into account 201 samples, and it is calculated only for sample and channels requested by client.

### *Implementation*

The stability of acquisition system is guaranteed by using of Xenomai, the sub-kernel real-time Linux framework. The tasks are distributed as follows:

- An acquisition task maximum up to  $4k\text{Hz}$ .
- A task of filtering applied to all channels using a 5th order Chebyshev filter.
- A surveillance task for each request to be served, sending messages with the required data. FIR filter is employed only for the specified sample channel since it is more computation power in a general purpose processor.
- A duty that awaits for client requests.

Otherwise, vehicle CAN bus is available in the acquisition system of the host PC. GPS and camera are directly connected to the computer for obtaining the vehicle path. It is noted that all the devices are located in the trunk of the car with the electric circuit system as shown in the above figure. The monitoring equipment is located on the back left seat. The operator can manipulate the configuration of the system with a monitor and keyboard.

## 7.2.2.2 Software architecture

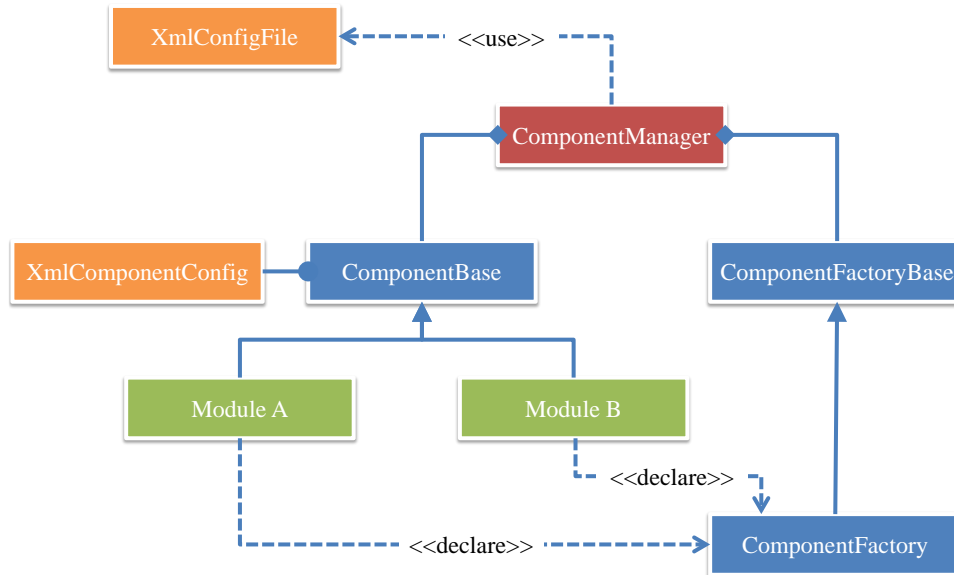
*Rapid prototyping environment: the framework PACPUS*

Figure 7.9: Software architecture

The laboratory has developed a rapid prototyping environment for designing software modules and testing them in real time on in-vehicle architecture. The framework PACPUS is available as an open source with free license CeCILL-C. The framework PACPUS was developed following the principle of component-oriented design to provide users more versatility in their developments. The rapid prototyping environment PACPUS is developed in C++ with multiple operating systems (Windows, Linux, Mac) in order to:

- keep a close compatibility with C and thus facilitate the development of lower layers (drivers, sensor interfaces, system calls, ...).
- able to use the mechanisms of object-oriented programming, meet the requirement for modularity.
- obtain a code compiled with higher execution speeds which are much closer to real-time constraint.

The framework PACPUS employs the Qt API for graphical interfaces and can be integrated with other development environment for multi-sensor fusion. The class diagram in Figure 7.9 presents the typical architecture of an application using the framework PACPUS. For instance, here two Module A and Module B components are created and managed by the ComponentManager class. This mechanism enables the communication between two modules become convenient for system design.

*Applications of state observation and risk prediction system*

This car is equipped with an industrial PC in the trunk. Particular software is developed for the acquisition system in C/C++. In the data structure, the data read by the acquisition task is stored in a circular buffer. The buffer is large enough to prevent the risk of exceeding, because FIR filters use a large amount of data. The cube sends the UDP packet by the Ethernet to the PC. The signal sequence after the filter FIR is  $100Hz$ . On the PC, we develop the application “CubeClient” for the task of communication between the cube and the PC. The component of this part is devoted to the task of sending the request, receiving the UDP packet and then decoding the UDP packet. Then the data is sent to the application which includes our algorithm written in C++. The schema is shown in Figure 7.10. Other components which are designed for the management of different equipments were constructed as well. In the system of the estimation process, the observer is developed in the .DLL form as a real-time application operating at  $200Hz$ . The following section will denote some performance validations which are able to be realized in real-time with respect to the applications of vehicle dynamics parameter estimation as well as risk predication and curve speed warning system.

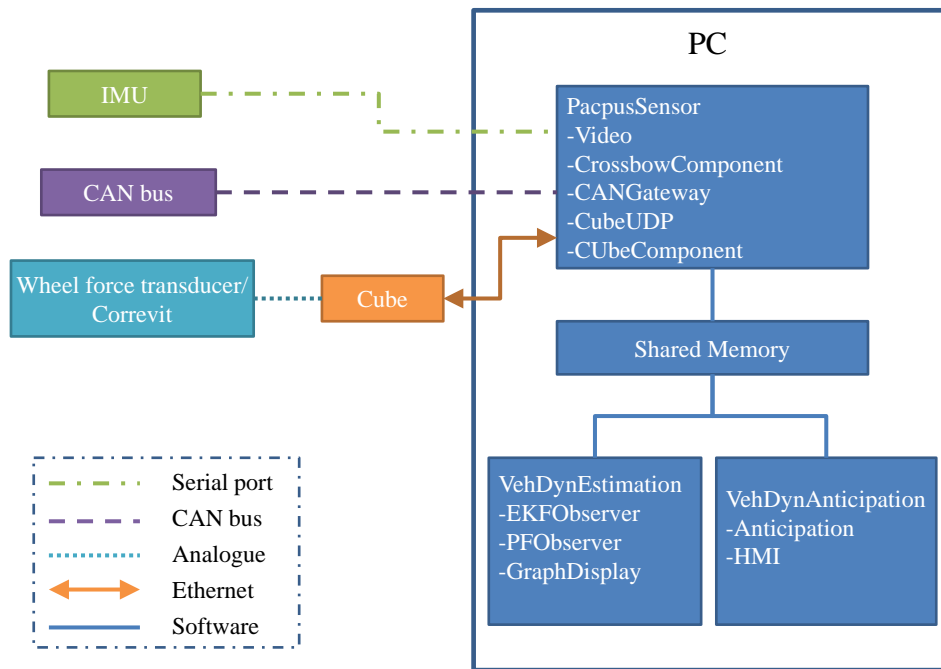


Figure 7.10: Application architecture of the vehicle dynamics parameter estimation and risk prediction

### 7.3 Experimental validation

In order to validate the entire system that is composed of data acquisition, data processing and particular modules developed as an embedded application in real-time, plenty of tests are performed either around our research center or at the professional testing track in CREAM (Centre d’Essais et de Recherche Automobile de Mortefontaine). It is noted that all tests are performed with our experimental vehicle DYNA, with 2 persons onboarded and full tank. First

application concerning vehicle dynamics parameter estimation can survey the vehicle dynamics state continuously and fleetly at current moment. The second application aiming at providing risk assessment and advisory speed for passing the curve is able to predict the potential danger in future instant. These two applications are designed to be activated independently or simultaneously depending on the users' initializing configuration.

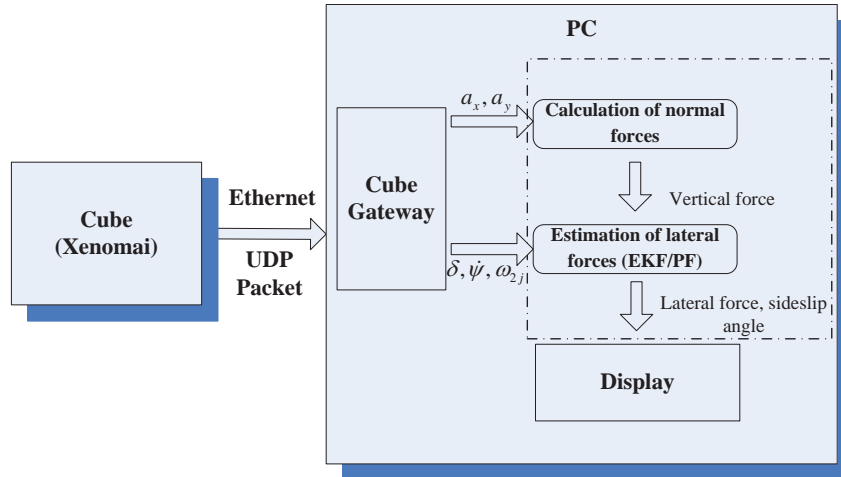


Figure 7.11: Real-time vehicle dynamics parameters estimation process schema

### 7.3.1 Vehicle dynamics parameters estimation

The basic theory has been presented hereinbefore, in this part we will validate the estimation process which is applied in our real-time system. The block diagram shown in Figure 7.11 illustrates the processing steps of our algorithm. The characteristic of simplicity and universality of such system structure is able to satisfy our requirements. The first block calculates the vertical force, these variables will be used as the input in the second block which aimed at estimating lateral forces and sideslip angle. The frame of the observer is simple and universal, for the requirement of the real-time system. The estimation process with EKF/PF has been developed as a real-time application. Particular software modules are developed for the acquisition system in C++ which is able to be embedded in the experimental vehicle. The user interface implemented by using Qt API provides the real-time surveillance about vehicle dynamics state in Figure 7.12.

For all the real-time test, the acquisition and estimation process were set at  $200Hz$  that can precisely reflect the dynamics characteristics. It is different from previous works, all the system operating at on-line state, the recorded sensor data and estimation results are plotted here using Matlab environment. The observer processing consists of the developed Extended Kalman filter ( $O_{EF_y}$ ) and Particle filter ( $O_{PF_y}$ ).

#### 7.3.1.1 Road circuit test

In order to validate the overall performance of two estimation methods as well as corresponding system, a maneuver was carried out on the dynamics behavior track at CREAM, The length of road circuit is  $5,200m$ , which consists of curves, bank angle, slope angle as well as bumpy obstacle. The track is marked with orange line in the following figure 7.13. A professional driver



Figure 7.12: Onboard real-time estimation surveillance interface

was hired to achieve extensive speed test. Some sections of the test are selected in order to clearly analyze the compartment of the estimation performance.

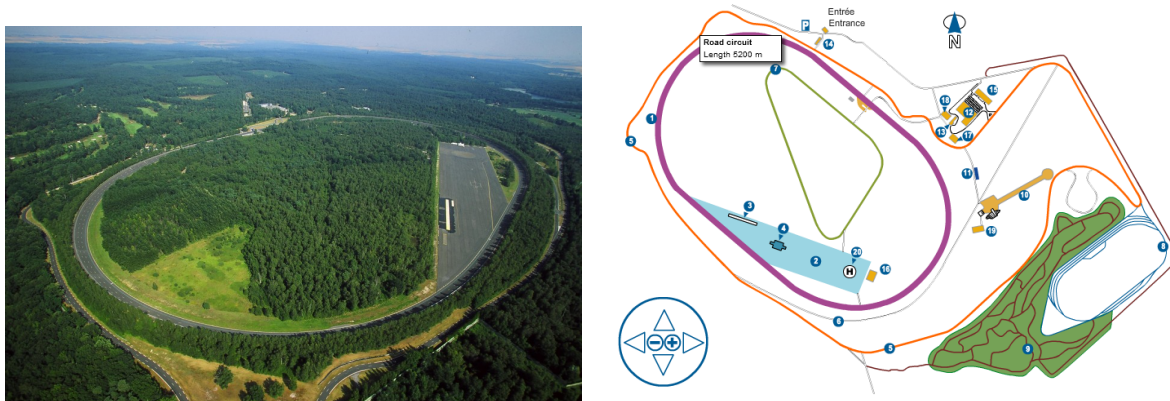


Figure 7.13: The trajectory of road circuit on plan

### *S-curve test*

The first maneuver is selected in a certain section where vehicle negotiates a S-curve, the trajectory is illustrated in Figure 7.15. S-curve represents a combination maneuver, in which vehicle dynamics plays an important role. The selected section takes 35s, in order to describe more precisely about the negotiating maneuver, longitudinal acceleration, lateral acceleration, steering wheel angle and vehicle velocity are represented in Figure 7.14. The vehicle reaches the start of the curve at speed of 65km/h, then the vehicle begins to brake with longitudinal acceleration of  $-3.4m/s^2$ . During the time interval of  $(15s < t < 18s)$ , vehicle passes first curve. The lateral acceleration reaches up to  $7.1m/s^2$ , while the maximum steering wheel angle

attains at  $0.12rad$ . These parameters ensure that the vehicle is passing a rough turning. In other words, the observer will be profoundly solicited in this transient period. Then the vehicle leaves first curve and enters the following one immediately. In the second curve ( $18s < t < 23s$ ), vehicle begins to accelerate, meanwhile vehicle undergoes it with maximum lateral acceleration of  $-6.1m/s^2$  and the steering wheel angle keeps constant at  $-0.07rad$  until vehicle leaves the S-curve.

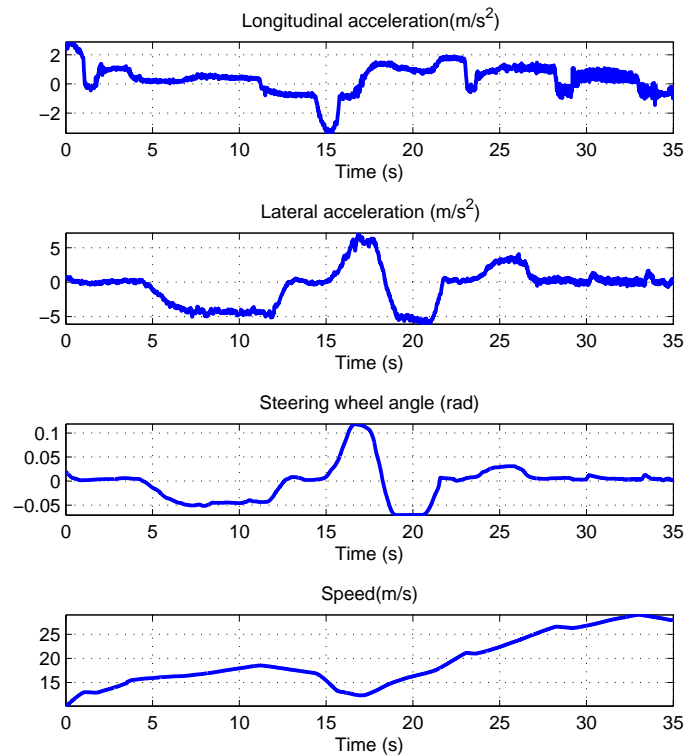


Figure 7.14: Maneuver time history: S-curve test

In Figure 7.17 and 7.18, the plotted data illustrate the comparison between calculated vertical tire force and the measurement from wheel force transducers. Globally, the direct calculation from relevant equations report satisfactory results. An efficient solution for the vertical tire force leads to a good evaluation of the lateral load transfer. In section ( $5s < t < 13s$ ), vehicle undergoes a smooth circle, here vertical tire force maintains constant, where the lateral load transfer in Figure 7.16 keeps at  $6000N$ . After that, a sudden tuning in S-curve causes a sharp variation of the vertical load distribution. During the S-curve section ( $15s < t < 23s$ ), the comportment of result follows with the variation trend of lateral acceleration. The lateral load transfer even reaches up to  $8000N$ , which means that driving maneuver is quite intense. In addition, from the statistics report of normalized root mean square error (NRMSE) in 7.28(a), the deviation level is around 6%. The estimated and measured lateral force applying EKF and PF techniques is depicted in Figure 7.20, different load distribution leads to assorted lateral force at each tire. During the S-curve section ( $15s < t < 23s$ ), lateral force at front right wheel

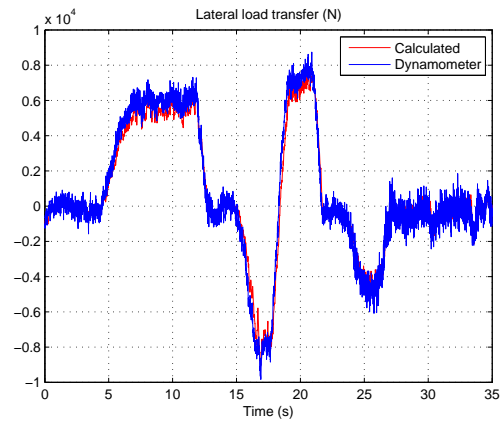
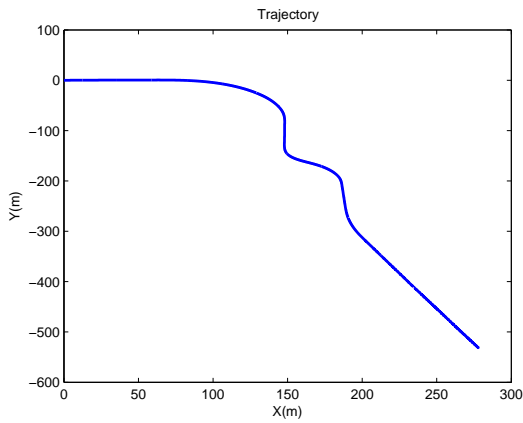
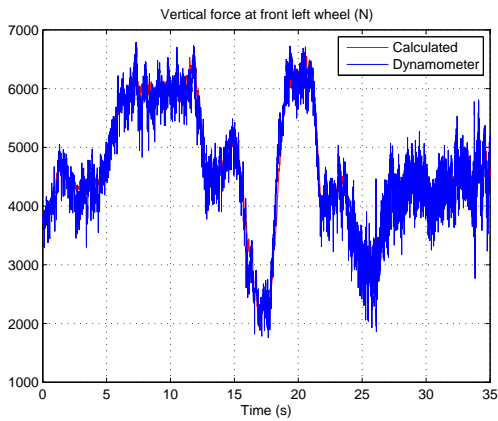
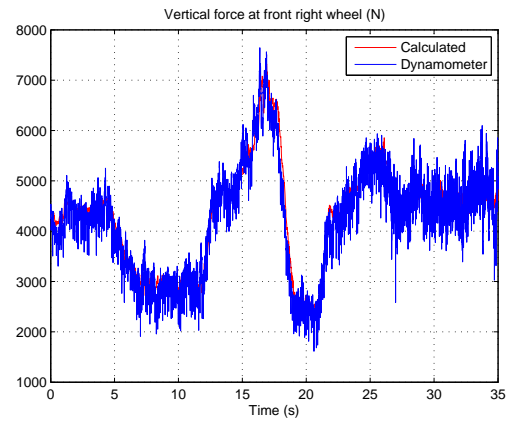


Figure 7.15: The trajectory of vehicle body Figure 7.16: Lateral load transfer: S-curve test movement: S-curve test

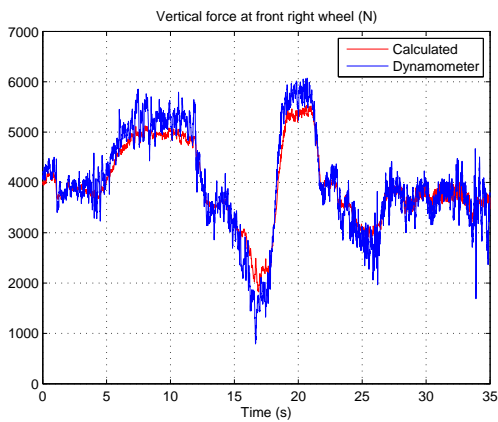


(a) Front left vertical tire force

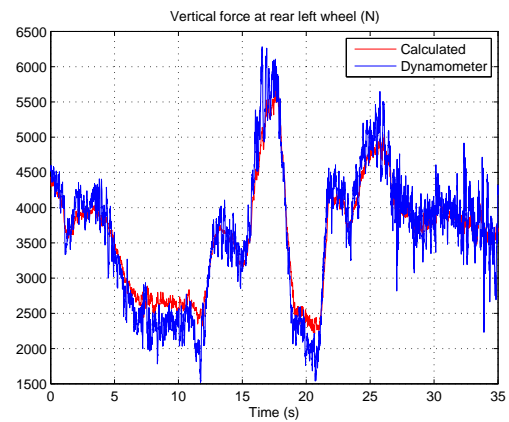


(b) Front right vertical tire force

Figure 7.17: Comparison of front vertical tire forces: S-curve test



(a) Rear left vertical tire force



(b) Rear right vertical tire force

Figure 7.18: Comparison of rear vertical tire forces: S-curve test

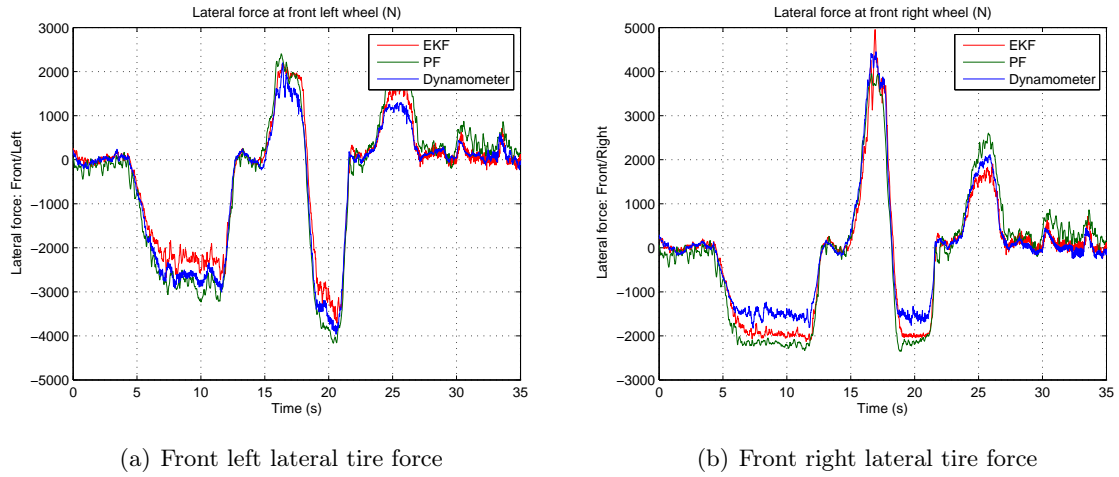


Figure 7.19: Comparison of front lateral tire forces: S-curve test

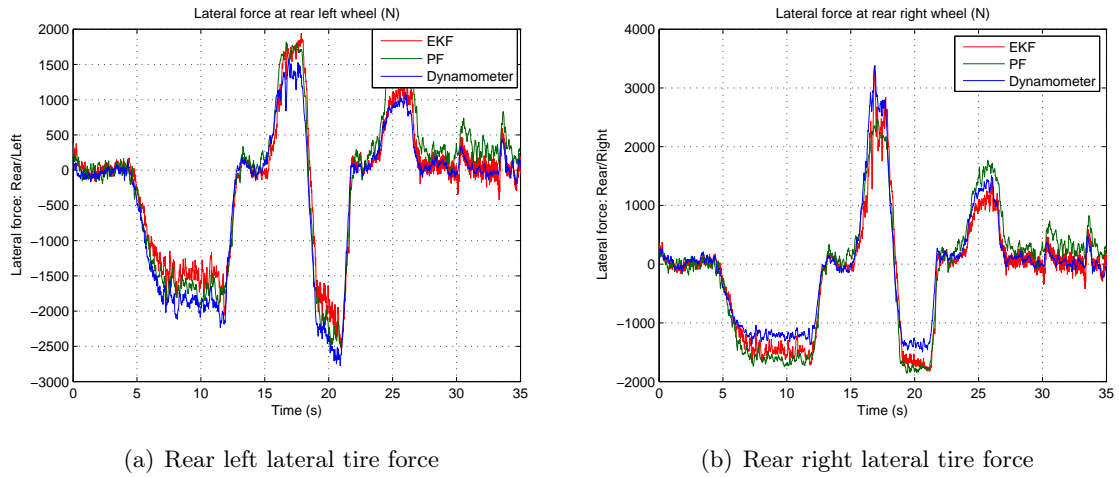


Figure 7.20: Comparison of rear lateral tire forces: S-curve test

attains at  $4000N$  on the first curve, as well as  $-4000N$  appeared at front left wheel on the second curve. It is definitely confirmed that force behavior is pushed into the nonlinear region. However, some error takes place due to the imperfection of reconstructed model. In this test, Particle filter is inferior to Extended Kalman filter. This phenomenon can be found both in figures and NRMSE statistics analysis in 7.28(a).

### ***Bend test***

The second section is intercepted from the entire road circuit test in Figure 7.22. This trajectory contains three characteristics: a semi-circle, a sharp bend and a straight gravel bumpy pathway. Figure 7.21 illustrates the maneuver time history that obtained by driving Peugeot 308sw around the dynamics behavior track. The first interval is between  $0s < t < 15s$  at the speed of  $80km/h$ , lateral acceleration decreases from  $-5m/s^2$  to  $-2m/s^2$  due to the reducing of vehicle speed. The second interval is defined at  $15s < t < 25s$ , a sharp bend following with the previous semi-circle. During this period, lateral acceleration exceeds  $5m/s^2$  that stating intense driving conditions, while steering wheel angle reaches up to  $0.2rad$ . In the last interval of  $25s <$

$t < 35s$ , vehicle passes a bumpy pavement full of gravel, meanwhile vehicle is accelerating until  $80km/h$ . This composite road condition makes the overall evaluation of the system performance available in the reality.

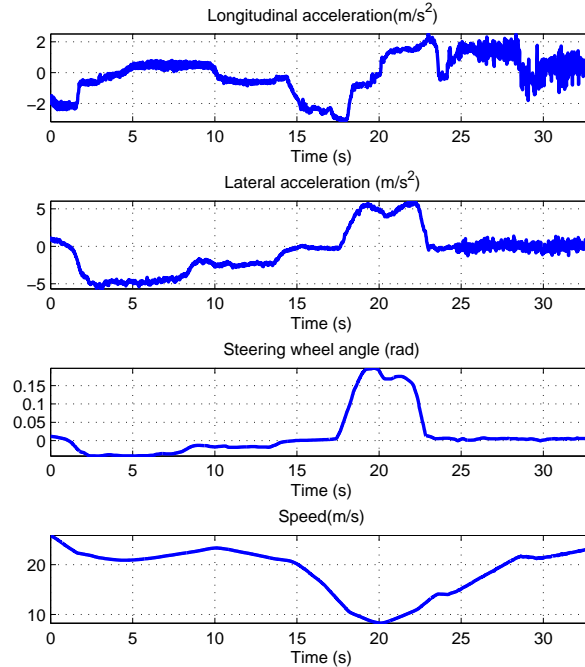


Figure 7.21: Maneuver time history: Bend test

Seen from Figure 7.25, calculated vertical force successfully follows with the measured data. Front wheels provide quite good quality, while the rear ones have some bias. It is explained by simplification of the model and disuse of observer technique. In the first interval  $0s < t < 15s$  of semi-circle negotiation, lateral load transfer in Figure 7.23 is approaching at  $7000N$ . Furthermore, it reaches up to  $-8000N$  in the second interval. The excessive value manifests the situation of severe driving handling. At the end of this scenario, vehicle undergoes the bumpy road, it is evident that measured data is erratic with a lot of noise. This segment is conducted to verify the observer robustness to the input noise.

Figure 7.26(a) - 7.27(b) represent two observers' performance in real-time. EKF result in red line is much closer to the measurement comparing with PF estimation. In the first segment, lateral force at front left wheel exceeds  $3000N$ , some deviation can be explained by the negligence of modeling of tire deformation with excessive running speed during turning, and the camber angle and suspension mechanism are not considered in our model. Similarly, this phenomenon appears on rest three wheels. Although a little difference can be found during sharp bend, however they point out that the accuracy and fast responses of the observer  $O_{EF_y}$  and  $O_{PF_y}$  are good.

Definitely, the observer technique reduces the effect of the input noise caused by irregular bumpy road, the estimation results become much smoother. Even though  $O_{PF_y}$  reveals better performance in chapter 5, when the vehicle undergoes with an excessive speed, the unmodeling factors may bring some errors in the system. In this test,  $O_{EF_y}$  obviously surpass  $O_{PF_y}$  in precision. This point is also evidently demonstrated from the statistics histogram in Figure 7.29(b).

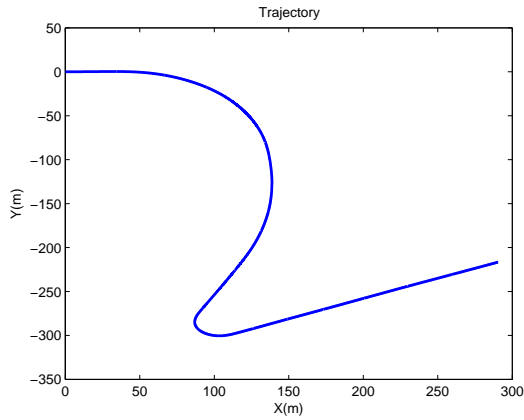


Figure 7.22: The trajectory of vehicle body movement: Bend test

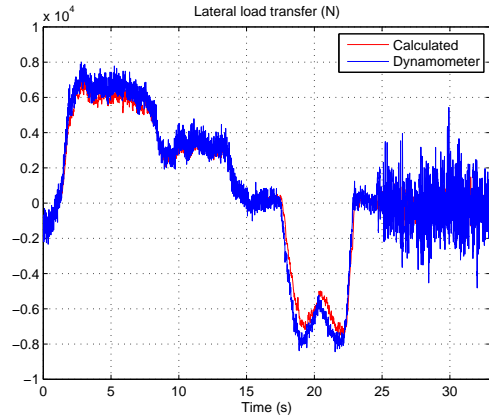
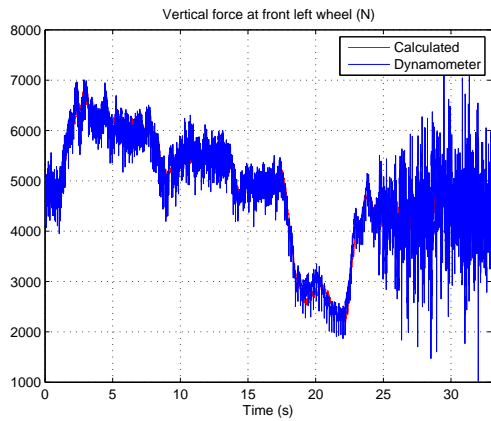
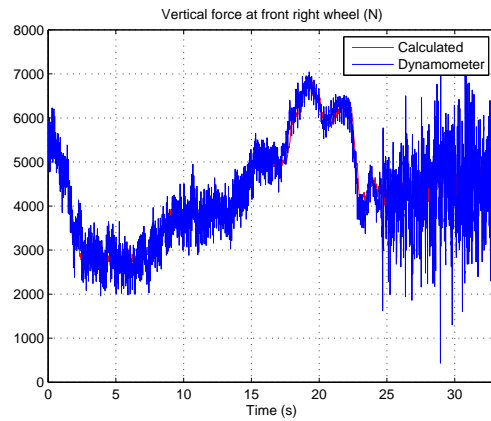


Figure 7.23: Lateral load transfer: Bend test

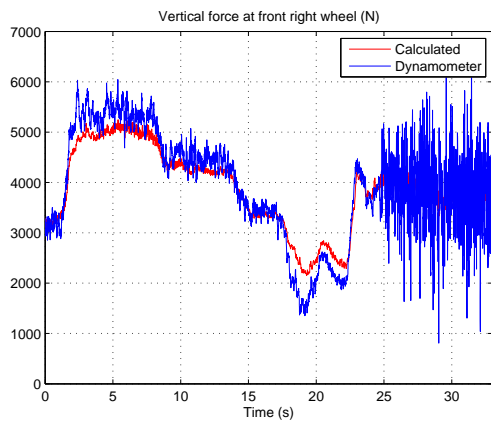


(a) Front left vertical tire force

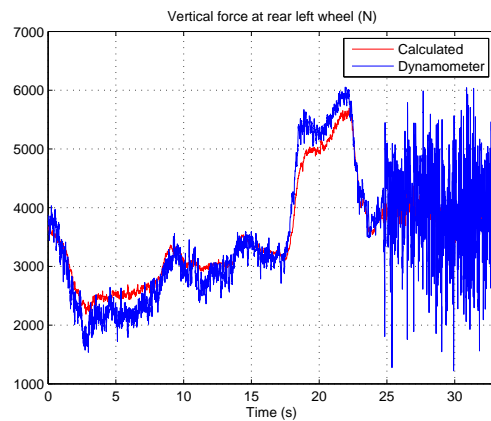


(b) Front right vertical tire force

Figure 7.24: Comparison of front vertical tire forces: Bend test



(a) Rear left vertical tire force



(b) Rear right vertical tire force

Figure 7.25: Comparison of rear vertical tire forces: Bend test

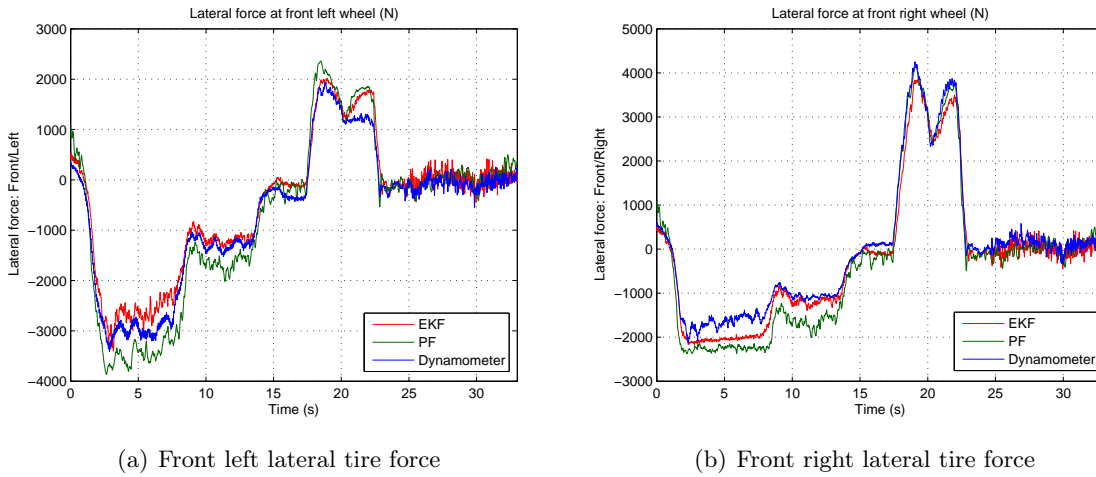


Figure 7.26: Comparison of front lateral tire forces: Bend test

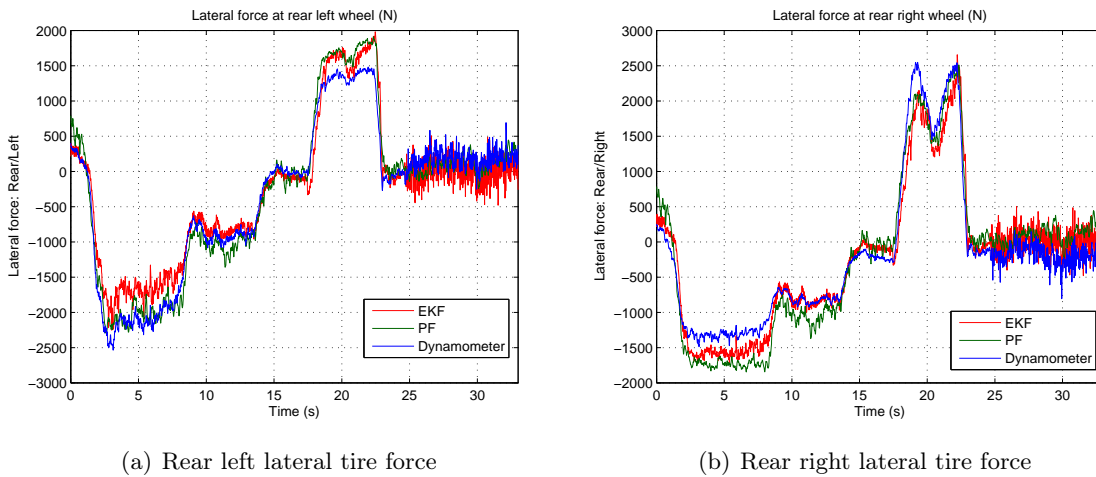


Figure 7.27: Comparison of rear lateral tire forces: Bend test

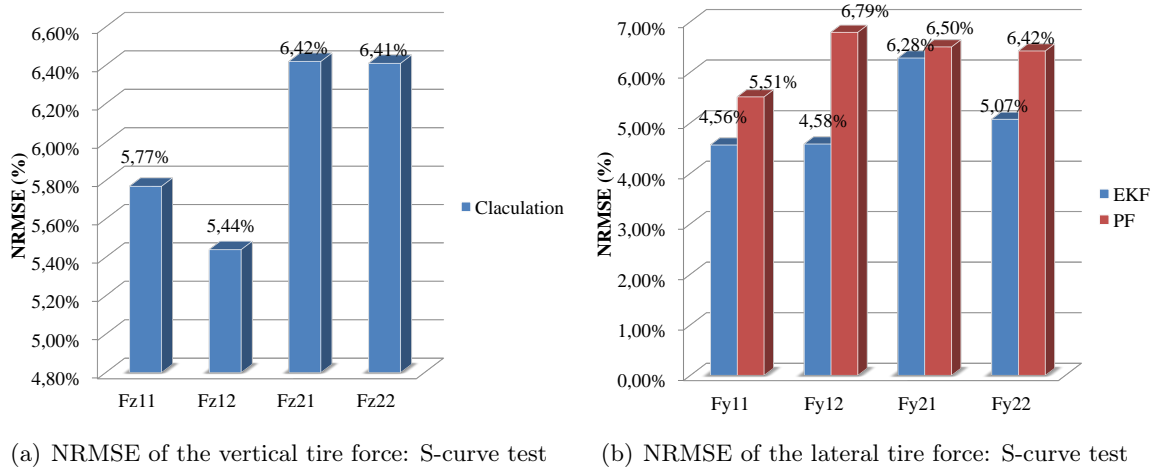


Figure 7.28: NRMSE analysis of S-curve test

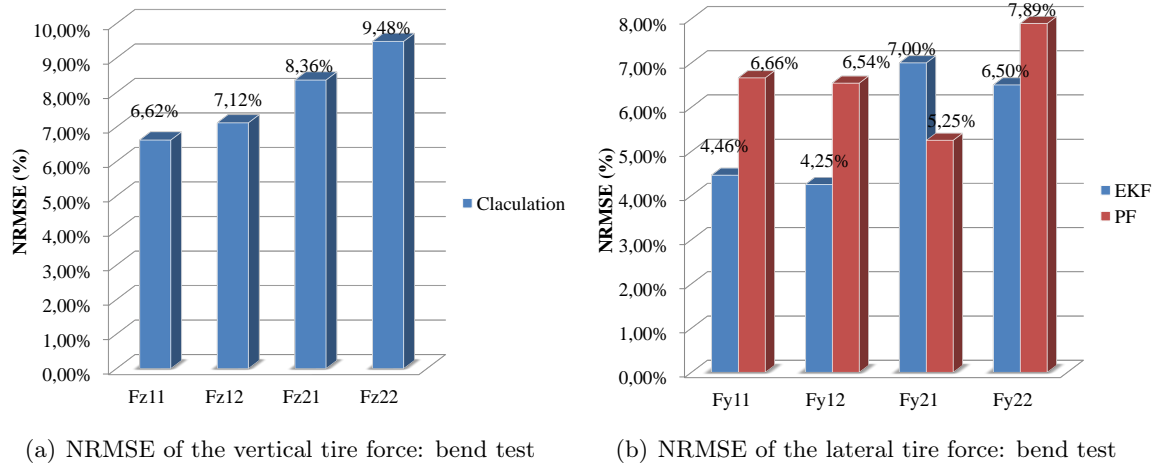


Figure 7.29: NRMSE analysis of bend test

### 7.3.2 Risk predication and curve speed warning system

The theoretical presentation concerning this system has been presented in chapter 6. This work contributes to SEDVAC project by the Picardie-region. The integrated observer in the part of the risk prediction system chooses Extended Kalman filter due to its fast response, an fundamental factor should be taken into account is the computing time. The system procedures as described in principle part are implemented by using Qt API in C++. The vehicle-infrastructure wireless communication application is combined with our project partner. The real-time system architecture is described in Figure 7.30, it consists of three principal modules, which are respectively responsible for data acquisition, risk prediction and driver interface. The collected data are sent to main computing module through shared memory, then prediction output is transmitted to HMI by using Qt signal&slot communication mechanism. The V2I communication, risk prediction applying observer technique, risk evaluation and advisory curve speed warning components execute sequentially within the principal prediction module.

#### *Installation of road-side infrastructure*

Two road-side units (DYNETAIRBORNE01 and DYNETAIRBORNE04) are installed on the campus of our university, the location is marked in Figure 7.31, where the server (DYNETAIRBORNE06) is fixed at the garage. The GPS coordinate is denoted in the following Table 7.3.2:

Tab	Coordinate
DYNETAIRBORNE01	(49.3998, 2.799649)
DYNETAIRBORNE04	(49.398539, 2.798852)
DYNETAIRBORNE06	(49.399087, 2.79941)

Table 7.2: GPS coordinate of the road-side infrastructure

Figure 7.32 illustrates the installation of DYNETAIRBORNE04, electricity supply relying on solar energy supports the operation of the device.

#### *Experimental test*

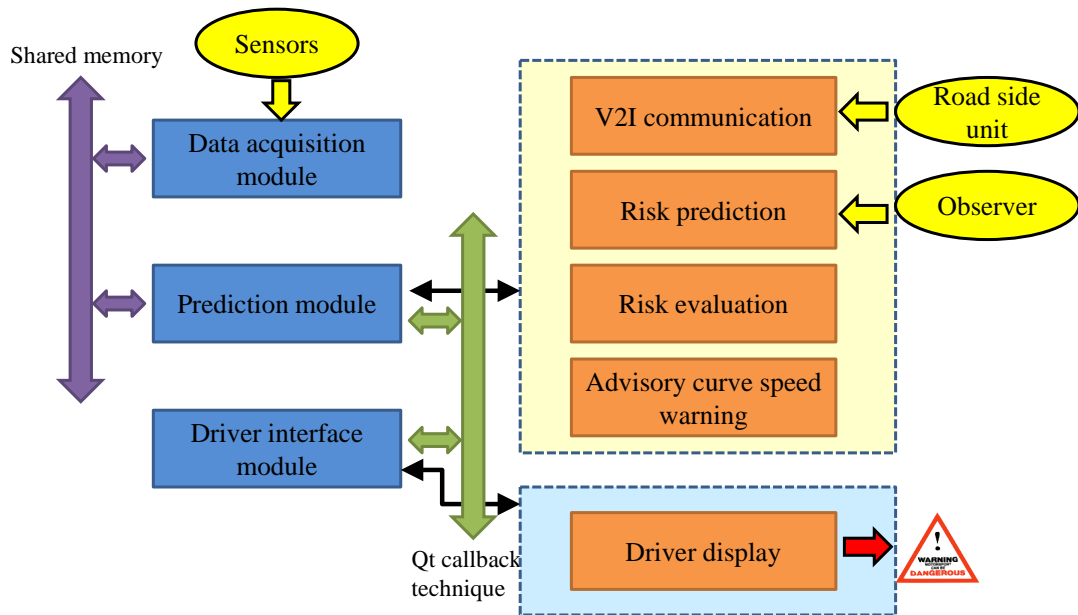


Figure 7.30: Architecture of real-time risk prediction and advisory curve speed warning system

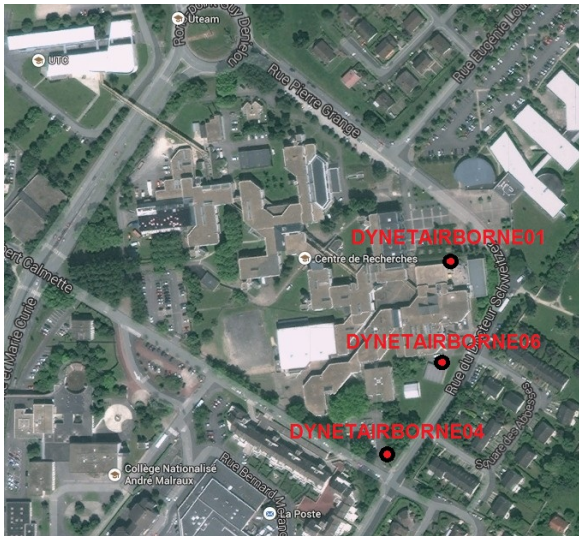


Figure 7.31: Road-side unit located on Google map



Figure 7.32: Road-side infrastructure

The experimental test performed with DYNA around the campus, the detailed trajectory and orientation are illustrated in Figure 7.33. Otherwise, the reconstructed Cartesian coordinate is represented in Figure 7.34. For instance, we take the first curve at Point B to explain and analyze the risk prediction and curve speed warning system. The experimental test starts from garage marked as point A on the map 7.33.

To give a clear description of the approach how the entire system works in real-time, we adopt the developed HMI and captured instantaneous image from camera. The phase of data

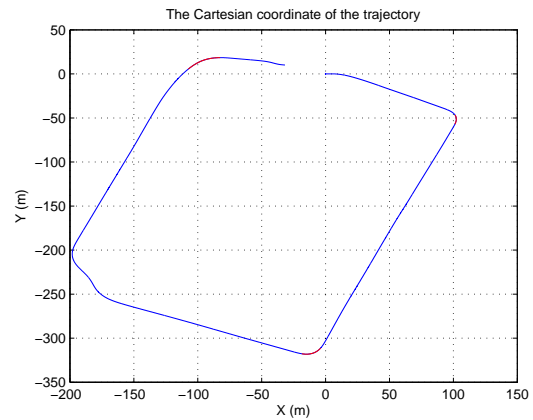
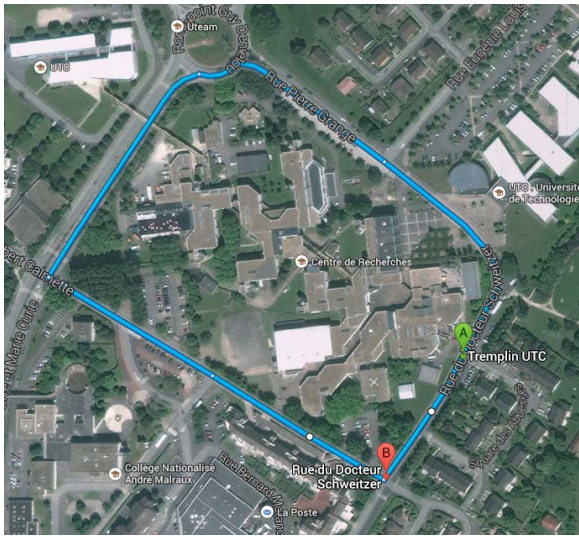


Figure 7.33: Tracked trajectory on Google map    Figure 7.34: Reconstructed Cartesian coordinate of trajectory

collection and the activation of the systems through V2I wireless communication (see Figure 6.4(a) and 6.4(b)) is not reflected directly in the driver display interface. They are designed as a background process running automatically. When the vehicle's location recorded by onboard GPS is approaching the starting point of the curve, this point is defined by the static information stored in road-side unit which is transmitted through V2I communication module. Vehicle speed and longitudinal acceleration are registered with a segment of 3s until it is distancing 2s from the starting point of the curve. As soon as vehicle reaches at this distance, the prediction procedure presented in Figure 6.5 starts to operate. If the risk evaluation module detects potential danger basing on current state, HMI in Figure 7.35 will alert driver with red danger signal icon and denotes advisory curve speed. This step is corresponding to the third phase in 6.4(c).

Afterwards, the system will monitor vehicle speed until it is decreased below the warning speed. The momentary captured image shown in Figure 7.36 illustrates that vehicle velocity at present is  $16.35\text{km/h}$ , it does not exceed the warning speed. Meanwhile, the green alarm lamp taking place of the red one manifests that vehicle is passing the curve safely. This phase realizes the theoretical introduction in Figure 6.4(d). Last phase in Figure 6.4(e) relating to the vehicle leaving off the curve is demonstrated in the screen-shot picture 7.37, vehicle negotiates the curve with safety. Up to present, we have explained five phases as presented theoretically in last chapter with corresponding captured images in real test situation. Another question we are wondering is the computing time, it is reported that the execution time of the whole phases need  $0.12\text{s}$ , hence it meets the requirement of the fast response characteristic. Finally, to give a global view of the test, vehicle trajectory is reported within the sub-window in Figure 7.38. The segment of the curve was marked in red line where the prediction system detected potential risk. Therefore, we can successfully draw the conclusion that the in-vehicle integrated system is efficient to denote risk assessment and safe speed for negotiating the curve not only with the simulator environment but also with the embedded systems in real-time.

In order to describe more clearly about the phase three in Figure 6.4(c) aimed at evaluating the potential risk and proposing safe advisory speed, the method schema has been presented in Figure 6.5. The first risk evaluation is performed applying the predicted parameters represented



Figure 7.35: Captured instantaneous scenario that entering the curve

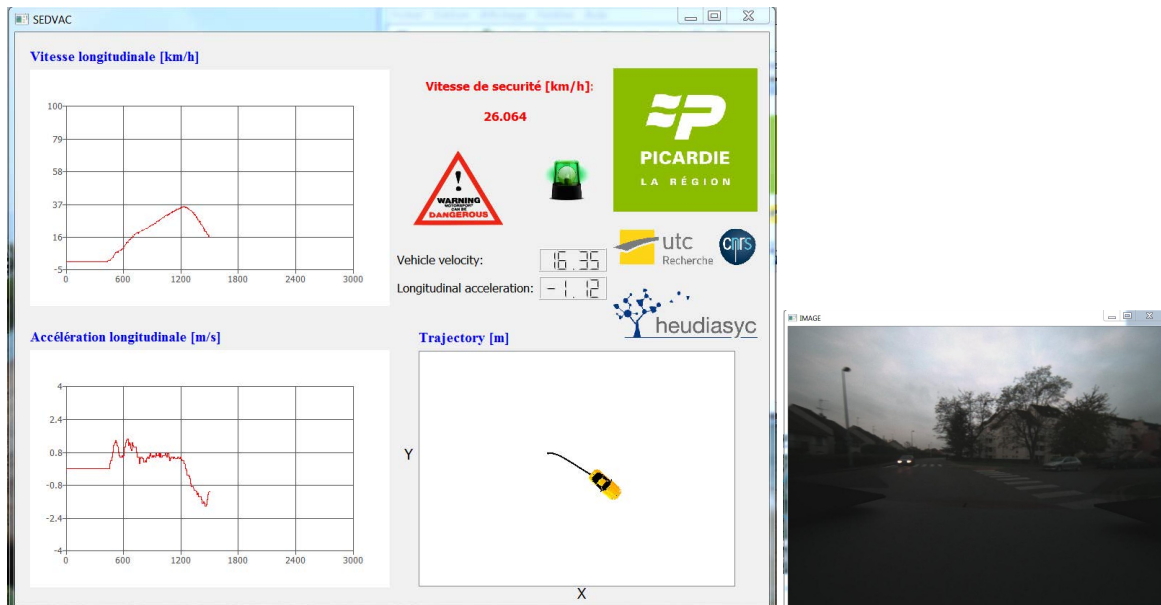


Figure 7.36: Captured instantaneous scenario that undergoing the curve

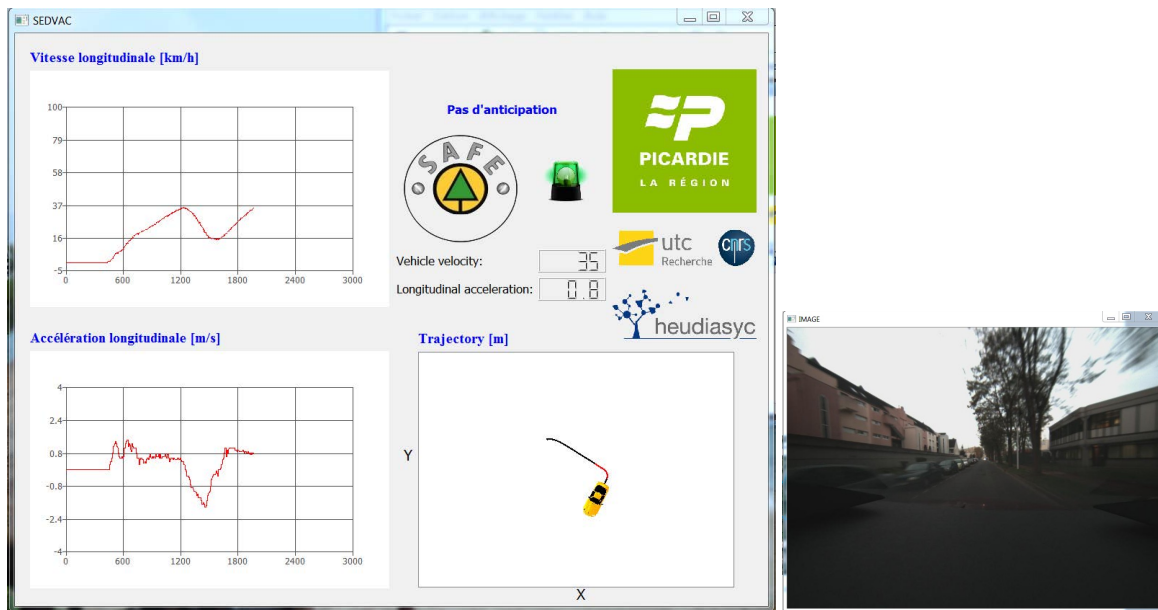


Figure 7.37: Captured instantaneous scenario that leaving the curve

in 7.39. Vertical and lateral tire forces are estimated with observer technique, the predicted results are shown in Figure 7.40 and 7.41. Lateral drift risk is discovered at two front wheels (see 7.43(a) 7.43(b)) and rear right one (see Figure 7.43(d)). Consequently, the system is willing to calculate the safe speed to pass the curve without danger. Risk eliminates until when inner vehicle speed decreasing to  $26\text{km/h}$ . The last illustrations of prediction sequence are represented from Figure 7.44 to 7.48, there is no danger to be appeared.

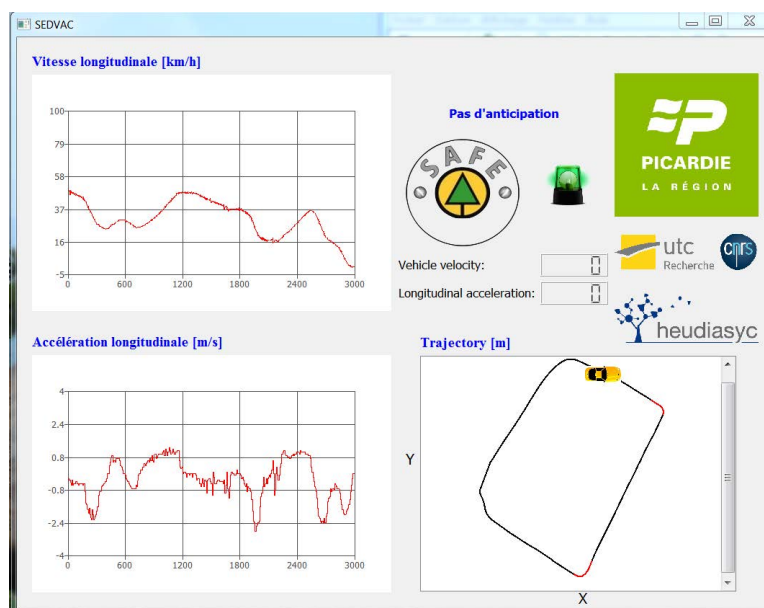
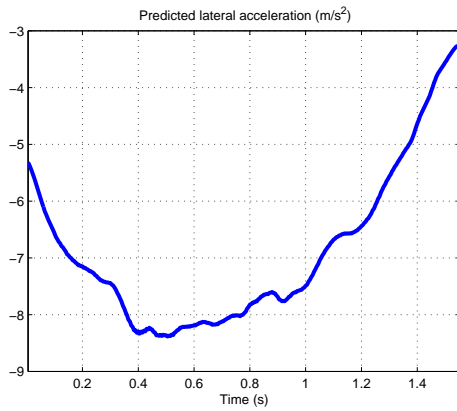
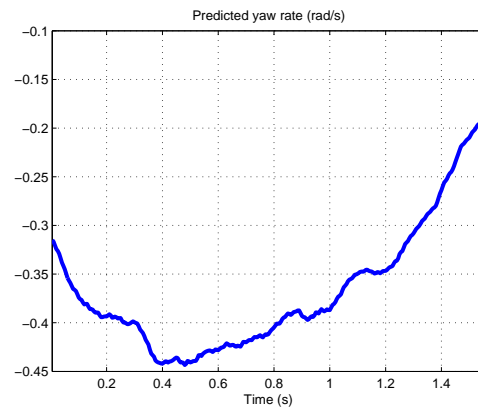


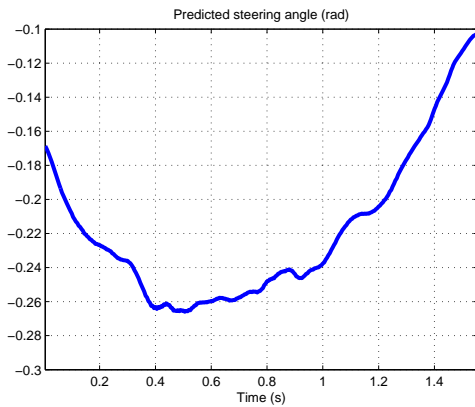
Figure 7.38: Final illustration of the overall experimental test around the campus



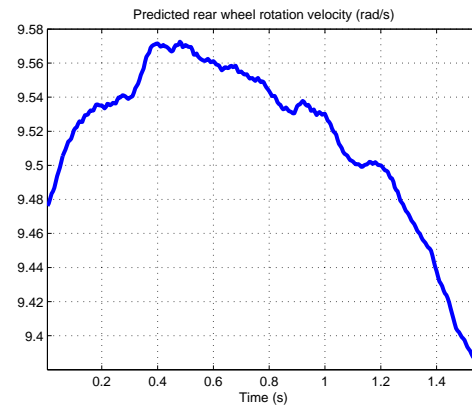
(a) Predicted lateral acceleraion: first sequence



(b) Predicted yaw rate: first sequence

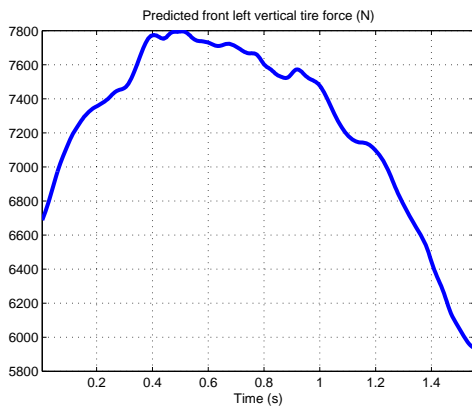


(c) Predicted steering wheel angle: first sequence

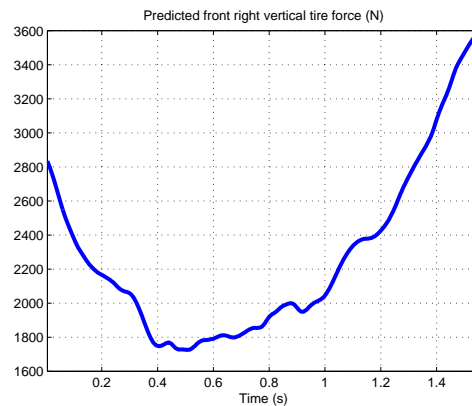


(d) Predicted rear wheel rotation speed: first sequence

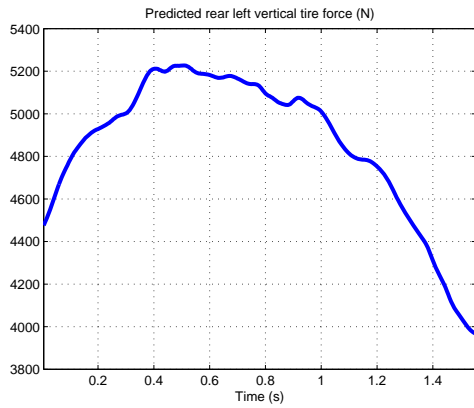
Figure 7.39: Predicted input parameters for the risk prediction system: first sequence



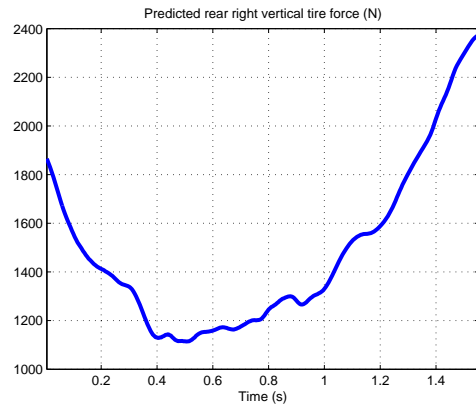
(a) Preticted vertical force at front left wheel: first sequence



(b) Preticted vertical force at front right wheel: first sequence

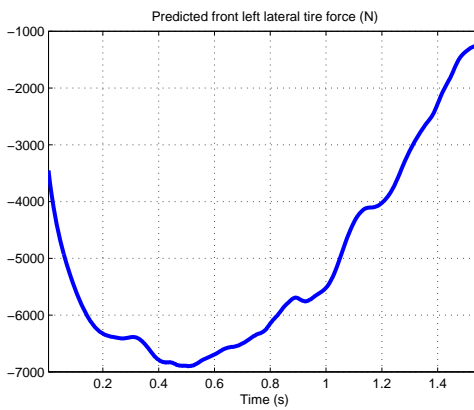


(c) Predicted vertical force at rear left wheel: first sequence

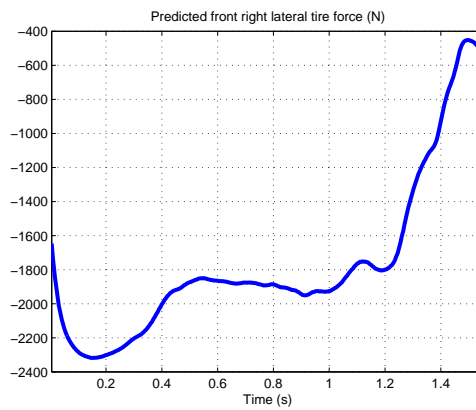


(d) Predicted vertical force at rear right wheel: first sequence

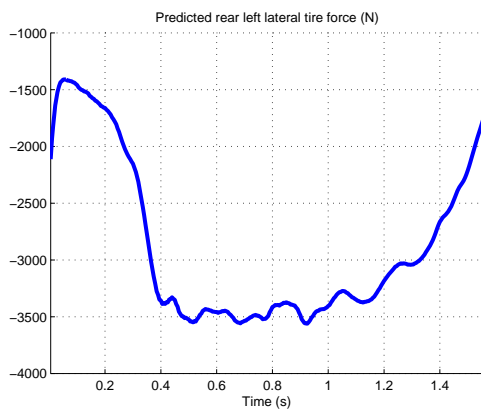
Figure 7.40: Predicted vertical force: first sequence



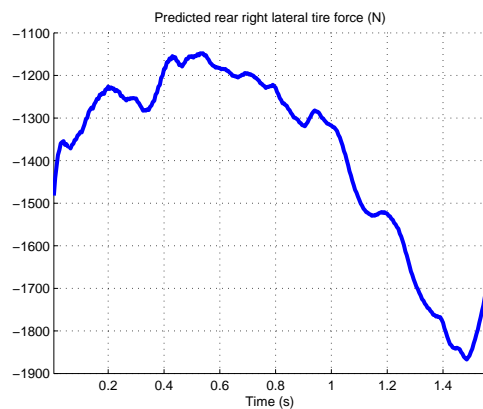
(a) Predicted lateral force at front left wheel: first sequence



(b) Predicted lateral force at front right wheel: first sequence



(c) Predicted lateral force at rear left wheel: first sequence



(d) Predicted lateral force at rear right wheel: first sequence

Figure 7.41: Predicted lateral force: first sequence

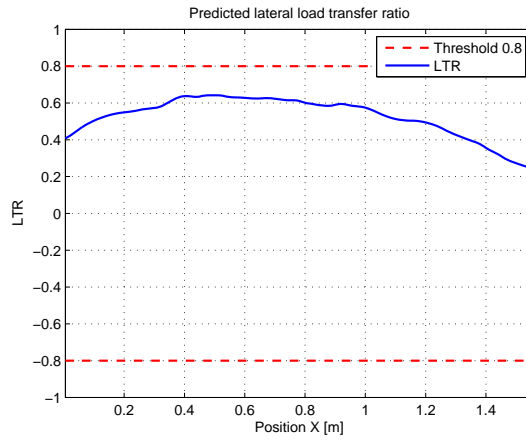
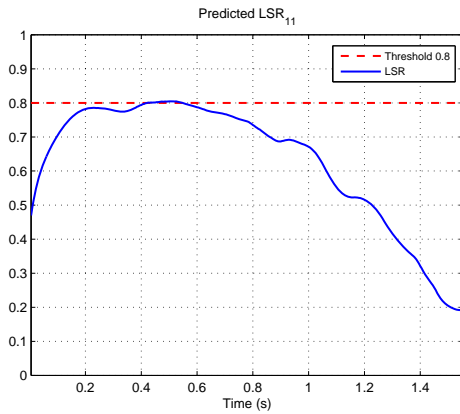
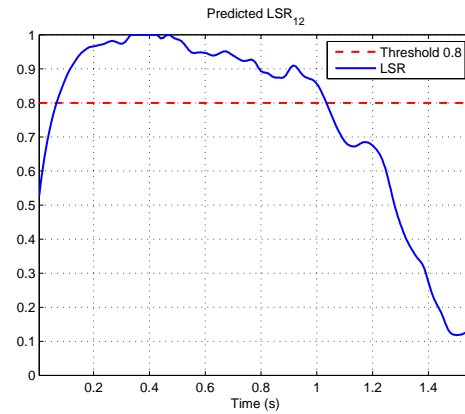


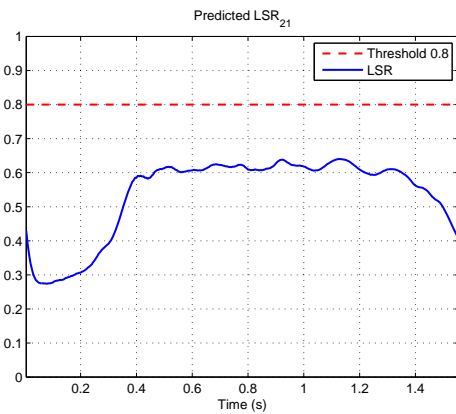
Figure 7.42: Predicted lateral load transfer ratio: first sequence



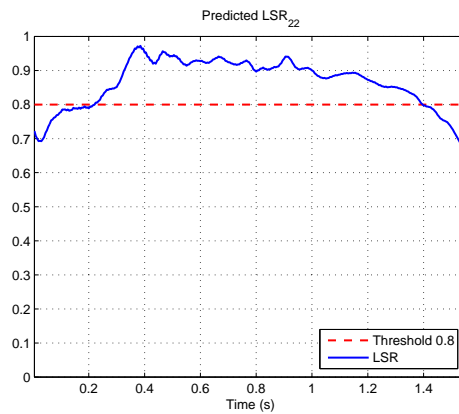
(a) Predicted lateral skid ratio at front left wheel: first sequence



(b) Predicted lateral skid ratio at front right wheel: first sequence

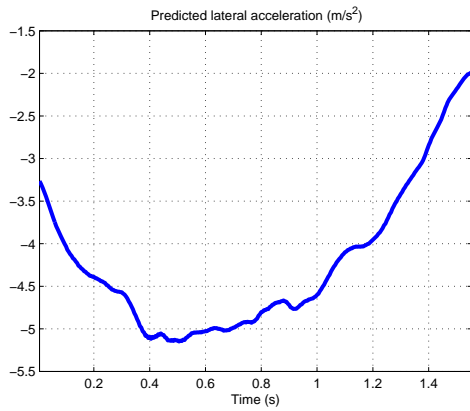


(c) Predicted lateral skid ratio at rear left wheel: first sequence

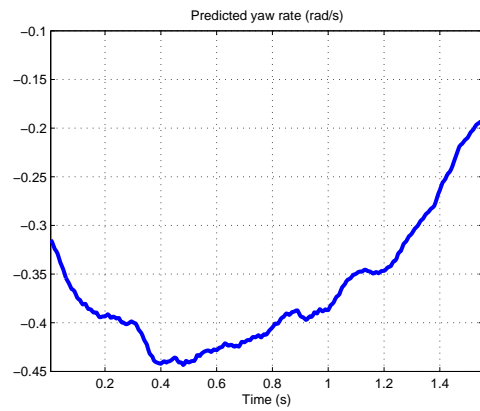


(d) Predicted lateral skid ratio at rear right wheel: first sequence

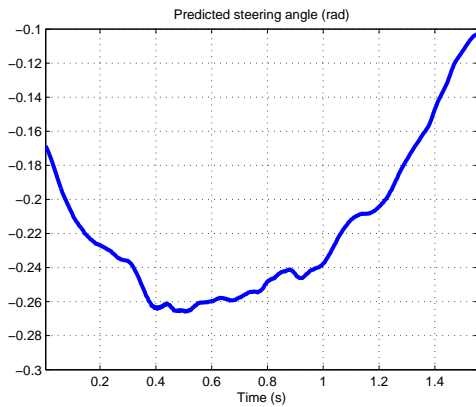
Figure 7.43: Predicted lateral skid ratio: first sequence



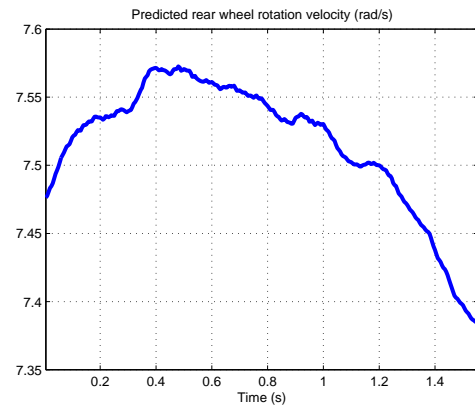
(a) Predicted lateral acceleration: final sequence



(b) Predicted yaw rate: final sequence

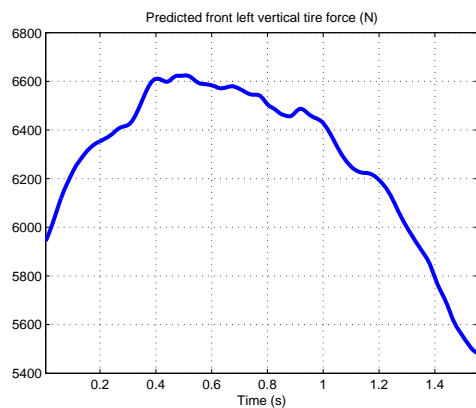


(c) Predicted steering wheel angle: final sequence

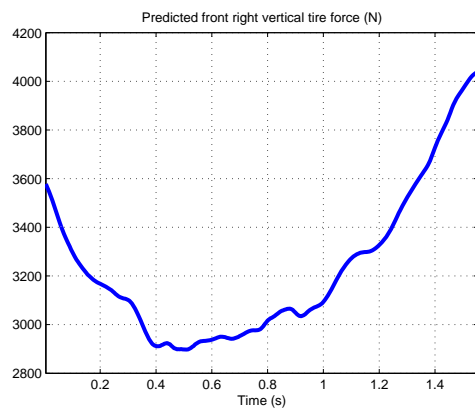


(d) Predicted rear wheel rotation speed: final sequence

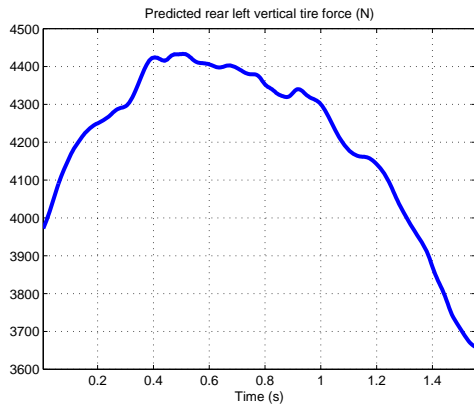
Figure 7.44: Predicted input parameters for the risk prediction system: final sequence



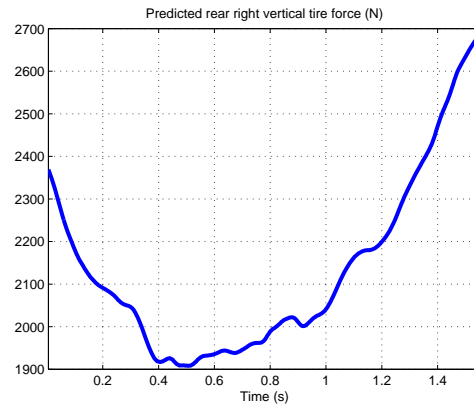
(a) Predicted vertical force at front left wheel: final sequence



(b) Predicted vertical force at front right wheel: final sequence

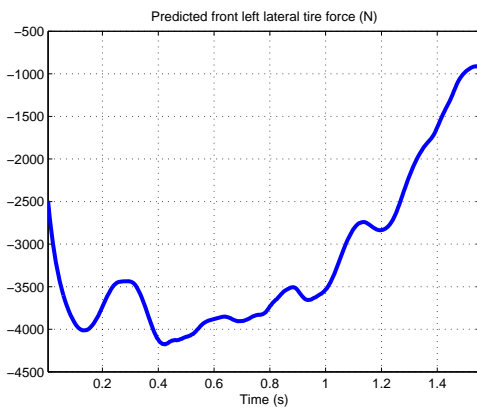


(c) Predicted vertical force at rear left wheel: final sequence

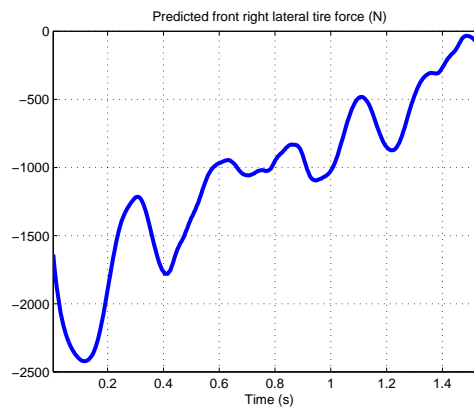


(d) Predicted vertical force at rear right wheel: final sequence

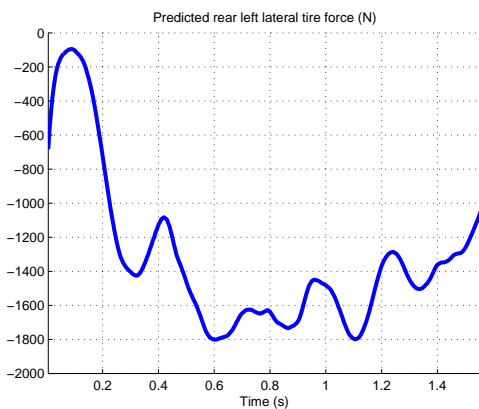
Figure 7.45: Predicted vertical force: final sequence



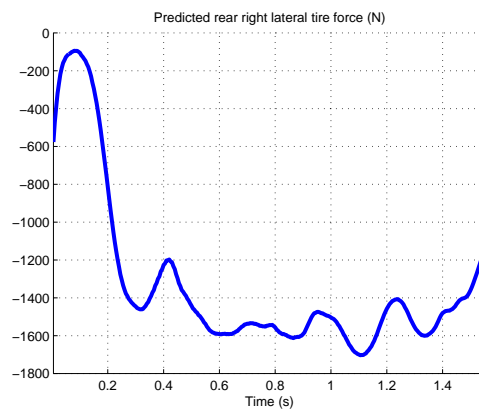
(a) Predicted lateral force at front left wheel: final sequence



(b) Predicted lateral force at front right wheel: final sequence



(c) Predicted lateral force at rear left wheel: final sequence



(d) Predicted lateral force at rear right wheel: final sequence

Figure 7.46: Predicted lateral force: final sequence

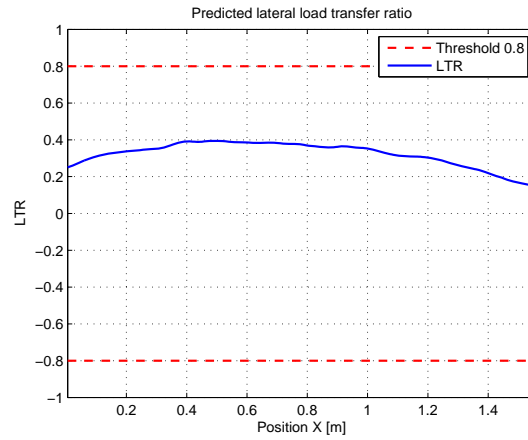
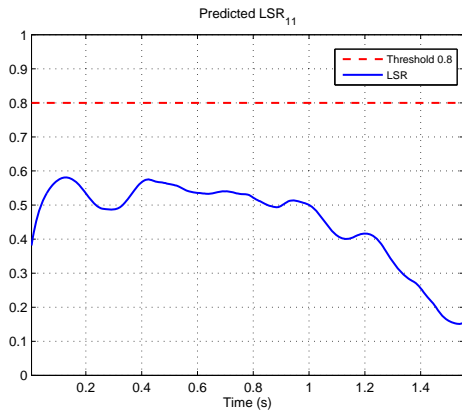
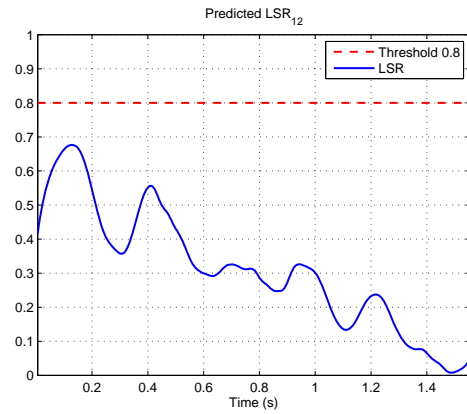


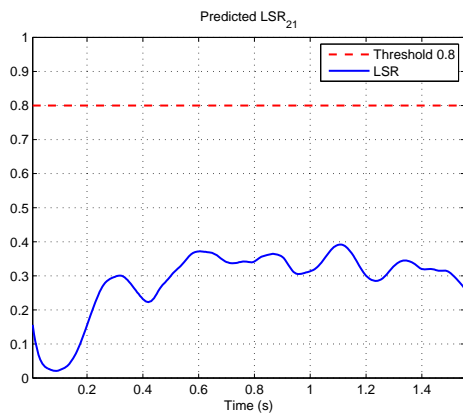
Figure 7.47: Predicted lateral load transfer ratio: final sequence



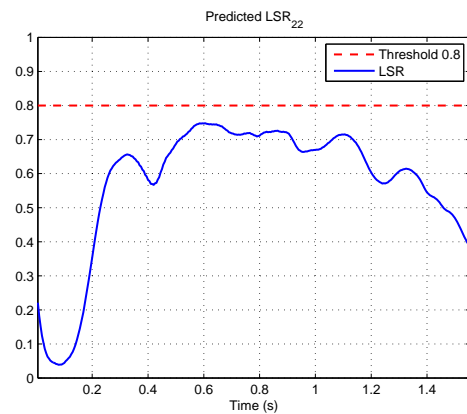
(a) Predicted lateral skid ratio at front left wheel: final sequence



(b) Predicted lateral skid ratio at front right wheel: final sequence



(c) Predicted lateral skid ratio at rear left wheel: final sequence



(d) Predicted lateral skid ratio at rear right wheel: final sequence

Figure 7.48: Predicted lateral skid ratio: final sequence

## 7.4 Conclusion

This chapter outlines the experimental vehicle developed in our laboratory aimed at research on vehicle dynamics characteristics. Hardware and software architectures are implemented to validate estimation approach of the vehicle dynamics parameters, evaluating of potential risk as well as establishing advisory speed on curves. This chapter is considered as the application of the entire theoretical development in this thesis.

The first part focuses on the presentation of the equipped sensors and in-vehicle embedded system modules. An essential module is about the acquisition system, the accessible vehicle parameters are listed in this section, it is noted that the acquisition system supplies these parameters at  $200Hz$ . Moreover, a rapid prototyping environment of component-design aiming at testing in real-time are employed to construct our testbed. We integrate the applications of Extended Kalman filter ( $O_{EF_y}$ ) and Particle filter ( $O_{PF_y}$ ), in addition, the risk prediction system is also implemented in our system architecture. The different modules reflect well incorporation, the fast response allows them to run at  $200Hz$  within the embedded real-time system.

The section of experimental validation principally presents and analyzes the performance of the estimation and prediction modules integrated in the system. Test performed on the dynamics behavior track at CERAM evaluates two observers, the estimation results demonstrate good performance in the real onboard test. The second application with respect to the risk prediction and advisory speed evaluation is tested around the research center. HMI component alerts visually driver the potential risk and safe speed to negotiate the upcoming curve. It is efficient to improve the road safety.

In the future, we plan to raise the stability of our system and implement more functions for road safety and vehicle diagnostics. The prediction system is planned to be realized in the open trajectory, i.e. it is not limited by the predefined itinerary.

# Conclusions and perspectives

---

## Contents

---

<b>8.1</b>	<b>Conclusions</b> . . . . .	<b>167</b>
<b>8.2</b>	<b>Future work</b> . . . . .	<b>168</b>

---

## 8.1 Conclusions

Nowadays, a dramatic increase in numbers of accidents and cause in human error invokes the motivation to develop driver assistance system. Some active safety systems have been integrated as standard options in our quotidian cars. These safety systems use simple vehicle parameters which are available on the vehicle on-board informatics system. However, the complex safety system or the advanced control unit on-board on the car may need more precise parameters describing the vehicle dynamics in an accurate way. The tire/road force and sideslip angle, which are not available on the on-board informatics system of standard cars and cannot be measured by inexpensive sensors, can give a direct description of the vehicle dynamics state. In other hand, such system describes current vehicle state, the ability to simultaneously predict dynamics state beyond the current state is another important aspect for the potential risk evaluation. Therefore, this work focus on the extension of accurate vehicle dynamics estimation to long-term in order to provide risk assessment both in current and future instant.

As motivated by practical requirement, this dissertation firstly reviews the back-stone in this filed. Some typical driver assistance systems are presented concerning to vehicle lateral drift and rollover. Tire and vehicle models are presented to give a detailed comparison, in order that the accurate model helps us develop a precise estimation method for desired parameters. In addition, some approach for road-traffic risk assessment is introduced. The basic review of the state of the art is conducive to the establishment of theory development in this work. As discussed hereinabove, to obtain the knowledge of unmeasured parameters, the observer technique is intervened to estimate these essential parameters. Consequently, we take a chapter to elaborate the foundation of different observer techniques. Kalman filter for linear system, Extended Kalman filter and Particle filter for nonlinear system are respectively presented and compared with its merit/drawback features.

The vertical dynamics is firstly discussed in chapter 4, we have compared the existing method and analyzed its restrictions where the hypothesis about the horizontal road is opened to real environment. Some fundamental variables are analyzed with the road banked condition, since road geometry affects the sensor accuracy. We propose an effective method using suspension deflection to identify suspension roll angle, it is separated with road bank angle from the gyrometer's measurement. We develop two adaptive models providing a precise description of the vehicle vertical dynamics on banked road, the first model is deduced by using accelerometer in

three axes, second one adds a roll dynamics term in the formulation of the vertical load distribution at each tire. Open-loop method denotes a satisfactory result comparing with ancient model. As well as, Kalman filter is implemented for providing better results, it successfully matches with the simulation data.

Chapter 5 gives a description of the vehicle lateral dynamics estimation, we employ simplified double track model and Dugoff tire model to describe the dynamics characteristics. With certain reasonable assumptions, we are able to make the calculation block easier but still remain at an accurate level. The required vertical tire force is calculated directly with a simple open-loop approach which depends on the longitudinal and lateral acceleration. All above mentioned solutions are based on the consideration of the balance of computational cost and precision. Extended Kalman filter and Particle filter aiming at disposing nonlinear system provide good convergence using experimental data. In particular, they are programmed as a real-time application embedded in the vehicle mounted system. Several tests performed demonstrate the performance of our developed algorithm in different road conditions. Particle filter presents more stable performance than Extended Kalman filter, in addition it seems more robust to the variations of not only the external environmental condition (road pavement, friction change) but also the vehicle parameters (mass, height of gravity).

In chapter 6, we lays the emphasis on describing a method of predicting vehicle dynamics parameters, evaluating potential risk as well as establishing advisory speed on curves. The statistics traffic accident report reveals that accidents usually happen due to the lateral drift and rollover, especially on curves. Therefore, we are absorbed in finding an efficient approach of reducing road crash on curves. We develop a method of predicting fundamental parameter basing on the proposed hypothesis and road geometry in our laboratory. The implemented procedure is based on three global steps: (i) detection of the curve ahead the vehicle (thanks to V2I communications procedure); (ii) anticipation phase (where the dynamics, which the vehicle will develop at the ahead curve, is predicted); (iii) rollover and lateral drift risk evaluation, and driver warning. The proposed method is validated through simulation scenario. It is noted that, this system is proved to be effective to improve the vehicle safety and help drivers avoid accident threat on curves.

Last but not the least, the overall methodology has been shown to be capable of addressing the issue of estimating the vehicle state in current instant and predicting potential risk beyond current instant. Nonetheless, how they perform when they are integrated in the embedded system running in real-time? Consequently, we develop an experimental test vehicle in our laboratory. The experimental validation of in-vehicle system is also considered as an essential feature in this dissertation. We present the sensors and in-vehicle embedded system modules installed on the Heudiasyc experimental vehicle. The acquisition system and developed application modules run at  $200Hz$ . The performed experimental test taken on CERAM test track and the open-road around our campus demonstrated good performance in the reality.

## 8.2 Future work

Although the methodologies proposed in this dissertation begin to address one of the fundamental problems facing road safety improvement through vehicle dynamics parameters estimation and risk prediction in real environment, many areas of research exist as opportunities for future work:

- The first obvious aspect of the future work is to develop a nonlinear vertical tire force model considering the influence of road bank and slope angle. Our current model only deals with the case with respect to banked road, however the real road geometry always introduced with both bank and slope angle. Consequently, our method is limited by the hypothesis of zero-slope condition. Otherwise, the results presented in this part are based on the CALLAS simulation environment. Although this simulator software has been validated by many research laboratories and automobile manufacturers, it cannot replace a real driving test. The stability and precision metrics, as well as the capability and robustness of the state estimators need to be evaluated in reality. Meanwhile, it is also desirable to be implemented as an embedded application module in the entire processing architecture in order to provide more accurate vertical force to the subsequent lateral tire force estimation modules.
- The second aspect of future work hopes to extend the lateral tire force model to a wider environment. Since the current double track model is no more available for a large scale change in both bank and slope, hence we are highly desirable to reconstruct a new physical vehicle model which is adapted to the variation of road geometry in reality. A feasible solution may be explored along the approach of treating these perturbations as unknown input. As well as, the unknown input observation (UIO) technique allows dealing with the situation where there are many disturbances present, or some of the inputs to the system are inaccessible [Guan 1991]. The combination of reformulation of the vehicle dynamics model extending to larger scale and considering the UIO techniques may greatly improve the accuracy and robustness relating to the lateral force estimation system, in which superposition of terrain effects are considered.
- Another improvement that should be taken into account concerns the negligence of suspension kinematic motion and camber angle effect. Camber angle generates a lateral force with the name of camber thrust or camber force due to the tilting angle of tire about the longitudinal x-axis [Reza 2007]. High camber angle at certain extent affects the precision of the estimated lateral tire force.
- Future work can also be projected to integrate longitudinal motion within our system, the coupling of longitudinal/lateral motion will be able to provide more accurate descriptions of above vertical and lateral tire force, especially during emergency braking/acceleration situations.
- Another essential field of potential future research would be the extension of risk assessment system, the simple LTR and LSR indexes denote a glib generalization of the risk evaluation using load distribution and coefficient of friction. The development of more advanced risk assessment methods is extremely expectant to evaluate the potential risk situation during the vehicle current movement or in future instant.
- In order to extend the risk prediction and the advisory curve warning algorithm to a larger using scale, the limitation of predefined trajectory will be abandoned in the future. As discussed in this dissertation, the trajectory and road curve geometric information are predefined before the test, however we are desirable to define a scenario with random trajectory, the prediction system itself could detect and obtain the road curve characteristics. Vehicle perception and localization techniques may be integrated to achieve this objective. More tests should be performed to complete validations on different road curves.

- The last perspective concerns in-vehicle embedded system. It is noted that in this dissertation, vehicle dynamics parameter estimation, risk prediction and advisory speed curve systems are applied as real-time applications. More developments and tests are planned to be performed to validate the stability and efficiency of the entire architecture.

# Bibliography

- [Arulampalam 2002] M. S. Arulampalam, S. Maskell, N. Gordon and T. Clapp. *A tutorial on particle filters for online nonlinear/non-Gaussian Bayesian tracking*. Signal Processing, IEEE Transactions on, vol. 50, no. 2, pages 174–188, 2002.
- [Baffet 2007] G. Baffet. *Développement et validation expérimentale d’observateurs des forces de contact pneumatique/chaussée d’une automobile*. PhD thesis, Université de Technologie de Compiègne, 2007.
- [Baruya 1997] A. Baruya. A review of speed-accident relationship for european roads. Master’s thesis, Traffic and Transport Resource Centre, 1997.
- [Batavia 1999] P. H. Batavia. *Driver-adaptive lane departure warning systems*. PhD thesis, Carnegie Mellon University, 1999.
- [Beadle 1997] E. R. Beadle and P. M. Djuric. *A fast-weighted Bayesian bootstrap filter for nonlinear model state estimation*. Aerospace and Electronic Systems, IEEE Transactions on, vol. 33, no. 1, pages 338–343, 1997.
- [Bevly 2001] D. M. Bevly, R. Sheridan and J. C. Gerdes. *Integrating INS sensors with GPS velocity measurements for continuous estimation of vehicle sideslip and tire cornering stiffness*. In Proceedings of the 2001 American Control Conference, volume 1, pages 25–30. IEEE, 2001.
- [Bolic 2003] M. Bolic, P. M. Djuric and Sangjin H. *New resampling algorithms for particle filters*. In Proceedings of 2003 IEEE International Conference on Acoustics, Speech, and Signal Processing, volume 2, pages II–589–92 vol.2, 2003.
- [Bouton 2007] N. Bouton, R. Lenain, B. Thuilot and J. C. Fauroux. *A rollover indicator based on the prediction of the load transfer in presence of sliding: application to an All Terrain Vehicle*. In 2007 IEEE International Conference on Robotics and Automation, pages 1158–1163, 2007.
- [Boyden 1994] F. D. Boyden and S. A. Velinsky. *Dynamic modeling of wheeled mobile robots for high load applications*. In 1994 IEEE International Conference on Robotics and Automation, pages 3071–3078 vol.4, 1994.
- [Cai 2011] G. Cai, B. M. Chen and T. H. Lee. *Coordinate Systems and Transformations*. In Unmanned Rotorcraft Systems, pages 23–34. Springer, 2011.
- [Candy 2007] J. V. Candy. *Bootstrap particle filtering*. IEEE Signal Processing Magazine, vol. 24, no. 4, pages 73–85, 2007.
- [Carlson 2003] C. R. Carlson and J. C. Gerdes. *Optimal rollover prevention with steer by wire and differential braking*. In Proceedings of IMECE, pages 16–21, 2003.
- [Casey 1996] J. Casey. Exploring curvature. Vieweg Wiesbaden, 1996.

- [Chen 1995] M. Chen, T. Jochem and D. Pomerleau. *AURORA: A vision-based roadway departure warning system*. In Proceedings of 1995 IEEE/RSJ International Conference on Intelligent Robots and Systems, volume 1, pages 243–248, 1995.
- [Chen 1999] B. Chen and H. Peng. *A real-time rollover threat index for sports utility vehicles*. In Proceedings of the 1999 American Control Conference, volume 2, pages 1233–1237, 1999.
- [Chen 2001] B. C. Chen and H. Peng. *Differential-braking-based rollover prevention for sport utility vehicles with human-in-the-loop evaluations*. *Vehicle System Dynamics*, vol. 36, no. 4-5, pages 359–389, 2001.
- [Chen 2008] B. C. Chen and F. C. Hsieh. *Sideslip angle estimation using extended Kalman filter*. *Vehicle System Dynamics*, vol. 46, no. S1, pages 353–364, 2008.
- [Cheng 2011] Q. Cheng, A. Victorino and A. Charara. *Nonlinear observer of sideslip angle using a particle filter estimation methodology*. In IFAC World Congress, Milan, Italy, 2011.
- [Chih-Li 2012] H. Chih-Li, Y. Yu-Hsaing and S. Tsung-Ying. *Lane departure warning system based on dynamic vanishing point adjustment*. In 2012 IEEE 1st Global Conference on Consumer Electronics (GCCE), pages 25–28, 2012.
- [Cho 2010] W. Cho, J. Yoon, S. Yim, B. Koo and K. Yi. *Estimation of Tire Forces for Application to Vehicle Stability Control*. *Vehicular Technology, IEEE Transactions on*, vol. 59, no. 2, pages 638–649, 2010.
- [Cunha 2011] F. Cunha, A. Victorino, R. Ghandour and A. Charara. *Vehicle Dynamics Prediction Based on State Observers Entries Anticipation*. In IFAC World Congress, volume 18, pages 2260–2265, 2011.
- [Dahmani 2010] H. Dahmani, M. Chadli, A. Rabhi and A.E. Hajjaji. *Fuzzy uncertain observer with unknown inputs for Lane departure detection*. In 2010 American Control Conference (ACC), pages 688–693, 2010.
- [Dakhlallah 2008] J. Dakhlallah, S. Glaser, S. Mammar and Y. Sebsadji. *Tire-road forces estimation using extended Kalman filter and sideslip angle evaluation*. In American Control Conference, 2008, pages 4597–4602, 2008.
- [Dherbomez 2013] G. Dherbomez, T. Monglon, P. Crubillé, B. Wang, A. C. Victorino and A. Charara. *DYNA, véhicule expérimental pour la Dynamique du Véhicule*. Quatrièmes Journées des Démonstrateurs en Automatique, 2013.
- [Ding 2006] E. Ding, T. Massel and S. Ding. *Estimation of vehicle pitch angle*. *ATZ worldwide*, vol. 108, no. 2, pages 22–24, 2006.
- [Ding 2010] N. Ding and S. Taheri. *A Modified Dugoff Tire Model for Combined-slip Forces*. *Tire Science and Technology*, vol. 38, no. 3, pages 228–244, 2010.
- [Dixon 1996] J. C. Dixon. *Tires, suspension, and handling*. 1996.

- [Douc 2005] R. Douc and O. Cappe. *Comparison of resampling schemes for particle filtering*. In Proceedings of the 4th International Symposium on Image and Signal Processing and Analysis, pages 64–69, 2005.
- [Doucet 2001] A. Doucet, N. De Freitas and N. Gordon. *An introduction to sequential Monte Carlo methods*. In Sequential Monte Carlo methods in practice, pages 3–14. Springer, 2001.
- [Doumiati 2009] M. Doumiati. *Estimation embarquée des efforts verticaux et latéraux d'un véhicule pour le diagnostic du comportement sur route*. PhD thesis, Université de Technologie de Compiègne, 2009.
- [Dugoff 1969] H. Dugoff, P. S. Fancher and L. Segel. Tire performance characteristics affecting vehicle response to steering and braking control inputs. 1969.
- [Durrant-Whyte 2001] H. F. Durrant-Whyte. *Introduction to estimation and the Kalman Filter*. Australian Centre for Field Robotics, 2001.
- [El Ali 2010] F. El Ali and Bertrand D. *A light architecture for opportunistic vehicle-to-infrastructure communications*. In Proceedings of the 8th ACM international workshop on Mobility management and wireless access, pages 60–67. ACM, 2010.
- [Emmanuel 2003] D. B. Emmanuel. On the control aspects of semiactive suspensions for automobile applications. Master's thesis, Virginia Polytechnic Institute and State University, 2003.
- [Eric Tseng 2007] H. Eric Tseng, L. Xu and D. Hrovat. *Estimation of land vehicle roll and pitch angles*. Vehicle System Dynamics, vol. 45, no. 5, pages 433–443, 2007.
- [Gertsch 2003] J. Gertsch and O. Eichelhard. *Simulation of dynamic rollover threshold for heavy trucks*. Simulation, vol. 1, page 3385, 2003.
- [Ghandour 2011] R. Ghandour. *Diagnostic et évaluation anticipée des risques de rupture d'itinéraire basés sur l'estimation de la dynamique du véhicule*. PhD thesis, Université de Technologie de Compiègne, 2011.
- [Glaser 2007] S. Glaser, L. Nouveliere and B. Lusetti. *Speed limitation based on an advanced curve warning system*. In Intelligent Vehicles Symposium, 2007 IEEE, pages 686–691, 2007.
- [Godthelp 1984] H. Godthelp, P. Milgram and G. J. Blaauw. *The development of a time-related measure to describe driving strategy*. Human Factors: The Journal of the Human Factors and Ergonomics Society, vol. 26, no. 3, pages 257–268, 1984.
- [Gordon 1993] N. J. Gordon, D. J. Salmond and A. F. M. Smith. *Novel approach to nonlinear/non-Gaussian Bayesian state estimation*. IEEE Proceedings on Radar and Signal Processing, vol. 140, no. 2, pages 107–113, 1993.
- [Grewal 1993] M. S. Grewal and A. P. Andrews. Kalman filtering: theory and practice. Prentice-Hall information and system sciences series. Prentice-Hall, 1993.

- [Grip 2009] H. F. Grip, L. Imsland, T. A. Johansen, J. C. Kalkkuhl and A. Suissa. *Vehicle sideslip estimation*. IEEE Control Systems, vol. 29, no. 5, pages 36–52, 2009.
- [Guan 1991] Y. Guan and M. Saif. *A novel approach to the design of unknown input observers*. IEEE Transactions on Automatic Control, vol. 36, no. 5, pages 632–635, 1991.
- [Guermah 2008] S. Guermah, S. Djennoune and M. Bettayeb. *Controllability and observability of linear discrete-time fractional-order systems*. International Journal of Applied Mathematics and Computer Science, vol. 18, no. 2, pages 213–222, 2008.
- [Gunia 2008] D. Gunia, T. Wey and J. Meier. *Advanced Driver Assistance Systems (ADAS)-Development at Ford Motor Company*, 2008.
- [Hac 2004a] A. Hac. *Influence of active chassis systems on vehicle propensity to maneuver-induced rollovers*. PROGRESS IN TECHNOLOGY, vol. 101, pages 60–67, 2004.
- [Hac 2004b] A. Hac, T. Brown and J. Martens. *Detection of vehicle rollover*. Vehicle Dynamics & Simulation, 2004.
- [Halfmann 1999] C. Halfmann, O. Nelles and H. Holzmann. *Semi-physical modeling of the vertical vehicle dynamics*. In IEEE American Control Conference, volume 3, pages 1707–1711, 1999.
- [Haykin 2001] S. S. Haykin *et al.* Kalman filtering and neural networks. Wiley Online Library, 2001.
- [Hayward 1971] J. C. Hayward. Near misses as a measure of safety at urban intersections. Near Misses as a Measure of Safety at Urban Intersections. Pennsylvania State University, Department of Civil Engineering, 1971.
- [Hermann 1977] R. Hermann and A. Krener. *Nonlinear controllability and observability*. IEEE Transactions on Automatic Control, vol. 22, no. 5, pages 728–740, 1977.
- [Hol 2004] J. D. Hol. *Resampling in particle filters*. PhD thesis, Linköping, 2004.
- [Hol 2006] J. D. Hol, T. B. Schon and F. Gustafsson. *On Resampling Algorithms for Particle Filters*. In 2006 IEEE Nonlinear Statistical Signal Processing Workshop, pages 79–82, 2006.
- [Hsu 2007] Y. Hsu and J. C. Gerdes. *Experimental studies of using steering torque under various road conditions for sideslip and friction estimation*. In Proceedings of the 2007 IFAC Symposium on Advances in Automotive Control, Monterey, California, 2007.
- [Hsu 2009] L. Y. Hsu and T. L. Chen. *Vehicle Full-State Estimation and Prediction System Using State Observers*. IEEE Transactions on Vehicular Technology, vol. 58, no. 6, pages 2651–2662, 2009.
- [Ibrahim 2010] F. A. Ibrahim. *Curve warning system*, 2010. US Patent 7,751,973.
- [Imine 2007] H. Imine and V. Dolcemascolo. *Rollover risk prediction of heavy vehicle in interaction with infrastructure*. International Journal of Heavy Vehicle Systems, vol. 14, no. 3, pages 294–307, 2007.

- [Imine 2008] H. Imine and V. Dolcemascolo. *Sliding mode observers to heavy vehicle vertical forces estimation*. International Journal of Heavy Vehicle Systems, vol. 15, no. 1, pages 53–64, 2008.
- [Jacob 2007] S. Jacob. Tire modeling and friction estimation. 2007.
- [Jun 2010] L. Jun, W. Sumei, P. Ke, X. Jun, W. Yun and Z. Tao. *Research on On-line Measurement and Prediction for Vehicle Motion State*. In 2010 International Conference on Digital Manufacturing and Automation (ICDMA), volume 2, pages 247–250, 2010.
- [Jung 2005] C. R. Jung and C. R. Kelber. *A lane departure warning system using lateral offset with uncalibrated camera*. In Intelligent Transportation Systems, 2005. Proceedings. 2005 IEEE, pages 102–107, 2005.
- [Kalman 1960] R. E. Kalman *et al.* *A new approach to linear filtering and prediction problems*. Journal of basic Engineering, vol. 82, no. 1, pages 35–45, 1960.
- [Kamnik 2003] R. Kamnik, F. Boettiger and K. Hunt. *Roll dynamics and lateral load transfer estimation in articulated heavy freight vehicles*. Proceedings of the Institution of Mechanical Engineers, Part D: Journal of Automobile Engineering, vol. 217, no. 11, pages 985–997, 2003.
- [Kawashima 2009] K. Kawashima, T. Uchida and Y. Hori. *Rolling stability control based on electronic stability program for in-wheel-motor electric vehicle*. system, vol. 2, page 4, 2009.
- [Kawashima 2010] K. Kawashima, Y. Hori, T. Uchida and O. Sehoon. *Robust bank angle estimation for rolling stability control on electric vehicle*. In 2010 11th IEEE International Workshop on Advanced Motion Control, pages 448–453, 2010.
- [Keall 2007] M. D. Keall and S. V. Newstead. *Four-wheel Drive Vehicle Crash Involvement Risk, Rollover Risk and Injury Rate in Comparison to Other Passenger Vehicles: Estimates Based on Australian and New Zealand Crash Data and on New Zealand Motor Vehicle Register Data*. Rapport technique, Monash University Accident Research Center, 2007.
- [Khalil 2002] H. K. Khalil. Nonlinear systems, volume 3. Prentice hall Upper Saddle River, 2002.
- [Kiencke 2005] U. Kiencke and L. Nielsen. Automotive control systems for engine, driveline, and vehicle. Springer, 2005.
- [Kim 2004] S. S. Kim and H. K. Jung. *Functional suspension modeling for real-time vehicle dynamics analysis using K&C test data*. In 2004 FISTA Conference, pages 231–237, 2004.
- [Kim 2009] J. Kim. *Identification of lateral tyre force dynamics using an extended Kalman filter from experimental road test data*. Control Engineering Practice, vol. 17, no. 3, pages 357–367, 2009.
- [Kitagawa 1996] G. Kitagawa. *Monte Carlo filter and smoother for non-Gaussian nonlinear state space models*. Journal of computational and graphical statistics, vol. 5, no. 1, pages 1–25, 1996.

- [Lechner 2002] D. Lechner. *Analyse du comportement dynamique des véhicules routiers légers: développement d'une méthodologie appliquée à la sécurité primaire*. PhD thesis, Ecole Centrale de Lyon, 2002.
- [Lee 1976] D. N. Lee et al. *A theory of visual control of braking based on information about time-to-collision*. Perception, vol. 5, no. 4, pages 437–459, 1976.
- [Lee 1999] S. Lee, W. Kwon and J. W. Lee. *A vision based lane departure warning system*. In Proceedings of 1999 IEEE/RSJ International Conference on Intelligent Robots and Systems, volume 1, pages 160–165, 1999.
- [Lee 2002] J. W. Lee. *A machine vision system for lane-departure detection*. Computer vision and image understanding, vol. 86, no. 1, pages 52–78, 2002.
- [Li 2008] K. Li, H. S. Tan, J. A. Misener and J. K. Hedrick. *Digital map as a virtual sensor—dynamic road curve reconstruction for a curve speed assistant*. Vehicle System Dynamics, vol. 46, no. 12, pages 1141–1158, 2008.
- [Li 2010] L. Li, H. Li, X. Zhang, L. He and J. Song. *Real-time tire parameters observer for vehicle dynamics stability control*. Chinese Journal of Mechanical Engineering, vol. 23, no. 5, pages 620–626, 2010.
- [Liebemann 2004] E. K. Liebemann, K. Meder, J. Schuh and G. Nenninger. *Safety and Performance Enhancement: The Bosch Electronic Stability Control (ESP)*. Rapport technique, Robert Bosch GmbH, 2004.
- [Liu 1998] J. S. Liu and R. Chen. *Sequential Monte Carlo Methods for Dynamic Systems*. Journal of the American Statistical Association, vol. 93, no. 443, pages 1032–1044, 1998.
- [Ljung 1979] L. Ljung. *Asymptotic behavior of the extended Kalman filter as a parameter estimator for linear systems*. IEEE Transactions on Automatic Control, vol. 24, no. 1, pages 36–50, 1979.
- [Louwerse 2004] W. J. R. Louwerse and S. P. Hoogendoorn. *ADAS safety impacts on rural and urban highways*. In 2004 IEEE Intelligent Vehicles Symposium, pages 887–890, 2004.
- [Mammar 2004] S. Mammar, S. Glaser, M. Netto and J-M Blosseville. *Time-to-line crossing and vehicle dynamics for lane departure avoidance*. In Proceedings of the 7th International IEEE Conference on Intelligent Transportation Systems, pages 618–623, 2004.
- [Mammar 2006a] S. Mammar, S. Glaser and M. Netto. *Time to line crossing for lane departure avoidance: a theoretical study and an experimental setting*. IEEE Transactions on Intelligent Transportation Systems, vol. 7, no. 2, pages 226–241, 2006.
- [Mammar 2006b] S. Mammar, S. Glaser and M. Netto. *Vehicle lateral dynamics estimation using unknown input proportional-integral observers*. In American Control Conference, 2006.
- [Menhour 2010] L. Menhour. *Synthèse de commandes au volant d'une automobile pour le diagnostic de rupture d'un itinéraire. Développement et validation expérimentale*. PhD thesis, Université de Technologie de Compiègne, 2010.

- [Menhour 2011] L. Menhour, D. Lechner and A. Charara. *Steering control and road bank angle estimation to evaluate the vehicle behaviour under high dynamic loads: Experimental evaluation*. In Proceedings of the 18th World Congress of the International Federation of Automatic Control (IFAC WC 2011), Milano, Italy, 2011.
- [Milanese 2004] M. Milanese, C. Novara, F. Mastronardi and D. Amoroso. *Experimental modeling of vertical dynamics of vehicles with controlled suspensions*. In SAE world congress,, Detroit, Michigan, March 2004.
- [Milliken 2003] D. L. Milliken, E. M. Kasprak, L. Daniel Metz and W. F. Milliken. Race car vehicle dynamics. SAE International, 2003.
- [Minderhoud 2001] M. M. Minderhoud and P. HL Bovy. *Extended time-to-collision measures for road traffic safety assessment*. Accident Analysis & Prevention, vol. 33, no. 1, pages 89–97, 2001.
- [Mokhiamar 2002] O. Mokhiamar and M. Abe. *Active wheel steering and yaw moment control combination to maximize stability as well as vehicle responsiveness during quick lane change for active vehicle handling safety*. Proceedings of the Institution of Mechanical Engineers, Part D: Journal of Automobile Engineering, vol. 216, no. 2, pages 115–124, 2002.
- [Moraal 1995] P. E. Moraal and J. W. Grizzle. *Observer design for nonlinear systems with discrete-time measurements*. IEEE Transactions on Automatic Control, vol. 40, no. 3, pages 395–404, 1995.
- [Morellas 1997] V. Morellas, T. Morris, L. Alexander and M. Donath. *Preview based control of a tractor trailer using DGPS for preventing road departure accidents*. In Intelligent Transportation System, 1997. ITSC'97., IEEE Conference on, pages 797–805, 1997.
- [NHTSA ] NHTSA. National highway traffic safety administration (NHTSA) website: [www.nhtsa.dot.gov](http://www.nhtsa.dot.gov).
- [NHTSA 2006] NHTSA. *PROPOSED FMVSS No. 126 Electronic Stability Control Systems*. Rapport technique, Office of Regulatory Analysis and Evaluation National Center for Statistics and Analysis, 2006.
- [NHTSA 2013] NHTSA. *Early Estimate of Motor Vehicle Traffic Fatalities for the First Quarter of 2013*, August 2013.
- [Nilsson 2011] A. Nilsson and H. Lingefelt. Estimation of vehicle roll angle. 2011.
- [Oh 2013] J. Oh and S. B. Choi. *Vehicle roll and pitch angle estimation using a cost-effective six-dimensional inertial measurement unit*. Proceedings of the Institution of Mechanical Engineers, Part D: Journal of Automobile Engineering, vol. 227, no. 4, pages 577–590, 2013.
- [ONISR 2012] ONISR. *L'accidentalité en 2012 France entière*, 2012.
- [Osborn 2006] R. P. Osborn and T. Shim. *Independent control of all-wheel-drive torque distribution*. Vehicle system dynamics, vol. 44, no. 7, pages 529–546, 2006.

- [Pacejka 1987] H. B. Pacejka, E. Bakker and L. Nyborg. *Tyre modelling for use in vehicle dynamics studies*. SAE paper, vol. 870421, 1987.
- [Pacejka 2006] H. B. Pacejka. *Tire and vehicle dynamics*. SAE International, second édition, 2006.
- [Palkovics 2001] L. Palkovics and A. Fries. *Intelligent electronic systems in commercial vehicles for enhanced traffic safety*. *Vehicle System Dynamics*, vol. 35, no. 4-5, pages 227–289, 2001.
- [Phanomchoeng 2011] G. Phanomchoeng. *State, Parameter, and Unknown Input Estimation Problems in Active Automotive Safety Applications*. PhD thesis, University of Minnesota, 2011.
- [Piyabongkarn 2009] D. Piyabongkarn, R. Rajamani, J. A. Grogg and J. Y. Lew. *Development and Experimental Evaluation of a Slip Angle Estimator for Vehicle Stability Control*. *Control Systems Technology, IEEE Transactions on*, vol. 17, no. 1, pages 78–88, 2009.
- [Pomerleau 1999] D. Pomerleau, T. Jochem, C. Thorpe, P. Batavia, D. Pape, J. Hadden, N. McMillan, N. Brown and J. Everson. *Run-off-road collision avoidance using IVHS countermeasures*. US Department of Transportation. National Highway Traffic Safety Administration. Report DOT HS, vol. 809, page 170, 1999.
- [Popp 2010] K. Popp and W. Schiehlen. *Ground vehicle dynamics*. Springer, 2010.
- [Prem 1998] H. Prem, R. George and J. McLean. *Methods for evaluating the dynamic-wheel-load performance of heavy commercial vehicle suspensions*. In *The 5th international symposium on heavy vehicle weights and dimensions*, Maroochydore, Queensland, Australia, pages 252–278, 1998.
- [Rajamani 2006] R. Rajamani, D. Piyabongkarn, J. Y. Lew and J. A. Grogg. *Algorithms for real-time estimation of individual wheel tire-road friction coefficients*. In *American Control Conference*, 2006.
- [Rajamani 2012] R. Rajamani. *Vehicle dynamics and control*. Springer, 2012.
- [Ray 1997] L. R. Ray. *Nonlinear Tire Force Estimation and Road Friction Identification: Simulation and Experiments*. *Automatica*, vol. 33, no. 10, pages 1819 – 1833, 1997.
- [Ray 1998] L. R. Ray. *Experimental determination of tire forces and road friction*. In *Proceedings of the 1998 American Control Conference*, volume 3, pages 1843–1847, 1998.
- [Reza 2007] N. J. Reza. *Vehicle dynamics theory and application*. Springer, 2007.
- [Ryu 2002] J. Ryu, E. J. Rossetter and J. C. Gerdes. *Vehicle sideslip and roll parameter estimation using GPS*. In *Proceedings of AVEC 2002 6th International Symposium of Advanced Vehicle Control*, 2002.
- [Ryu 2004] J. Ryu and J. C. Gerdes. *Estimation of vehicle roll and road bank angle*. In *Proceedings of the 2004 on American Control Conference*, volume 3, pages 2110–2115 vol.3, 2004.

- [SAE 2008] *Vehicle Dynamics Terminology*. Warrendale, PA, 2008.
- [Sayer 2005] T. B. Sayer, J. R. Sayer and J. M. Devonshire. *Assessment of a driver interface for lateral drift and curve speed warning systems: mixed results for auditory and haptic warnings*. Proceedings of Driving Assessment, pages 218–224, 2005.
- [Schiehlen 2009] W. Schiehlen. *Dynamical analysis of vehicle systems*. Springer, 2009.
- [Segel 1956] L. Segel. *Theoretical prediction and experimental substantiation of the response of the automobile to steering control*. Proceedings of the Institution of Mechanical Engineers: Automobile Division, vol. 10, no. 1, pages 310–330, 1956.
- [Senger 1989] K. H. Senger and W. Kortum. *Investigations on state-observers for the lateral dynamics of four-wheel steered systems*. The Dynamics of Vehicles on Roads and on Tracks, pages 515–527, 1989.
- [Sentouh 2006] C. Sentouh, S. Glaser and S. Mammar. *Advanced vehicle–infrastructure–driver speed profile for road departure accident prevention*. Vehicle System Dynamics, vol. 44, no. sup1, pages 612–623, 2006.
- [Sentouh 2007] C. Sentouh. *Analyse du risque et détection de situations limites: application au développement des systèmes d’alerte au conducteur*. PhD thesis, Université d’Evry-Val d’Essonne, 2007.
- [Shiang-Lung 2004] K. Shiang-Lung, T. Han-Shue and M. Tomizuka. *Nonlinear tire lateral force versus slip angle curve identification*. In Proceedings of the 2004 on American Control Conference, volume 3, pages 2128–2133 vol.3, 2004.
- [Shino 2001] M. Shino and M. Nagai. *Yaw-moment control of electric vehicle for improving handling and stability*. JSAE review, vol. 22, no. 4, pages 473–480, 2001.
- [Smeed 1949] R. J. Smeed. *Some statistical aspects of road safety research*. Journal of the Royal Statistical Society. Series A (General), vol. 112, no. 1, pages 1–34, 1949.
- [Smith 1995] D. E. Smith and J. M. Starkey. *Effects of model complexity on the performance of automated vehicle steering controllers: Model development, validation and comparison*. Vehicle System Dynamics, vol. 24, no. 2, pages 163–181, 1995.
- [Smith 2004] N. D. Smith. *Understanding parameters influencing tire modeling*. Department of Mechanical Engineering, Colorado State University, 2004.
- [Solomon 1964] D. Solomon. *Accidents on main rural highways related to speed, driver, and vehicle*. 1964.
- [Song 2013] R. T. Song. *Estimation of vehicle’s vertical and lateral tire/road forces with non-zero road bank angle*. Master’s thesis, Université de Technologie de Compiègne., 2013.
- [Sorenson 1960] H.W. Sorenson. *Kalman filtering: Theory and application*. IEEE Press selected reprint series. 1960.
- [Stéphane 2004] J. Stéphane. *Contribution à l’étude et à la validation expérimentale d’observateurs appliqués à la dynamique du véhicule*. PhD thesis, Université de Technologie de Compiègne, 2004.

- [Sun 2007] L. Sun, X. Cai and J. Yang. *Genetic algorithm-based optimum vehicle suspension design using minimum dynamic pavement load as a design criterion*. Journal of Sound and Vibration, vol. 301, no. 1-2, pages 18–27, 2007.
- [Suzuki 2003] K. Suzuki and H. Jansson. *An analysis of driver's steering behaviour during auditory or haptic warnings for the designing of lane departure warning system*. JSAE review, vol. 24, no. 1, pages 65–70, 2003.
- [Takano 2001] S. Takano and M. Nagai. *Dynamics control of large vehicles for rollover prevention*. In Proceedings of the IEEE International Vehicle Electronics Conference, pages 85–89, 2001.
- [Taylor 2000] M. Taylor, D. A. Lynam, A. Baruya and G. Britain. *The effects of drivers' speed on the frequency of road accidents*. Transport Research Laboratory Crowthorne, 2000.
- [Thomas 1997] D. G. Thomas. *Fundamentals of vehicle dynamics*. SAE International, 1997.
- [Tseng 1999] H. E. Tseng, B. Ashrafi, D. Madau, T. Allen B. and D. Recker. *The development of vehicle stability control at Ford*. Mechatronics, IEEE/ASME Transactions on, vol. 4, no. 3, pages 223–234, 1999.
- [Tseng 2001] H. E. Tseng. *Dynamic estimation of road bank angle*. Vehicle System Dynamics, vol. 36, no. 4-5, pages 307–328, 2001.
- [Tsourapas 2009] V. Tsourapas, D. Piyabongkarn, A. C. Williams and R. Rajamani. *New method of identifying real-time predictive lateral load transfer ratio for rollover prevention systems*. In American Control Conference, 2009. ACC'09., pages 439–444, 2009.
- [Van der Horst 1994] R. Van der Horst and J. Hogema. *Time-to-collision and collision avoidance systems*. VERKEERSGEDRAG IN ONDERZOEK, 1994.
- [Van Zanten 2002] A. T. Van Zanten. *Evolution of electronic control systems for improving the vehicle dynamic behavior*. In Proceedings of the 6th International Symposium on Advanced Vehicle Control, pages 1–9, 2002.
- [Von Vietinghoff 2005] A. Von Vietinghoff, M. Hiemer and U. Kiencke. *Nonlinear observer design for lateral vehicle dynamics*. In Proc. 16th IFAC World Congress, 2005.
- [Wan 2000] E. A. Wan and R. Van der Merwe. *The unscented Kalman filter for nonlinear estimation*. In The IEEE 2000 Adaptive Systems for Signal Processing, Communications, and Control Symposium, pages 153–158, 2000.
- [Wang 1992] Y. C. Wang and B. J. Frost. *Time to collision is signalled by neurons in the nucleus rotundus of pigeons*. 1992.
- [Wang 2013] B. Wang, A. Correa Victorino, A. Charara, K. Augsburg and K. Höpping. *Assessment of Rollover Stability Based on Risk Indicator*. In Symposium Series on Computational Intelligence, 2013 IEEE, 2013.
- [Welch 1995] G. Welch and G. Bishop. *An introduction to the Kalman filter*, 1995.

- [Wenzel 2006] T. A. Wenzel, K. J. Burnham, M. V. Blundell and R. A. Williams. *Dual extended Kalman filter for vehicle state and parameter estimation*. *Vehicle System Dynamics*, vol. 44, no. 2, pages 153–171, 2006.
- [Wong 2008] J. Y. Wong. *Theory of ground vehicles*. John Wiley & Sons Ltd, 2008.
- [Xu 2007] L. Xu and H. E. Tseng. *Robust model-based fault detection for a roll stability control system*. *IEEE Transactions on Control Systems Technology*, vol. 15, no. 3, pages 519–528, 2007.
- [Yu 2008] H. Yu, L. Güvenc and Ü. Özgüner. *Heavy duty vehicle rollover detection and active roll control*. *Vehicle System Dynamics*, vol. 46, no. 6, pages 451–470, 2008.
- [Yu 2013] G. Z. Yu, D. Wang, Q. Li, P. W. Wang and Y. P. Wang. *Road Bank Estimation for Bus Rollover Prediction*. *Appl. Math*, vol. 7, no. 5, pages 2027–2034, 2013.
- [ZANTEN 2000] A. T. VAN ZANTEN. *Bosch ESP systems: 5 years of experience*. In SAE Technical Paper, volume 109, pages 428–436, New York, NY, ETATS-UNIS, 2000.
- [Zhan 2000] W. Z. Zhan, Y. Lin, G. B. Shi and L. G. Wang. *Study on Non-Linear Dynamic Characteristic of Vehicle Suspension Rubber Component*. In International ADAMS User Conference, 2000.
- [Zhang 1998] Y. L. Zhang, D. H. Hong, J. H. Chung and S. A. Velinsky. *Dynamic model based robust tracking control of a differentially steered wheeled mobile robot*. In Proceedings of the 1998 American Control Conference, volume 2, pages 850–855 vol.2, 1998.
- [Zhu 2011] X. Zhu, C. Qiu, L. Guo and Y. Zhang. *New method for slip and tire force estimation of wheeled mobile robot on inclined terrain*. In 2011 IEEE International Conference on Robotics and Biomimetics, pages 2264–2269, 2011.